

EIGHTH NATIONAL CONFERENCE ON ELECTRON PROBE ANALYSIS

PRESENTED BY

THE ELECTRON PROBE ANALYSIS SOCIETY OF AMERICA

AUGUST 13 - 17, 1973

JUNG HOTEL  
NEW ORLEANS, LOUISIANA

## PREFACE

The Eighth National Conference on Electron Probe Analysis marks a major change for our Society. This is the first joint meeting with EMSA. Since both societies have mutual interests in many areas, this joint venture was an obvious one.

The program of both societies is open to all, and hopefully it will be of mutual benefit to members of both groups. The exhibit is the largest to date and should be patronized by all attendees.

As usual, these meetings are not one- or two-man efforts. Thanks are due to John Colby - publicity, Arnold Hakkila - program, Don Beaman - publications, and Art Chodos - arrangements. Special thanks are due to Joseph Miller and G. W. Bailey of EMSA who have handled the bulk of the local and program arrangements. Lastly, the program--which is the heart of any meeting--relies heavily on the authors and thanks are due them.

Let us hope that this meeting will provide the stimulation for many similar meetings in the future.

Paul Lublin  
General Chairman

NATIONAL OFFICERS -- 1973

President

D. R. Beaman  
The Dow Chemical Company

President-Elect

P. Lublin  
General Telephone & Electronics Laboratories

Secretary

J. W. Colby  
Bell Telephone Laboratories

Treasurer

D. B. Brown  
U. S. Naval Research Laboratories

Members At Large

J. B. Woodhouse  
University of Illinois

J. I. Goldstein  
Lehigh University

D. F. Kyser  
IBM

EIGHTH NATIONAL CONFERENCE COMMITTEE

General Chairman

P. Lublin  
General Telephone & Electronics Laboratories

Arrangements

A. A. Chodos  
Cal Tech

Publicity

J. W. Colby  
Bell Telephone Laboratories

Program

E. A. Hakkila  
Los Alamos Scientific Laboratory

W. F. Chambers  
Sandia Corporation

J. R. Coleman  
University of Rochester

K. Keil  
University of New Mexico

P. Walitsky  
Westinghouse Electric Corporation

Publication

L. K. & D. R. Beaman  
The Dow Chemical Company



INVITED SPEAKERS

R. Castaing  
Universite de Paris-Sud  
Orsay, France

K. Kandiah  
United Kingdom Atomic Energy Authority  
Harwell, England

K. F. J. Heinrich  
National Bureau of Standards  
Washington, D.C.

J. Philibert  
CNRS  
Saint Germain-en-Laye, France

J. E. Houston  
Sandia Corporation  
Albuquerque, New Mexico

W. F. Chambers  
Sandia Corporation  
Albuquerque, New Mexico

L. V. Sutfin  
Children's Hospital  
Boston, Massachusetts

C. E. Johnson  
Argonne National Laboratory  
Argonne, Illinois

D. O'Boyle  
University of Wisconsin  
Madison, Wisconsin  
&  
Argonne National Laboratory  
Argonne, Illinois

SUSTAINING MEMBERS

1973

AMR CORPORATION  
Burlington, Massachusetts

APPLIED RESEARCH LABORATORIES  
Glendale, California

CAMECA INSTRUMENTS INC.  
Elmsford, New York

CANBERRA INDUSTRIES, INC.  
Meriden, Connecticut

COATES AND WELTER INSTRUMENT CORPORATION  
SUBSIDIARY OF AMERICAN OPTICAL CORPORATION  
Sunnyvale, California

CORNING GLASS WORKS  
Corning, New York

EDAX INTERNATIONAL, INC.  
Prarie View, Illinois

ETEC CORPORATION  
Hayward, California

FINNIGAN CORPORATION  
Sunnyvale, California

FORD MOTOR COMPANY  
Dearborn, Michigan

SUSTAINING MEMBERS

1973

HI-REL LABORATORIES  
San Marino, California

IMAGE ANALYSING COMPUTERS, INC.  
Monsey, New York

JEOL USA INCORPORATED  
Medford, Massachusetts

KENT CAMBRIDGE SCIENTIFIC INC.  
Morton Grove, Illinois

McCRONE ASSOCIATES  
Chicago, Illinois

NUCLEAR DATA, INC.  
Palatine, Illinois

ORTEC INC.  
Oak Ridge, Tennessee

PERKIN-ELMER ULTEK, INC.  
Palo Alto, California

PHYSICAL ELECTRONICS INDUSTRIES, INC.  
Edina, Minnesota

TRACOR NORTHERN  
NORTHERN SCIENTIFIC INC.  
Middleton, Wisconsin

### VICTOR MACRES MEMORIAL AWARD

Early this year the Executive Council established the Victor Macres Memorial Award for the outstanding contribution in instrumentation presented at the annual meeting. The recipient will receive a citation and a \$250 award. Selection will be announced during the annual meeting.

STUDENT AWARD RECIPIENTS

JEOL AWARD

E. J. BARRETT

University of Rochester

Paper Number 60

"Sodium and Potassium Content of Single Cells:  
Effects of Metabolic and Structural Changes"

EPASA AWARDS

W. N. LIN

University of Southern California

Paper Number 73

"Study of GaAs Using Infrared Modulated Cathodoluminescence"

A. J. GANCARZ

California Institute of Technology

Papers Number 45 and 77

"Microprobe Analysis of the Bulk Composition of Phase Aggregates"  
and  
"Optimization of Computer Controlled  
Quantitative Analysis of Minerals"

PREVIOUS AWARD WINNERS

- 1971: M. R. Jackson, W. K. Jones, J. Lebiedzki, J. C. Potosky, and  
R. Warner.
- 1972: T. E. Keller, H. C. Marciniak, B. J. Panessa, and R. R. Warner.

MEETING ANNOUNCEMENT

NINTH NATIONAL CONFERENCE ON ELECTRON PROBE ANALYSIS

Location: Carleton University  
Ottawa, Ontario, Canada

Date: July 22 - 26, 1974

For information concerning this meeting, please contact:

Dr. Don Harris	Program Chairman
Dr. George Plant	Arrangements Chairman
Dr. Rod Packwood	Secretary

At: Mines Branch  
Department of Energy, Mines and Resources  
555 Booth Street  
Ottawa, Ontario, Canada, K1A-0G1

Phone: 613-994-5100

The meeting will include a tutorial session on Monday, July 22, planned by Dr. Jim Brown, and technical sessions on Tuesday through Friday, July 23 - 26. The technical sessions will include all aspects of electron probe analysis, energy dispersive spectrometry, scanning electron microscopy, secondary ion mass analysis, Auger electron spectroscopy, ion scattering spectrometry, electron spectroscopy chemical analysis, soft x-ray emission, instrumentation, computer control and data reduction, and applications.

Contributed papers are welcome and instructions to authors will be provided through meeting announcements and the MicroNews.

## EPASA COMMITTEES

### CONFERENCE COMMITTEE

P. Lublin	Present
R. Packwood	Future
R. J. Ruscica	Past

### EMPLOYMENT SERVICE

G. Judd  
J. B. Woodhouse

### FUTURE MEETING SITES

A. A. Chodos  
J. W. Colby  
P. Lublin

### LEGAL

P. Lublin

### MEMBERSHIP

J. W. Colby

### SPEAKER'S TOUR

J. W. Colby  
D. B. Wittry

### STANDARDS

D. R. Beaman  
A. A. Chodos (Chairman)

### STUDENT AWARDS

L. S. Birks (Chairman)  
J. W. Colby  
J. R. Coleman  
O. C. Wells

### SUSTAINING MEMBERS

D. R. Beaman  
J. Tabock

### VICTOR MACRES MEMORIAL AWARD

L. S. Birks (Chairman)  
D. R. Beaman  
J. Bomback  
K. F. J. Heinrich  
J. Tabock  
J. B. Woodhouse

# EIGHTH NATIONAL CONFERENCE ON ELECTRON PROBE ANALYSIS

## — PROGRAM —

---

Monday, August 13, 1973

### TUTORIAL SESSION

Hall of the Americas, South Hall  
Arnold Hakkila, Chairman

8:00 AM	Registration
9:45	Introductory Remarks by P. Lublin, President-Elect EPASA
10:00	"Interpretation of Metallurgical Data" J. I. Goldstein, Lehigh University.
11:00	"Methods for Obtaining Topographic Images with Resolutions $\sim 100\text{\AA}$ in the Surface SEM" Oliver C. Wells, IBM.
12:00	Lunch
1:30 PM	"Secondary Mass Spectrometry - 'The Ion Probe'" Charles A. Evans, Jr., University of Illinois.
2:30	"X-ray Analysis with Energy Dispersive Spectrometers" D. R. Beaman, The Dow Chemical Company.
3:30	Workshop at Conclusion of Session
4:00	Executive Council Meeting



Tuesday Morning, August 14, 1973

ION MICROPROBE I

Hall of the Americas, South Hall  
Charles Evans, Jr., Chairman

- 8:00 AM Registration
- 9:00 Introduction of EPASA Officers
- 1 9:15 INVITED PAPER: "Secondary Ion Microanalysis - Crystalline and Temperature Effects"; R. Castaing, Universite de Paris-Sud.
- 2 10:00 "Study of a Duoplasmatron with a Quadrupole Mass Spectrometer"; J. C. Potosky and D. B. Wittry, University of Southern California.
- 3 10:15 Intermission
- 4 10:30 "Characterization of Layered Materials with the Ion Microprobe"; K. F. J. Heinrich and R. L. Myklebust, National Bureau of Standards.
- 5 11:10 "Primary Ion Implantation Effects on Depth Profiles Obtained by Secondary Ion Mass Spectrometry"; R. K. Lewis and B. Autier, Cameca Instruments, and J. M. Morabito and J. C. C. Tsai, Bell Telephone Laboratories.
- 6 11:30 "Application of the Ion Microprobe to Semiconductor Problems"; J. W. Colby, Bell Laboratories.
- 11:50 Lunch
- 

Tuesday Afternoon, August 14, 1973

ION MICROPROBE II

Hall of the Americas, South Hall  
John W. Colby, Chairman

- 7 1:30 PM "Reduction of Spectral Interferences in Ion Probe Mass Spectrometry"; D. K. Bakale, B. N. Colby, C. A. Evans, Jr., and J. B. Woodhouse, University of Illinois.
- 8 1:50 "An Investigation of Three-Component Diffusion (Platinum Phosphorus, Silicon) by Sputtering-Auger and Secondary Ion Emission Techniques"; J. M. Morabito and M. J. Rand, Bell Telephone Laboratories.

- 9 2:10 "Geological Applications of the Ion Microprobe Mass Analyzer"; J. R. Hinthorne and C. A. Andersen, Applied Research Laboratories.
- 10 2:30 "Determination of Ion-Implanted Dopant Distribution in Semiconductors by Ion Microanalysis"; R. D. Dobrott, F. N. Schwettmann, and J. L. Prince, Texas Instruments, Inc.
- 11 2:50 "Inter-element Effects in the Ion Probe"; Michael Bayard, W. C. McCrone Associates.
- 3:05 Intermission
- 3:20 Panel Discussion on Ion Microprobe Analysis:  
C. A. Anderson, Applied Research Laboratories  
R. Baxter, Battelle Columbus  
R. Castaing, University of Paris  
J. W. Colby, Moderator, Bell Telephone Labs  
C. A. Evans, Jr., University of Illinois  
K.F.J. Heinrich, National Bureau of Standards  
R. K. Lewis, Cameca Instruments Inc.
- 4:30 End Session. Vendor and Photographic Exhibits open.
- 

Tuesday Afternoon, August 14, 1973

ENERGY DISPERSIVE ANALYSIS

Meeting Room No. 1  
Eric Lifshin, Chairman

- 12 1:30 PM INVITED PAPER: "Some Limitations of Energy Dispersive X-ray Spectrometers"; K. Kandiah, UKAEA.
- 13 2:15 "Quantitative Electron Microprobe Analysis Using An Energy Dispersive Spectrometer"; A. G. Plant and G. R. Lachance, Geological Survey of Canada.
- 14 2:35 "Rapid Energy Dispersive Analysis Utilizing a Field Emission SEM"; Richard G. Vadimsky, Bell Telephone Laboratories.
- 15 2:55 "Microanalysis of Particulate Materials"; R. E. Ferrell and G. G. Paulson, Louisiana State University. In EMSA Proceedings.
- 16 3:10 "Element and Compound Distribution Mapping in the SEM"; J. C. Russ, M. W. Barnhart, and J. L. Christopher, EDAX International, Inc. In EMSA Proceedings.
- 17 3:30 "Improvements in High Counting Rate Performance of Si(Li) Energy Spectrometers with a Novel Baseline Restoration Technique"; N. Karlovac and D. A. Gedcke, ORTEC.
- 3:40 End Session. Vendor and Photographic Exhibits open.
-

Wednesday Morning, August 15, 1973

SURFACE ANALYSIS I (Joint with EMSA)

Hall of the Americas, South Hall  
W. P. Ellis, Chairman

- 18 9:00 AM INVITED PAPER: "Use of Advanced Analytical Techniques for Characterization of the Chemical, Physical, and Crystallographic Nature of a Surface"; R. E. Herfert, Northrop Corporation. In EMSA Proceedings.
- 19 9:40 INVITED PAPER: "The Third Dimension in Scanning Electron Microscopy: Scanning Auger Microscopy"; N. C. MacDonald, Physical Electronics Industries, Inc. In EMSA Proceedings.
- 10:20 Intermission
- 20 10:35 "SEM-Auger Spectroscopy Characterization of Semiconductor Structures"; E. K. Brandis, IBM East Fishkill Facility.
- 21 10:55 "Applications of Auger Electron Spectroscopy (AES) to Problems in Microelectronic Manufacturing Processes"; D. K. Conley, Western Electric Company.
- 22 11:15 "Analysis of Gas and Solid Samples by ESCA"; J. F. Rendina, McPherson Instrument Corporation.
- 23 11:35 "Ion Scattering Spectrometry - Sensitivity, Resolution, and Quantitative Considerations"; J. A. Leys and J. T. McKinney, 3M Company.
- 11:55 Lunch
- 

Wednesday Morning, August 15, 1973

QUANTITATIVE ANALYSIS

Terrace Suites 1, 2, 3  
W. F. Chambers, Chairman

- 24 9:00 AM INVITED PAPER: "Progress in Quantitative Electron Probe Microanalysis"; K. F. J. Heinrich, NBS.
- 25 9:30 "Statistical Check of Electron Probe Microanalysis Measurements"; M. Ancey and R. Tixier, IRSID.
- 26 9:45 "Performance Evaluation of FRAME - An On-Line Theoretical Program for Electron Probe Microanalysis"; R. L. Myklebust, H. Yakowitz, and K. F. J. Heinrich, NBS.

10:05 Intermission

27 10:20 INVITED PAPER: "Electron Probe Microanalysis of Thin Specimens"; J. Philibert, University of Paris, and R. Tixier, IRSID.

28 10:50 "Quantitative Electron Microprobe Analysis of Thin Films with Monte Carlo Calculations"; D. F. Kyser and K. Murata, IBM Research Laboratory.

29 11:10 "Determination of the Energy Distribution of the Continuum and Ratio of Indirect to Direct X-Ray Fluorescence"; E. Lifshin, M. F. Ciccarelli, and R. B. Bolon, GE Corporate R&D Center.

30 11:30 "Quantitative Electron Probe Microanalysis of Particles"; J. C. Russ, EDAX Laboratories.

31 11:50 "The Use of Monte Carlo Calculations for Quantitative Analysis at Non-Normal Electron Beam Incidence"; R. B. Bolon and E. Lifshin, GE Corporate R&D Center.

12:05 Lunch

---

Wednesday Afternoon, August 15, 1973

SURFACE ANALYSIS II (Joint with EMSA)

Hall of the Americas, South Hall  
W. Bottoms, Chairman

32 1:30 PM INVITED PAPER: "Analysis by Appearance Potential Techniques"; J. E. Houston and R. L. Park, Sandia Laboratories.

33 2:10 "Surface Capabilities of the Electron Microprobe Using Threshold Isochromat Integrated Intensities and Other Techniques"; J. S. Solomon, T. J. Wild, University of Dayton Research Institute, and W. L. Baun, Air Force Materials Lab.

34 2:30 "Prospects and Difficulties in High Spatial Resolution Surface Electron Probes"; T. W. Rusch and W. P. Ellis, Los Alamos Scientific Laboratory.

35 2:50 "An Experimental System Combining Medium Energy Electron Diffraction and Scanning Electron Microscopy"; J. M. Cowley, F. A. Koch, and J. L. Albain, Arizona State University. In EMSA Proceedings.

3:10 Intermission

- 36 3:25 "Soft X-Ray Absorption Spectroscopy Using the Electron Microprobe"; D. G. W. Smith, University of Alberta, and K. Norrish, CSIRO.
- 37 3:55 "A Universal Type Pressure Controller for Thin Window Flow Proportional Counters"; C. E. Hugenberg and W. J. Steele, Lawrence Livermore Laboratory.
- 38 4:05 "A Photoemission Electron Microscope Using An Electron Multiplier Array"; W. J. Baxter and S. R. Rouze, General Motors Corporation. In EMSA Proceedings.
- 39 4:25 "Photo Stimulated Exoelectron Emission From Slip Lines - A New Microscopy of Metals Deformation"; W. J. Baxter and S. R. Rouze, General Motors Corporation. In EMSA Proceedings.
- 40 4:45 "Auger Electron Emission Micrography and Microanalysis of a Stained Surface of Pure Iron Plate"; S. Hayakawa, H. Okano, S. Kawase, and S. Yamamoto, Hitachi Ltd. In EMSA Proceedings.
- 5:05 End Session. Vendor and Photographic Exhibits open.
- 

Wednesday Afternoon, August 15, 1973

AUTOMATION AND COMPUTER APPLICATIONS

Terrace Suites 1, 2, 3  
A. A. Chodos, Chairman

- 41 1:30 PM INVITED PAPER: "The Sandia Approach to Electron Probe Automation"; W. F. Chambers, Sandia Laboratories.
- 42 2:15 "Time-Shared Computer Control of Electron Microprobe and X-Ray Diffraction Equipment"; W. Holzwarth, E. Quigg, and C. T. Prewitt, State University of New York.
- 43 2:35 "Practical Aspects of Microprobe Automation"; W. B. Estill and D. E. Benthussen, Sandia Laboratories.
- 2:45 Intermission
- 44 3:05 "On-Line Quantitative Microprobe Analysis with a Hosted IBM SYSTEM/7 Computer"; D. F. Kyser, G. L. Ayers, and D. E. Horne, IBM Research Laboratory.
- 45 3:25 "Optimization of Computer-Controlled Quantitative Analysis of Minerals"; A. A. Chodos, A. L. Albee, A. J. Gancarz, and J. Laird, Cal Tech.
- 46 3:45 "Microprobe Digital Data Acquisition with the Multichannel Analyser"; W. T. Kane, Corning Glass Works.
- 4:05 End Session. Vendor and Photographic Exhibits open.
-

Thursday Morning, August 16, 1973

SCANNING ELECTRON MICROSCOPY I (Joint with EMSA)

Hall of the Americas, South Hall  
D. B. Wittry, Chairman

- 47 9:00 AM INVITED PAPER: "Electron Microscopy and X-Ray Microanalysis in Forensic Science"; J. W. Johnson and J. L. Brown, Georgia Tech. In EMSA Proceedings.
- 48 9:40 "Direct Observation of Ferroelectric Domains Using the SEM"; C. Michel and A. Sicignano, Philips Laboratories.
- 49 10:00 "Magnetic Contrast in the Secondary Emission Mode of the SEM"; R. P. Ferrier and D. F. Kyser, IBM Research Laboratory.
- 10:20 Intermission
- 50 10:35 "Crystal Habit of Iron in Apollo 14, 15 and 16 Recrystallized Breccias"; U. S. Clanton, D. S. McKay, R. B. Laughon, NASA, and G. H. Ladle, Lockheed Electronics Corporation.
- 51 10:55 "Considerations in Making Stereo Micrographs with the Scanning Electron Microscope"; E. R. Walter, Union Carbide Corporation. In EMSA Proceedings.
- 52 11:15 "SEM Observations of Magnetic Domain Contrasts in Silicon-Iron Crystals"; A. Gervais, J. Philibert, A. Riviere, and R. Tixier, CNRS.
- 

Thursday Afternoon, August 16, 1973

SCANNING ELECTRON MICROSCOPY II (Joint with EMSA)

Hall of the Americas, South Hall  
O. Wells, Chairman

- 53 1:30 PM "Test Specimens for High Resolution Scanning Electron Microscopy"; R. T. Greer, Iowa State University. In EMSA Proceedings.
- 54 1:50 "SEM Resolution and Test Specimen"; J. T. Black, University of Rhode Island. In EMSA Proceedings.
- 55 2:10 "Metal Cutting in the Scanning Electron Microscope"; J. T. Black, University of Rhode Island, and S. Ramalingam, State University of New York. In EMSA Proceedings.
- 56 2:30 "An Efficient Reduced Raster and Manual Line Set Control System for JEOL JSM-U2 and JSM-U3 SEMs"; H. W. Estry, L. F. Allard, and W. C. Bigelow, University of Michigan. In EMSA Proceedings.

- 57 2:50 "A Combined Scanning Electron Microscope - Electron Probe Microanalyzer"; A. E. Zolla, R. S. Willing, A. Falco, and J. R. Seward, ARL.
- 58 3:10 "Modular Magnetic Lense Accessory to Basic Field Emission SEM"; A. C. Holms, J. H. Cooper, J. J. God, and L. M. Welter, Coates and Welter Instrument Corporation. In EMSA Proceedings.
- 3:30 EPASA Business Meeting.
- 

Friday Morning, August 17, 1973

BIOLOGICAL APPLICATIONS

Meeting Room No. 1  
J. R. Coleman, Chairman

- 59 9:00 AM INVITED PAPER: "Electron Probe Analysis of Subcellular Structures in Biological Tissues"; L. V. Sutfin, Children's Hospital Medical Center.
- 60 9:30 "Sodium and Potassium Content of Single Cells: Effects of Metabolic and Structural Changes"; E. J. Barrett and J. R. Coleman, University of Rochester.
- 61 9:50 "Evaluation of the Electron Microprobe for Medical Applications"; P. S. Ong, W. O. Russell, M. Mandavia, and G. Sroka, University of Texas.
- 10:10 Intermission
- 62 10:25 "Pure Crystals as Secondary Standards for Quantitative Electrolyte Studies of Soft Biological Tissue"; F. D. Ingram, M. J. Ingram, and C. A. M. Hogben, University of Iowa.
- 63 10:35 "Electron Probe Analysis of Calcium Containing Lipid Droplets in Tetrahymena pyriformis"; J. R. Coleman, University of Rochester.
- 64 10:55 "Electron Probe Microanalysis of Age Differences in Human Red Blood Cells"; L. C. Burns, Northrup Services, and S. L. Kimzey, Johnson Space Center.
- 65 11:15 "Immature Muscle Sodium and Potassium; Electron Microprobe Investigation"; B. L. Nichols, D. J. Sachen, and C. F. Hazlewood, Baylor College of Medicine, and L. C. Burns and S. L. Kimzey, Johnson Space Center.
- 66 11:35 "Ultrahistochemical Studies of Mucosubstances: Electron Microscope Observations and Microprobe Analysis of the Chick Embryo Cornea"; T. Ohkura, H. Iwatusuki, and T. Watanabe, Kawasaki Medical College.

- 67 11:55 "Specific Metal Staining of Biological Tissues for the SEM Using Backscatter Electron or Specimen Current Imaging"; J. L. Abraham, P. B. DeNee, and A. H. Gelderman, U. S. Department of Health, Education, and Welfare.

12:05 PM Lunch

---

Friday Morning, August 17, 1973

NUCLEAR APPLICATIONS

Meeting Room No. 10  
D. O'Boyle, Chairman

- 68 9:00 AM INVITED PAPER: "Application of Electron and Ion Microprobe Techniques to the Study of Nuclear Fuels"; C. E. Johnson, Argonne National Laboratory.
- 69 9:45 "Microprobe Examinations of Irradiated Nuclear Fuels"; W. F. Zelezny, W. B. Hutchinson, R. E. Smith, and E. A. Hakkila, Los Alamos Scientific Laboratory.
- 70 10:05 "Intergranular Attack of LMFBR Cladding - A Comparison of Laboratory and In-Reactor Results"; T. E. Lannin, E. A. Aitkin, and S. K. Evans, General Electric Company.
- 71 10:25 "Electron Microprobe Determination of U, Zr, and C in Mixed Carbide Fuel Elements"; E. A. Hakkila, Los Alamos Scientific Laboratory.
- 10:35 End Session. Intermission

APPLICATIONS TO THE ELECTRONICS INDUSTRY

P. Lublin, Chairman

- 72 10:50 "Determining Thickness of SiO<sub>2</sub> and Si<sub>3</sub>N<sub>4</sub> Ultra-Thin Film Composites of FED Wafers and Devices"; G. Di Giacomo, IBM.
- 73 11:10 "Study of GaAs Using Infrared Modulated Cathodoluminescence"; W. N. Lin and D. B. Wittry, University of Southern California.
- 74 11:30 "Investigation of the Electron Burn of MgF<sub>2</sub> Dielectric Material"; P. J. Walitsky, Westinghouse Electric Corporation.
- 75 11:50 "Theoretical Model of EBIC Bipolar Circuit Testing"; P. C. Arnett, IBM.

12:10 PM End Session. Lunch

---



Friday Afternoon, August 17, 1973

APPLICATIONS TO METALLURGY AND CERAMICS

Meeting Room No. 10  
P. Walitsky, Chairman

- 76 1:30 PM INVITED PAPER: "Metallurgical Applications of the Electron Microprobe"; D. O'Boyle, University of Wisconsin and Argonne National Laboratory.
- 77 2:10 "Microprobe Analysis of the Bulk Composition of Phase Aggregates"; A. J. Gancarz and A. L. Albee, Cal Tech.
- 78 2:30 "Use of EBM Analysis in the Process Development of a New Gear Material"; N. M. Walter, The Boeing Verton Company.
- 79 2:50 "Ion Plated Copper-Steel Graded Interface"; R. Swaroop and I. Adler, Kelsey-Hayes R&D Center.
- 3:10 End Session.
- 

Friday Afternoon, August 17, 1973

NEW INSTRUMENTATION AND LATE BREAKING DEVELOPMENTS

Meeting Room No. 1  
D. R. Beaman, Chairman

- 80 1:30 PM "Reducing Background at the Short Wavelength End of ARL Crystal Spectrometers"; W. C. Bigelow, F. Bleicher, L. F. Allard, and A. J. Mardinly, University of Michigan.
- 81 1:40 "New X-Ray Spectrometers for a Multipurpose Scanning Electron Microprobe"; B. Kenessey, L. K. Griffith, and E. Davidson, ARL.
- 82 2:00 "A Simple Device for Volume Fraction Analysis in the Scanning Electron Microscope"; W. T. Hatfield, E. Lifshin, and M. R. Jackson, G. E. Corporate R&D Center.
- 83 2:10 "An Image Comparison System for Electron Optics Instruments"; G. Judd and R. Wilson, Rensselaer Polytechnic Institute, and H. Weiss, Raytheon Company.
- 84 2:20 "Microprobe Techniques for the Analysis of Radioactive Materials"; D. O'Boyle, University of Wisconsin, and Argonne National Laboratory.
- 85 2:35 "A New Technique for Deconvolution of Complex X-Ray Energy Spectra"; F. H. Schamber, Northern Scientific, Inc.
- 86 2:55 "Observations on the Practical Applications of Selected Area Electron Channelling Patterns to Deformation Studies"; J. A. Cornie, D. L. Harrod, and C. W. Hughes, Westinghouse Research Laboratories.
- 3:10 Adjourn



S U M M A R I E S

O F

P A P E R S



## SECONDARY ION MICROANALYSIS - CRYSTALLINE AND TEMPERATURE EFFECTS

R. Castaing

Laboratoire de Physique des Solides, Université de Paris-Sud  
91405 Orsay (France)

The specific advantages of secondary ion microanalysis, as compared to electron probe analysis, are balanced by the fact that quantitative analysis is much more difficult; the emission of the secondary ions is strongly dependent on the chemical bonds so that the interpretation of the measurements is complicated, except in simple cases such as isotope mixtures or very low concentrations; even in such simple cases, care must be taken for avoiding the presence of spurious molecular ions which could falsify the measurements. On the other hand, advantage may be taken frequently of that dependence of the emission on the chemical bonds. For example, a precipitation at the scale of the electron microscope cannot be detected by the electron microprobe; the same would be true for secondary ion analysis if the ion emission were insensitive to chemical bonds; the instrument would be unable to discriminate between such an heterogeneous state and a solid solution of the same average composition. In fact the measurement of composite secondary ions, which are emitted essentially by the precipitates, makes possible such a discrimination.

The essential point, in quantitative analysis, is to get figures depending only on the bulk properties of the analyzed phases, and independent of other parameters such as crystalline orientation or etching speed for example. In that respect, the best procedure, in quantitative secondary ion microanalysis consists in comparing the emissions of the various ions at the same point; the errors due to the differences in sputtering rate at the various points of the sample are automatically eliminated; moreover, such a procedure reduces to a low level the important errors which could result from differences of orientation of the sample lattice with respect to the primary ion beam. The sputtering rate and the secondary ion emission are strongly dependent on that respective orientation. When the ion is impinging along a direction of "transparency" of the lattice, both sputtering rate and ion emission are much lower than when it impinges along an "opaque" direction. That orientation dependence has been studied in detail by Bernheim and Slodzian in our laboratory. They found that, for an alloy AB bombarded with noble gas ions, the  $A^+$  and  $B^+$  emissions vary by a factor of 2 or more when passing from a transparent direction to an opaque direction, whereas the ratio  $B^+/A^+$  is practically independent of the orientation. For some metals such as Al, the orientation dependence of the emission may be lowered by using oxygen primary ions; it is completely eliminated (see Fig. 1) by introducing a partial pressure of oxygen in the vicinity of the sample so as to produce an amorphous oxide layer at the free surface.

The situation is quite different in the case of a Ni-Cr alloy for example. The adsorption of oxygen enhances the  $Ni^+$  and  $Cr^+$  emissions, but the ratio  $Cr^+/Ni^+$  is practically independent of the orientation. Incidentally, it was found that the orientation dependence of the ion emission ( $Ni^+$  or  $Cr^+$ ) is strongly modified at intermediate stages of the oxygen adsorption, indicating a modification of the crystalline structure of the surface layer; in that respect, secondary ion emission could be a valuable tool for studying the atomic arrangements of such adsorbed layers. On the other hand, the adsorption of nitrogen has very little effect on the  $Ni^+$  emission, but it enhances the  $Cr^+$  emission by a factor of 3 in the opaque directions and by a factor of 10 in the transparent directions (Fig. 2), with the very unhappy result that the  $Cr^+/Ni^+$  ratio depends strongly on the crystal orientation. The influence

of such effects on quantitative analysis will be discussed. They are highly sensitive to the temperature of the sample, as the thermal vibrations reduce the differences in transparency between the various directions. A detailed study of the effect of temperature has been made by Laurent and Slodzian, up to the melting point of the sample. As an example, Figs. 3 and 4 show in the case of an Al crystal that an increase in temperature reduces the emission in the opaque directions (maxima) and increases the emission in transparent directions (minima). Both maxima and minima converge towards a common limit which is identical to the emission of the liquid metal.

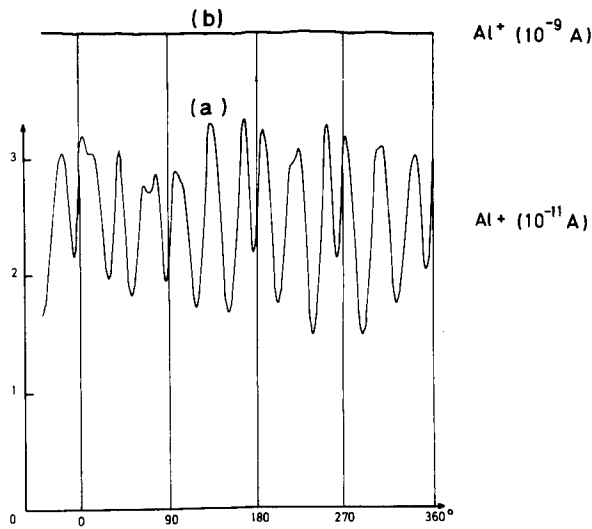


Fig. 1.  $\text{Al}^+$  emission vs orientation  
(a) bare sample  
(b) sample covered with oxygen

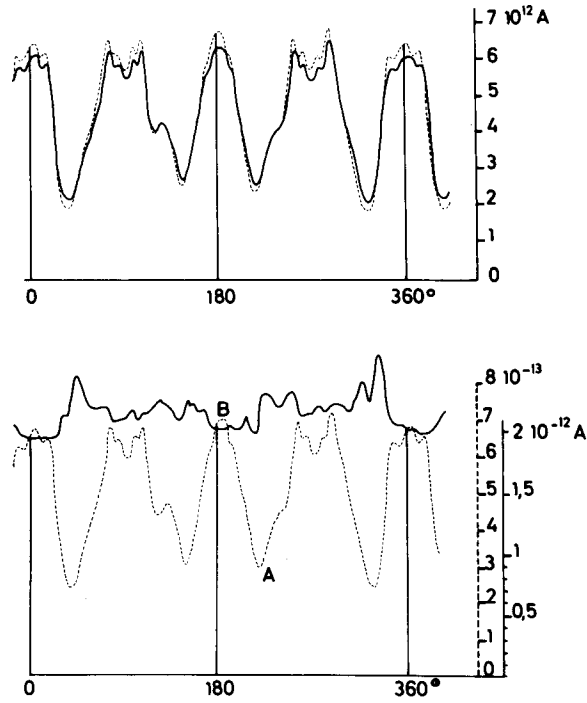


Fig. 2. Ni-Cr crystal. Emission of  $\text{Ni}^+$  (upper curves) and  $\text{Cr}^+$  (lower curves) versus orientation  
-----: bare sample  
——: sample covered with nitrogen

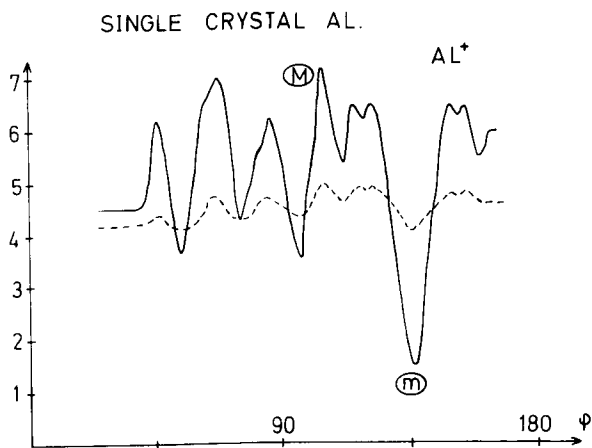


Fig. 3.  $\text{Al}^+$  emission vs orientation  
——: room temperature  
-----: near the melting point

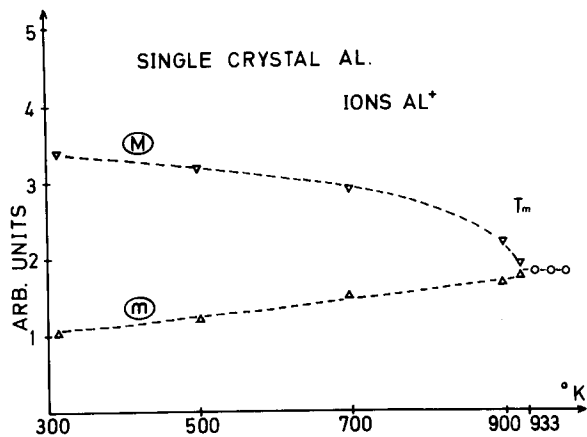


Fig. 4. Maximum emissions (M) and minimum emissions (m) vs temperature. Open circles (ooo): liquid metal.

## STUDY OF A DUOPLASMATRON WITH A QUADRUPOLE MASS SPECTROMETER\*

J.C. Potosky and D.B. Wittry  
 Departments of Electrical Engineering and Materials Science  
 University of Southern California  
 Los Angeles, California 90007

An ideal ion source for an ion microprobe is characterized by high brightness, small virtual source size, and stability. It is also desirable to produce beams of different atomic or molecular species and charge. The duoplasmatron, invented by Von Ardenne<sup>1</sup> can meet the above requirements<sup>2</sup> and have been used previously as an ion source for ion microprobes.

The duoplasmatron operates by initiating a discharge through a low pressure gas. The gas is ionized and a plasma is produced in the discharge region. An electric field produced by an intermediate electrode, and a longitudinal magnetic field serve to confine the plasma along the central axis and to produce a high ion density in a small region near the anode. The ion beam is extracted from this region with a suitable electrode.

The duoplasmatron shown in Fig. 1 was constructed for use as an ion source for an ion microprobe. In order to produce ions of reactive gases a cold hollow cathode was used in place<sup>3</sup> the conventional thermionic cathode as in the work of Liebl et al.<sup>3</sup> Initially a 1/4" dia. hollow tantalum tube was used as the cathode. However, it was not satisfactory because of higher pressures required by Paschen's law. The cathode of an OB2 electron tube was found to be a useful hollow cathode because of its low work function and ease of replacement. This cathode provided a larger area of high emissivity and resulted in satisfactory operation. Four inexpensive ring-shaped ferrite magnets (Edmund Scientific Co. #40,482) produce the required magnetic field.

An adjustment was provided to offset the cathode-intermediate electrode axis with respect to the anode aperture. The offset optimizes the extraction of negative ions while reducing electron loadings as shown by Lawrence et al.<sup>4</sup> A standard 100 micron platinum electron microscope aperture was used in the anode to limit the diameter of the extracted beam. The small aperture also serves to isolate the higher pressure discharge region from the high vacuum column which is maintained at  $\sim 5 \times 10^{-5}$  torr by a LN<sub>2</sub> trapped oil diffusion pump (Veeco EP2A-1). Typical duoplasmatron pressures<sup>5</sup> were .05 to .50 torr with corresponding system pressures of 1 to  $5 \times 10^{-5}$  torr.

The I-V characteristics of the discharge are shown in Fig. 2. This curve is pressure dependent. For maximum beam current the intermediate electrode is biased at +50 volts with respect to the cathode.

The mass spectra of the extracted ion beam were obtained with a quadrupole mass spectrometer (Extranuclear Laboratories Inc. model QPS and Special

D-1 High-Q-Head). The body of the spectrometer and mean pole potential was biased near the anode potential for best resolution. It was found desirable to use an electron lens to focus the ion beam into the quadrupole. The experimental arrangement is shown schematically in Fig. 3. The duoplasmatron was run on oxygen and air with negative and positive beams extracted. The spectra obtained are shown in Fig. 4. It should be noted that the intermediate electrode was adjusted to maximize the ion output in each case.

The brightness was not measured. However, if the virtual source size is assumed to be 50 microns, for the ion currents measured (without the quadrupole mass filter but with electron filtering) the brightness could be estimated to be  $\sim 2 \text{ A/cm}^2 \text{ ster}$  at 3KV. This may be compared with reported values of 100-200  $\text{A/cm}^2 \text{ ster}$  obtained at voltages of 12KV and higher.<sup>2</sup>

#### Acknowledgements

N. Gardner assisted in the construction of the apparatus and J. Norris performed some initial tests. H. Roden contributed valuable advice during the construction of the plasmatron.

---

\* This work was sponsored by the Joint Services Electronics Program through the Air Force Office of Scientific Research under grant F44620-71-C-0067 and by the Advanced Research Projects Agency under grant OAHC 15-72-67.

1. M. Von Ardenne, "Tables of Electron Physics, Ion Physics, and Electron Microscopy," Deutscher Verlag der Wissenschaften, Berlin 1, 544-557, 845-862 (1956).
2. H. Liebl, J. Appl. Phys. 38, 5277-83 (1967).
3. C.R. Robinson, H.J. Liebl, and C.A. Anderson, Third Nat. Conf. Electron Microscope Analysis, Chicago, (1968).
4. G.P. Lawrence, R.K. Beuchamp, J.L. McKibben, Nuclear Inst. and Meth. 32, 357-9 (1965).



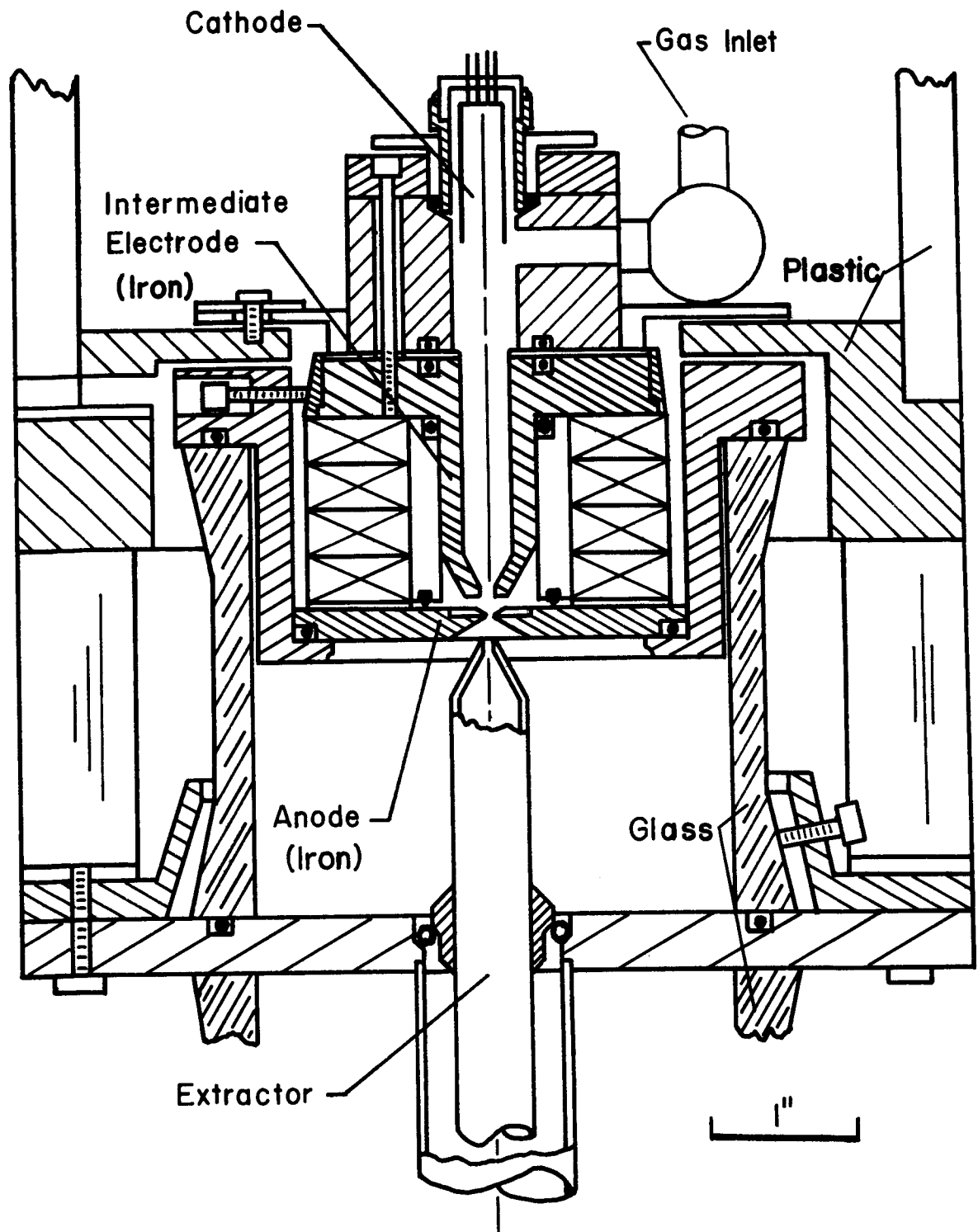


Fig. 1

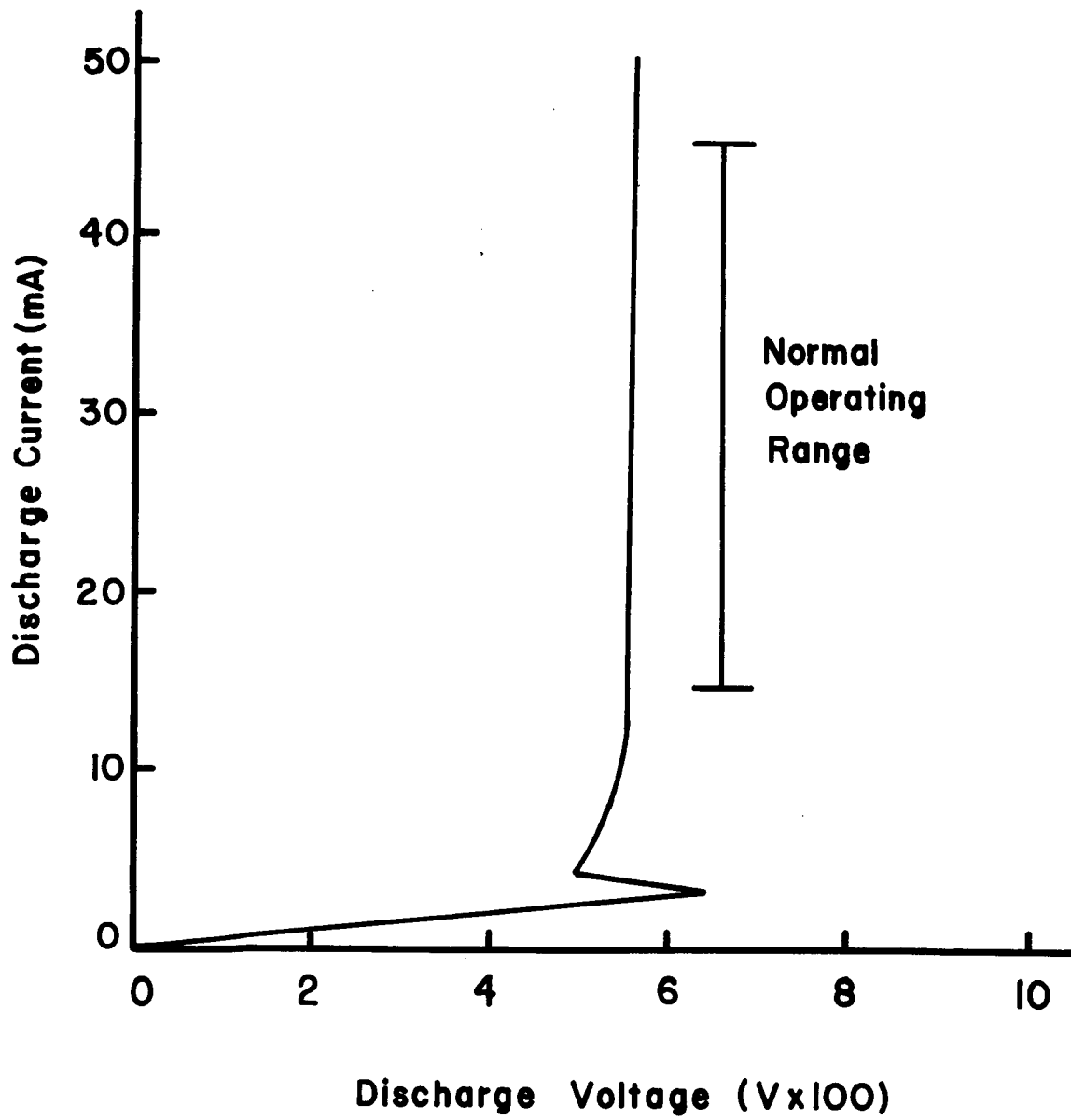


Fig. 2

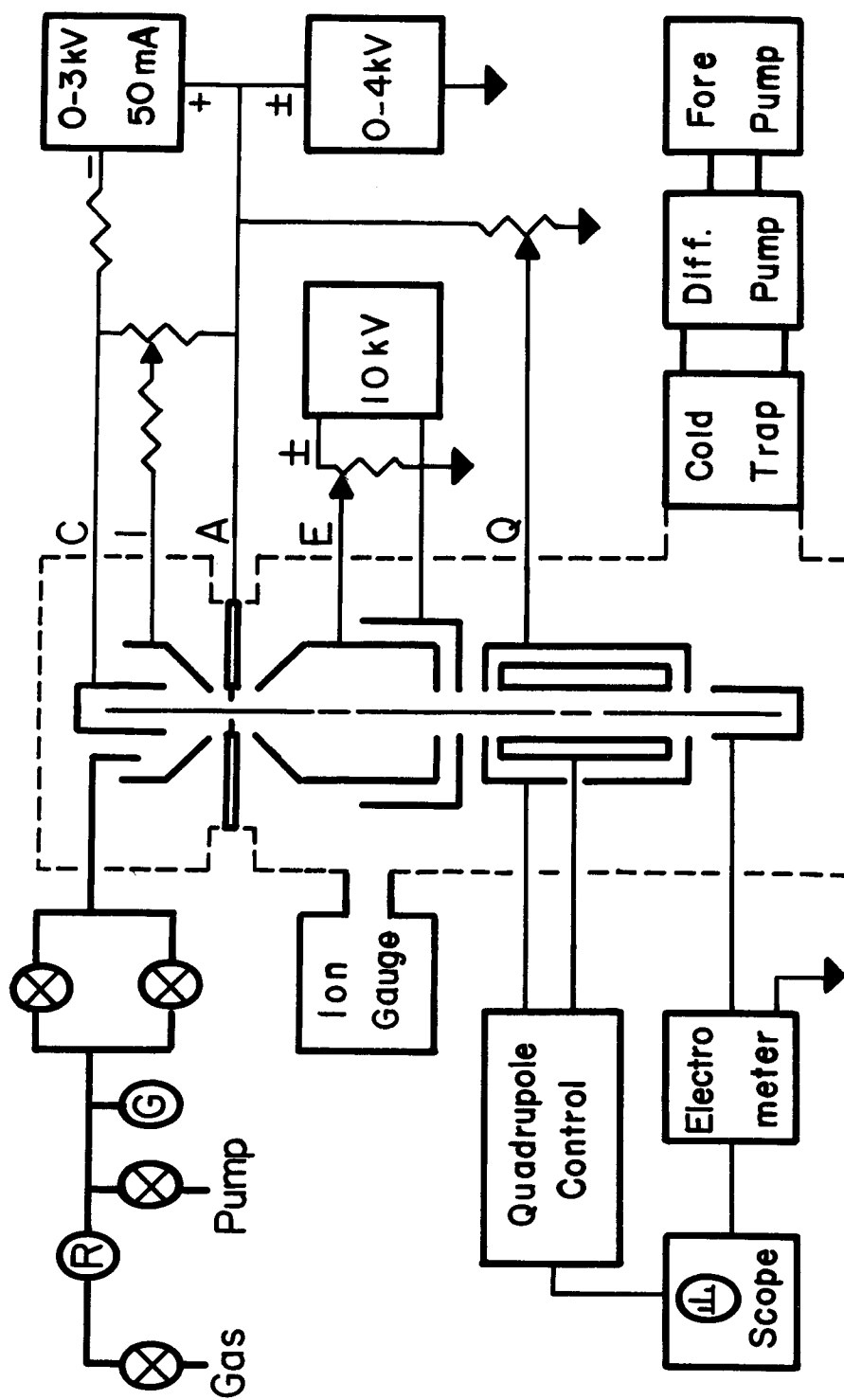


Fig. 3

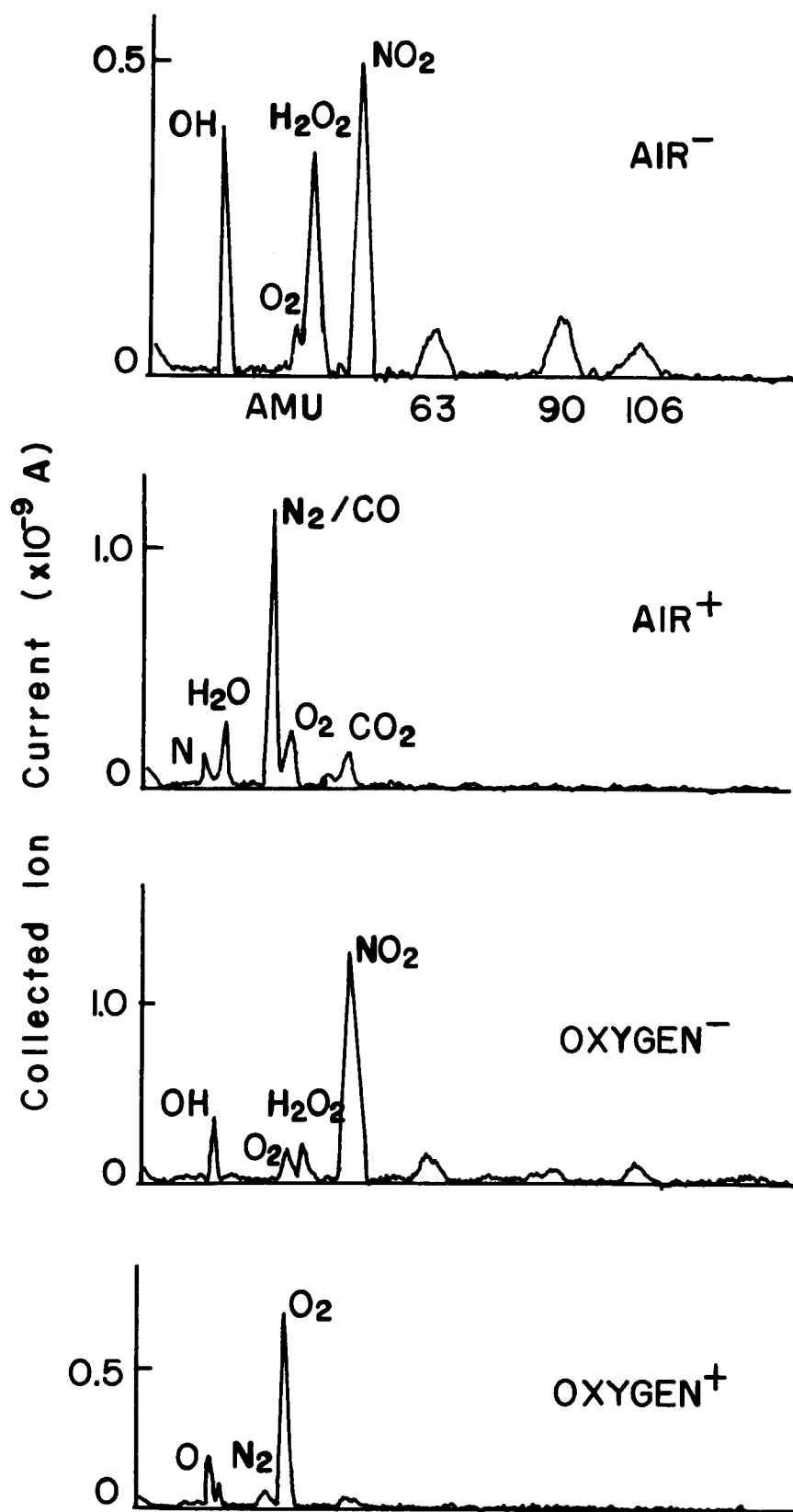


Fig. 4

Characterization of Layered Materials with  
the Ion Microprobe

K. F. J. Heinrich and R. L. Myklebust  
Institute for Materials Research  
National Bureau of Standards  
Washington, D. C. 20234

In many natural and technological products, the characterization of concentration gradients with depth is of interest. The electron probe microanalyzer can be used to investigate such materials. However, its usefulness is, in general, limited to depths above  $1\mu\text{m}$ , elements of atomic number above 10, and concentrations above the trace (0.01%) level. When the layered structures are distributed at shallow depths, the localization of the elements in question is hindered, not only by the depth range of the electrons exciting characteristic x-rays, but also by the difficulties and limitations in the preparative steps which are required to provide a cross-section through the specimens.

The ion microprobe mass analyzer is useful in the investigation of specimens which do not conform with the above mentioned limitations of electron probe microanalysis. Cases of eminent technical interest in this category include silicon wafers doped with various elements of low atomic number (B, Li).

The scanning IMMA is an excellent tool for preshaping the specimens by ion-etching with a programmed scanning beam (Figure 1). In homogeneous materials, one can obtain very well-controlled geometrical configurations. For fairly deep etching ( $>1000\text{ \AA}$ ), it is advisable to use a positive beam (e.g.,  $^{32}\text{O}_2^+$ ). This, however, precludes the concurrent analysis of insulators, in which local charging may severely alter the observed secondary ion intensities. It is, therefore, preferable to first prepare the specimen by etching a shallow ramp with a positive beam, and then characterize the depth distribution with a negative beam of lower intensity, by means of line- or step scans.

The quantitative calibration of relative ion emission can be aided by the use of the electron probe. For instance, in the investigation of the distribution of phosphorus in silica layers of  $\sim 1.5\mu\text{m}$  thickness, it was possible to calibrate the ion emission intensities by analyzing the average layer composition with the electron probe. The resulting plot of the ratio of the mass number 31 to 30 ( $^{31}\text{P}/^{30}\text{Si}$ ) as a function of the mass ratio of phosphorus to silicon is linear (Figure 2).

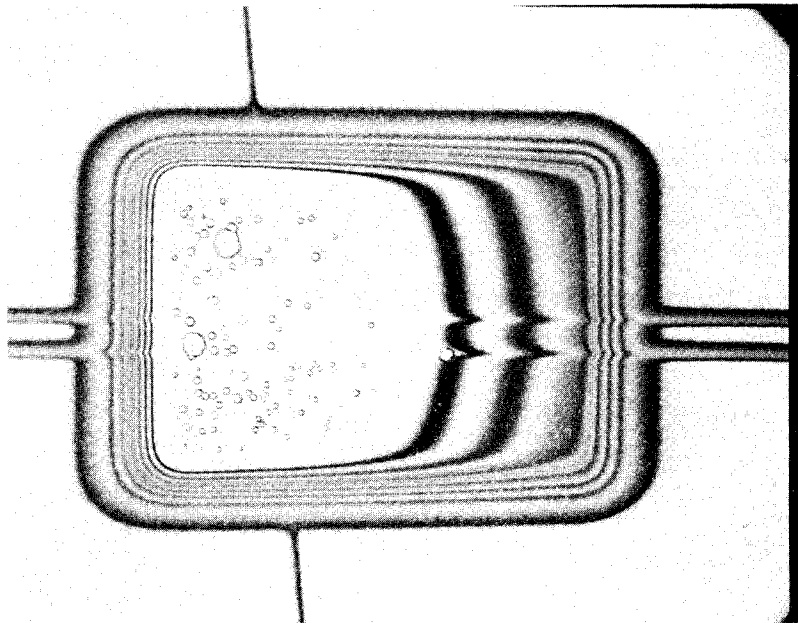
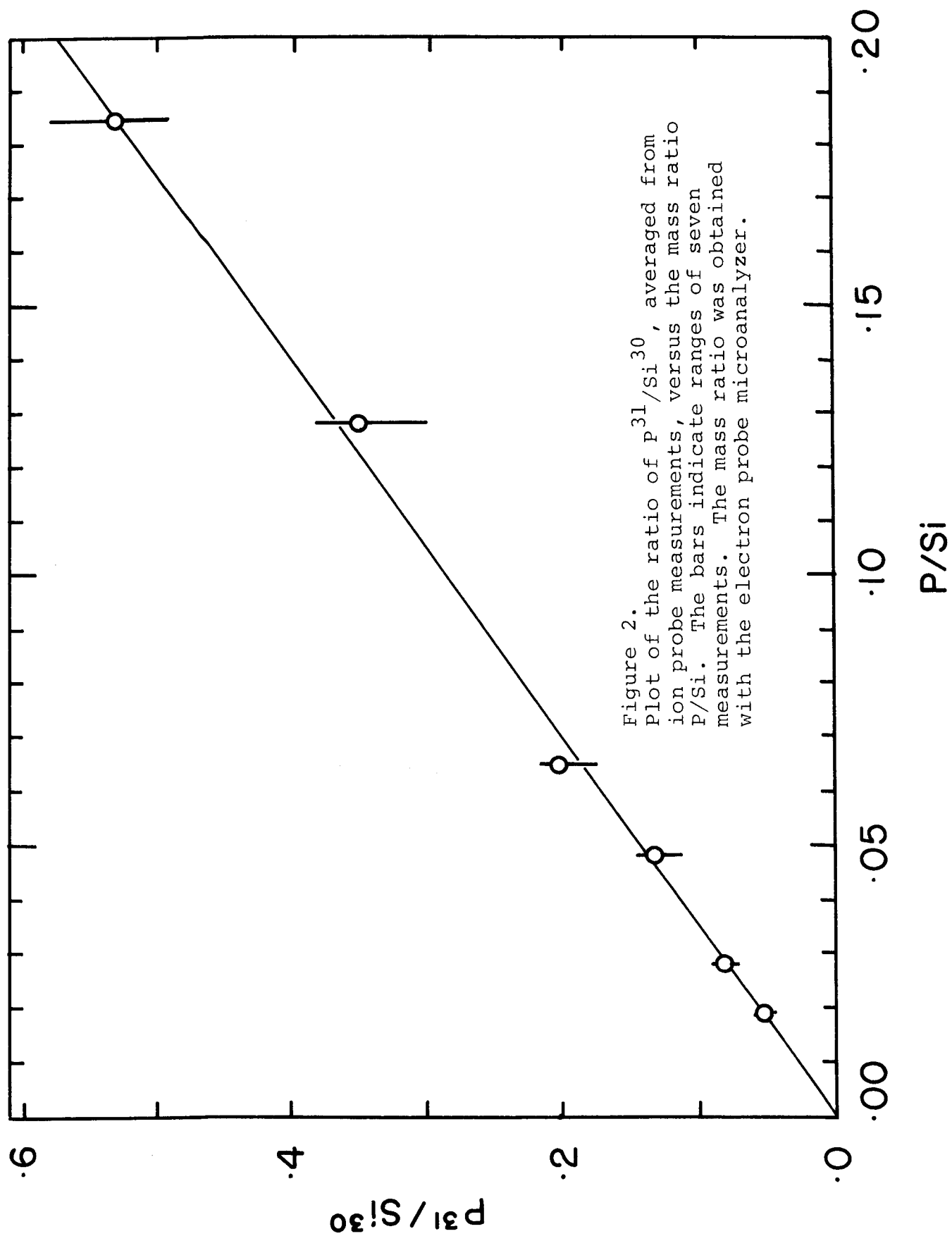


Figure 1. Micrograph (300X) of an etching pit produced in a silicon chip covered by a  $\text{SiO}_2$  layer. The depth of the layer was  $\sim 1.5\mu\text{m}$ . In the central part, the silicon has been reached. The beam consisted of  $^{32}\text{O}^+$  ions accelerated to 20 kV. Three line-scans are superposed.



## RECENT ADVANCES IN QUANTITATIVE ION MICROPROBE MASS ANALYSIS

C. A. Andersen

and

J. H. Hinthorne

Hasler Research Center  
Applied Research Laboratories  
95 La Patera Lane  
Goleta, California 93017

An analytical method for the quantitative interpretation of sputtered ion intensities based on a thermal equilibrium model has been developed (1). The model states that the majority of sputtered ions, atoms, molecules and electrons are in thermal equilibrium with each other and that these equilibrium concentrations can be predicted through use of the proper Saha equations. This calculation is the basis for a quantitative correction method, CARISMA™, which has been successfully applied to a wide variety of elements and materials (2). The analytical method used involves controlling the electronic work function of the bombarded surface by the use of high energy beams of reactive gases.

New work suggests that, as previously postulated, the electrons and ions are also in equilibrium with the surface of the sample which at the point of bombardment appears to attain temperatures of several thousand degrees. This apparent equilibrium is demonstrated, for example in figure 1, by use of a Richardson-Dushman type plot where the observed positive sputtered ion yields of standard samples have been plotted as a function of the temperature of the emitting surface. The slope of the line through the data points, on such a graph, gives the effective electronic work function of the surface of the sample. The effective electronic work functions obtained from these experimental data appear to be in reasonable agreement with accepted values for these materials. The temperatures used in this analysis are those obtained from CARISMA™, which is based on the Saha-Eggert ionization equations. We suspect that the elevated temperatures are related to large decreases in the thermal conductivity of the bombarded region of the sample due to gross lattice damage resulting from the heavy ion bombardment.

The equilibrium model can be employed to provide analyses of molecular species that exist as known entities within the crystal structure of the sample. The equilibrium model states that the dissociation of a molecule at the surface of the sample is controlled by equilibrium reactions and that the concentration of the molecule is directly related to the concentrations of its dissociation products



through the appropriate dissociation constant. We have used this idea to explore the possibility of water analysis in minerals by using the intensity of the sputtered  $H^+$  ion to indicate the concentration of water, as  $OH$ , in the mineral. For example:

$$n_{OH} = n_H \cdot n_O \cdot \frac{1}{K_{OH}}$$

where  $n$  is concentration and  $K_{OH}$  is the dissociation constant of  $OH$ . Our preliminary results of this type of analysis are given in figure 2 where we plot the measured  $H^+$  ion intensity of minerals with known  $OH$  content. The measured  $H^+$  ion intensity is normalized to the measured  $Si^+$  ion intensity and the known silicon content of each sample. The water content of the minerals is taken from the chemical composition of the minerals. A lunar olivine, which is known to represent a dry system, has been used to establish the zero water concentration level. In this approximation it is assumed that the surface temperatures attained during sputtering of the various minerals analyzed are approximately the same and that likewise the oxygen concentrations of the different minerals are also approximately equal. Within these assumptions the maximum errors is approximately 33% and the average error is 13%. Analyses of other gases such as fluorine in minerals and oxygen in metals will also be discussed.

#### REFERENCES

- (1) C.A. Andersen, Third, Fourth, Fifth and Sixth Natl. Electron Microprobe Conf. Chicago 1968; Pasadena 1969; New York 1970; Pittsburgh 1971; J. Mass Spect. and Ion Physics, 2 (1969) 61; 3 (1970) 413; C.A. Andersen and J.R. Hinthorne, Science, 175.
- (2) C.A. Andersen and J.R. Hinthorne, Seventh Natl. Electron Microprobe Conf. San Francisco 1972, Analytical Chemistry, in press.

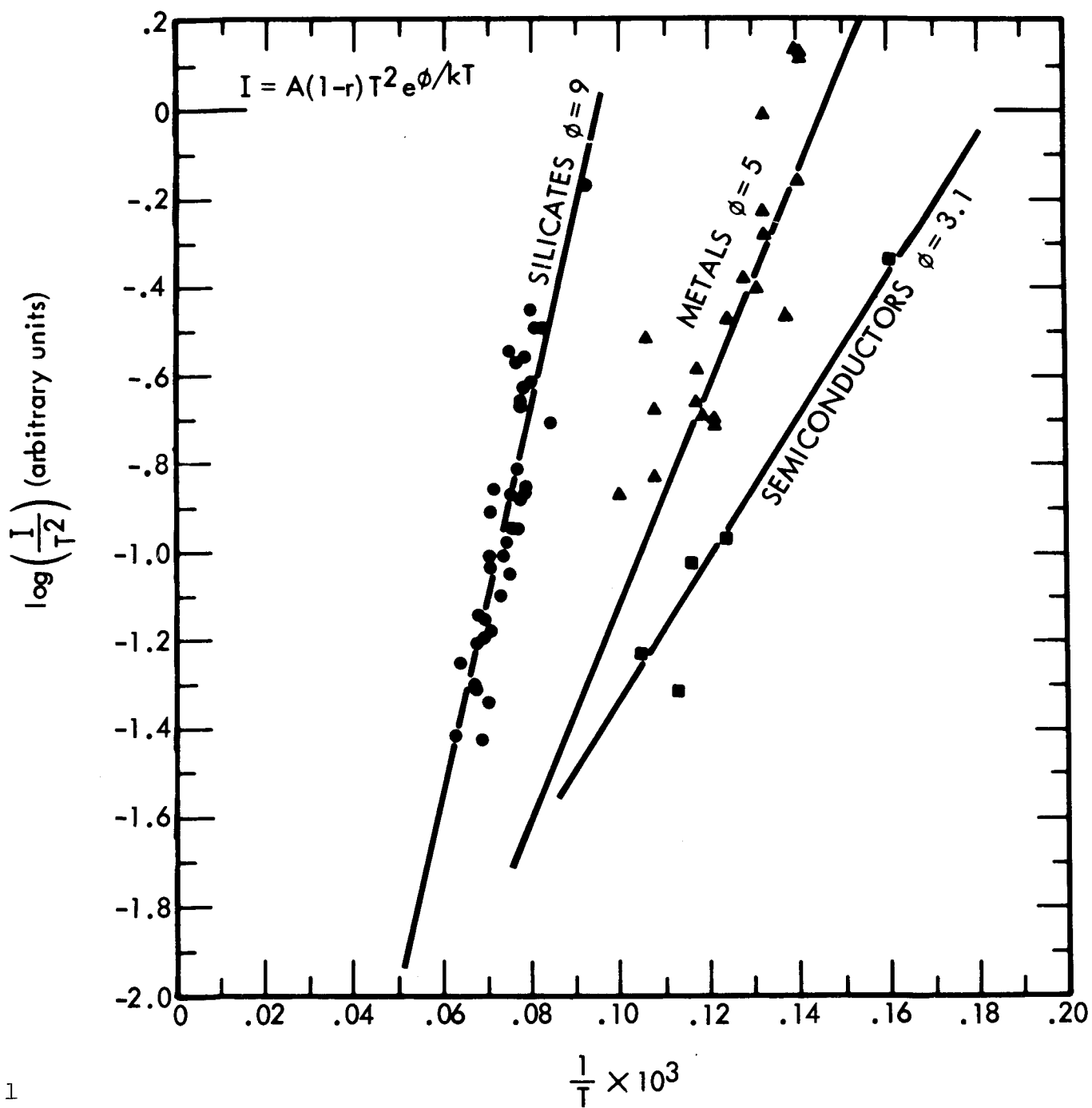


FIGURE 1

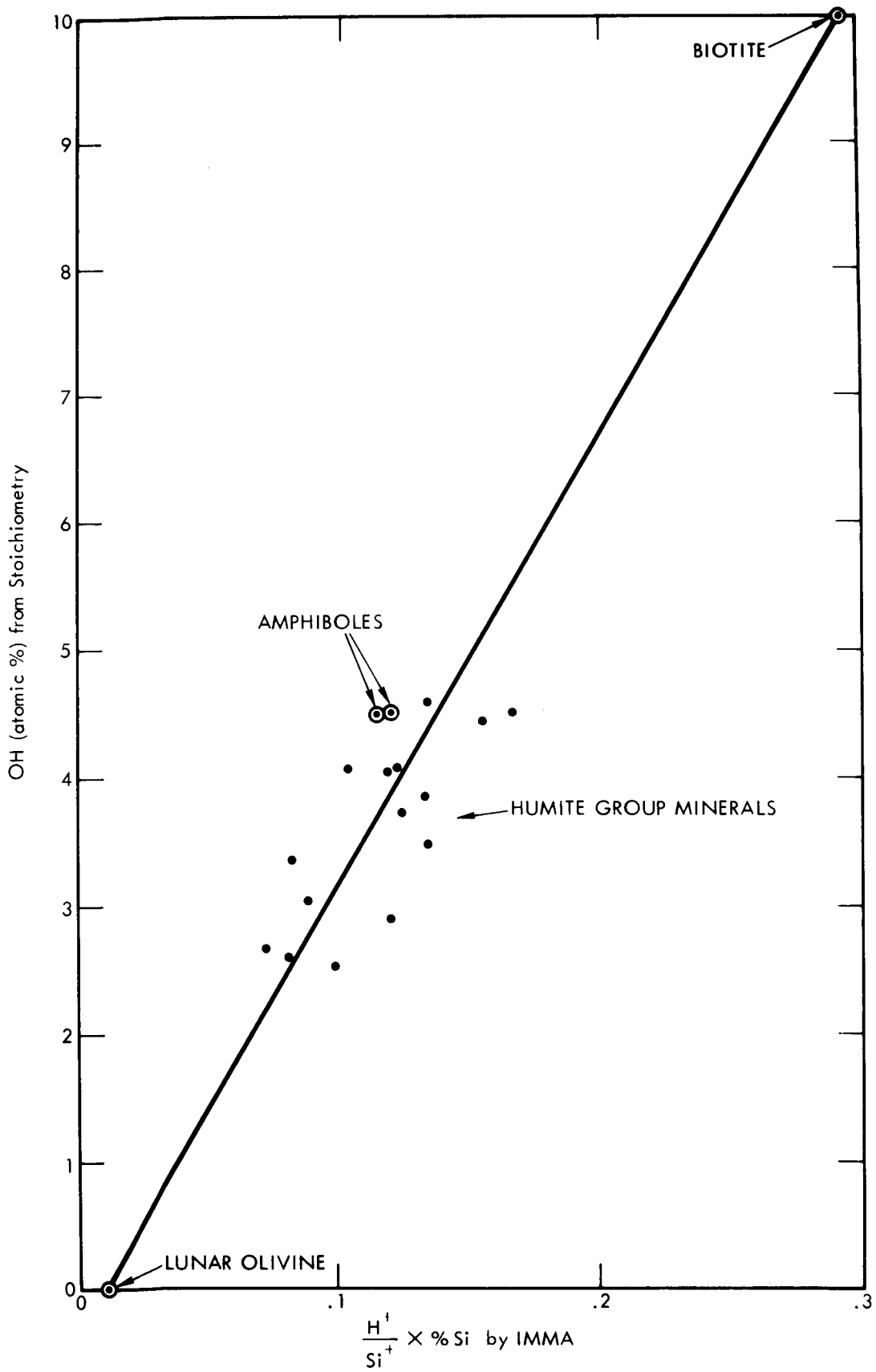


FIGURE 2

Primary Ion Implantation Effects on Depth Profiles  
Obtained by Secondary Ion Mass Spectrometry

R. K. Lewis and B. Autier, Cameca Instruments, Inc., Elmsford, N. Y.  
J. M. Morabito, Bell Telephone Laboratories, Allentown, Pa.  
J. C. C. Tsai, Bell Telephone Laboratories, Reading, Pa.

Secondary ion mass spectrometry (SIMS) has been demonstrated to be a highly effective analytical technique for depth profiling measurements.<sup>1-4</sup> This technique employs energetic primary ion bombardment to sputter away successive surface layers, and the secondary ions released by the collision process are then analyzed with a mass spectrometer. Monitoring a specific ion species and controlling the sputtering process allows variations in chemical concentrations at the trace element level to be measured from a material's surface into its interior. Profiles have been measured with a depth resolution of better than 50 Å using this technique.

Extensive depth profile analyses with the CAMECA IMS 300 have shown that it is possible to reproduce the SIMS depth profiles to better than a few percent if careful attention is given to the primary beam operating conditions. These conditions include ion gun operating voltage and pressures, beam focusing and rastering, and finally location of the beam on the sample.

Two anomalous surface effects have been observed. The first is related to the adsorbed reacted surface oxygen and the second to the primary ion beam implantation range into the analyzed sample. These effects are observed as an anomalous variation in secondary ion yield over the first few hundred angstroms of depth sputtered and can complicate the interpretation of depth profile measurements over this range. These effects have been neglected in the past because the mechanism of secondary ion emission<sup>5</sup> related to depth profiling have not been completely understood.<sup>6</sup> This paper discusses these effects, suggests an explanation of the causes and describes methods of minimizing the problem.

Depth profiles with the two surface effects superimposed are shown in Fig. 1a. O<sup>-</sup> primary ion bombardment of pure silicon has been used and the Si<sup>+</sup> species monitored. The first effect is delineated better in the expanded display shown in Fig. 1b. An enhanced Si<sup>+</sup> yield occurs over the first few angstroms of depth sputtered. This enhancement results from the presence of adsorbed ambient gas on the surface which has reacted with the first few monolayers (chemical emission). The second effect produces a decreased Si<sup>+</sup> signal extending over several hundred angstroms from the surface. This "self-induction" depth range effect is due to the fact that at the initiation of the sputtering process the beginning of the projected range of the primary oxygen implantation occurs at a depth over several hundred angstroms below the surface; consequently, over this range the silicon remains essentially oxygen free, leaving the ion production mechanism principally a kinetic process. The enhancement effect on secondary ion yield due to the presence of reacted oxygen from the primary beam (chemical emission) cannot occur until the sputtering front reaches the beginning of the implanted oxygen distribution. When the sputtering depth reaches the

peak of the oxygen implant distribution, the signal from the measured ion species then reaches a stabilized oxygen enhanced value, and it now accurately follows concentration variations. It is necessary, of course, to achieve this stabilized condition when using any reactive gas for quantitative analysis in SIMS.

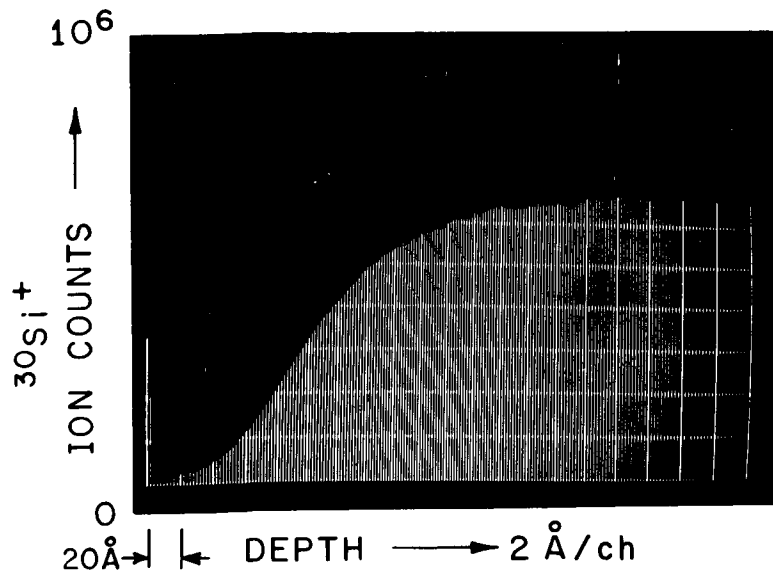
The effect of these anomalous ion yields on a typical depth profile is shown in Fig. 2a. The sample was silicon, ion implanted with arsenic to  $5 \times 10^{15}$  atoms/cm<sup>2</sup> and diffused for 15 minutes at 1050°C. Bombarding with O<sub>2</sub><sup>+</sup> and monitoring AsO<sup>-</sup> offered the best compromise for achieving high detection sensitivity. It is obvious that the "self-induction" depth range effect produces an artifact in the AsO<sup>-</sup> profile measurement when this profile is compared with the <sup>30</sup>Si<sup>-</sup> profile obtained on pure silicon as shown in Fig. 2b. The AsO<sup>-</sup> signal should have started at about  $5 \times 10^4$  counts at the surface and continued at about this level over the next 400 Å.

The validity of the primary ion implanted range assumption used to describe the mechanism of the "self induction" depth range effect has been substantiated by measuring the in-depth distribution of the primary oxygen ion beam. This measurement was made using both SIMS and Auger spectroscopy employing argon bombardment. The SIMS profiles are shown in Fig. 3. This oxygen distribution profile is consistent with the assumption of an initial gaussian distribution with subsequent sputtering. A gaussian distribution would be predicted by LSS theory<sup>7</sup> for static (without sputtering) ion implantation of oxygen into silicon.

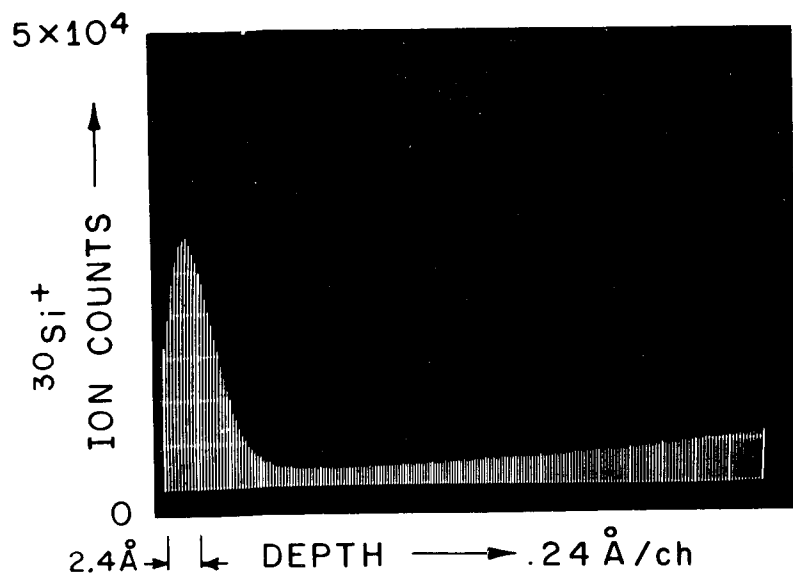
We have shown that a controlled oxygen stream blowing across the surface of the sample eliminates the "self-induction" depth range effect. The effect of this high ambient oxygen pressure on the secondary ion yield has been described by Slodzian and Hennequin.<sup>8</sup>

#### REFERENCES

1. C.A.Evans, jr., Anal.Chem., Vol. 44, No.13, pp.72A-80A, 1972.
2. J.M.Morabito and J.C.C. Tsai, Sur.Sci., Vol.33, pp.422-426, 1972.
3. J.M.Morabito and R.K.Lewis, Anal.Chem., Vol. 45, No.5, pp 869-880, 1973.
4. J.C.C.Tsai, J.M. Morabito, R.K.Lewis, Proc. of 3rd Int'l Conf. on Ion Implantation, New York, Dec. 1972, to be published.
5. G.Blaise and G.Slodzian, Le Journal de Physique, Vol.31, pp.1-29, 1970.
6. R.K.Lewis, Pittsburgh Conf. on Anal.Chem. and Applied Spectroscopy, Cleveland, Ohio, paper 170, 1973.
7. L. Lindhard, M. Scharff and H. Schiott, Mat. Pys. Medd. Oan.Vid.Selsk 33, (1963) 1.
8. G. Slodzian and J. F. Hennequin, C.R. Acad. Sci., Paris, 263B, p. 1246, 1968.



1 a.

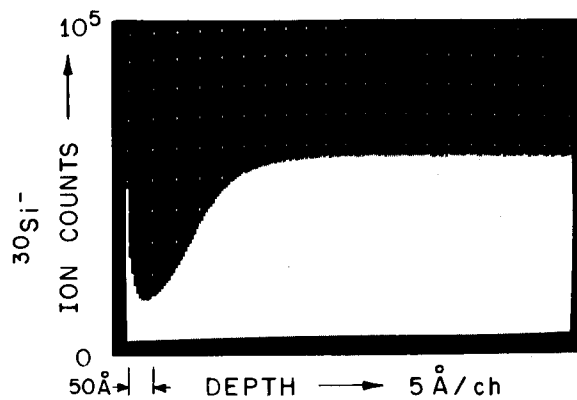


$P : 2 \times 10^{-7} \text{ torr}$   
 $\dot{Z} : .24 \text{ \AA/s}$

1 b.

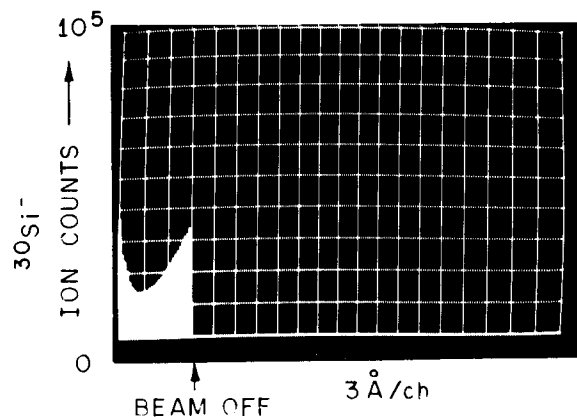
**FIG. 1** SILICON PROFILES OF BULK GROWN SILICON  
 a. PROFILE RANGE 0 -  $400 \text{ \AA}$   
 b. PROFILE RANGE 0 -  $48 \text{ \AA}$   
 PRIMARY ION,  $^{16}\text{O}^-$  AT  $14.5 \text{ keV}$

5D



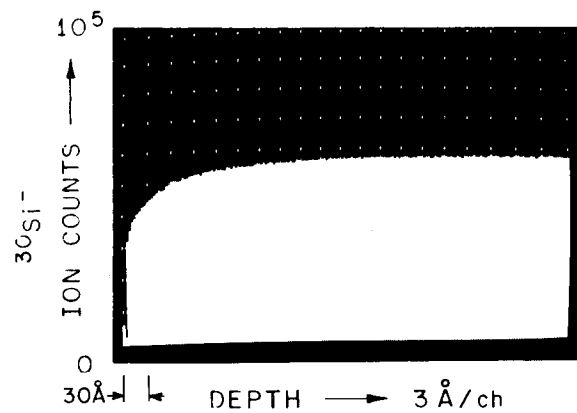
PROFILE FROM THE  
SURFACE IN NEW AREA

2 a.



PROFILE FROM THE  
SURFACE IN NEW AREA

2 b.



PROFILE CONTINUED  
IN CRATER ABOVE AFTER  
EXPOSURE TO AIR

2 c.

P :  $2 \times 10^{-7}$  torr  
Z : 80 Å/s

FIG. 2. EFFECT OF INTERRUPTION OF MEASUREMENTS  
ON SILICON PROFILE

PRIMARY ION  $^{16}\text{O}_2^+$  AT 14.5 keV

SPUTTERING RATE 80 Å/s

a. INITIAL MEASUREMENT

b. INTERRUPTED MEASUREMENT IN A  
NEW CRATER

c. CONTINUATION OF 3b.

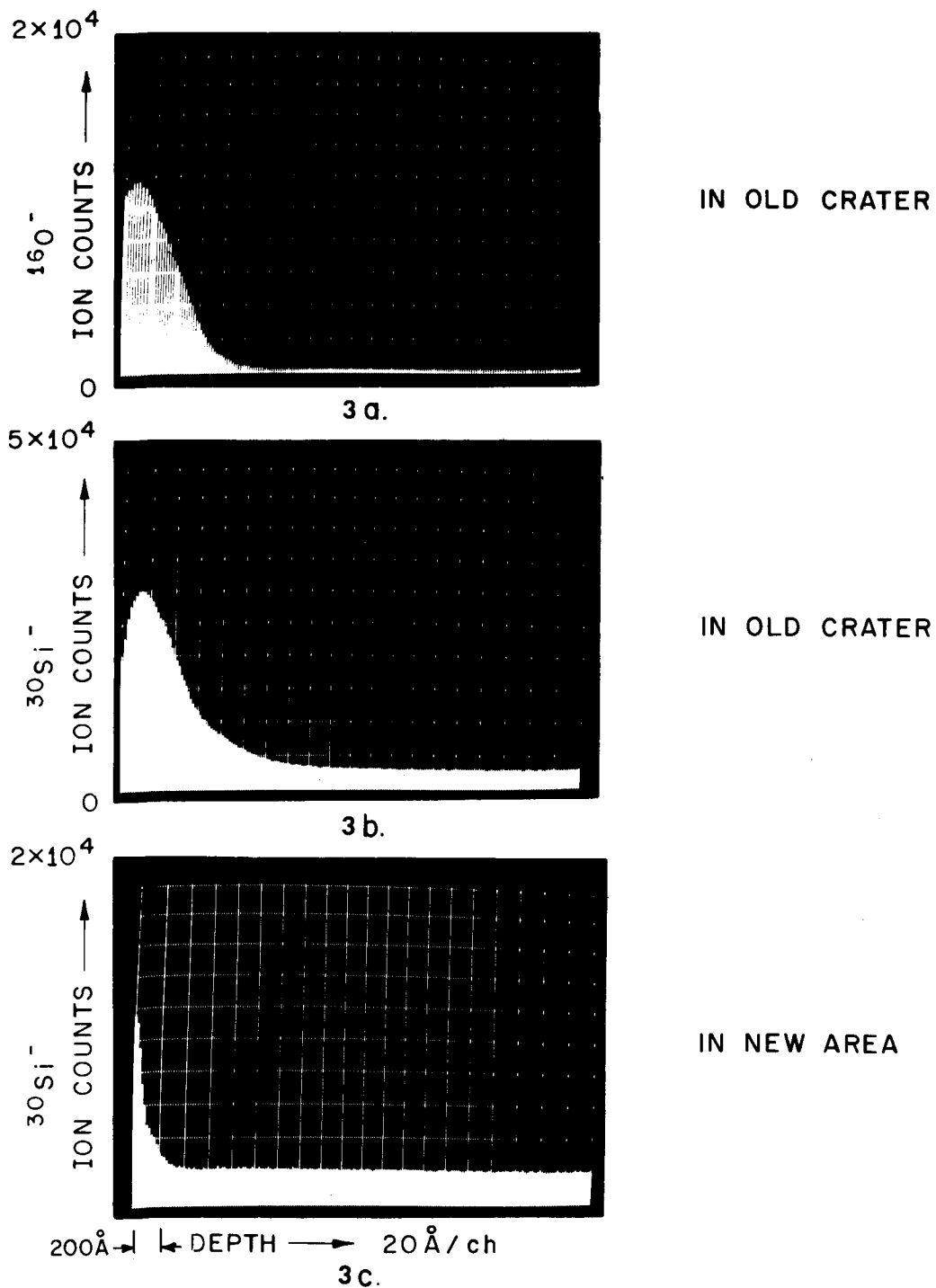


FIG. 3. COMPARISON OF OXYGEN AND SILICON SIGNALS  
 IN A PREVIOUSLY MEASURED CRATER  
 (3a, 3b) AND A NEW CRATER (3c)  
 PRIMARY ION ARGON AT 14.5 keV  
 SPUTTERING RATE 100 Å/s



APPLICATION OF THE ION MICROPROBE  
TO SEMICONDUCTOR PROBLEMS

J. W. Colby  
Bell Laboratories  
555 Union Boulevard  
Allentown, Pennsylvania 18103

Through the pioneering work of Andersen<sup>1-3</sup>, the ion microprobe has progressed from a qualitative imaging ion microscope<sup>4</sup>, to a quantitative analytical tool. Through the use of a reactive gas as a primary ion source, and the use of a computer program CARISMA<sup>3</sup>, it has been demonstrated by Anderson and Hinthorne<sup>3</sup> that quantitative analysis is quite possible, with good accuracy on many systems. Whereas the model is not perfect, that is it may not work universally well in all systems, it is adequate nevertheless, and is somewhat reminiscent of the first correction scheme proposed by Castaing<sup>5</sup> for the electron probe. It too gave excellent results on some systems, and failed miserably on others.

However, when the volume of data to be reduced is large as in an in-depth profile the use of such a program becomes impractical from a cost standpoint, and one usually employs an internal standard approach<sup>6</sup>, as described below. However, CARISMA can be utilized to calculate in effect, a constant multiplier for a given system, such that data reduction then becomes trivial. We have had numerous, uniformly-doped silicon samples analyzed on the ARL ion microprobe, and the concentrations determined through the use of CARISMA. These same samples have been analyzed by various other techniques, primarily by electrical resistivity, Hall measurements, and electron microprobe. The agreement has usually been excellent. These same samples have been analyzed on the Cameca ion microscope and through the use of standards as described below, concentrations were determined which are also in excellent agreement with the CARISMA results. Thus it may be concluded that quantitative ion probe analyses are possible, at least as far as doped silicon is concerned, and that both instruments and techniques yield comparable results, providing suitable standards are available. This may not be the case when analyzing alloys, or diffusion couples, where concentration may vary over a much larger concentration range. In these cases it may be necessary to use a correction model such as CARISMA. There are also significant instrumental differences, which will be discussed in more detail.

When analyzing silicon systems, the secondary ion intensity of the analyte is ratioed to the secondary ion intensity of the silicon matrix. It is found in practice, that this ratio is linearly proportional to concentration, and has a slope of unity, as shown in Figure 1. Thus a single multiplier may be determined, which is independent of the ion microprobe operating conditions, for all practical purposes. Whereas

the constants obtained on the ARL microprobe differ from those obtained on the Cameca ion microscope, due to differences in the acceptance energy of the two mass spectrometers, the same approach may be utilized with either machine. The use of a correction scheme such as that proposed first by Werner<sup>7</sup>, and subsequently by Morabito and Lewis<sup>8</sup> essentially reduces to the internal standard method described above, since the "absolute ionization yields" obtained by them are matrix dependent, and must be modified by a "suitable factor."

It may be shown that sputtering rate, other things being equal, is directly proportional to the effective current density, and is given by<sup>9</sup>

$$R = \frac{1.04 J A S}{\rho}$$

where

R = sputtering rate (angstroms/second)

J = current density (milliamps/sq cm)

A = atomic weight of matrix

$\rho$  = density (g/cc)

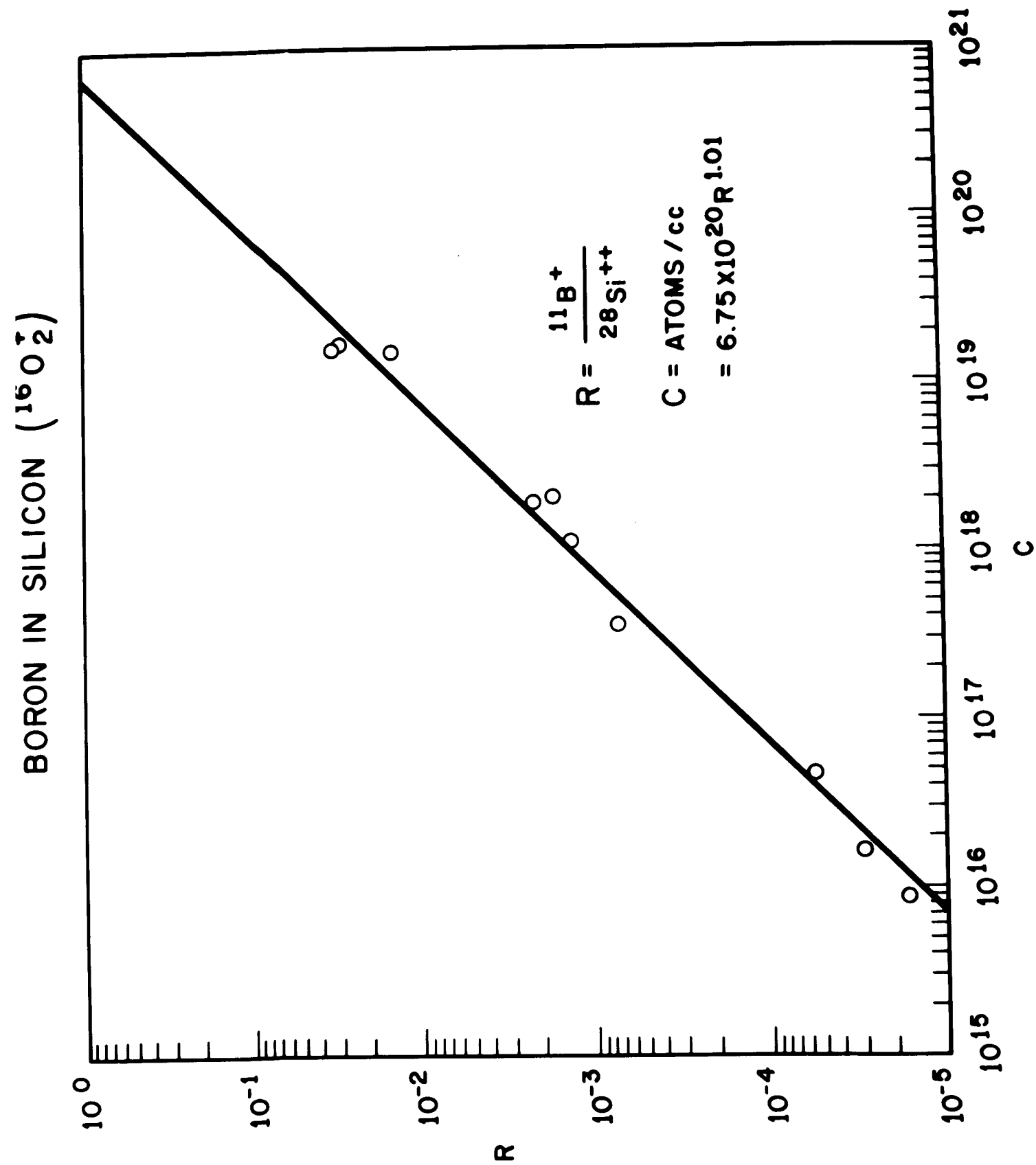
and S = sputtering yield (atoms/ion)

The sputtering yield varies with accelerating potential, angle of incidence of the primary beam and primary ion species for a given material. These variations may be easily determined for an unknown matrix material, and some are available in the literature.<sup>10</sup>

The ion microprobe and ion microscope have both been used effectively to determine variations in the segregation coefficient for silicon crystals having different orientation<sup>11</sup>, for in depth profiles of ion implanted species<sup>12</sup>, and for analysis of micron sized defects.<sup>13</sup> Several examples will be given showing the utility of the ion microprobe and ion microscope in these types of applications.

6c  
REFERENCES

1. C. A. Andersen, J. Mass Spectrom & Ion Physics, 2, p. 61 (1969).
2. C. A. Andersen, J. Mass Spectrom & Ion Physics, 3, p. 412 (1970).
3. C. A. Andersen and J. R. Hinthorne, Science, 175, p. 853 (1972).
4. R. Castaing and G. Slodzian, J. Micros. (Paris), 1, p. 395, (1962).
5. R. Castaing, PhD Thesis, Univ. of Paris, 1951.
6. J. W. Colby, SAS Speaker Tour, 1972.
7. H. W. Werner, Develop Appl. Spectros., 7A, p. 239, (1969).
8. J. M. Morabito and R. K. Lewis, Anal. Chem, 45, p. 869 (1973).
9. J. W. Colby, Workshop on SEM, EMP, AES, & IMMA, Surface Reliability Physics Conf., April 1973, to be published.
10. G. Carter and J. Colligon, Ion Bombardment of Solids, Elscuier, (1968).
11. J. W. Colby and L. E. Katz, to be published.
12. J. W. Colby, P. Miller, and A. D. Bridges, to be published.
13. L. E. Katz and J. W. Colby, to be published.



Reduction of Spectral Interferences in Ion Probe Mass Spectrometry\*

by

D. K. Bakale, B. N. Colby, C. A. Evans, Jr., and J. B. Woodhouse

Materials Research Laboratory

University of Illinois, Urbana, Illinois 61801

Characterization of a material using ion probe mass spectrometry is accomplished by bombarding a sample with 1-20 KeV primary ions and by mass analysis of the resultant sputtered secondary ions. In addition to the analytically important singly-charged monoatomic ions, there are several types of ions produced by the bombardment process which can result in spectral interferences and can dramatically complicate the qualitative evaluation and quantitative analysis of a sample. This discussion will consider five interfering ion types and instrumental operating modes which can be employed to reduce them. In particular we will consider the role of high mass spectral resolution in separating the analytically important monoatomic elemental lines from the interference lines in a secondary ion mass spectrum.

Types of Spectral Interferences

Ion bombardment produces multiply-charged positive ions of the elements present. However, doubly-charged ions are generally only  $10^{-3}$  of the intensity of the singly-charged species (1) and, consequently, do not usually present a significant interference problem. The first significant source of interference results from hydrocarbon ions and oxygen-containing hydrocarbon ions. Since hydrocarbons can be easily introduced during sample preparation or formed from interaction of a clean sample surface with residual vacuum species, they are common spectral contaminants; however, a mass resolution of approximately 1000 is generally sufficient to separate these peaks from the peaks of analytical interest.

Three other sources of secondary ions--hydrides, polyatomic ions resulting from sample interactions with the primary beam, and polyatomic combinations of the various elemental sample constituents including self-polymers of the matrix--present a major source of spectral complexity. Hydrogen is a common impurity in metals and in the residual vacuum of most mass spectrometers. Hydride formation poses a special problem when analyzing for a low intensity ion which is one atomic mass unit higher than a very intense peak such as in the analysis of small amounts of manganese in iron. Spectral interferences related to the primary ion beam arise from the formation of oxides or nitrides when bombarding samples with oxygen or nitrogen primary ions. This is illustrated by the analysis of As in Si or Co in Al when using oxygen primary ions since the species  $\text{Si}_2\text{O}^+$  and  $\text{AlO}_2^+$  have the same nominal masses as As and Co in these systems.

---

\* This research was supported in part by the National Science Foundation Grants GH-33634 and GP-33273 and U. S. Atomic Energy Commission under Contract AT(11-1)-1198.

The extent of the last type of interference is related to matrix complexity. In a multicomponent sample such as a mineral or a biological specimen, the possible polyatomic ions resulting from combinations of matrix elements is large. In these complex matrices, the a priori prediction of all potential interferences is difficult. Thus, the problem of determining that the analytical line does not contain contributions from molecular ions becomes acute.

### Instrumental Parameters

There are several instrumental operating modes which help to reduce or remove the spectral interferences.

1. The "tail" of the initial kinetic energy distribution of atomic ions extends to a much higher energy than that of the molecular ions (2). By using an "energy window" to discriminate against lower energy ions, the ratio of atomic to molecular ions can be increased and, hence, signal purity improved (2,3,4). 2. Alteration of the chemical nature of the primary ion beam can reduce molecular interferences which result from interactions with the primary ion beam. 3. For some analytical situations, a change in relative ion yields and ion types which results from switching to negative secondary ion mass analysis may solve the interference problem.

There are, however, innumerable spectral interferences which will defy the use of the techniques discussed above. Thus, the analyst turns to a classic spectroscopic method to reduce interferences, higher spectral resolution.

### High Resolution Ion Probe Mass Spectrometry

The utility of high mass resolution in interpreting the secondary ion spectra of complex samples is illustrated by the mass 43 portion of the secondary ion spectrum from oxygen ion bombardment of the mineral fluorapatite [ $3\text{Ca}_3(\text{PO}_4)_2 \cdot \text{Ca F}_2$ ] as exemplified in Figure 1. The three mass scans shown at  $m/e = 43$  are at nominal (50% valley definition) resolutions of 300, 1000, and 3000, respectively. What appeared to be one major peak with a high mass shoulder at 300 resolution is shown to be much more complex at 3000 resolution. The middle spectrum at 1000 resolution shows separation of the higher-mass hydrocarbon peak from the other components. A resolution of approximately 1000 is often termed "hydrocarbon resolution." At 3000 resolution the nominal mass 43 line is shown to actually contain six different ion species.

The assignment of exact masses to within a few millimass units (0.001 amu  $\equiv$  1 millimass unit) on the basis of peak position is a widely used technique in high mass resolution studies of organic compounds. In order to assign the exact mass of an unknown peak on a photoplate, it is necessary to know the identity of two other peaks (preferably bracketing the unknown) and to relate the positions of all three peaks to an arbitrary reference point. If  $M$ ,  $M_a$ , and  $M_b$  refer to the masses of the unknown and two known peaks, respectively, and  $X$ ,  $X_a$ , and  $X_b$  are their distances from an arbitrary reference point, the exact mass of the unknown is calculated as follows:

$$M = \left[ \frac{\sqrt{M_b} - \sqrt{M_a}}{X_b - X_a} \left[ \frac{X_b \sqrt{M_a} - X_a \sqrt{M_b}}{\sqrt{M_b} - \sqrt{M_a}} + X \right] \right]^2$$

This exact mass measurement technique was used to identify the mass 42 and mass 43 peaks of the fluorapatite sample using the  $^{42}\text{Ca}^+$  and the  $^{43}\text{Ca}^+$  as the known masses. The process of choosing known masses relies on whatever information is available concerning the characterization of the sample in question. In many cases the process is one of trial and error in that if a wrong reference assignment is made, the resulting set of calculated exact masses for the unknown peaks will be unassignable to any set of possible ions. Figure 2 illustrates the assignments which were made for the peaks at 42 and 43 of fluorapatite. The numbers in parenthesis are the differences in millimass units between the experimentally obtained masses and the known exact masses of the assigned ions. It can be seen that in this sample there are several examples of hydride formation, oxide formation, inter-element molecular ion formation, and hydrocarbon interferences.

Figure 3 provides an excellent illustration of the problems caused by molecular interferences in the analysis of trace metals in complex samples. The densitometer trace of masses 51, 52, 55, and 56 are shown with exact mass assignments for all peaks from a sample of an experimental ceramic bone implant from a dog's leg. Without the aid of high resolution, the conclusive determination of the presence or absence of V, Cr, Mn, and Fe would have been impossible. If, indeed, the singlet peaks which would have been obtained at a resolution of 300 were mistakenly assigned to these elements without realization of the presence of interfering ions, the estimates of their concentrations would be high by factors of 3 to 8.

Additional examples where high resolution is the only or best answer to a particular problem of mass spectral interference will be presented.

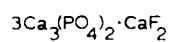
### Conclusions

Unfortunately, the use of high resolution is not without cost to the analyst since increased resolution is accompanied by a decrease in spectrometer transmission and, hence, sensitivity. The particular analytical problem at hand will dictate the extent to which high resolution or, perhaps, some other interference-reducing technique or a combination of techniques is the answer. The examples we have shown have demonstrated that there will be numerous situations in which there is a definite need for higher resolution to perform trace analysis in complex materials. It is important to remember that the ability to provide exact mass assignments and the resulting qualitative peak identifications is a valuable aspect of high resolution. In addition, molecular ions, once characterized by exact mass measurement techniques, may override their nuisance character in some cases by providing additional information about the composition of the sample and its interactions with the bombarding ion species.

### References

1. B. N. Colby and C. A. Evans, Jr., "Spectral Interferences in Secondary Ion Mass Spectrometry", accepted for publication by Applied Spectroscopy.
2. R. F. K. Herzog, V. P. Poschenrieder, and F. A. Satkiewicz, GCA Corp., Bedford, Mass., for NASA, NASR-CR-89326(N67-39205) (1967).
3. J.-M. Rouberol, Private Communication, Paris, France (1972).
4. R. K. Lewis, Private Communication, Elmsford, New York (1972).

## FLUORAPATITE



Mass 43

Fig. 1

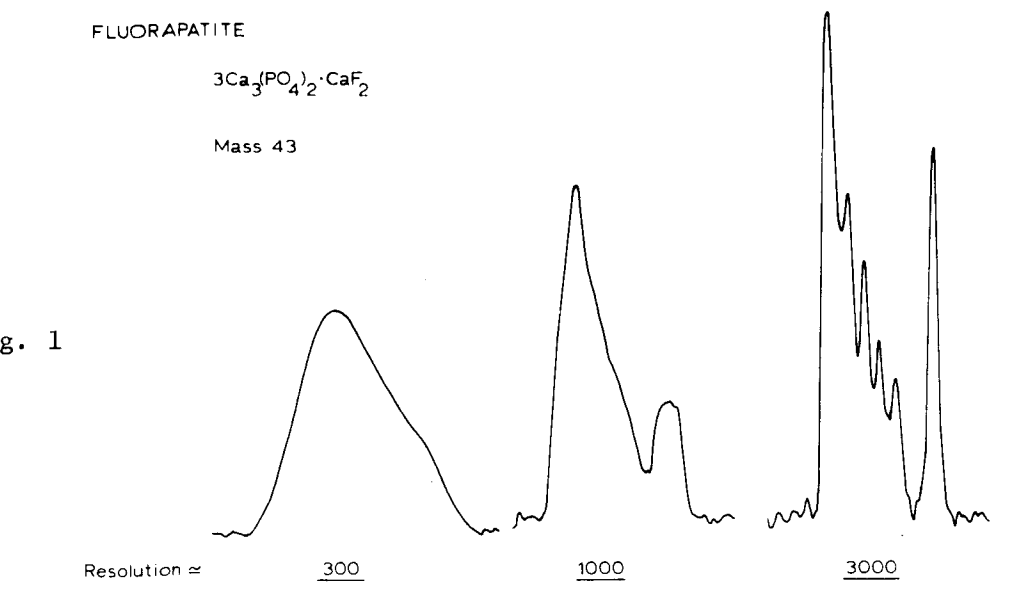
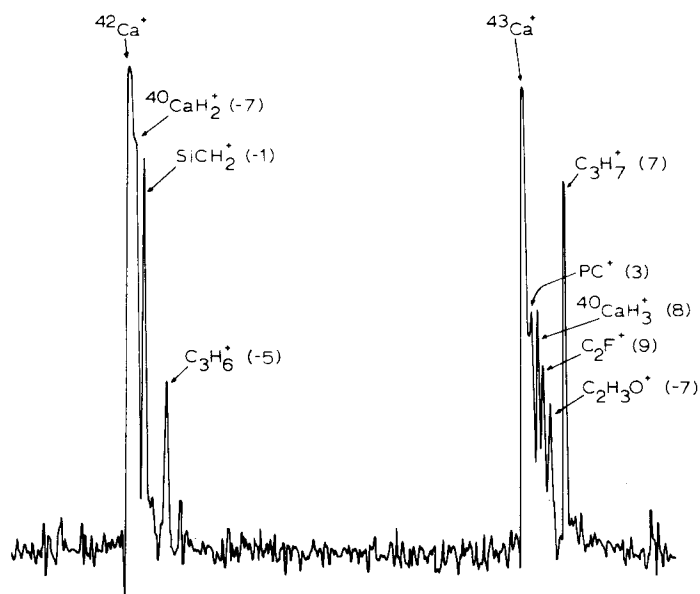
FLUORAPATITE  $3\text{Ca}_3(\text{PO}_4)_2 \cdot \text{CaF}_2$ 

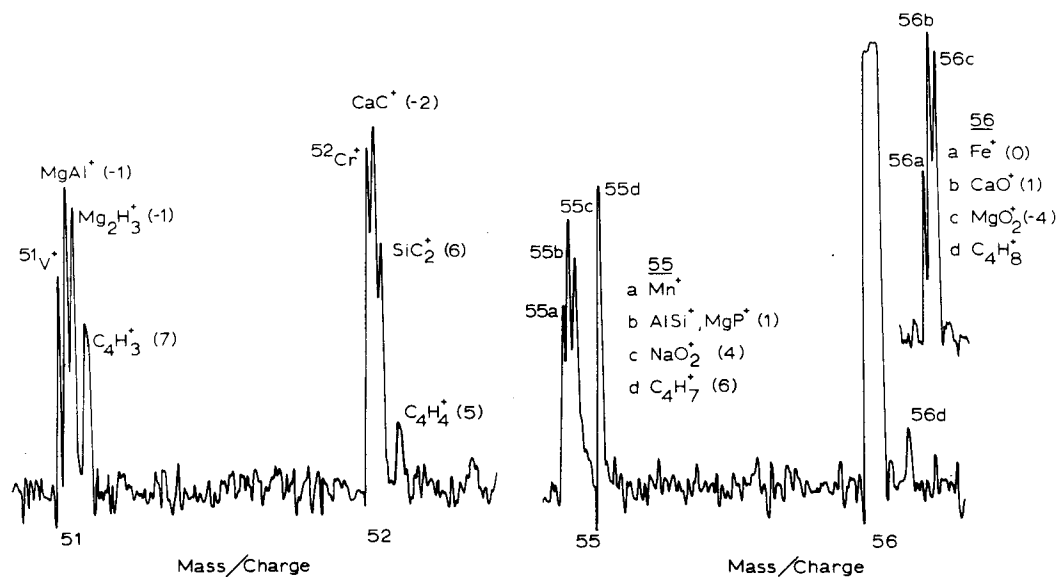
Fig. 2



## CERAMIC BONE IMPLANT

## REACTION ZONE

Fig. 3





AN INVESTIGATION OF THREE-COMPONENT DIFFUSION  
(PLATINUM, PHOSPHORUS, SILICON) BY  
SPUTTERING-AUGER AND SECONDARY ION EMISSION TECHNIQUES

by

J. M. Morabito and M. J. Rand  
Bell Telephone Laboratories, Incorporated  
Allentown, Pennsylvania 18103

Various combinations of thin metal films are used in silicon integrated circuit technology for producing silicide contacts to the various silicon areas, and for subsequent application of metal conductor patterns. Some useful metals, e.g., Pt, W, Ta, are difficult to filament-evaporate, and are usually deposited by sputtering or electron-beam evaporation. These energetic processes can cause radiation damage to thin film insulators, and in the case of the gate insulation of field-effect devices the resulting electrical instabilities may be unacceptably severe.

To avoid this effect in the case of Pt, a pyrolytic deposition from the volatile compound  $\text{Pt}(\text{PF}_3)_4$  has been developed.<sup>1</sup> Adherent, bright films of 300 to 2000Å of Pt are readily produced. However, electron microprobe analyses have detected residual phosphorus in the Pt and in the PtSi produced by interdiffusion with the Si substrate. The location and distribution of this third component in the Pt-Si system was of concern, since concentration at the interfaces (the surface, the Pt-Si interface, the PtSi-Si interface) might greatly influence the mechanical, chemical, and electrical properties of the system. Typical areas

of concern include:

- 1) Adherence of the CVD Pt, and the adherence of other films to the CVD Pt.
- 2) Surface mobility of Pt atoms; recrystallization upon heating of the Pt; possibility of a liquid phase appearing locally (there is a Pt-P eutectic at 588°C).
- 3) Possibility of changing the doping level of the Si substrate immediately adjacent to the PtSi layer, with attendant changes in the electrical characteristics of the silicide contacts.
- 4) Effects on the chemical etching resistance of PtSi.
- 5) Rate of interdiffusion between Pt, Si and other metals.

Figures 1-3 show the Pt, P, and Si profiles obtained on the as-deposited Pt on Si and the diffused PtSi by the ion sputtering-Auger<sup>2</sup> and secondary ion emission<sup>3</sup> techniques. The latter is more sensitive,<sup>4,5</sup> and one of the objectives of this study was to compare the results of the two methods. Fig. 1 shows the ion sputtering-Auger profiles in the as-deposited Pt. All the phosphorus appears to be within 60Å of the film surface, with a corresponding Pt deficiency. The Pt-Si interdiffusion zone was ~ 400Å even though the deposition temperature was only 225°C.

The secondary ion profiles in the as-deposited Pt (Fig. 2) were complicated by chemical enhancement effects which are known to influence profile shape.<sup>6</sup> Chemical enhancement, mass interference, and primary ion bombardment effects<sup>7</sup> are of particular importance at the surface and interface. Phosphorus does, however, appear to be present throughout the film, and in

higher amounts at the Si interface. The amount of this phosphorus was below the detectability limit ( $\sim 0.5$  at %) by Auger analysis (c.f. Fig. 1). The  $^{195}\text{Pt}^+$  secondary ion yield was enhanced by the presence of Si and P (Fig. 2). The rather large phosphorus signal increase at the interface could be attributed in part to a chemical enhancement effect.

The ion sputtering-Auger profiles of phosphorus in as-deposited and sintered ( $450^\circ\text{C}$ ,  $625^\circ\text{C}$ ) CVD Pt are shown in Fig. 3. Sintering resulted in the migration of phosphorus to the surface. The secondary ion profiles of phosphorus in sintered CVD Pt films were in agreement with this result.

#### REFERENCES

1. M. J. Rand, J. Electrochem. Soc., in press, May, 1973.
2. J. M. Morabito, Tenth Natl. Meeting of Soc. of Applied Spectroscopy, St. Louis, Mo., Oct. 1971; P. W. Palmberg, Fifth Intl. Vacuum Congr., Boston, Mass., Oct. 1971.
3. R. Castaing and G. Slodzian, J. Microscopie 1 (1962) 395.
4. J. M. Morabito and J. C. Tsai, Sur. Sci., 33 (1972) 422-426.
5. J. M. Morabito and R. K. Lewis, Anal. Chem. (April Issue, 1973).
6. J. C. Tsai, J. M. Morabito, R. K. Lewis, Proc. of 3rd Intl. Conf. on Ion Implantation, New York, Dec. 1972, to be published.

FIG. 1. ION-SPUTTERING-AUGER PROFILES  
OF CVD Pt ON Si AS DEPOSITED, 225°

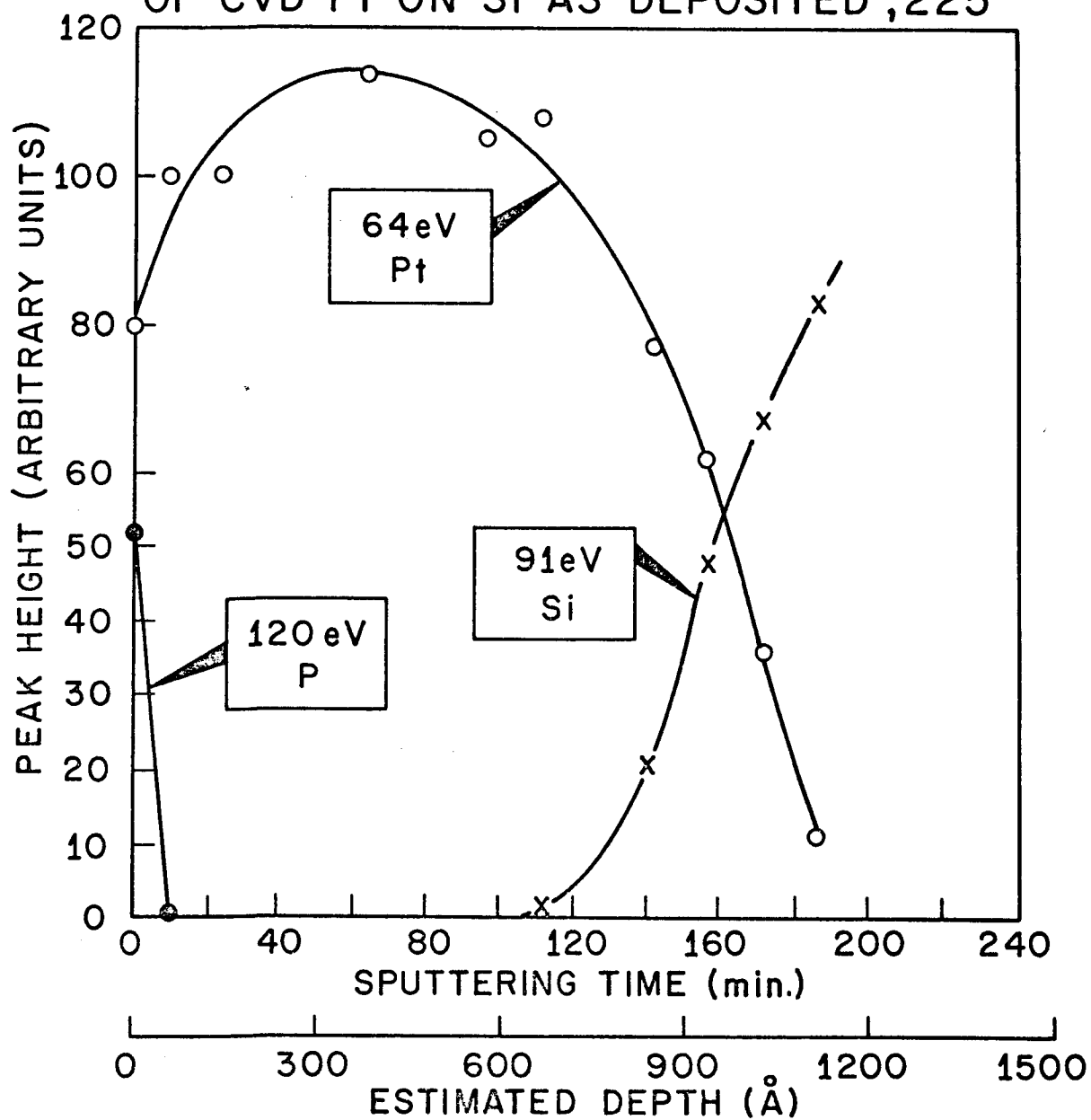


FIG. 2. SECONDARY ION PROFILES  
OF CVD Pt ON Si AS DEPOSITED,  $225^\circ$

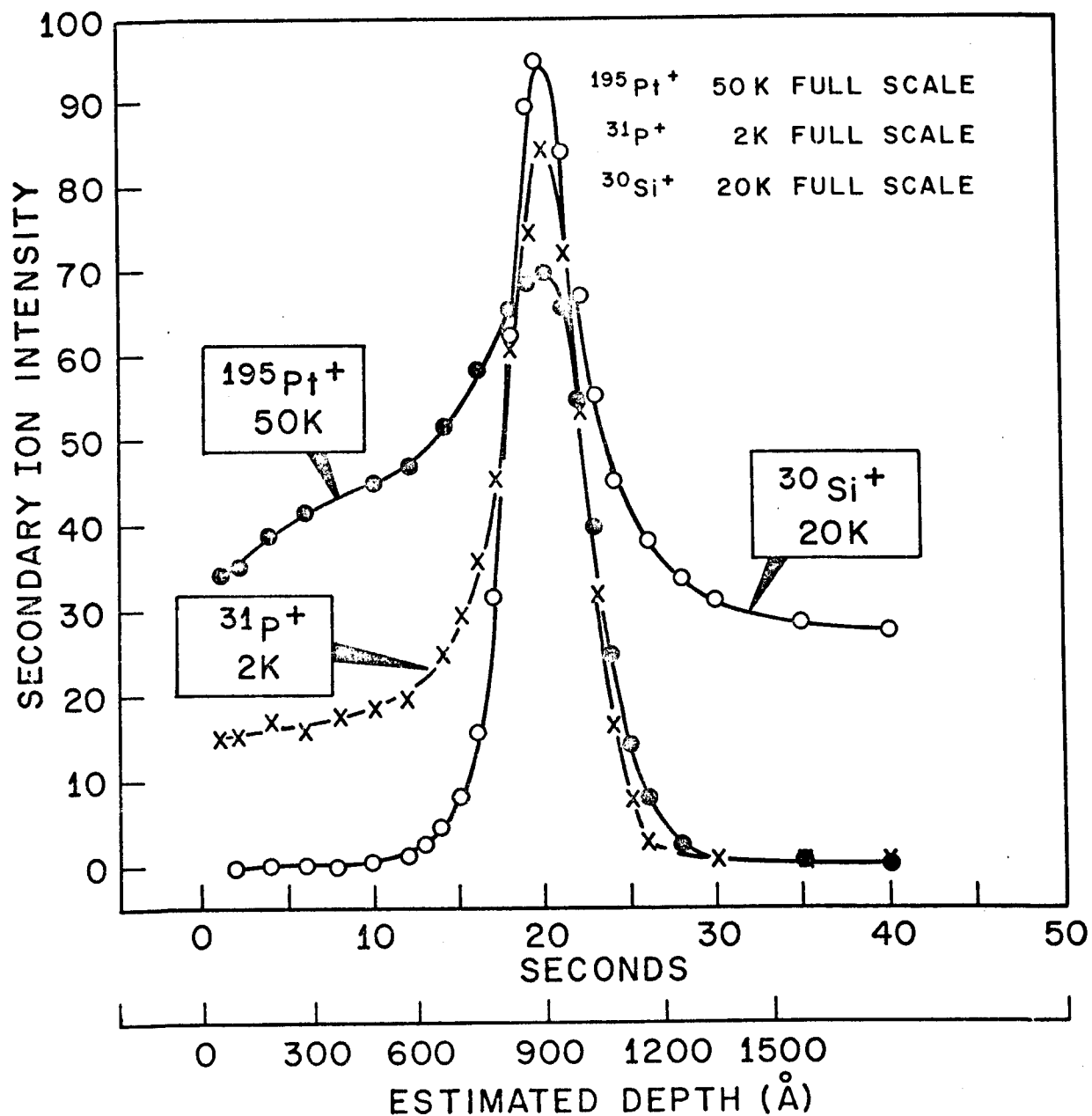
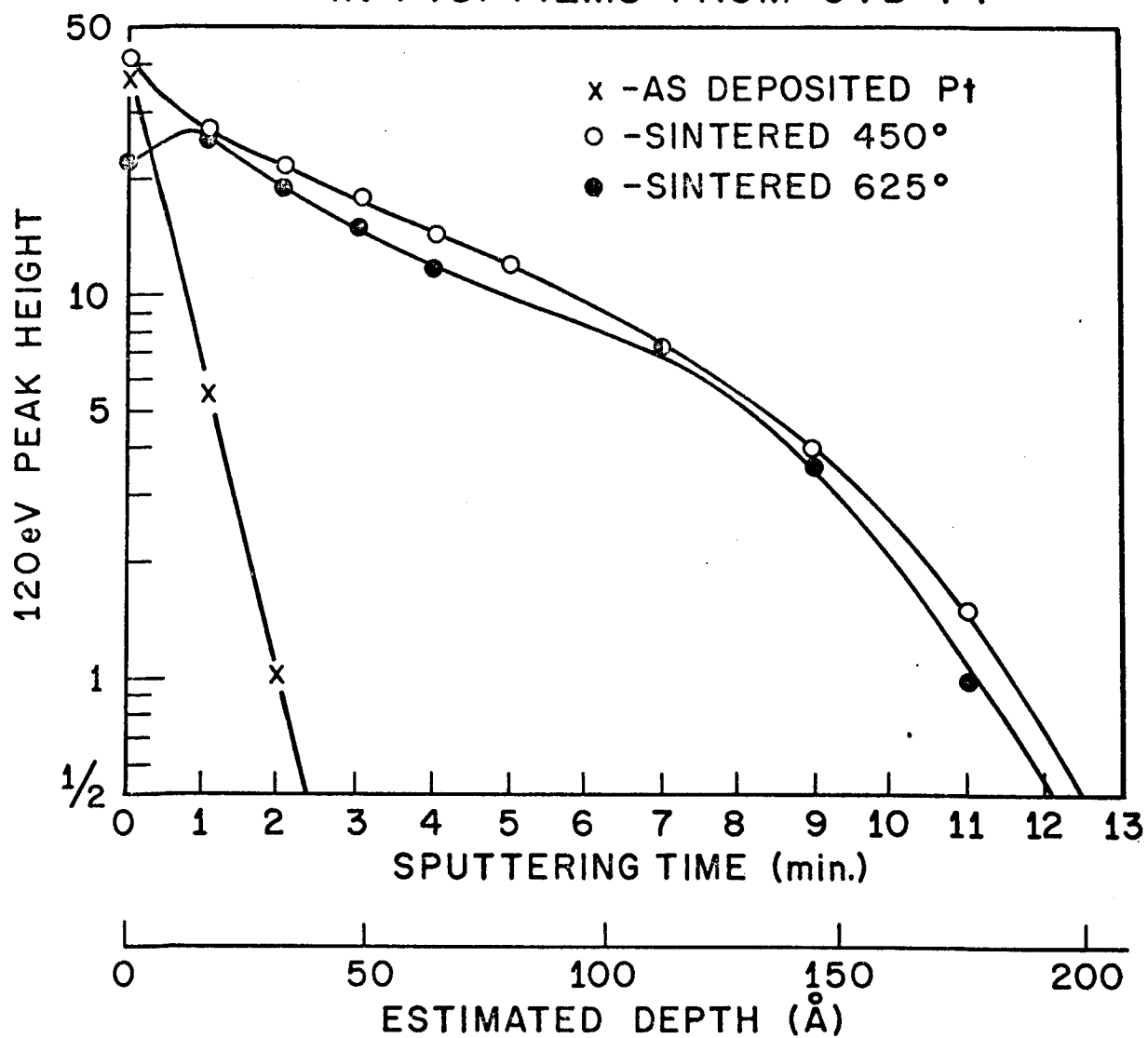


FIG. 3. ION SPUTTERING-AUGER PHOSPHORUS PROFILES  
IN PtSi FILMS FROM CVD Pt



## GEOLOGICAL APPLICATIONS OF THE ION MICROPROBE MASS ANALYZER

J. R. Hinthorne

and

C. A. Andersen

Hasler Research Center  
Applied Research Laboratories  
95 La Patera Lane  
Goleta, California 93017

The ion microprobe mass analyzer has been applied to a wide variety of geochemical problems. The applications generally fall into two groups: high sensitivity elemental microanalysis, and isotopic microanalysis.

A study was made of the amphibole mineral group to determine the distribution of trace elements between coexisting calcium-poor amphiboles of monoclinic and orthorhombic symmetry (1). Ion microprobe analyses were performed in situ using standard polished thin sections. Consistent partition coefficients between cummingtonite-gedrite mineral pairs and cummingtonite-anthophyllite mineral pairs were determined for several elements at concentrations ranging from 1 percent to 1 ppma. The elements studied include Li, B, F, Na, P, K, Ca, Ti, V, Cr, Mn, Co, Sr and Y. Figure 1 shows the concentrations and distribution coefficients for Li between various amphibole species. Two samples with a calcium-rich amphibole (hornblende) are shown for comparison.

The substitution of boron for silicon in silicate minerals is widely observed in bulk mineral analyses, but quantitative microanalysis for boron has been found to be difficult or impossible with the electron probe at minor and trace concentrations levels. A suite of humite group minerals, previously studied with the electron microprobe (2), were found by ion microprobe analysis to have significant amounts of boron. The electron probe analyses of the same mineral grains had suggested a slight silicon deficiency in some samples (up to 2% of the Si contents). Figure 2 shows the inverse relationship found between the electron probe (EMX) silicon values and the ion microprobe boron values indicating a direct substitution of boron in the silicon lattice sites. Small amounts of aluminum (about 100 ppma) were also found with the ion microprobe and since Al may also substitute for Si, the B+Al values are also compared to Si in figure 2. The average deviation of the measured silicon content from the theoretical boron-for-silicon substitution line is 0.64% and the maximum deviation is 1.8%. The good correlation indicates that most of the measured silicon deficiencies are due to real differences in

silicon contents rather than analytical errors in the electron probe analyses. The precision of the ion microprobe boron analyses is suggested by the measured peak/background ratio of about 100 for the  $^{11}\text{B}^+$  isotope in a sample containing 100 ppma of boron.

Anion determinations are important in many geochemical studies. Applications will be presented showing the utility of the ion microprobe in the quantitative determination of fluorine (detection limit less than 30 ppma) and water (as hydrogen) in silicate minerals.

Trace element abundances determined in major silicate phases in terrestrial and lunar basalts indicate that some elements, such as Li and V, are incorporated into different phases depending on the conditions of crystallization as well as the crystal chemistry of the phases. The rare earth elements in lunar basalts occur highly concentrated in several kinds of accessory minerals including phosphates, oxides and silicates. The relative abundances of the rare earths determined with the ion microprobe in these phases are quite distinct and reflect crystal-chemical control during crystallization.

Much of our isotopic microanalysis work has been concerned with the determination of crystallization ages of lunar minerals using measurements of the lead 207/206 ratio (3). Several terrestrial zircons ranging in age from 3.3 to 1.0 billion years have also been successfully dated with this technique. In addition, we have determined that large inhomogeneities in uranium concentration are present in some zircons. The inhomogeneities are caused by zoning and by the presence of micron-size inclusions of other mineral phases. The ion microprobe has been used to date the inclusions as well as the distinct zones in some zircons and the results will be presented.

Preliminary lithium isotope measurements have been made on lunar and terrestrial basaltic glass and on a terrestrial zircon. The measurements yield essentially the same values ( $^7\text{Li}/^6\text{Li} = 12.188 \pm 0.013$ ) for the three samples with counting statistic standard deviations on the order of 0.5%.

The ion microprobe has also been applied to the determination of the diffusion rate of potassium in mica. Biotite flakes were placed in a solution enriched in  $^{41}\text{K}$  and heated (4). The ion microprobe was used to study the resulting  $^{39}\text{K}/^{41}\text{K}$  ratios in step scans across a single flake and as a function of depth into the flake. The analysis revealed that the potassium apparently diffused more than 100 times as fast parallel to the perfect cleavage plane (001) of the mica as it did in the direction perpendicular to this plane.

- (1) Stout, J. and Hinthorne, J.R. In preparation.
- (2) Jones, N.W., Ribbe, P.H., and Gibbs, G.V., Am. Min., 54, 391(1969).
- (3) Andersen, C.A. and Hinthorne, J.R., Earth Planetary Sci. Letters (1973) In press.
- (4) Enriched samples obtained from P. Hoffman.

This work was partially supported by NASA Contract NAS 9-11566.



# LITHIUM

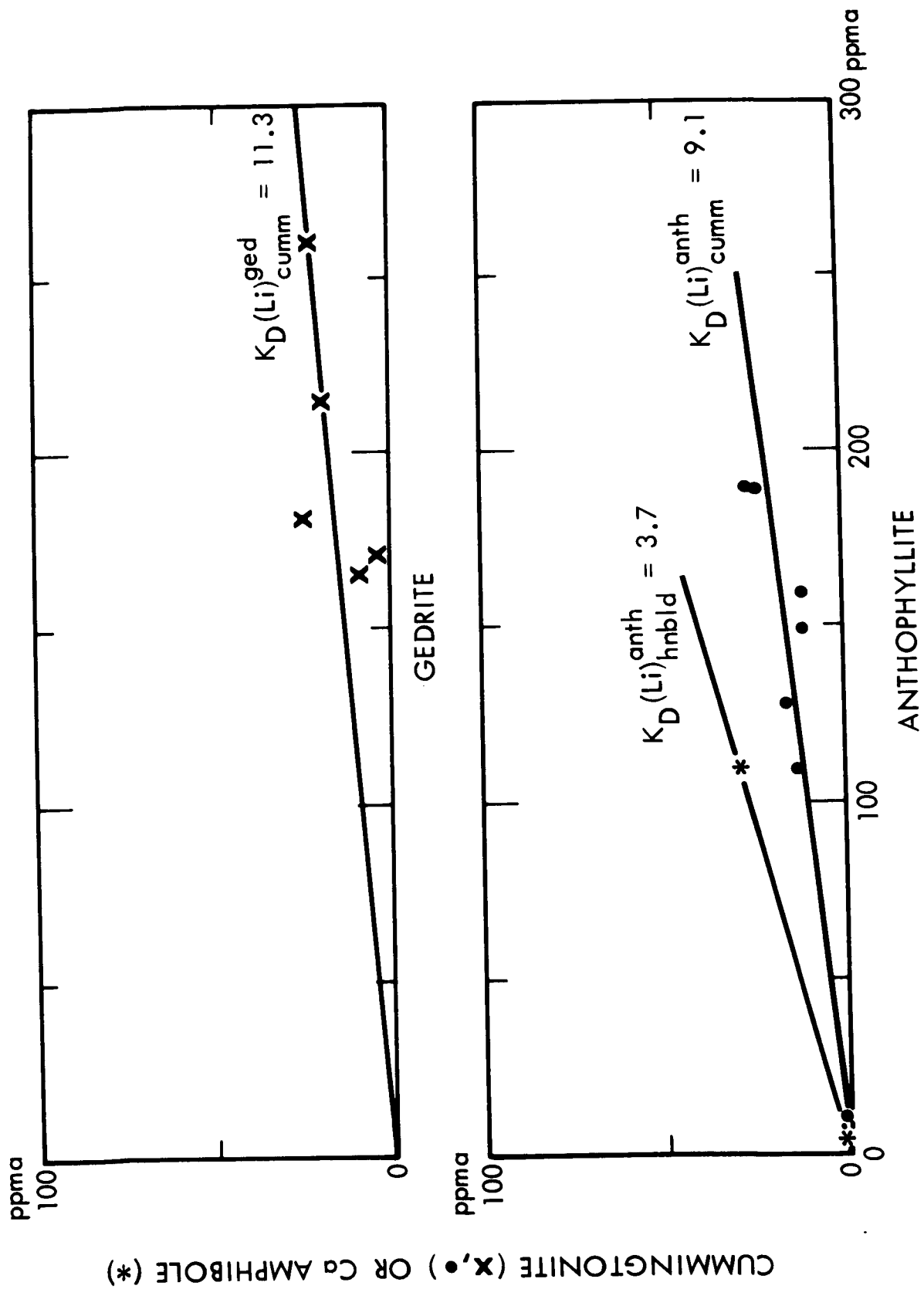


FIGURE 1

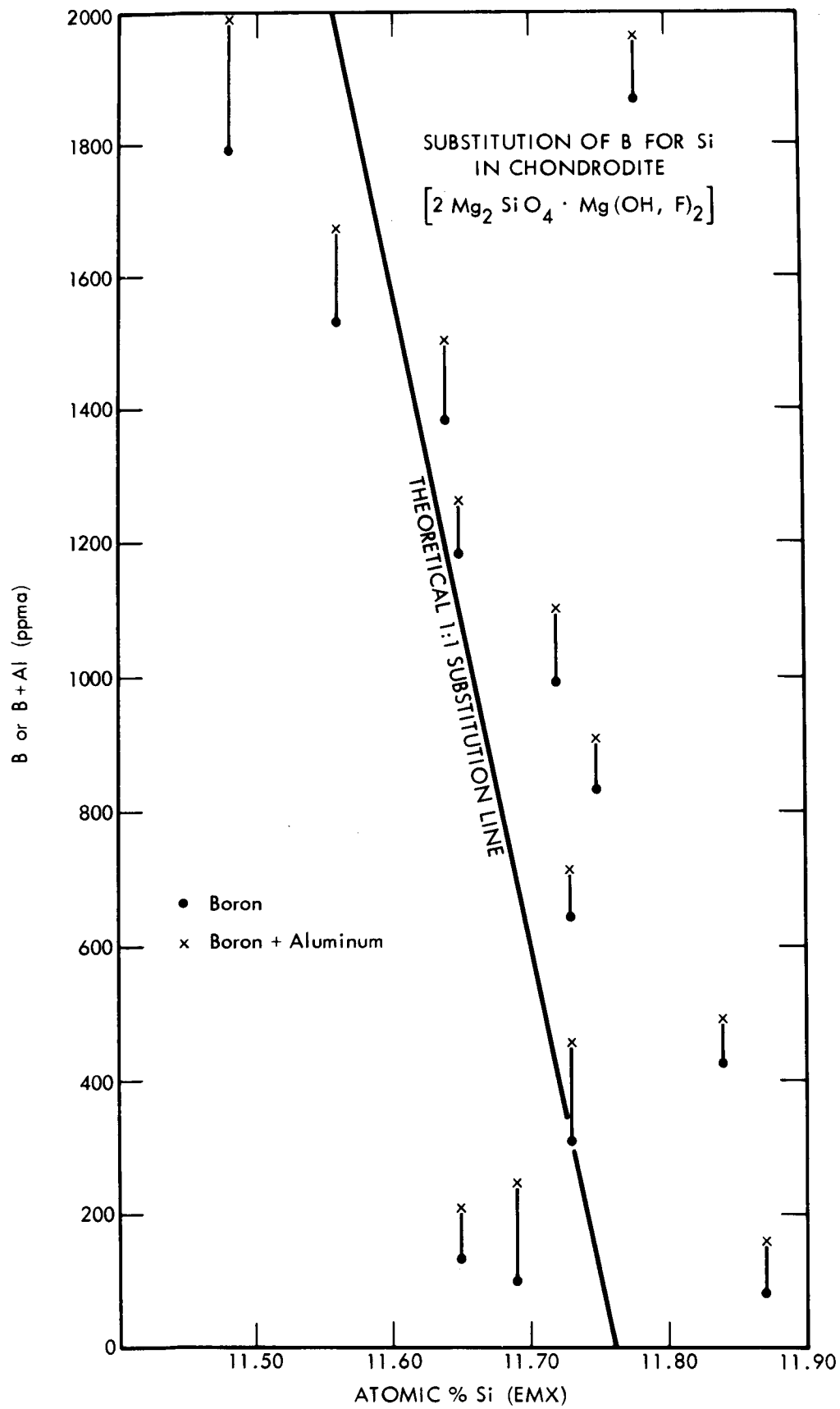


FIGURE 2

DETERMINATION OF ION-IMPLANTED DOPANT DISTRIBUTION IN  
SEMICONDUCTORS BY ION MICROANALYSIS

R. D. Dobrott, F. N. Schwettnann and J. L. Prince  
Texas Instruments Incorporated, P. O. Box 5936,  
Dallas, Texas 75222

Ion implantation is currently receiving much attention by most semiconductor device manufacturers in that the implantation process theoretically allows very precise control of dopant species, concentration, and depth distribution. Also, the implantation process is adaptable to novel device fabrication techniques, for example, a shallow emitter layer may be formed before a deep base eliminating the so-called emitter push effect which occurs frequently with current diffusion techniques. In actual practice some convenient means of determination of the actual distribution in depth in the as implanted material, after annealing and oxidation treatments, and for multi-species implants is necessary to successfully employ all of the flexibility of ion implantation. The ion microanalyzer is the ideal tool for this task in that it has excellent sensitivity for all elements; its sputtering ability renders concentration in depth; and it is not sensitive to the crystalline state of the matrix.

Figure 1 is the in-depth profiles of boron-arsenic-boron triple implant scheme used in the fabrication of silicon bipolar transistors. This experimentally determined profile clearly reveals that the base exhibits retarded diffusion during the oxidation and anneal cycles in agreement with R. Fair's<sup>1</sup> theoretical treatment for conventional diffusions of n-p-n structures. The ion-microanalysis is probably the only instrumental technique other than electrical measurements inference which is capable of confirming the theory. Many other profiles have been collected on boron single, boron double, and boron-arsenic-boron triple implants to demonstrate the usefulness of this technique. Also, profiles have been accumulated from a matrix of samples where 500 to 1000 Å surface layers have been chemically removed, profiles from back side to surface, profiles as of primary ion species, have

all been investigated in order to gain some in-sight on the validity of the ion-microanalyzer depth profiles. These latter experiments were designed to determine the effects of surface equilibrium delay time, the so called knock-on phenomenon, redeposition of the secondary ion species, and crater-wall ambiguities.

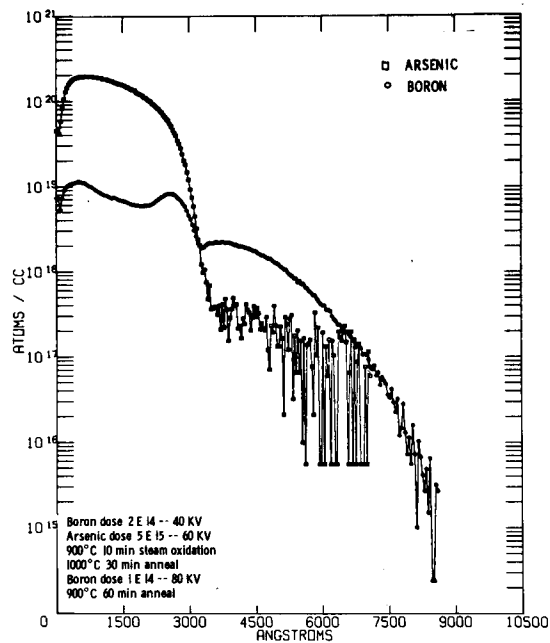


Figure 1. In-depth concentration profiles of a B-As-B triple implanted silicon wafer.

Title: Inter-element Effects in the Ion Probe

Author: Michael Bayard, Senior Research Microscopist, Walter C. McCrone Associates

Under any one given set of operating conditions the ion microprobe has a wide range in sensitivities for the different elements in the periodic table. If one is looking at a positive spectrum and bombarding with negative oxygen, it is very easy to get large signals from comparatively small amounts of sodium. However, under the same conditions, it is almost impossible to see gold in a pure gold sample. Accordingly, we have investigated different methods to increase the signal output from various elements which are normally blind. These methods are mainly applied to analysis of small particles, but should be applicable, in some cases at least, to large area analyses.

The effect of photoelectrons on quenching the signal from electro-positive elements and enhancing the signal for electro-negatives has been investigated. Ten to fifteen percent reductions in  $\text{Na}^+$  and order of magnitude increases in  $\text{Cl}^-$  were noted when investigating cadmium sulfide photo-emitters under various lighting conditions. The effect of alkali metals on enhancing the negative signal from noble metals has been put to use in practical cases. Signals from gold films have been enhanced by several orders of magnitude by evaporating an overlayer of cesium iodide or cesium bromide. We have investigated the simultaneous evaporation of an enhancing elements while bombarding with the normal gaseous species available from a duoplasmatron.

A very important factor that enters into small particle analysis is the range over which enhancement phenomena occur. Experimental evidence indicate that we have some mixing over a range of 0.5-1  $\mu\text{m}$  from a particle. This means that we can easily enhance the signal from very small particles of a normally poor ion emitter.

Some Limitations of Energy Dispersive X-ray Spectrometers

K. Kandiah

United Kingdom Atomic Energy Authority, Harwell, Didcot, Berks

The main attraction of an energy dispersive spectrometer is the ability to see the entire spectrum of the X-rays absorbed in the silicon detector. The fact that it responds to a wide range of energies and has a poor resolution in comparison with a wavelength dispersive spectrometer introduces some limitations in its use. In order to obtain reliable and accurate quantitative analysis with an energy dispersive spectrometer it is necessary to appreciate the nature and magnitude of the spectral distortions which arise from its basic properties and enhanced by deficiencies in individual forms of the instrument.

The poor peak-to-background ratio of an energy dispersive system dictates longer counting times. In a typical electron probe assembly it is possible to place the silicon detector close to the sample and obtain high counting rates in an effort to reduce the measurement time. The increased counting rate leads to the presence of sum peaks due to chance coincidence of X-rays detected within the pair-pulse resolving time and to appreciable line broadening unless active signal filtering<sup>(1,2)</sup> is used.

Pulse shaping

Owing to the presence of noise in the amplifier it is necessary to shape the pulse before the analysis into the spectrum in order to obtain the best signal-to-noise ratio. The intensity of sum-peaks can be reduced by means of pile-up rejectors but these too employ pulse shaping circuits in order to optimise the speed of pulse recognition and interference from noise. The line width of a spectrometer at an energy  $E$  is  $(2.5E + E_0^2)^{1/2}$  where  $E_0$  is the line width due to electronic noise assuming a Fano factor for the detector of 1.25. The electronic noise  $E_0$  varies with the pulse shaping time  $T$  as shown in fig 1. It is seen that the X-ray line width will be limited by electronic noise at low energies and by detector statistics at energies greater than a few keV when a shaping time of say 20 $\mu$ s is used. The pile-up rejector should use shaping times much shorter than those used in the pulse analysis channel in order to obtain a worthwhile reduction of the sum-peak intensity. The choice of the pile-up rejector depends to some extent on the X-ray spectrum.

### Pile-up rejection

The use of short pulses improves the rejection at high energies but the exact form of the shaping circuits and the rejection logic may affect its efficiency in the normal situation when there is a complex spectrum. Double differentiation is usually employed in order to avoid problems of base-line fluctuations but this gives a poor performance when a low energy event is detected after a high energy event. It is desirable to use zero-cross timing logic as well as recognition of the leading edge in order to improve protection. It will be noted that the use of event-by-event opto-electronic charge restoration at the detector<sup>(2)</sup> eases the pulse shaping problems in the pile-up rejector also since double differentiation is not necessary as would be the case in systems<sup>(3)</sup> where many pulses are allowed to accumulate in the head amplifier before restoring the charge at the detector.

For the sake of illustration all the following arguments relate to a pile-up rejector system which uses a 130 ns shaping time and also uses a logic circuit which imposes a maximum time limit of 300 ns from the threshold discriminator pulse to the zero-crossing discriminator pulse. It is seen from fig 1 that the electronic noise line width for 130 ns shaping is about 840 ev. Therefore the threshold discriminator level is set at about 1.3 kev and the efficiency of this discriminator as a function of energy is shown in fig 2. It is seen that the efficiency of the discriminator is virtually zero below about 800 ev and full efficiency is only obtained above 2 kev. In order to improve the pile-up problem at low energies the system uses an additional pulse recognition circuit with 2 $\mu$ s shaping time giving full efficiency at 1 kev.

### Results

The operation of the complete system which employs active signal filtering with processing time of 20 $\mu$ s for the main analysis as well as the pile-up protection described above will now be discussed. Reed<sup>(4)</sup> recognised the importance of choosing the correct pulse shaping time for rejection of pile-up at different parts of the spectrum. The system we are using employs more elaborate protection logic and two shaping times simultaneously. These factors combined with active filters for analysis give greatly improved performance as demonstrated in the results presented.

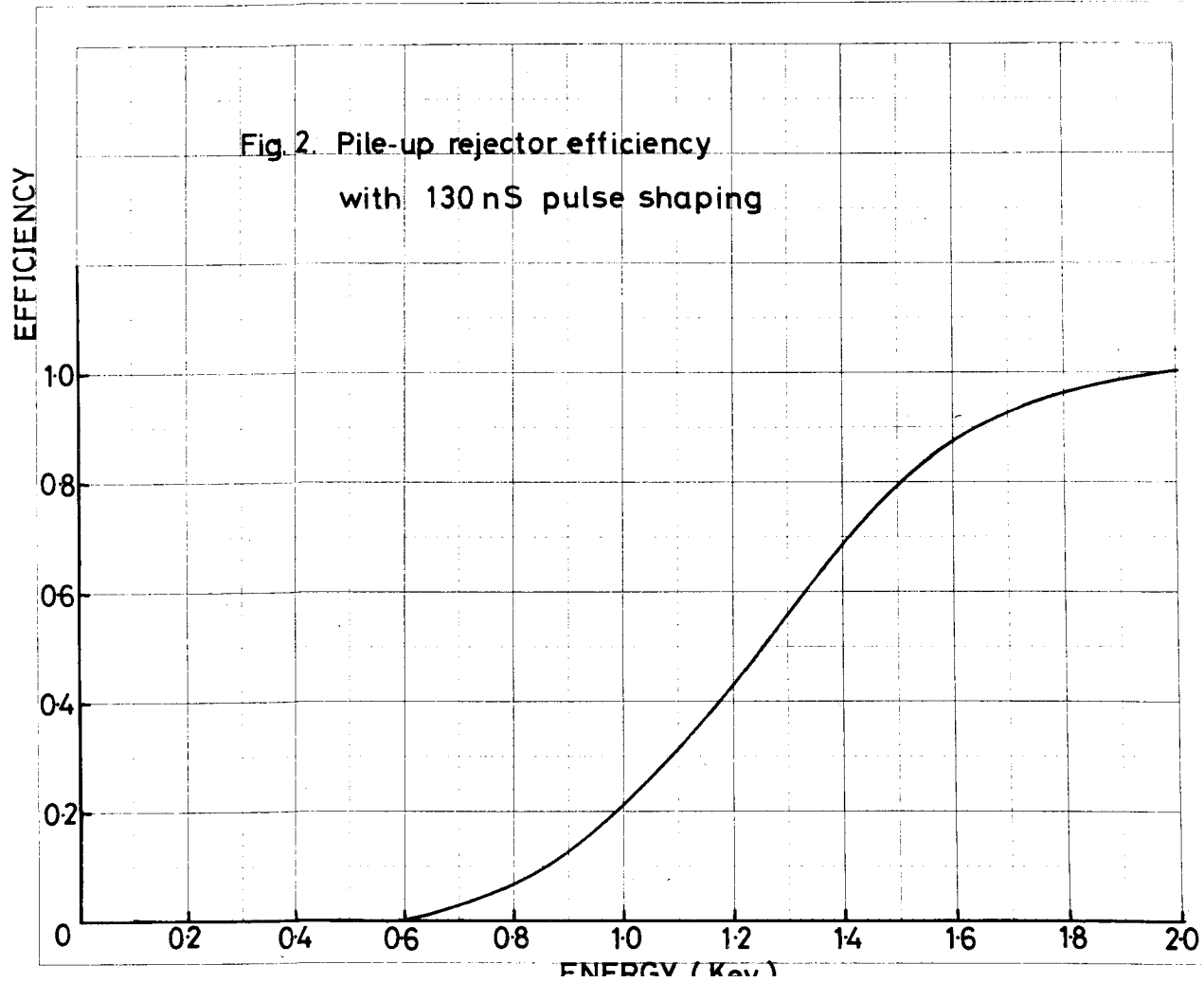
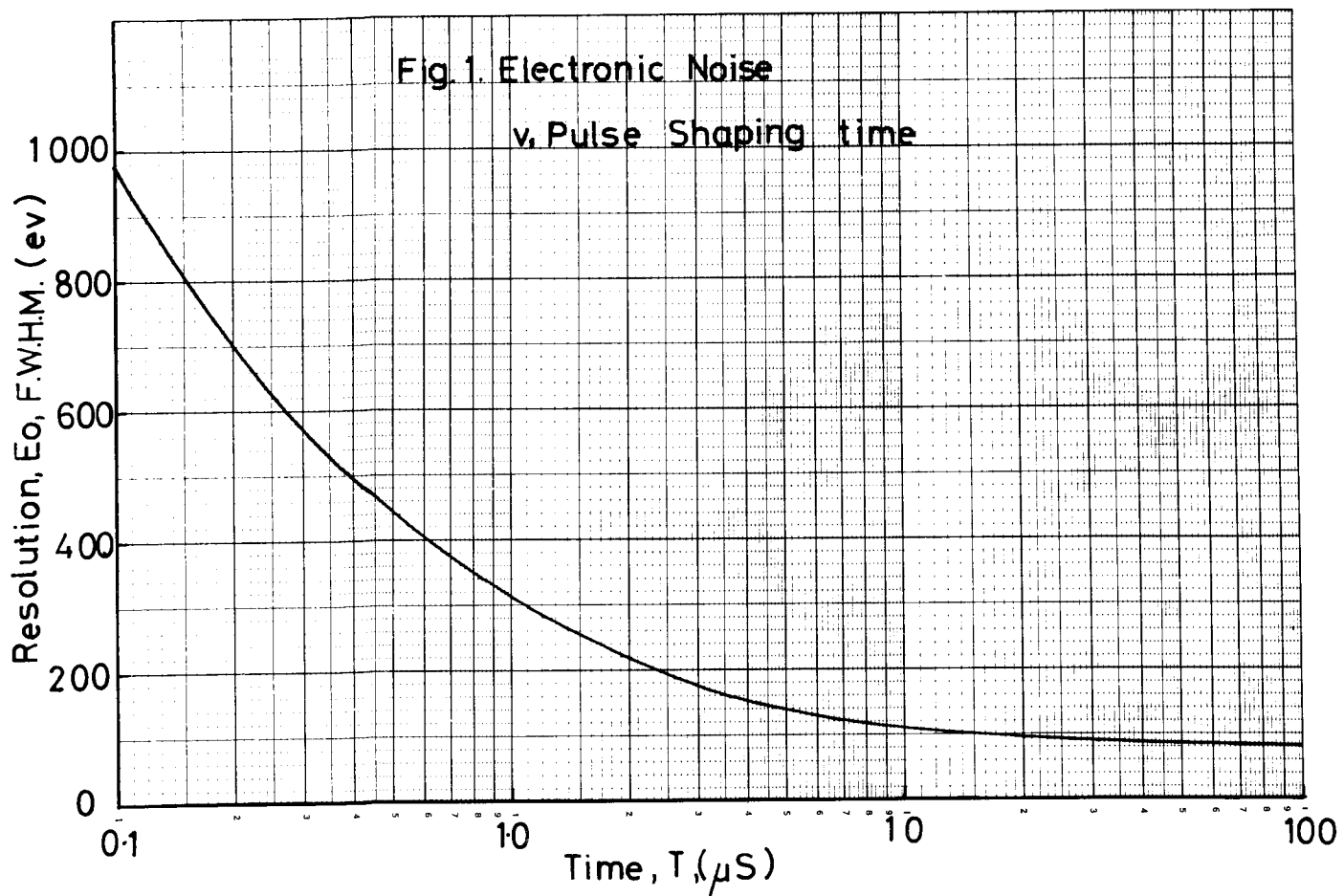
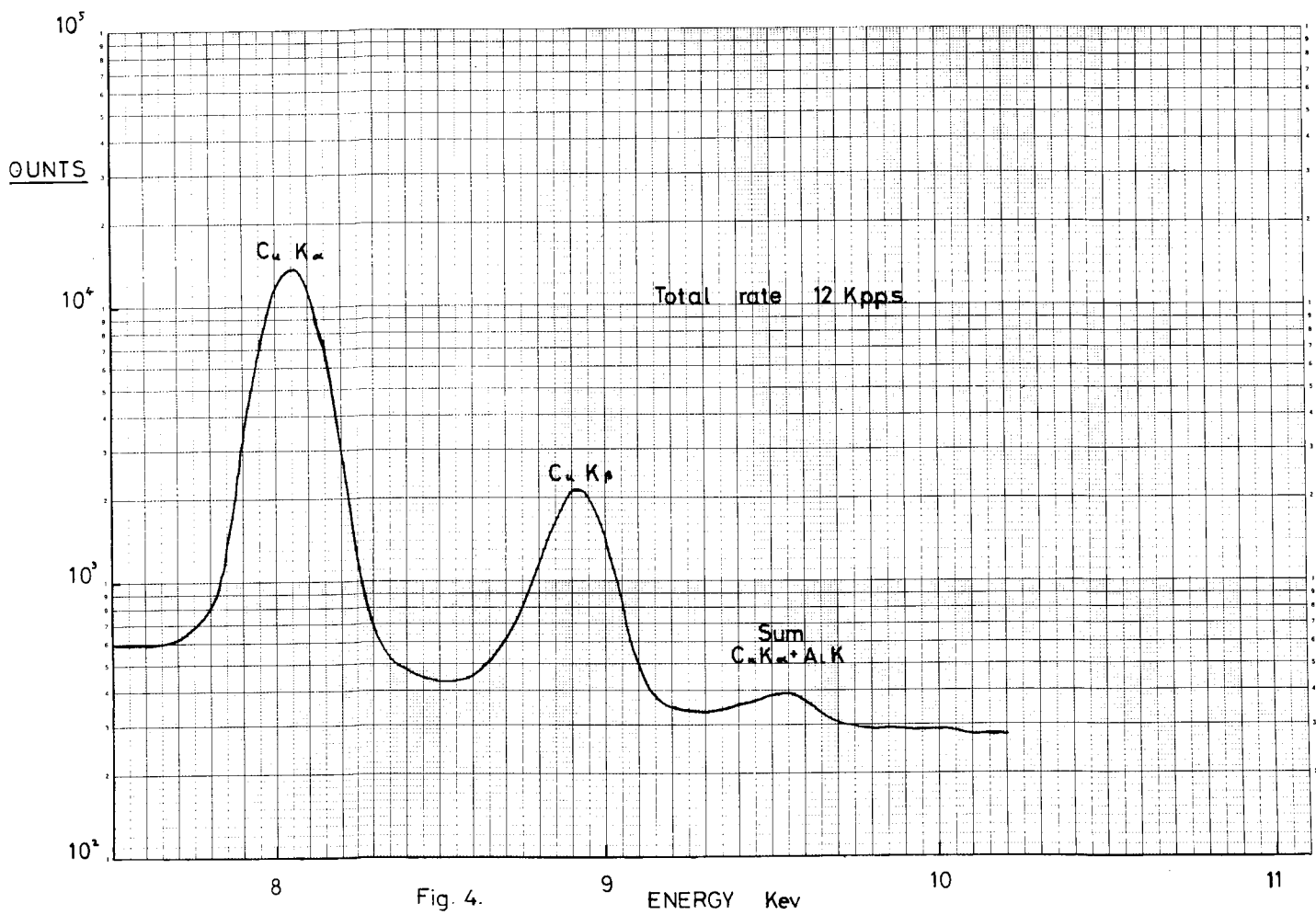
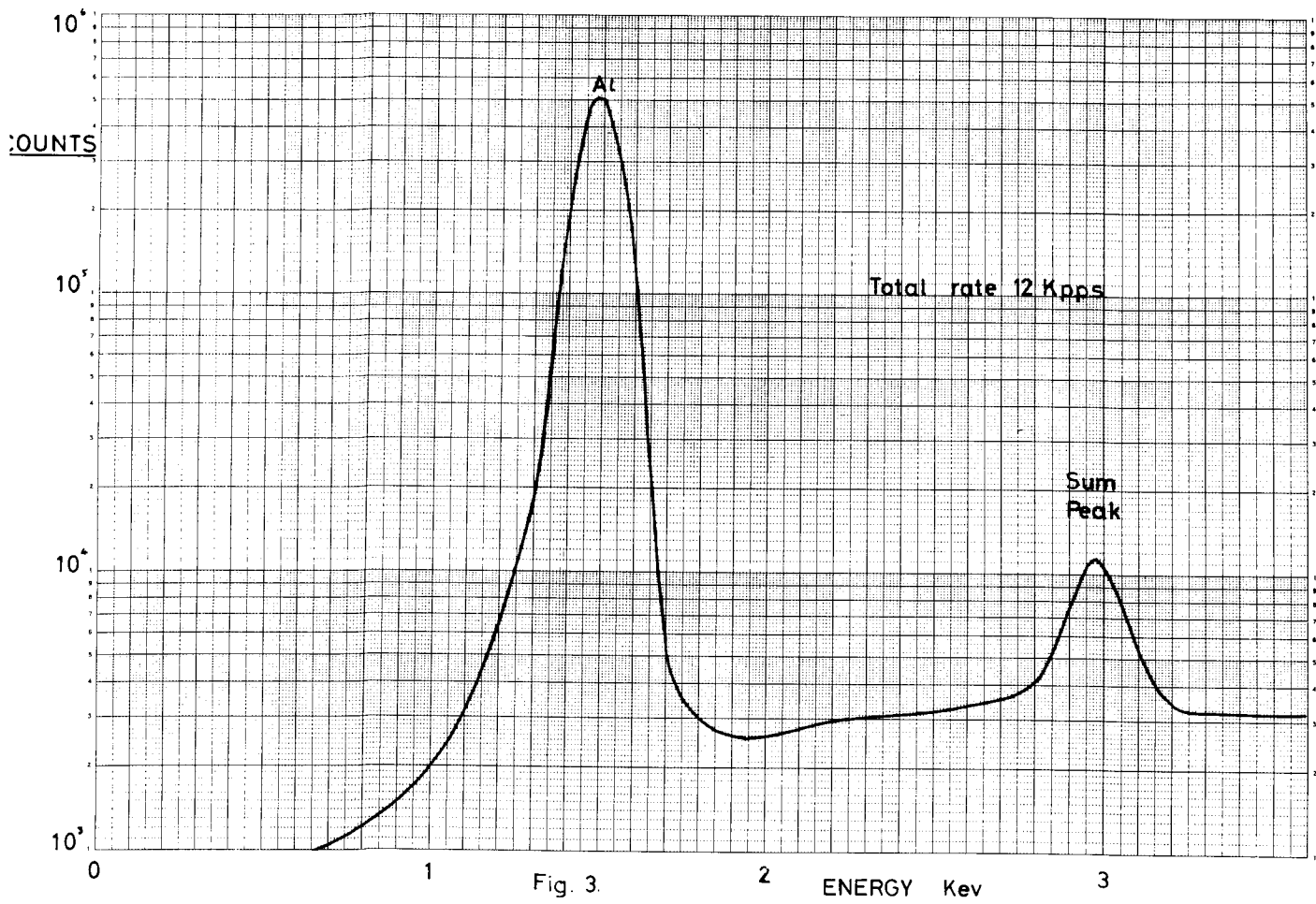




Fig 3 shows the spectrum from a pure Al sample at a counting rate of  $1.2 \times 10^4$  per second. It is seen that the intensity of Al + Al sum peak is about  $1/50$  of the Al peak corresponding to a pair pulse resolution of  $1.6 \mu\text{s}$ . This result is in reasonable agreement with the pulse shape of the slow recognition channel ( $2 \mu\text{s}$  shaping) and the 80% efficiency of the fast recognition channel at 1.49 keV as seen from fig 2. A more typical situation with a mixed Cu and Al sample with about  $2 \times 10^3$  counts/sec on the Al peak is shown in fig 4 where the sum peak is about  $1/1000$  of the main peak.

Owing to the presence of the Bremsstrahlung background it is not easy to obtain accurate measurements on the pile-up effect in an electron beam excited emission spectrum. Therefore signals from a Mn source were mixed at the head amplifier with a charge simulator which exactly simulates the pulses from the detector but with an accurately controllable amplitude and rate (true Poisson distribution in time). Fig 5 shows the spectrum obtained with this arrangement with a total counting rate of  $1.9 \times 10^4$  per second but with the test pulse rate set at  $7 \times 10^3$  per second so that the peak counting rates of the test pulse and Mn lines were nearly identical. In this run the amplitude of the test pulses was equivalent to 2 keV X-rays. The Test + Test sum peak is close to the Si escape peak from the detector but is seen to be about  $1/500$  of the single Test peak intensity indicating a pair pulse resolving time of 280 ns. However it is noted that the MnK $\alpha$  + MnK $\alpha$  sum peak is only about  $1/1000$  of the single MK $\alpha$  peak in spite of the fact that the counting rate on this is  $1.2 \times 10^4$  per second indicating a pair pulse resolving time of only 83 ns. This is to be expected since double differentiation is used in the fast recognition channel. The intensity of the MnK + Test sum peak is seen to be only  $1/100$  on the MnK peak indicating that the smaller test pulse sitting on the tail of the Mn pulses cannot be recognised for a time interval of about  $1.4 \mu\text{s}$ .

The existence of the more serious problem is demonstrated in fig 6. This run differs from that shown in fig 5 only in the amplitude of the test pulses which now simulates 1 keV X-rays. It is seen that the Test + Test sum peak is only  $1/50$  of the intensity of the single Test peak owing to the low efficiency of the fast rejector channel. Pile-up rejection is only effective because of the presence of the  $2 \mu\text{s}$  shaped pulses of the slow recognition channel giving a pair pulse resolving time of about  $2.8 \mu\text{s}$ . It is seen from fig 6 that the pair pulse resolving time for a 1 keV event following a 5.9 keV event is now about  $7 \mu\text{s}$ . As expected the pair pulse resolving time for MnK $\alpha$  + MnK $\alpha$  sums remains the same as in the previous run.



### Line shapes and positions

Identification of elements and calculations of recorded intensities are made easier if the line shapes and positions are independent of composition of the spectrum and counting rate. Using conventional passive pulse shaping and well designed base line restorers there should be little difficulty in maintaining linearity or reasonably clean lines when  $nT < \frac{1}{4}$  where  $n$  is the counting rate and  $T$  is the pulse shaping time (time to peak). At higher counting rates the line width increases very sharply and is unacceptably large when  $nT \approx \frac{1}{2}$ . The active filters used in our work do not show such gross errors. It has been shown by Deighton<sup>(5)</sup> that the electronic noise in the active filters used by us increases by only about 20% from the low rate value when the counting rate is nearly infinite. Furthermore this system permits the zero energy line shape also to be recorded during the run so that any distortions of the line shape can be quickly identified. We have established that the shape of the zero energy line remains gaussian down to a count level of less than 0.1% of the peak but we have noticed minor distortions in the main spectral lines at levels below 10% of the peak counts. These are reduced when the source is well collimated.

### Conclusions

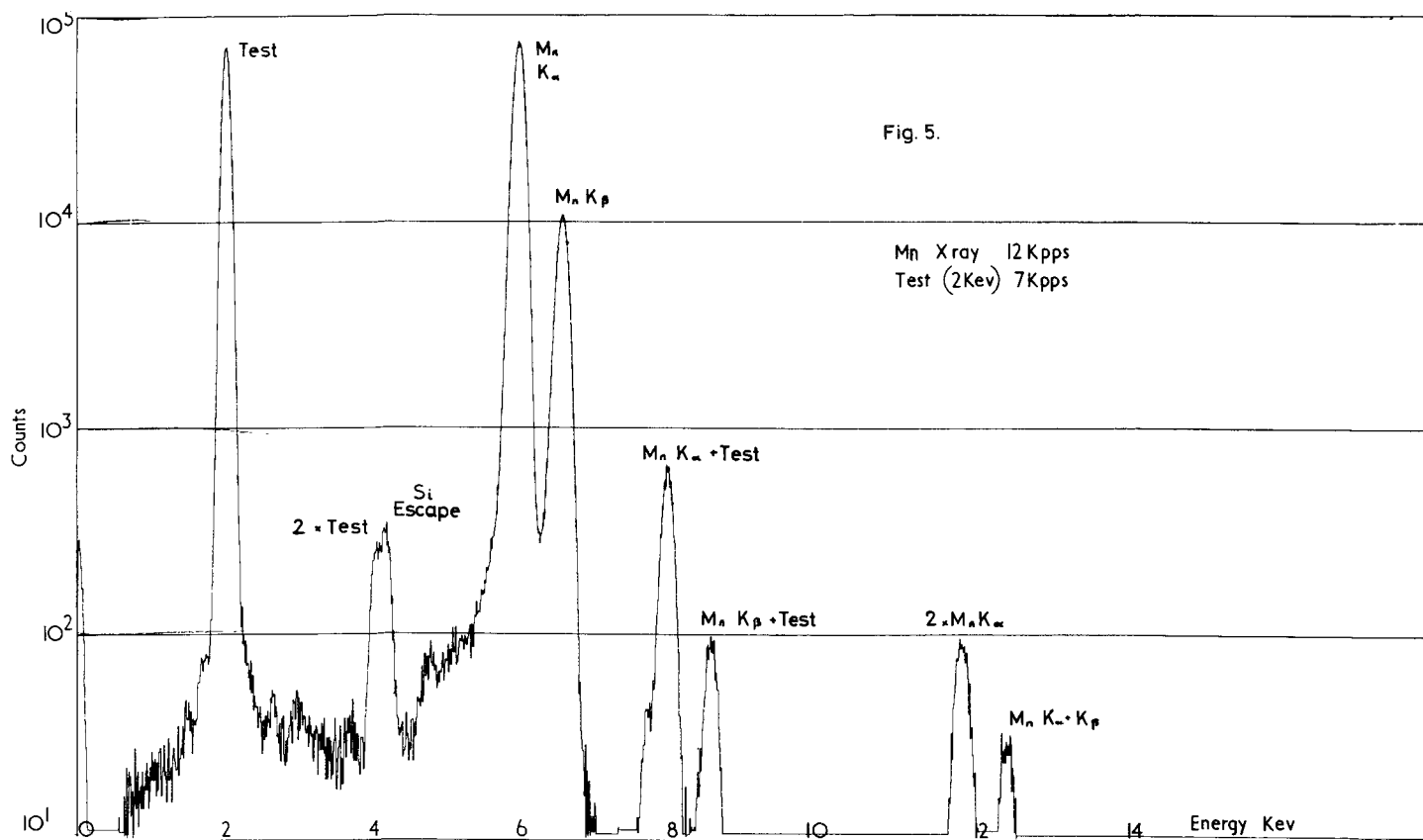
Owing to the steep increase in noise as pulse shaping times are reduced the effectiveness of pile-up rejectors deteriorates below about 2 kev. The pile-up spectrum is dependant on the shape of the true spectrum especially when there are components below about 4 kev. The use of detectors with very thin entrance windows is not to be recommended in situations where low energy X-rays are not to be studied. The optimum performance will be obtained only by judicious choice of absorber in front of the detector and pulse shaping in the pile-up rejector. It will be generally desirable to use more than a simple threshold discriminator and multiple shaping times may be desirable when unknown low  $z$  trace elements are to be analysed. Since the peak to background ratio in electron probe analysis is not very high the departure of the spectral lines from a true gaussian is not generally detectable. With good signal processing and pile-up protection measurements of emission lines, even of minor constituents to a fraction of 1% should be possible.

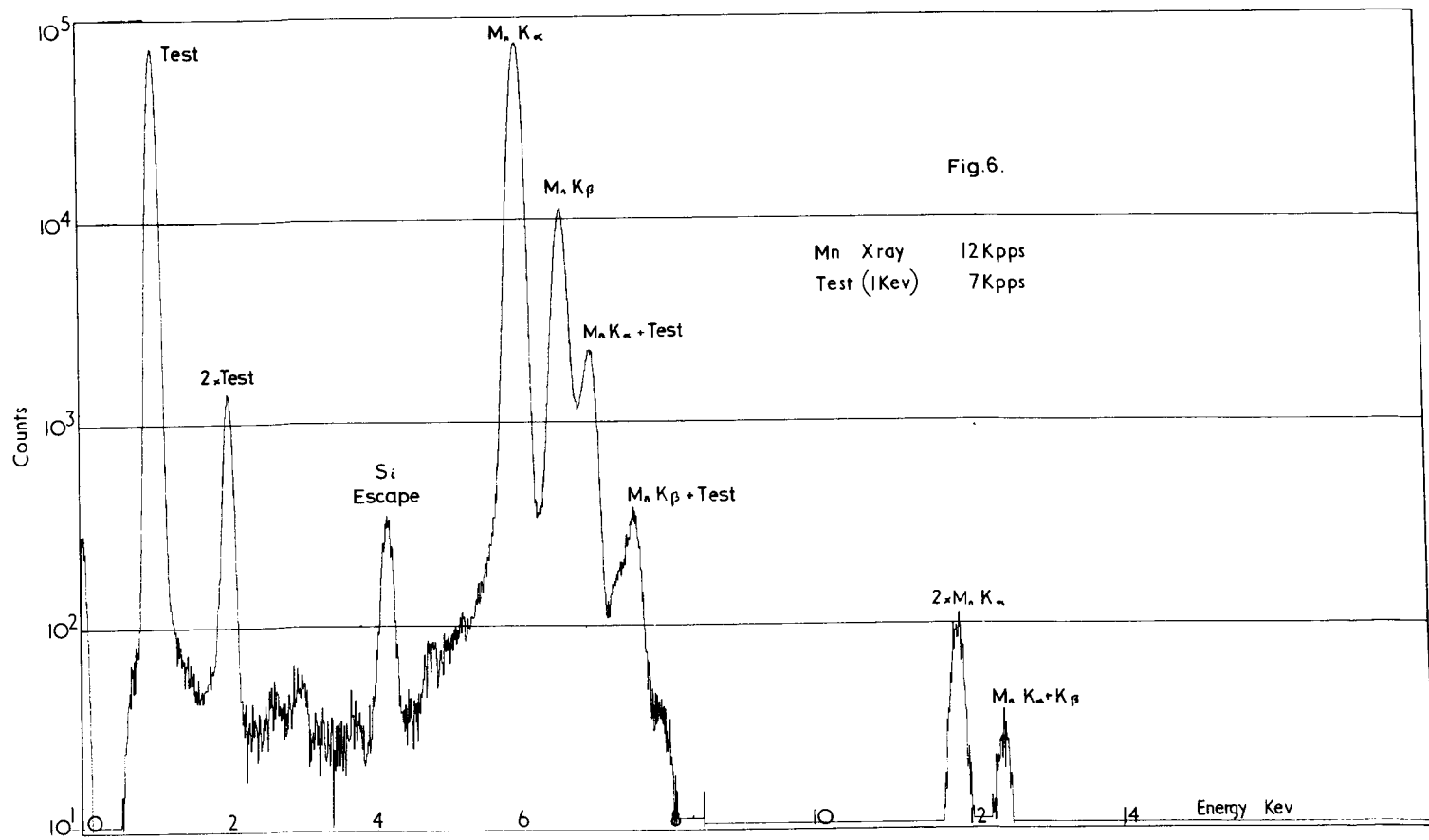
### Acknowledgements

The author is indebted to colleagues at Harwell, particularly Mr. G. White, and to Dr. J.V.P. Long of the University of Cambridge for their help in obtaining much of the data presented here.

# References

- (1) K. Kandiah, A. Stirling, D.L. Trotman and G. White, Intern. Symp. Nuclear Electronics (Versailles, 1968)
- (2) K. Kandiah, Nucl. Instr. and Meth. 95 (1971) 289
- (3) D.A. Landis, F.S. Goulding and J.M. Jaklevic, Nucl. Instr. and Meth. 87 (1970) 211
- (4) S.J.B. Reed, J. Phys. E. 5, 10 (Oct 1972) 997-1000
- (5) M.O. Deighton, Nucl. Instr. and Meth. 103 (1972) 1





QUANTITATIVE ELECTRON MICROPROBE ANALYSIS  
USING AN ENERGY DISPERSIVE SPECTROMETER

A. G. Plant and G. R. Lachance

Geological Survey of Canada  
Ottawa, Ontario  
Canada

The combination of an electron microprobe with an energy dispersive spectrometer and an on-line mini-computer forms a powerful system for the analysis of materials, and this paper outlines an empirical method for the quantitative analysis of rock-forming silicate minerals for up to 15 elements. By restricting ourselves to silicate minerals and by measuring at fixed operating parameters, the problems encountered in universal methods are minimized and their magnitude is such that, within the reproducibility of the data, their effects are negligible in the day to day analysis of samples and an empirical approach is feasible. For example, the problems that can arise from large variations in count rate and in the interference (non-resolution) of K, L and M spectra when the analyst is faced with analyzing a wide variety of materials for every element detectable by energy dispersive X-ray analysis are considerably reduced as silicate minerals usually contain fewer than 10 elements in reasonably well defined concentration ranges above the 0.1% level. Also, the programming aspects are simplified in that a number of elements can be fixed, for example, we always analyze for Na, Mg, Al, Si, K, Ca, Ti, Cr, Mn and Fe, with an option for adding up to five additional elements.

The principles of energy dispersive X-ray analysis are now well established (Beaman and Isasi, 1972) and in our laboratory we have used a M.A.C. Model 400 electron microprobe, a Kevex Si (Li) detector (resolution at Mn  $K\alpha$  = 157 eV) coupled to the 5000A X-ray energy spectrometer with 1024 channels and a 16K Hewlett Packard 2100 computer. The multi-channel analyzer is operated at 10eV/channel and thus when the system is correctly calibrated, channel 174 corresponds to the 1.74 keV peak of silicon; recalibration should be carried out if peaks drift by more than one or two channels. Following display of the integrated spectrum (usually 100-300 seconds) on a CRT, the data can be transferred directly to computer memory (approx. 35 secs.) or if the spectrum is to be added to a library of spectra, a paper tape can be produced.

The first step in the data reduction sequence (see Outline of Analytical Program) is to convert the measured intensities to counts per second. This allows the analyst to vary integration times when necessitated by mineralogical considerations. The data are then convoluted using the 19 point set of integers for quadratic-cubic curves proposed by Savitzky and Golay (1964). From the detailed study of many spectra obtained from a wide variety of minerals (silicates, oxides, carbonates), we have concluded that within the counting statistics of the data: (1) the channel position of the peak maxima is reproducible, (2) the distribution of the counts within the peaks is reproducible, (3) backgrounds for each element can be correlated with selected portions of the continuum, and (4) non-resolution effects and other minor residuals can be correlated to appropriate peaks in the spectrum. These

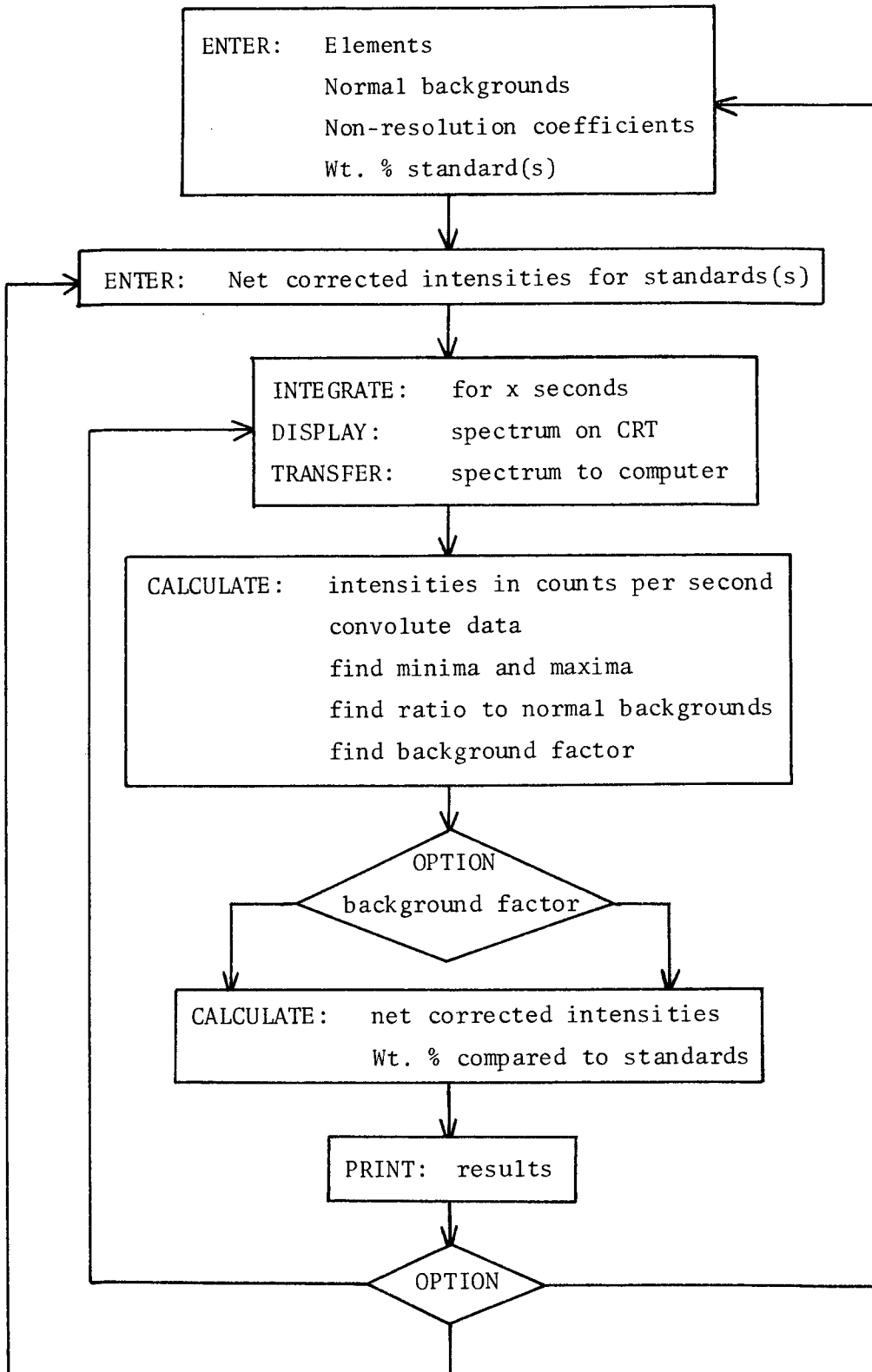
conclusions have led to the adoption of the following: (a) peak intensities are measured by integration over 13 channels centered on the maximum; (b) backgrounds are calculated by reference to a normal curve for peaks of 2.5 keV or more, and for peaks less than 2.5 keV, backgrounds are calculated by interpolation; (c) non-resolution effects are calculated by an iteration process and correct for peak overlap, peak trailing, background anomalies, etc.

The weight per cent oxides obtained by direct comparison to mineral standards are subject to the usual matrix corrections. We have used both ZAF and empirical  $\alpha$ -factor methods and examples will be presented of analyses of a variety of silicate minerals for both major and minor elements. The procedures developed in our empirical method give results comparable to those obtained using wavelength dispersive analysis. To ensure that the system is maintained in an optimum state of calibration, a standard sample of the mineral, Kaersutite, which contains 8 of the 10 fixed elements in concentrations greater than 1.5%, is analyzed during each analytical session. Our analyses of this mineral over a period of several months show that the short term reproducibility is excellent, but that during this time, the sensitivity of elements having a lower energy than silicon has dropped, while it has increased for elements of higher energy. A number of tests are being conducted to define the magnitude, rate of change, etc., as a function of energy in order to trace the cause of this long term drift.

Beaman, D.R. and Isasi, J.A. 1972. Electron Beam Microanalysis. ASTM STP 506.

Savitzky, A. and Golay, M.J.E. 1964. Smoothing and Differentiation of Data by Simplified Least Squares Procedures. Anal. Chem. 36, 1627-1639.

## OUTLINE OF ANALYTICAL PROGRAM





RAPID ENERGY DISPERSIVE ANALYSIS  
UTILIZING A FIELD EMISSION SEM

by

Richard G. Vadimsky  
Bell Telephone Laboratories  
Murray Hill, New Jersey 07974

## ABSTRACT

It has been well established that energy dispersive systems are powerful adjuncts to scanning electron microscopes (SEMs). This has again been demonstrated by our recent mating of a field emission source SEM<sup>(1)</sup> with a fast, convenient X-ray analyzer<sup>(2)</sup>. The resulting instrument provides excellent qualitative and semiquantitative X-ray microanalysis while allowing a high through-put of samples.

The inherently bright field emission source is one factor behind this achievement. Although the microscope is routinely operated at less than half the maximum available beam intensity, total spectrum X-ray count rates of 5000-10,000 cps are achieved while maintaining a secondary electron resolution of better than 500 Å.

The X-ray analyzer incorporates a minicomputer and compensates for pulse pile-up and deadtime losses. Having a cycle time of only 1.6 μsec., the unit can quickly present meaningful data for evaluation. Its major time

economizing feature, however, is its ability to acquire data in one memory subgroup while allowing manipulation of data previously stored in another. Hence, there is a great reduction in "operator deadtime."

Some of the data manipulation functions, simply available via pushbuttons, include spectrum smoothing (5 point least squares fit), background subtraction, peak identification, selected area totalizing, and spectrum stripping. Further, in the "learn" mode, one may program any sequence of operations (up to 52 steps in each of two memories) to reduce data manipulation time where repetitive operations are to be carried out.

The system's capability for quantitative analysis is being evaluated. Two major items under examination are beam current stability (which may be less than desirable) and correction program accuracy. The programs referred to are: the LINEAR CONCENTRATION routine which calculates a linear working curve for up to ten elements and then fits unknown samples to this curve, the MULTIPLE REGRESSION routine which uses intensities from standards to calculate coefficients for computing concentrations corrected for inter-element effects, and the KOREX routine which corrects for fluorescence, absorption and atomic number effects in calculating weight fraction concentrations. Finally, optimum operating parameters, minimum detectable limits, and sensitivity will be determined.

<sup>1</sup>CWIKSCAN 100.

<sup>2</sup>77-90S Qanta/Metrix with Kevex detector.

MICROANALYSIS OF PARTICULATE MATERIALS

R. E. Ferrell and G. G. Paulson  
Department of Geology, LSU, Baton Rouge, Louisiana

Abstract published in EMSA Proceedings

ELEMENT AND COMPOUND DISTRIBUTION MAPPING IN THE SEM

J. C. Russ, M. W. Barnhart, and J. L. Christopher  
EDAX International, Inc., Raleigh, North Carolina

Abstract published in EMSA Proceedings

IMPROVEMENTS IN HIGH COUNTING RATE PERFORMANCE OF SI(LI)  
ENERGY SPECTROMETERS WITH A NOVEL BASELINE RESTORATION  
TECHNIQUE

N. Karlovac and D. A. Gedcke  
ORTEC, Incorporated  
Oak Ridge, Tennessee 37830

---

Performance of Si(Li) energy spectrometers deteriorates at high counting rates. There are many reasons for this deterioration<sup>1,2,3</sup> and most of them are interdependent, but the most important one is the baseline restoration.<sup>2</sup> The baseline restoration is incorporated into the spectrometer to provide filtering of the low frequency noise and to stabilize the baseline level<sup>3</sup>, but at the same time causes a count rate dependent peak shift and line broadening because it acts as a partial AC coupling for the signal pulses. In an effort to improve the high count rate performance we designed a new baseline restorer based on the concept of the time variant differentiator.<sup>4</sup>

Figure 1 shows the block diagram of the amplifier and the baseline restorer. The main shaping amplifier is a linear amplifier employing semi-Gaussian shaping with three selectable shaping time constants ( $\tau = 2, 6, \text{ or } 10\mu\text{sec}$ ). The shaping amplifier output is fed through the baseline restorer to the "linear output". The baseline restorer operates as a conventional restorer in the absence of the signal pulse. The signal from the preamplifier is amplified and shaped with a 100 nsec time constant in the fast amplifier. The fast amplifier output triggers the discriminator, which in turn triggers the gate logic and pile-up rejector logic. The gate logic provides a logic pulse that gates off the operation of the baseline restorer for the duration of the signal from the main amplifier, and thus DC couples the signal pulse to the linear output and the multichannel pulse height analyzer (MCA). The gate logic pulse is also available as a "Busy output" to be used for live time correction in the MCA. The "Inhibit output" is used for the pile-up rejection in the MCA. The fast logic pulse is also available for the monitoring of true input counting rate.

The effect of counting rate on resolution is shown in Fig. 2. It is evident that the curves are remarkably flat and resolution degradation with counting rate very small. The baseline stability at high counting rates is shown in Fig. 3. The peak shift is also negligible up to very high counting rates. The line width increases less than 5 eV and the peak shift is less than 2 eV for counting rates up to 10000 cps with 10 $\mu\text{sec}$  shaping, up to 40000 cps with 6 $\mu\text{sec}$  shaping and up to at least 60000 cps with 2 $\mu\text{sec}$  shaping.

Figure 4 shows the percent deadtime measured at the amplifier output and the residual loss after the MCA livetime correction.<sup>3</sup> Deadtime loss correction accuracy is quite adequate up to the 40% deadtime loss point. At 40% losses the spectrometer is producing an output rate which is 83% of the maximum output rate a paralyzable deadtime system can pass.<sup>3</sup> There is little to be gained in statistical accuracy or counting time reduction beyond this counting rate.

In conclusion, the gated baseline restorer provides substantial improvement in high counting rate performance in comparison to previously reported results.<sup>2,3,5</sup> In practice, the amount of the spectral distortion due to count rate effects in the gated baseline restorer is negligible for all counting rates up to the limit set by the paralyzable nature of the deadtime.

- 
1. F. J. Walter, Special Technical Publication 485, American Society for Testing and Materials, Philadelphia, 1971.
  2. D. A. Gedcke, E. Elad, G. R. Dyer, Proc. Sixth National Conf. on Electron Probe Analysis, Pittsburgh, July 27, 1971.
  3. D. A. Gedcke, X-Ray Spectrometry 1, 129 (1972).
  4. V. Radeka, The Rev. of Scientific Instruments 38, 1397(1967).
  5. S. J. B. Reed and N. G. Ware, Journal of Physics E 5, 1112(1971).

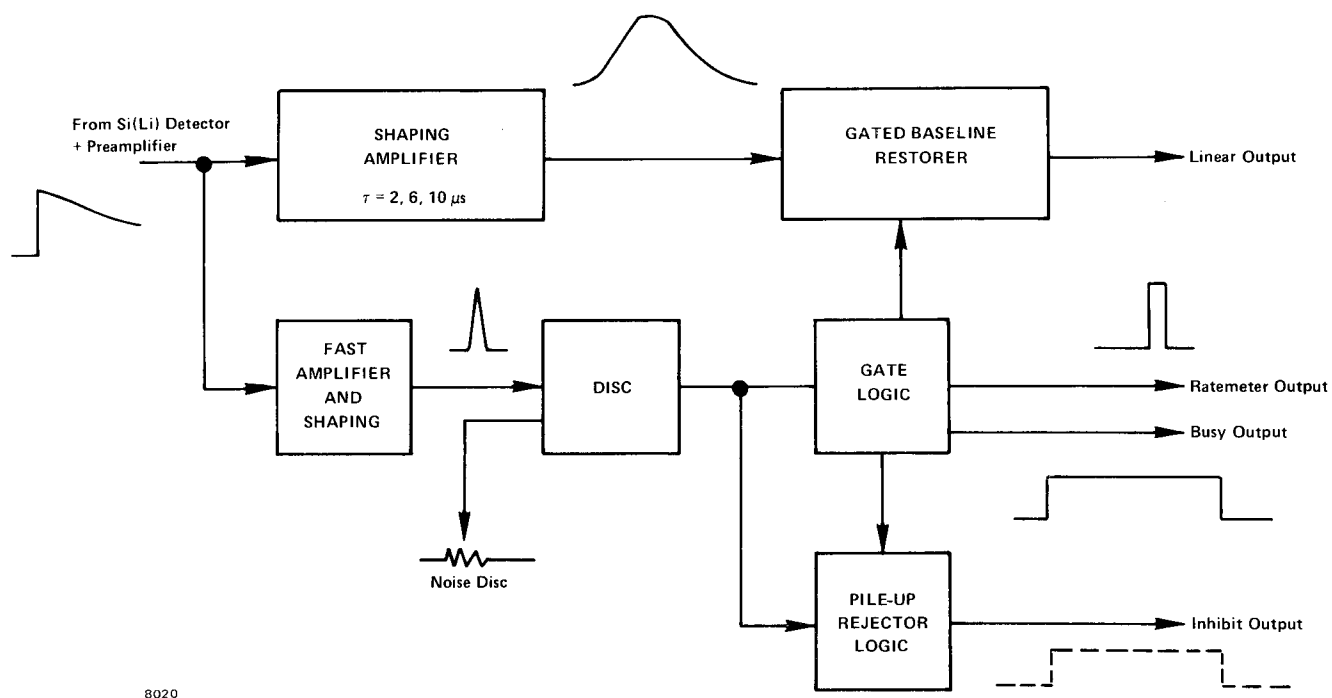


Figure 1. Amplifier and Baseline Restorer Block Diagram

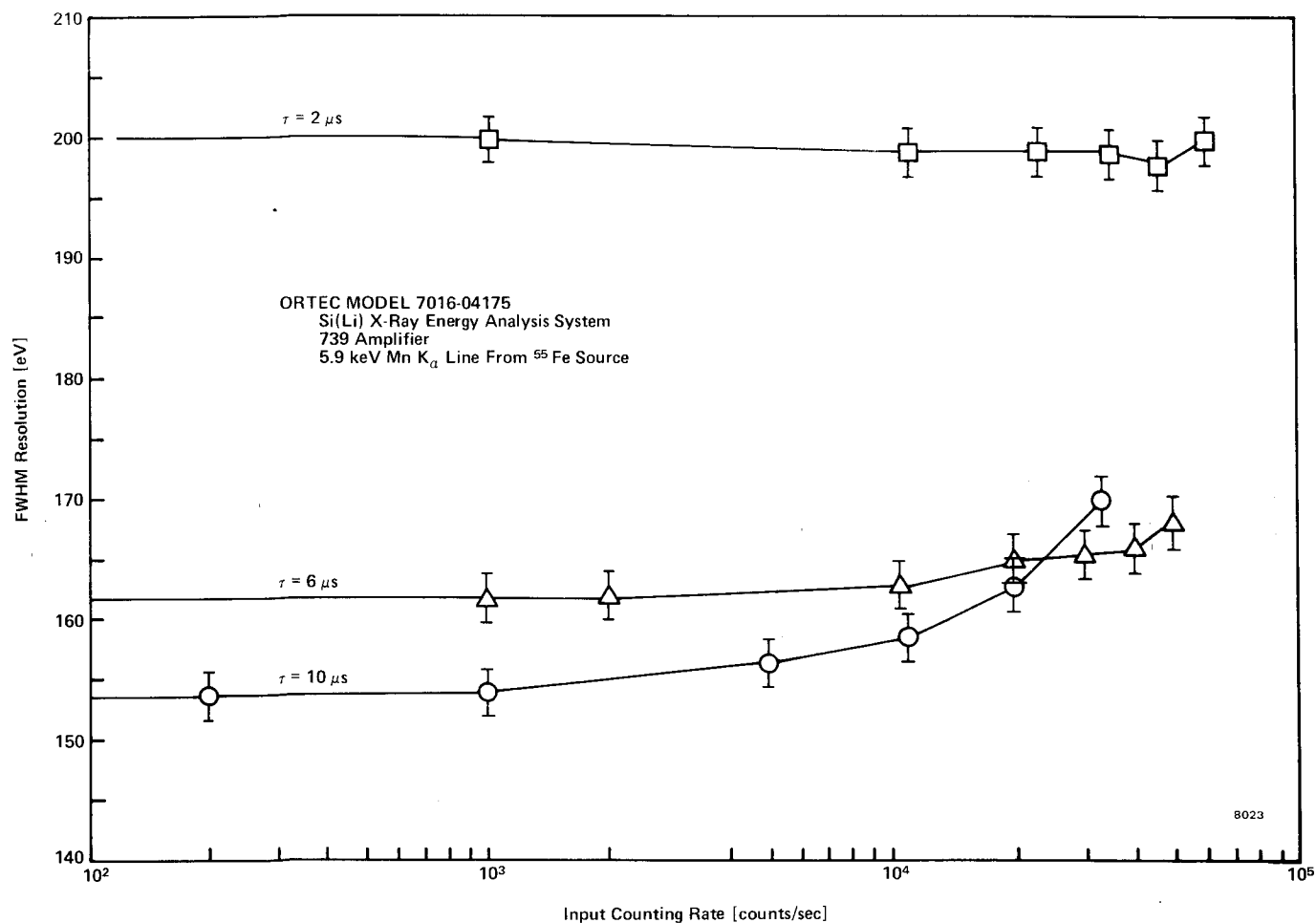


Figure 2. Resolution vs. Counting Rate

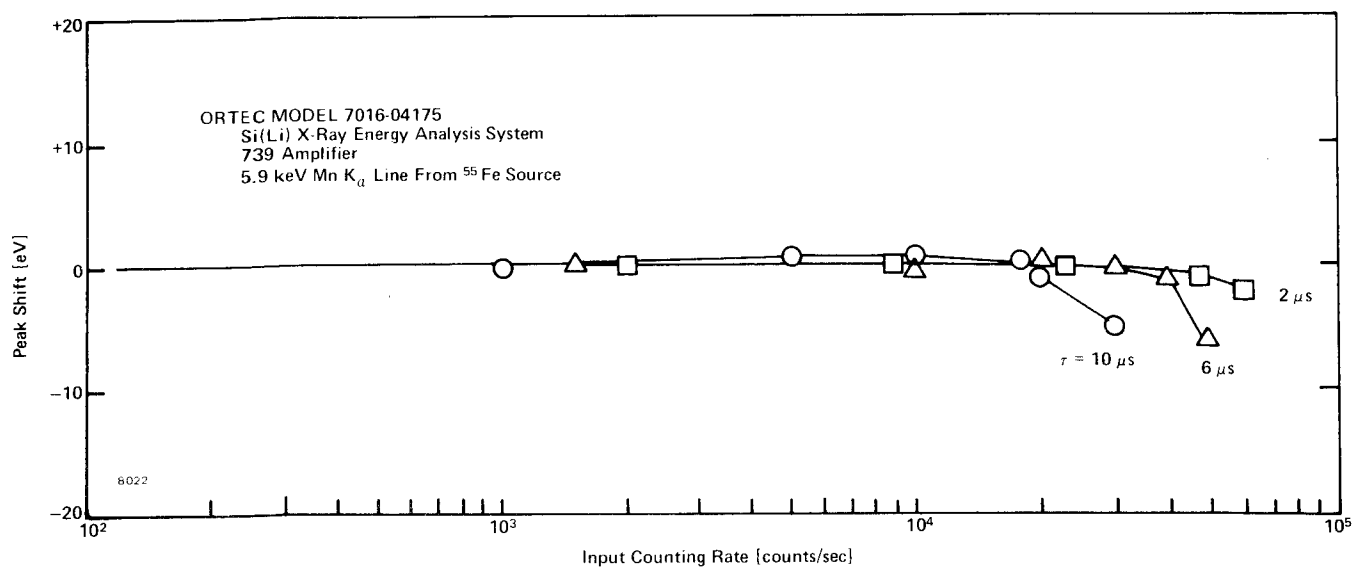


Figure 3. Baseline Stability vs. Counting Rate

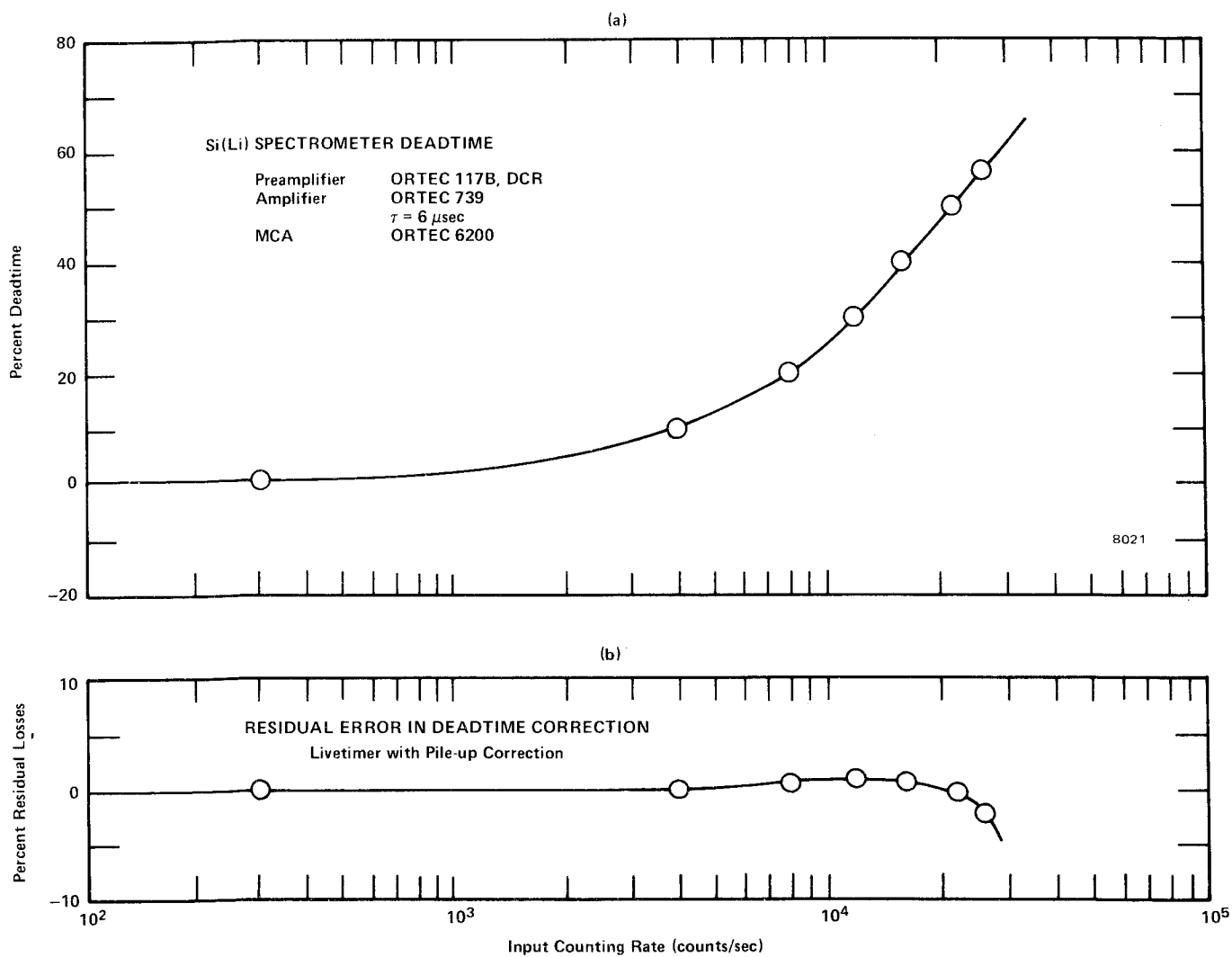


Figure 4. Si(Li) Spectrometer Deadtime



USE OF ADVANCED ANALYTICAL TECHNIQUES FOR CHARACTERIZATION OF THE  
CHEMICAL, PHYSICAL, AND CRYSTALLOGRAPHIC NATURE OF A SURFACE

R. E. Herfert  
Northrop Corp., Aircraft Division, Hawthorne, California

Abstract published in EMSA Proceedings

THE THIRD DIMENSION IN SCANNING ELECTRON MICROSCOPY: SCANNING  
AUGER MICROSCOPY

N. C. MacDonald  
Physical Electronics Industries, Inc., Edina, Michigan

Abstract published in EMSA Proceedings

SEM-AUGER SPECTROSCOPY  
CHARACTERIZATION OF SEMICONDUCTOR STRUCTURES

E. K. Brandis

IBM System Products Division  
East Fishkill Facility  
Hopewell Junction, New York 12533

Auger electron spectroscopy has become one of the most sensitive surface analysis tools. As first demonstrated by MacDonald<sup>1</sup> by combining electron spectroscopy with scanning electron microscopy, surface analysis with submicron spatial resolution can be obtained.

To prevent the carbon contamination observed with many commercial scanning electron microscopes, the vacuum system of the Cambridge Stereoscan was rebuilt and a gas jet technique incorporated.<sup>2,3</sup> With these SEM modifications it became possible to perform Auger analysis on relatively non-reactive samples like those encountered when analyzing processing steps of semiconductor materials.

P. Palmberg<sup>4</sup> pointed out that Auger electron spectroscopy is capable of providing information on chemical effects. For some materials the variation of the energy loss mechanism gives rise to a change of the low-energy side of the Auger peak. In the case of silicon, widely used in semiconductors, this effect can be exploited successfully to give information about the chemical environment of the surface.

Figure 1 depicts the differentiated  $\text{Si}_{\text{KLL}}$  Auger electron energy peaks of silicon ( $< 20\text{\AA}$  of  $\text{SiO}_2$ ),  $\text{SiO}_2$ ,  $\text{Si}_3\text{N}_4$  and PtSi. While there are minor variations between the last three peaks, there appear to be very noticeable changes in the peaks between silicon and bonded silicon.

One important step in semiconductor processing is the opening of transistor contact holes. Careful inspection after contact hole etching revealed a thin, rough surface film ( $< 1000\text{\AA}$  thick) on some transistor contacts as shown in the SEM micrographs (Fig. 2). The Auger spectrum of this film (Fig. 3) reveals the presence of Si, O and C. However, the  $\text{Si}_{\text{KLL}}$  peak resembles that recorded for bonded Si. This indicates the presence of  $\text{SiO}_2$  in the contact area.

During processing of another wafer, a thin, spotty film was observed as shown in the SEM micrographs (Fig. 4) after depositing silicon nitride. Auger spectra of the film and the area adjacent to it are shown in Fig. 5. The absence of nitrogen and the characteristic shape of the  $\text{Si}_{\text{KLL}}$  Auger peak in the spectrum from the residue suggest the presence of Si in an  $\text{SiO}_2$  matrix.

For the formation of ohmic contacts, sometimes thin PtSi films are formed at transistor contacts. Monitoring the integrity of the PtSi films can be performed with the SEM-Augur technique. For example, the excessive heat-treatment of the aluminum metal lands deposited over the PtSi contacts to provide connections between the various components of an integrated circuit caused the aluminum to react with the PtSi layer. SEM-Augur analysis of the PtSi surface after removing the aluminum lands by chemical etching



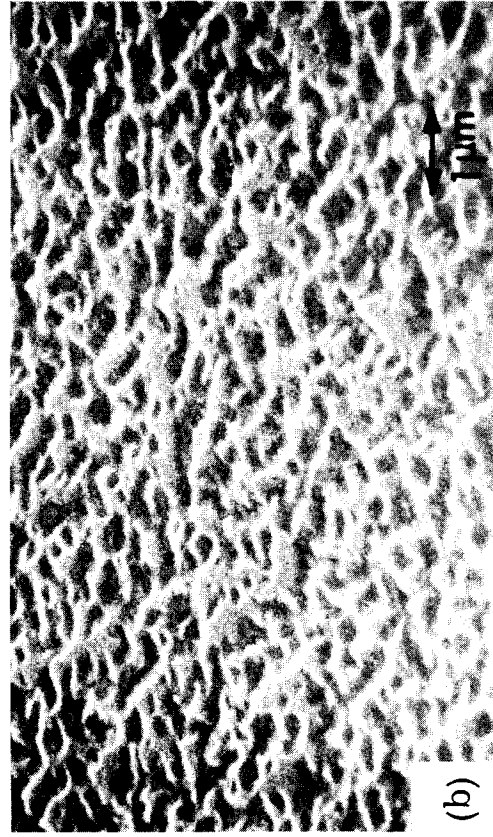
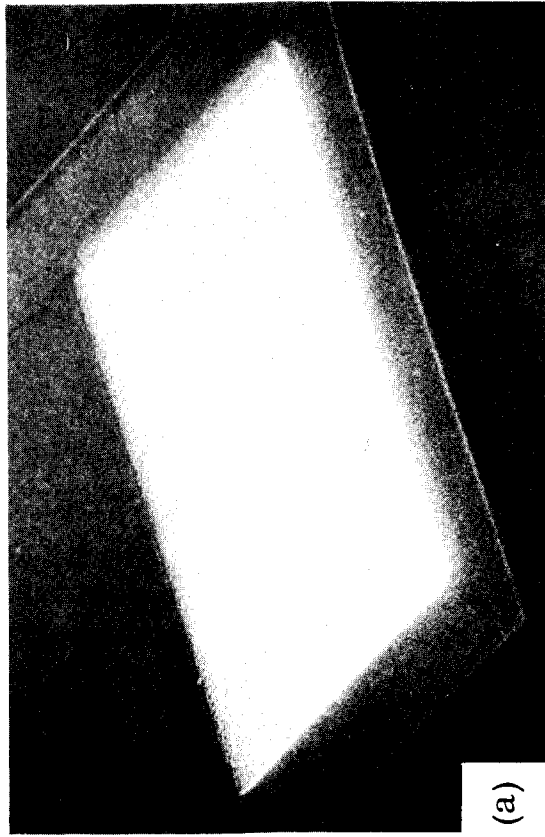


Fig. 2. Irregularity in contact area of a transistor.

(a) 800X,  $45^{\circ}$ ; (b) 9000X,  $45^{\circ}$ .

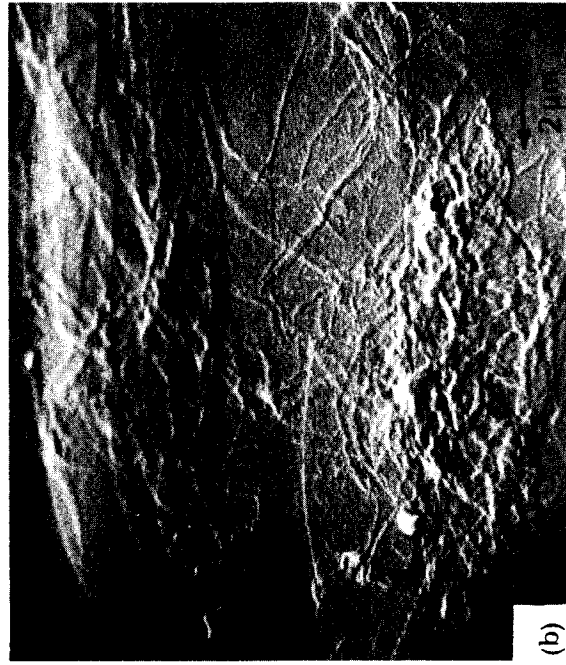
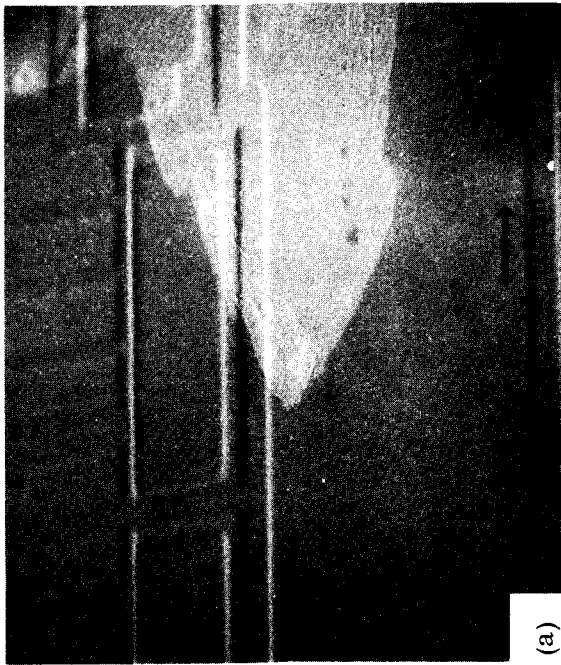


Fig. 4. Residue on silicon nitride.

(a) 600X,  $50^{\circ}$ ; (b) 6000X,  $50^{\circ}$ .

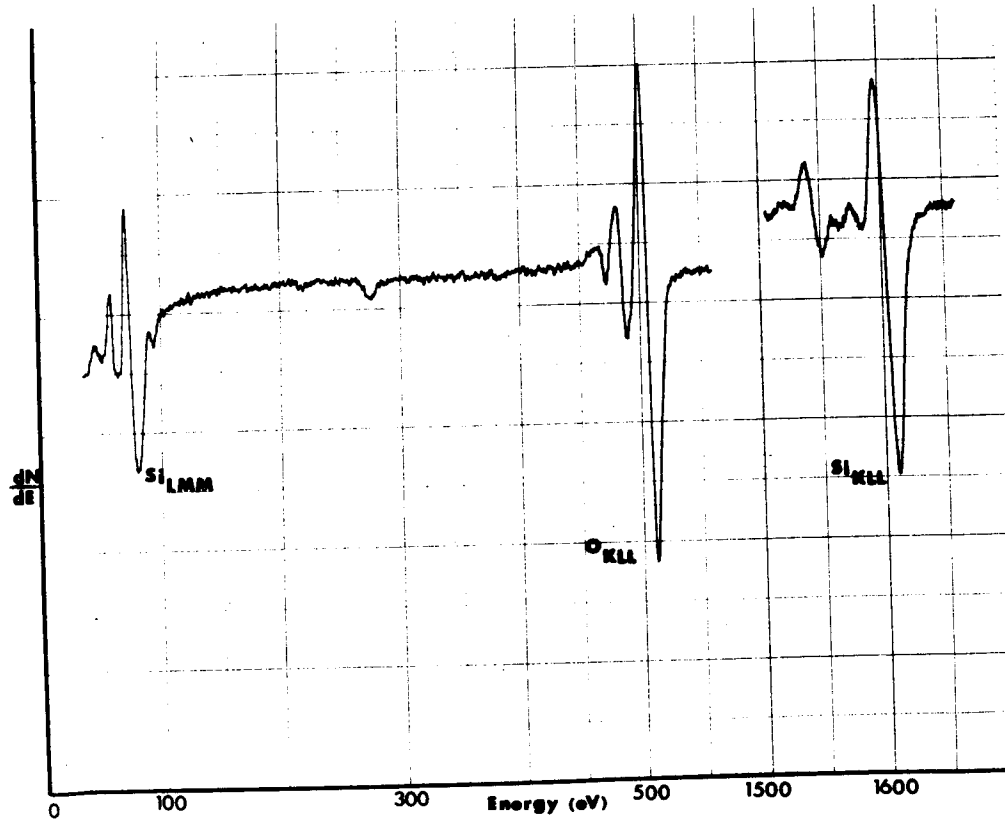


Fig. 3. Auger spectrum of irregularity in contact area.

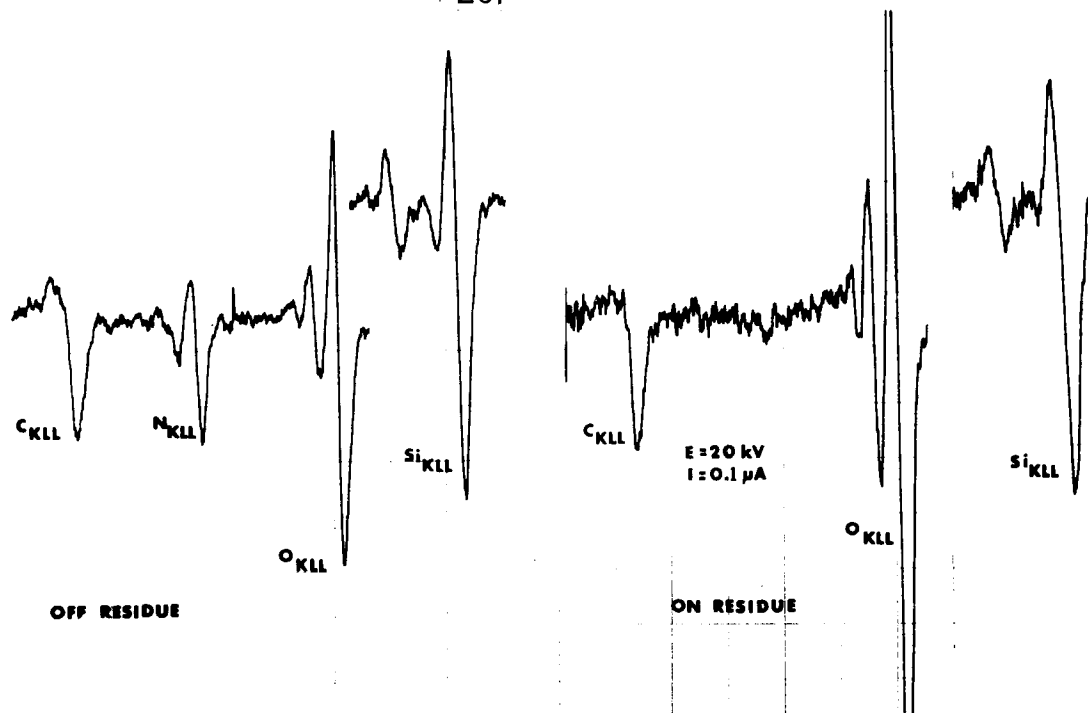


Fig. 5. Auger spectra of the residue and adjacent area (Fig. 4).

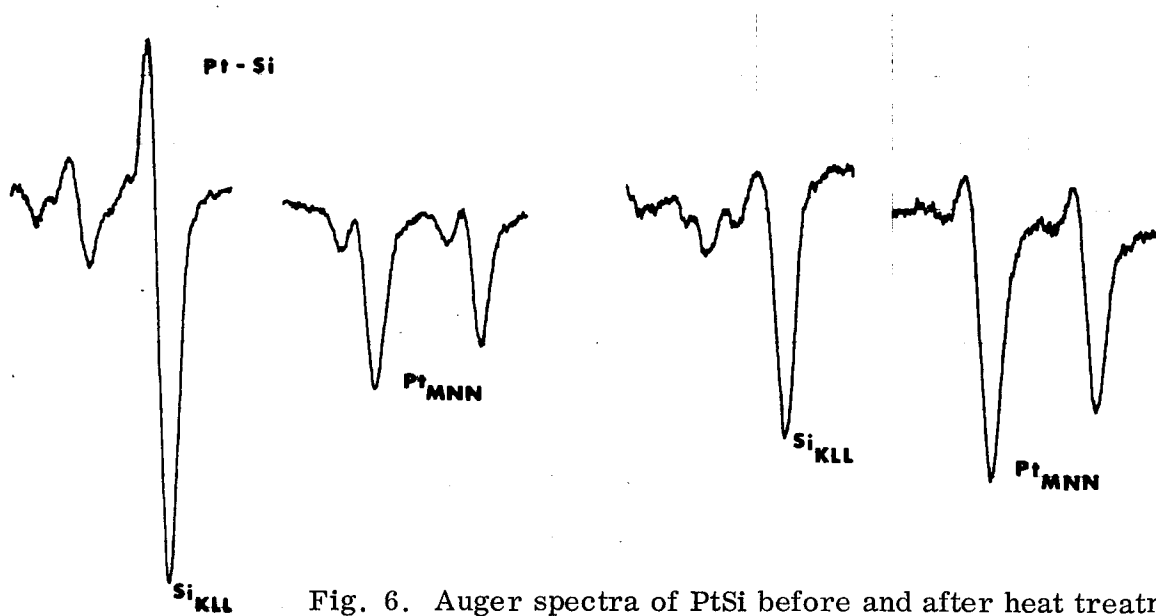


Fig. 6. Auger spectra of PtSi before and after heat treatment.



## APPLICATIONS OF AUGER ELECTRON SPECTROSCOPY (A.E.S.) TO PROBLEMS IN MICRO-ELECTRONIC MANUFACTURING PROCESSES

by

D. K. Conley  
Western Electric Company  
Allentown, Pennsylvania

In the production of semiconductor devices and microcircuitry, there are many processes involved which are very sensitive to surface chemistry. Examples are the evaporation or sputtering of a film to metallize a dielectric surface, lead attachment by solid-phase or thermocompression (T.C.) bonding, anodization of tantalum in the preparation of thin film resistors or capacitors, plating, etc.

Contamination in each of these manufacturing processes can result in immediate product failure or, even worse, could result in failure after the component has been integrated into a circuit and put into use. Therefore, as a precautionary measure the materials and the environment of the processes to be used in manufacturing Western Electric products are kept as clean as possible by cleaning cycles prior to many of the processing steps. This has necessitated investigations into in-process cleaning techniques. Examples will be shown where A.E.S. has been used to improve cleaning procedures and to eliminate cleaning cycles which were actually contaminating the product.

Conversely, A.E.S. has been used to show that the lack of a few monolayers of the necessary impurity oxides on alumina ceramic substrates can result in poor adhesion of metal conductor films.<sup>1</sup>

On one occasion we were bothered by gold-to-gold T.C. bonding problems simultaneously on three separate product lines. Although the problems were received individually by our laboratory, it soon became evident that they were associated.

A residue was sometimes evident on several types of copper lead frames after gold plating and the normal cleaning process. It was suspected that this residue was responsible for the poor gold-to-gold T.C. bonds. A.E.S. spectra will be presented of good and bad bond regions which will show that the residues are a mixture of a carbonaceous material and sodium carbonate. Identification of the residue constituents allowed one to postulate its origin and to suggest the necessary remedial action to eliminate it. In each case the contaminant was found to have originated from a lead frame, etc. which had been gold plated from a common bath.

The occurrence of carbon and sodium carbonate can be understood by a closer look at the gold plating bath and subsequent cleaning operations.

It is believed that carbon is present in the deposit as a polymer of HCN as reported by C. B. Munier.<sup>2</sup> This is supported by the presence of a nitrogen peak to be seen on the auger spectra. This polymer occurs in baths using cyanide as the reducible gold species. The sodium carbonate can be coming from (a) the City soft water rinses used after the plating operations and/or (b) the cyanide soak often used after plating to remove stains. The latter clean cycle is suspect since carbonates do build up in this system with time. It is also known that cyanides are difficult to rinse and if a thorough rinse does not follow the cyanide clean operation, residues containing cyanide and carbonates are quite feasible. The T.C. bonding problems virtually disappeared by (a) elimination of the cyanide cleaning step, (b) elimination of soft water rinsing, and (c) longer rinsing in D.I. water.

In our laboratory the usage of A.E.S. in conjunction with the electron microprobe has proved to be a powerful combination. Following is an example of such an instance:

A circuit was submitted to the laboratory from which leads were separating upon being touched. It was requested that we identify the interface at which the lead bond failure had occurred. X-ray images were taken with the electron microprobe of the failed leads and the region on the substrate from which they had separated. The X-ray images showed that there was a thick layer of chromium on the lead and no continuous film of tantalum nitride. From the X-ray images of the circuit bond area, it was seen that the tantalum nitride was a continuous film and that there was a thin discontinuous film of chromium on top of the tantalum nitride.

From this, one would have assumed that the bond failure occurred at the Cr-Ta<sub>2</sub>N interface and that the thin discontinuous film of chromium was due to carry over at separation.

Subsequent analyses of these samples by A.E.S. showed that there was a thin continuous film of carbon on top of the chromium film which was responsible for the bond failure. Thus one can see how the sensitivity of A.E.S. for very thin low atomic number films, e.g. carbides, nitrides, and oxides, can be utilized in this area where the electron microprobe is weak.

In addition to analyzing surface chemistry, the characterization of chemical concentration with depth can be obtained. This is possible since the auger analysis can be performed simultaneously with ion sputtering. Ion sputtering can be used to remove the surface atoms with rates varying from a fraction of a monolayer per minute up to approximately thirty monolayers per minute. This characteristic is very important in the micro-electronics industry since it allows us to analyze thin film interfaces with great in-depth resolution.

Concentration-depth profiles will be shown of anodized tantalum nitride which will show such features as the depth to which the anodization has proceeded, the interchange of carbon and nitrogen with the first several hundred angstroms of the anodized tantalum nitride, etc.

1. Conley, D.K., "Application of A.E.S. to Surface Chemistry Studies of Ceramic Substrates", Proceedings of 75th Annual Meeting of American Ceramic Society, Cincinnati, Ohio, May 1973.
2. Munier, G. B., Plating 56, 1151 (1969).

## ANALYSIS OF GAS AND SOLID SAMPLE BY ESCA

John F. Rendina, McPherson Instrument Corporation,  
Subsidiary of GCA Corporation, 530 Main Street,  
Acton, Massachusetts 01720

The photoelectron spectrometer for ESCA studies requires that the sample be in an ultra-high vacuum, present sufficient cross section to the ionizing source for measurable photoelectron emission and occasionally provide sample temperature control over a wide range. While many applications of ESCA are concerned with solid samples that are UHV compatible, the study of volatile samples and gases constitutes an appreciable application potential for ESCA. Furthermore, data interpretation may be significantly easier for samples in the gas phase with the elimination of solid state effects.

The McPherson Instrument Corporation ESCA 36 Photoelectron Spectrometer has been designed to overcome the typical restrictions described above.

A sample holder capable of temperature control from liquid nitrogen temperatures to over 400°C provides a means of measuring the photoelectron spectrum of liquids and gases in a condensed phase with the vapor pressure lowered to a sufficient value for UHV conditions. This variable temperature sample holder attaches to the ESCA 36 sample chamber and can be positioned from outside the chamber for sample deposition and then rotated for sample analysis, as shown in Figure 1. The sample temperature is controlled by a Dewar cold sink and/or a heater near the sample. A thermocouple is supplied to determine the temperature at the sample.

One of the most important aspects of low-temperature sample analysis is an ultra-high vacuum, free from residual gases that may condense on the sample itself. Since the concentration detectability of ESCA may typically be a fraction of a monomolecular layer of material on the surface, it is important that the pressure in the area of the sample be in the 10<sup>-10</sup> torr or better range. This is achieved in the ESCA 36 using a cryo pump virtually surrounding the sample and operating in the 10-18°K range.

Figure 2 is a carbon 1s photoelectron spectrum of acetone in the solid phase. Acetone vapor was condensed onto the sample holder at liquid nitrogen temperature and the photoelectron spectra obtained using Mg K $\alpha$  radiation.

A sample cell for gas and vapor analysis using X-ray photoionization for ESCA studies is shown in Figure 3, as used with the ESCA 36 sample chamber. The cell is sealed except for the entrance slit to the spectrometer which is small enough to maintain a pressure differential of better than 10<sup>4</sup>:1. The cryo pump within the sample chamber again insures an ultra-high vacuum in the X-ray area with up to 1 torr pressure in the sample cell. Figure 4 is a carbon 1s spectrum of acetone in the vapor state. Note the increased resultant resolution over the acetone data in the solid phase, which illustrates one of the advantages of gas phase ESCA.

A study of conduction band or valence electron binding energies with a photoelectron spectrometer may be limited by the natural half width of the ionizing radiation even when using an X-ray monochromator. Studies with the ESCA 36 using the helium resonance line at 21.2 eV indicate considerable improvement can be obtained in resolution, signal level and signal to background. Conventional X-ray monochromators may reduce the width of the X-ray characteristic line to about 0.3 eV; however, the natural width of the helium 21.2 eV line is much less than 0.01 eV or, in other words, contributes nothing to the final resolution of the spectrum.

Figure 5 illustrates the VUV/solid accessory for the ESCA 36. The sample may be any solid, with provisions made for evaporation or argon ion cleaning in the sample chamber. The cryo pump provides UHV conditions during deposition, cleaning and analysis. The 21.2 eV radiation from the source strikes the sample in front of the spectrometer entrance slit and the photoelectrons are subsequently analyzed. Figure 6 is a spectrum of a freshly-deposited gold film using the 21.2 eV source. While the basic shape of the conduction band remains similar to that of X-ray photoelectron spectroscopy, the Fermi level is much more pronounced with an overall improvement in resolution and signal to background.

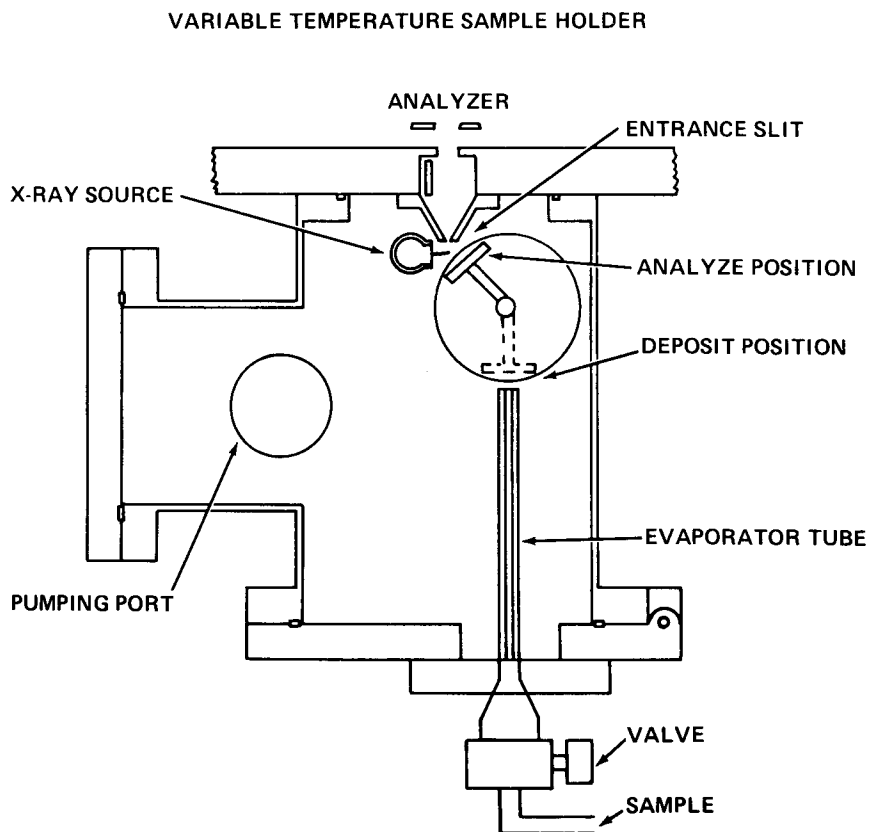


Figure 1

ESCA 36-G  
VARIABLE TEMPERATURE SAMPLE HOLDER

SAMPLE ACETONE (SOLID)  
TEMP. -196°C  
X-RAY Mg 280 WATTS  
SCAN TIME 80 SECONDS  
SCAN RANGE 12 eV

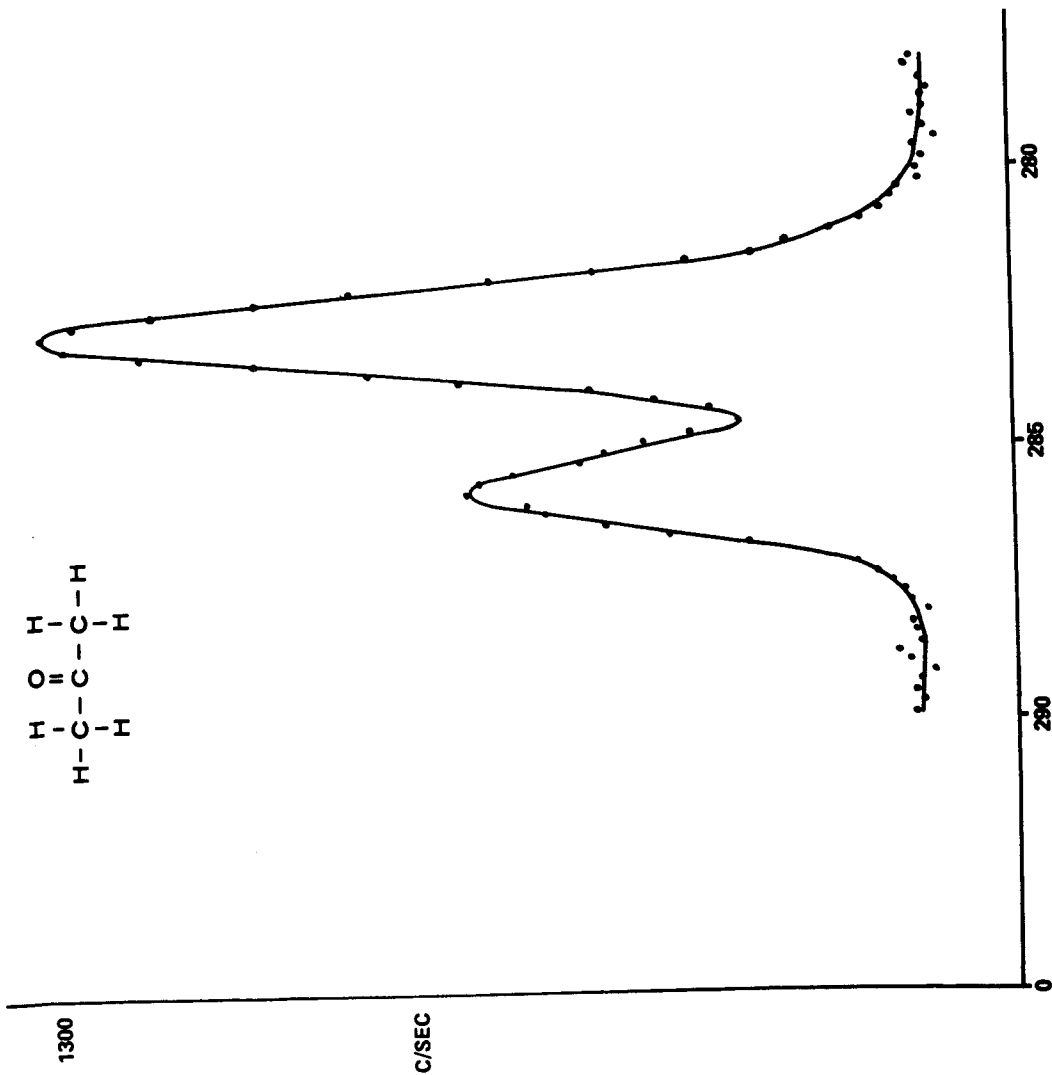


Figure 2

SAMPLE ACETONE  
EXCITATION Mg K $\alpha$  (340w)  
SCAN RANGE 11 eV  
SCAN TIME 23 min

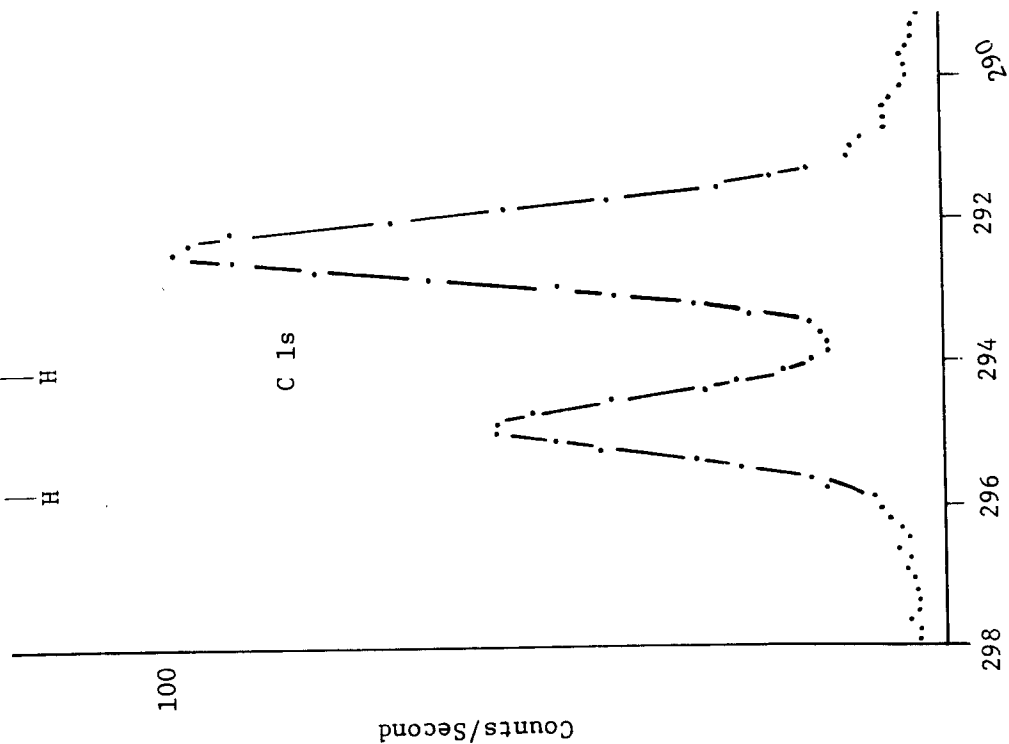
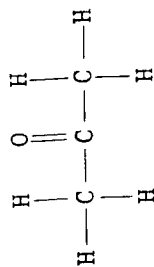
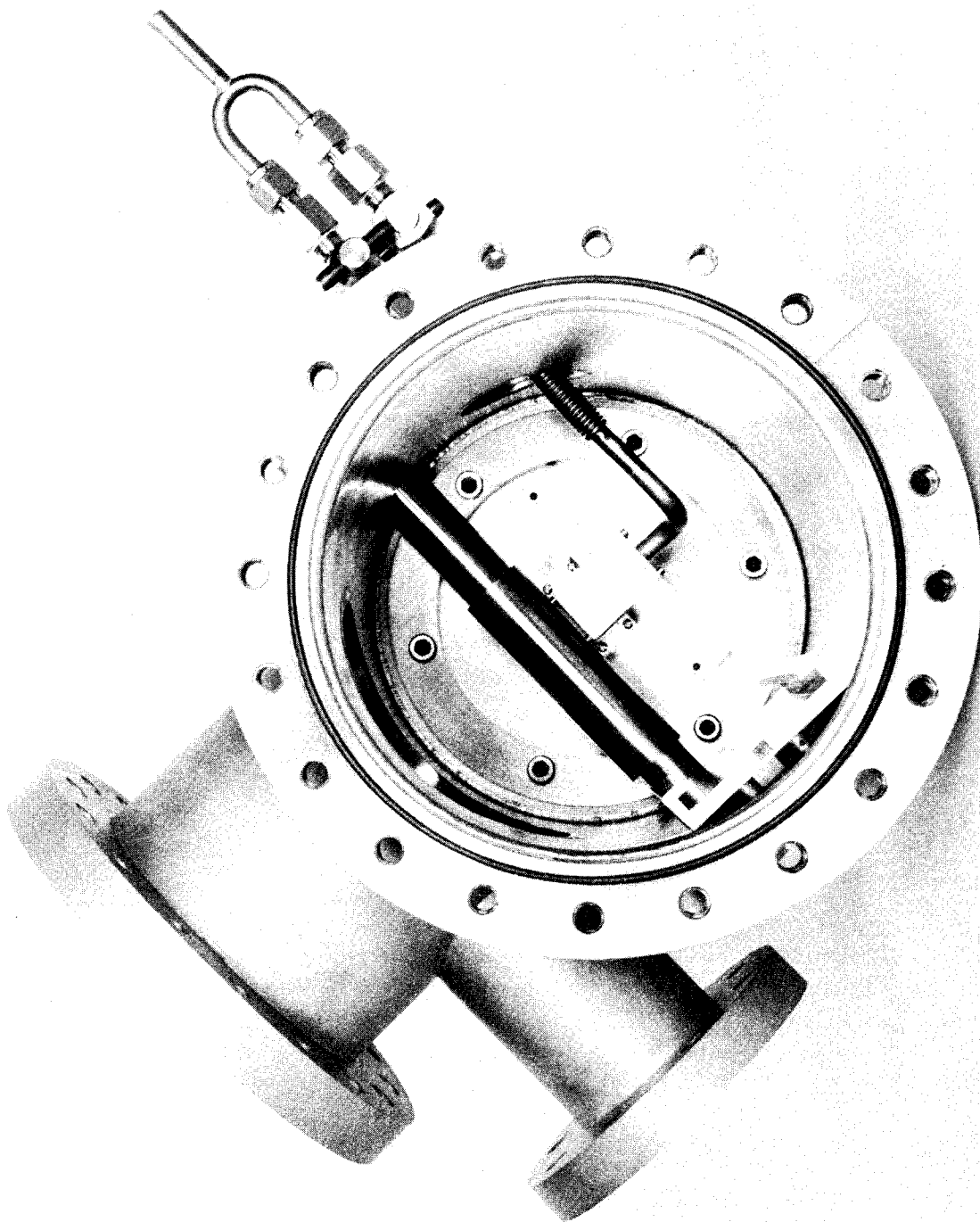


Figure 4



ESCA 36-U

GAS PHASE SAMPLE HOLDER

Figure 3

VUV PES OF SOLID SAMPLE

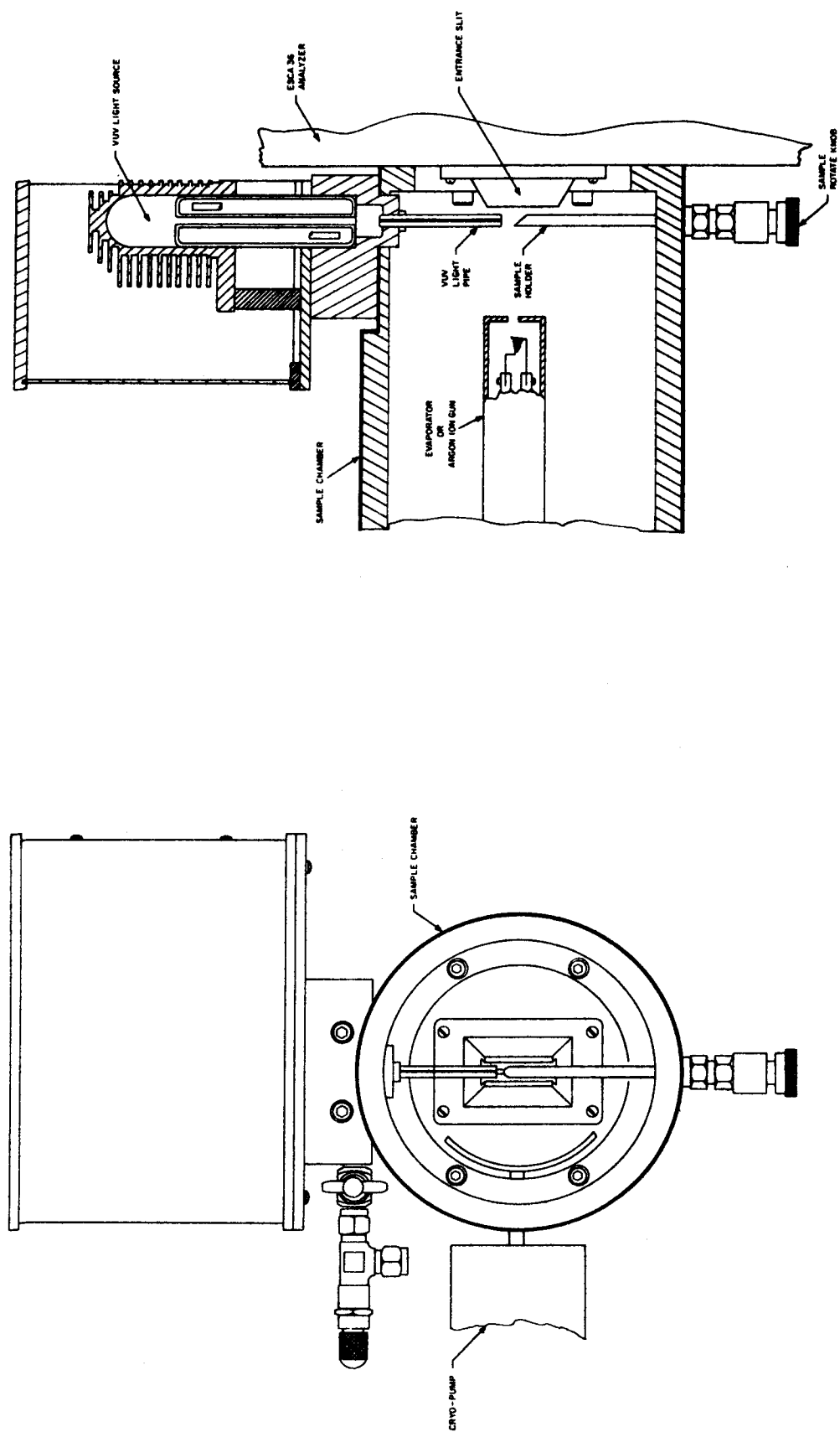


Figure 5

ESCA 36

Date 9/8/72

SAMPLE Au  
IE 11.0  
DE .036  
EXCITATION He 21.2eV  
S/B 80:1  
S/N 100:1

PRELIMINARY DATA  
Resolution not optimized

For comparison, see:  
D. E. Eastman, Phys. Rev. Lett.,  
26, 1108 (1971)

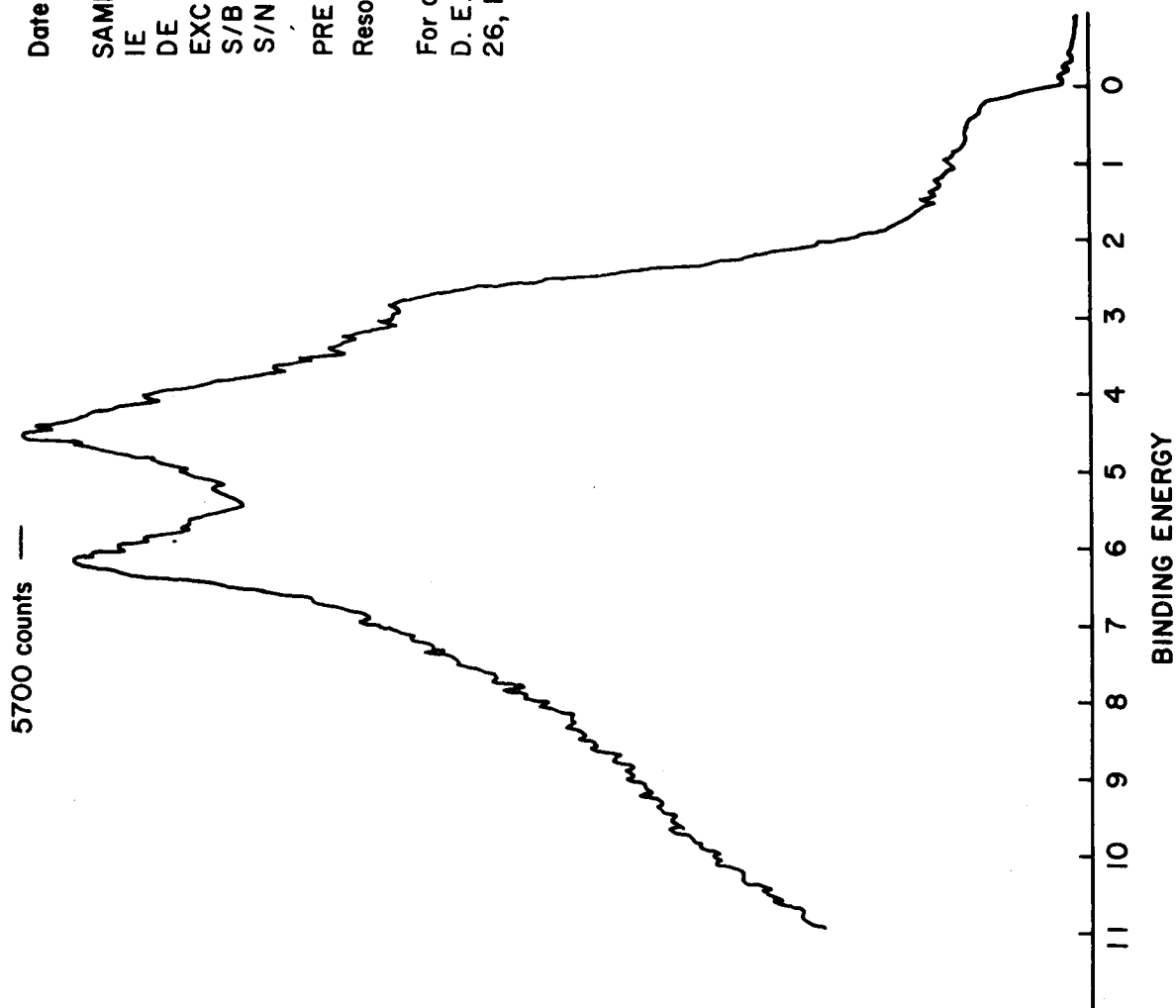


Figure 6



ION SCATTERING SPECTROMETRY -  
SENSITIVITY, RESOLUTION, and QUANTITATIVE CONSIDERATIONS

J. A. Leys and J. T. McKinney

3M Company, St. Paul, Mn. 55101

Since ion scattering is being used increasingly for analysis of surface layers, there is considerable interest in its quantitative possibilities. In this paper we point out the primary features to be considered in estimating the sensitivity and resolution of ion scattering as an analytical tool.

The basic principle of ion backscattering is illustrated in Figure 1. A beam of ions of well-defined energy impinges on a surface to be examined. The ions emerging from the surface at a particular angle to the incident beam are energy analyzed, and thus the energy loss in the scattering process is established. Since the dominant mode of energy loss at these energies is due to binary elastic collisions of the incident ion with the surface atoms, the mass of the scattering atom can be uniquely determined from the energy of the scattered ion. For the case of scattering through  $90^\circ$  this relation is very simple and can be expressed as shown in Figure 1.

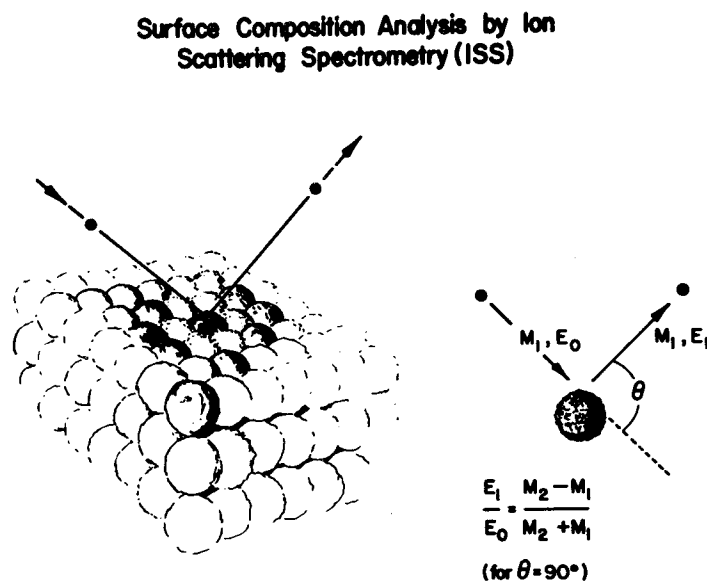


Figure 1  
Schematic representations of surface analysis by ion scattering. Upon scattering through  $90^\circ$ , incident ion of mass  $M_1$  suffers an energy loss ( $E_0 - E_1$ ) that is a function of the mass  $M_2$  of the surface atom.

A schematic of the instrument used in the analysis is shown in Figure 2. The ion gun is designed to provide a collimated mono-energetic beam of ions. The apertures of the energy analyzer are selected to give the highest sensitivity without sacrificing instrument resolution; the detector generally used is a channel electron multiplier in the pulse-counting mode.

With regard to sensitivity, there are two aspects to be discussed; the variation in sensitivity for different elements, and the lower limits on sensitivity. Basically, the number of back scattered ions per unit solid angle can be calculated using the appropriate potential; for the scattering of the ions at the energies of interest, the screened coulomb potential is valid, and the calculated cross sections are shown in Figure 3.<sup>1</sup> Assuming the validity of these calculations for scattering from atoms is a solid, it is still necessary to know the region over which scattering can occur and the probability of neutralization of the recoiling helium. It has been shown that the back scattered ions originate only in the outermost atomic layer.<sup>2</sup> Thus the surface area that can see both the exit aperture of the gun and the entrance aperture of the analyzer will be analyzed. For rough surfaces, this can be less than the total surface area, and makes absolute measurements difficult. The rate of neutralization has not been thoroughly investigated at the energies of interest here, but some indications of its importance can be established by scattering experiments using different isotopes of a given probe ion. The scattering cross sections shown in Figure 3, for instance, are virtually identical for scattering by <sup>3</sup>He and <sup>4</sup>He; the probability of neutralization, however, is generally felt to be a function of the residence time of the ion in the neighborhood of the surface, or the inverse of the ion velocity.<sup>3</sup> Thus at the same energies appreciable differences in signal levels for <sup>3</sup>He and <sup>4</sup>He are expected if the neutralization probability is a dominant consideration.

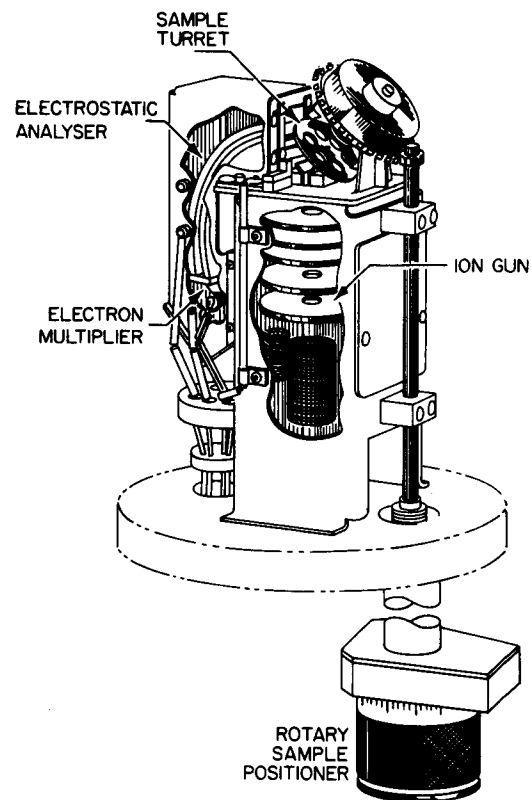


Figure 2  
Schematic of Ion Scattering instrumentation. Ion gun provides collimated, mono energetic ion beam 300 eV to 3 keV.

<sup>1</sup> Computed under these conditions by R. Honig, from reduced calculations of F. W. Bingham

<sup>2</sup> See, for instance, H. H. Brogersma & P. M. Mul, Chem. Phys. Lett. 14 (380) 1972

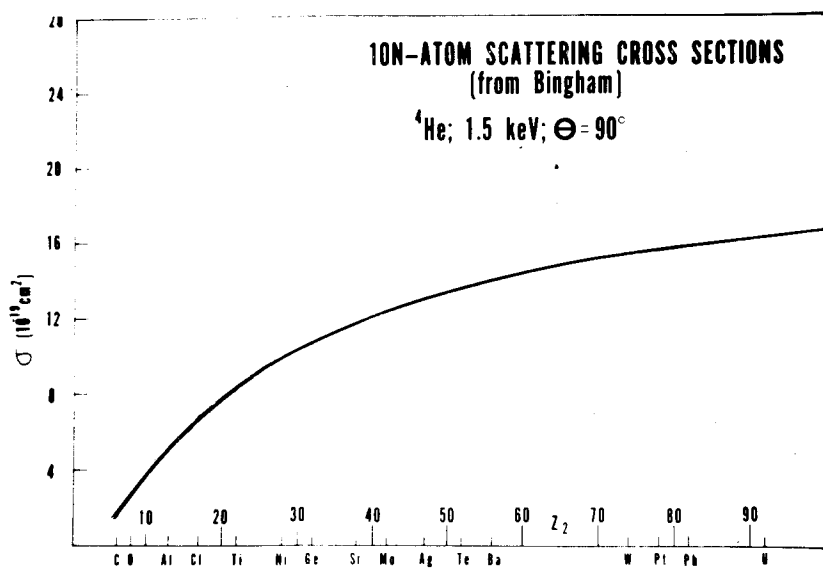


Figure 3  
Cross sections for ion-atom scattering, using screened-coulomb potential.

For scattering from heavy metals, the observed signal is the same for  ${}^3\text{He}$  and  ${}^4\text{He}$ , but the results for scattering from carbon indicate significantly enhanced sensitivity for the lighter isotope  ${}^3\text{He}$ . Further, changes in the observed sensitivity with incident ion beam energy substantiate the view that neutralization effects are considerably more important for scattering from light elements. Signal levels for the heavier elements generally decrease with increasing energy, as predicted from cross section calculations; the results for helium scattering from carbon, however are entirely different, as shown in Figure 4. These data show an increase in signal level that is exponential in  $1/\sqrt{E_0}$ , consistent with the idea that the carbon peak heights are determined primarily by the neutralization coefficient. Thus it is clear that a direct application of the calculated cross sections to determine concentrations from peak heights is insufficient for the case of light elements. This does not prevent the technique from making comparative studies of light element concentrations, however. Figure 5 shows an example of a beryllium copper alloy that was treated to change the surface concentration of beryllium; the degree to which this has been accomplished can be adequately investigated by the peak height ratio. The lower limit to the sensitivity of ion scattering is fixed by the noise, which is of two kinds. First is the shot noise, which is the statistics of counting random pulses. Increasing the integration time reduces this shot noise at a cost of averaging over more atomic layers, which are being sputtered during the integration time. Typically, with the collection efficiency presently obtainable, a reduction of the shot noise to a few percent of the peak height is obtainable while examining a single atomic layer. One other origin of ions is the background count rate which is evident, for instance, under the oxygen peak in the spectra of Figure 5. At present, the exact origin of these ions is uncertain, but it is felt that they are from inelastic collisions or multiple elastic collisions. In most cases this background presents no problem to the identification of a peak, since the background is smoothly varying and is free of structures that could be mis-construed as a spectral peak. It should be noted that this type of low energy tail is completely absent when Neon is used as the probe ion.

## HELIUM ION SCATTERING FROM CARBON

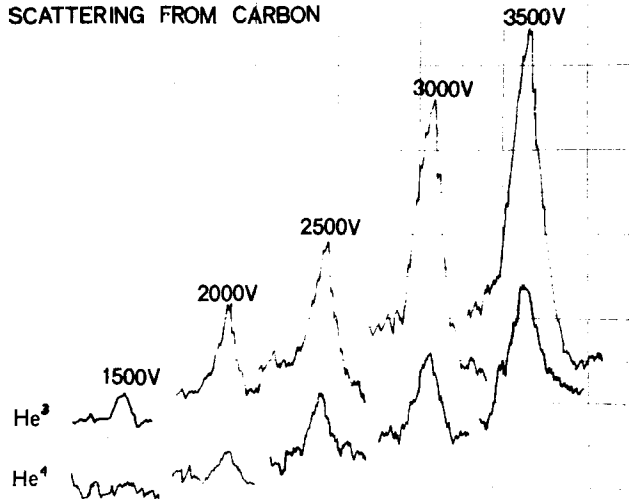


Figure 4

Scattering of helium from carbon. Difference between  $^3\text{He}$  and  $^4\text{He}$  scattered signal indicates the importance of the neutralization rate.

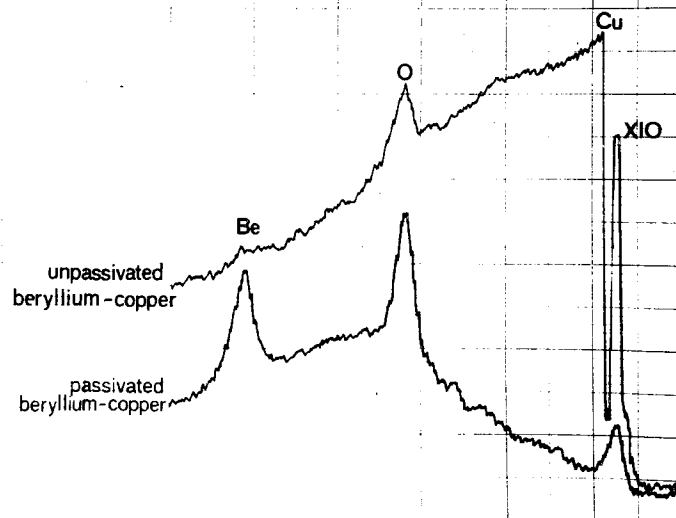
 $^3\text{He}$  SCATTERED ION SPECTRA OF BERYLLIUM COPPER ALLOY  
3500V

Figure 5

$^3\text{He}$  ion scattering spectra of beryllium copper alloy before and after passivation. Surface concentration of copper is markedly diminished and that of beryllium is increased by the passivation.

The resolution of the ion scattering spectrometer is determined by the peak separation and the experimental peak width. The peak separation is calculable from the equation in Figure 1; it is maximized for nearly equal probe ion and target atom masses and it becomes progressively less for a large ratio of the masses. The available inert gas ion masses present a reasonable sequence of probe ions so that a maximum separation is most often obtainable. The experimental resolution, however, is also dependent on the peak widths, as well as on their separation. For completely elastic binary collisions, one would expect the peak width to depend only on the resolution of the energy analyzer and the possible variation in scattering angle for those ions admitted to the analyzer. The energy resolution can be made as small as 0.5% without difficulty, but the variability in scattering angle is more uncertain. There can be a contribution to the variability from the width of the slits, the width of the illuminated area and the divergence of the focussed ion beam. For a given set of experimental parameters, i.e. a given variability in scattering angle, the resultant peak width is a function of the mass ratio. Thus it is difficult to generalize with complete accuracy about the attainable resolution, but most often a resolution of two peaks is possible if they are separated by 5% in mass.

From the standpoint of the practicing analyst, the most straightforward technique for establishing sensitivities, as well as resolution, is comparison with standards. Since the scattered signal originates from only the outer monolayer of the specimen surface the problems associated with electron probe analysis which are related to finite beam penetration and X-ray signal attenuation or enhancement by the specimen bulk should not be experienced. In addition, since ion scattering behaves according to classical binary collision formulae one would not expect "matrix" effects in the scattering signal between various atoms present in the specimen surface. Ion Scattering data have been taken on several known polycrystalline compounds in order to determine if quantitative measurements are as straight forward as anticipated. In each case the ion scattering spectrometer was calibrated in a manner analogous to that used for electron probe analysis i.e. by the use of polycrystalline elemental standards to perform analysis of surface atom populations of the compound. One example (Figure 6), shows the ion scattering spectra of zinc metal and a zinc oxide film using both neon 20 and helium 3 probe gases. Calculations based on the signal obtained from zinc metal and the zinc to zinc atomic distances in zinc metal and zinc oxide yielded the theoretical zinc peak height as shown for zinc oxide for each probe gas. The measured scattered ion intensity for zinc on zinc oxide using neon 20 probe gas agrees favorably with the theoretical value whereas with helium 3 probe gas the measured intensity is substantially less than theoretical.

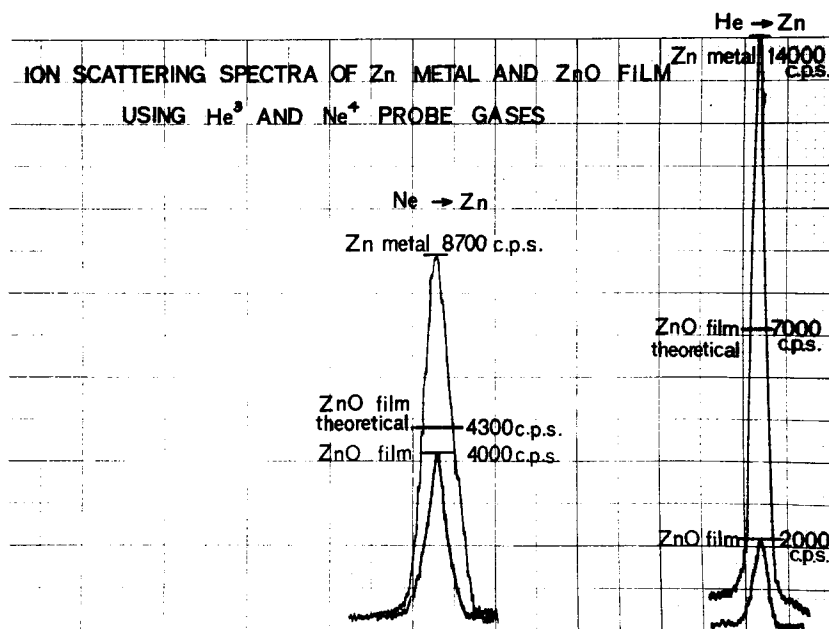


Figure 6  
Comparison of  $^3\text{He}$  and  $^{20}\text{Ne}$  zinc spectra from zinc metal and from zinc oxide.

All data taken to date on various "known" systems have shown the same type results i.e. agreement to within  $\pm 10\%$  of the theoretical value using neon 20 probe gas and significantly lower intensities than predicted with helium 3 probe gas. At this time it must be concluded that the suppressed helium ion signal must be due to greater helium ion neutralization by the compound than by the metal. For analyses using helium probe gas it remains then to work out these "neutralization" factors before a universally quantitative system can be established. Presently, it appears that Neon is the most useful probe gas, both because comparison between standards gives expected results, and because of the complete absence of the low energy tail observed with helium.

## Progress in Quantitative Electron Probe Microanalysis

Kurt F. J. Heinrich  
Institute for Materials Research  
National Bureau of Standards  
Washington, D. C. 20234

Electron probe microanalysis was considered a quantitative technique since its inception, and a considerable array of theoretical arguments tends to confirm this contention. It was not until the systematic investigations of Poole and Thomas [1] that the limitations of accuracy of the technique, as then performed, were put in evidence. An analysis of the sources of error in electron probe microanalysis [2-6] indicates the following significant causes for poor accuracy:

a. A poor choice of operating voltage and/or x-ray emergence angle frequently caused large errors in the absorption correction factors.

b. The "true" values of some of the analyzed specimens depended frequently on uncertain assumptions of perfect stoichiometry, microscopic homogeneity, and/or chemical analysis free of errors. Hence, the apparent error distribution may have been exaggerated.

c. Uncertainties in the theoretical assumptions — in parameters and constants — such as mass absorption coefficients — and simplifications in the calculation procedures, have increased the errors in some instances.

The failure or inaccuracy of theoretical assumptions has been discussed in great detail since the publication of Poole and Thomas' papers. The availability of large computers now permits the explicit treatment of some aspects, such as stopping power, which previously was treated in an abbreviated form. A particularly significant step in the theoretical treatment is the inclusion of the correction for fluorescence due to continuous radiation, which is the subject of detailed

studies by Hénoc [7] and Springer [8]. The effects of the fluorescence due to the continuum are incorporated in the program COR 2 [9] which should be considered the present state-of-the-art in data reduction for quantitative electron probe microanalysis.

A close inspection of the progress achieved in the last ten years discloses that the main factors in the improvement of the obtained accuracy are a more critical treatment of the absorption correction, and the operation variables related to it. Some apparent improvement is also due to the rejection of doubtful "known specimens".

Although the consideration of the fluorescence due to the continuum, and other theoretical improvements, are significant, in certain cases, the uncertainties arising from the theoretical factors can be minimized by a prudent selection of operating conditions, and by judicious adjustment to experimental evidence of the theoretical framework.

As a consequence, simplified programs applicable to on-line analysis become practical, without significant loss of accuracy, once the adjustment has been performed on the correction formulae so as to conform to experimental evidence. In the process, some of the formal rigor of the theoretical models is shown to be of more apparent than real value, and the semi-empirical nature of the well-adjusted model becomes evident.

The progress in computer availability has increased the use of Monte-Carlo calculations of parameters related to electron-target interaction. These calculations will be extremely useful for odd geometries such as thin films and particles. It is doubtful, however, that they will improve the accuracy of the analysis of semi-infinite specimens, since the uncertainties in the parameters concerning deceleration and scattering of electrons, as well as those relating to x-ray production, still exist.



Further improvement of the analytical accuracy will be difficult at best to achieve, and most customers seem content with the present state of quantitative analysis. Therefore, there appears to be little incentive for further refinements of the theoretical correction models.

#### References

- [1] Poole, D. M. and Thomas, P. M., in "The Electron Microprobe," McKinley, T. D., Heinrich, K. F. J., and Wittry, D. B., Editors, p. 269, John Wiley & Sons, Inc., New York (1966).
- [2] Heinrich, K. F. J., in "Advances in X-ray Analysis," 11, Newkirk, J. B., Mallett, G. R., and Pfeiffer, H. G., Editors, p. 40, Plenum Press, New York (1968).
- [3] Yakowitz, H. and Heinrich, K. F. J., Mikrochim. Acta, 182 (1968).
- [4] Heinrich, K. F. J. and Yakowitz, H., Mikrochim. Acta, 905 (1968).
- [5] Heinrich, K. F. J. and Yakowitz, H., Mikrochim. Acta, 123 (1970).
- [6] Heinrich, K. F. J., Anal. Chem. 44, 350 (1972).
- [7] Hénoc, J., in National Bureau of Standards Special Publication 298, Heinrich, K. F. J., Editor, p. 197, U.S. Government Printing Office, Washington, D. C. (1968).
- [8] Springer, J., Jb. Miner. Abh. 106, 241 (1967).
- [9] Hénoc, J., Heinrich, K. F. J., and Myklebust, R. L., National Bureau of Standards Technical Note 769, U.S. Government Printing Office, Washington, D. C. (in press).

STATISTICAL CHECK OF ELECTRON PROBE  
MICROANALYSIS MEASUREMENTS

M. ANCEY and R. TIXIER  
IRSID - 78104 Saint Germain en Laye - France

In electron probe microanalysis, X ray intensities are usually measured using gas flow or solid state proportional detectors.

X ray emission under electron bombardment is a random process. Photon conversion to electric impulses is also random by nature. Thus, the measured pulse number is random too.

On the other hand some scattering of measured values can occur due to various possible apparatus shifts. It should be detected and eliminated to insure good quality measurements.

Hardware.

Many interfaces have already been described for electron probe microanalysis data acquisition <sup>(1 - 5)</sup>, some include the computer. This hardware effort should be associated with instrument improvement : for instance in most electron probe analysers the accelerating voltage is still improperly measured.

Statistics.

In fixed time procedure the count distribution is generally of Poissonian type <sup>(6) (7)</sup>, and can be assimilated to a Laplace Gauss type, with the variance equal to the mean. In fixed total count number procedure the distribution of times is of Gamma type <sup>(8)</sup>, but can generally be considered as normal.

With a given series of n counts the problem consists in checking the validity of the measurement and eventually improving it by filtering

outlier count numbers.

### Outlying count numbers.

The tendency is to discard exceptional values as not belonging to the set. It is more correct to follow a policy for which the probability of wrong decisions is known. Among various statistical tests one must select those related to the experimental conditions.

Of course one first examine the extreme values  $x_1$  and  $x_n$  after having arranged the  $n$  counts in ascending order. The true mean and variance are not known and more than one value can be outlying. In such a case a convenient test has been described by DIXON <sup>(9)</sup>.

One forms the ratios

$$r_1^n = \frac{x_n - x_{n-1}}{x_n - x_1} \quad \text{and} \quad r_1^1 = \frac{x_2 - x_1}{x_n - x_1} \quad (n \leq 10)$$

$$r_2^n = \frac{x_n - x_{n-2}}{x_n - x_3} \quad \text{and} \quad r_2^1 = \frac{x_3 - x_1}{x_{n-2} - x_1} \quad (n > 10)$$

Table 1 gives the limit-values.

If  $r$  is too large, the count number is discarded and the test is continued for the next extreme value. In our program we have chosen the 5 % confidence level.

### Quality control.

The filtered count numbers must be examined in order to know whether they are really extracted from a normal distribution. The usual test consists in calculating the chi square. In some cases the chi square will be larger than the 5 % limit. In such cases it will be interesting to try and improve the measurement by using a more effective test for outlying observations.

### Consistency control.

A test described by GRUBBS makes it possible to discard the count numbers which cause asymmetry in the distribution. If  $x_a$  is the extreme count number in the measure with mean  $m$ , without  $x_a$  the mean

becomes  $m'$ .

One forms the ratio

$$\frac{S_n^2}{S^2} = \frac{\sum_{i=1}^{n-1} (x_i - m')^2}{\sum_{i=1}^n (x_i - m)^2}$$

Table II gives the limit values.

We reject the count number when the ratio is smaller than the 5 % limit and then the test is reiterated.

Of course all the tests are run by programs. If all count numbers are rejected one can conclude that the measurement is inconsistent and the instrument has to be checked.

If enough count numbers are saved one checks the new chi square. Then the new mean value is introduced in the correction programs.

#### Advantages.

It is to be emphasized that one saves a lot of money and computer time by filtering the values before corrections and not after.

Systematic use of such statistical controls results in more reliable data, continuous control of the instrument and also long term stability control. After some time the chi square obtained with the same  $n$  counts number can be tested, they should have a chi square distribution, otherwise the instrument needs a good check up.

#### References.

- (1) - E. LIFSCHIN, R. E. HANNEMAN (1966).

Electron Microbeam Probe Analysis.

II automated data collection and computer analysis.

General Electric Report n° 66 C 250.

- (2) - A. A. CHODOS, L. ALBEE (1971).

Quantitative microprobe analysis and data reduction using an on line mini computer.

EPASA Proceedings, 6, 15.

- (3) - F. KUNZ, E. EICHEN, G. MATTHEWS, S. PINER (1971).  
Electron Microprobe Automation.  
EPASA Proceedings, 6, 18.
- (4) - T.D. KIRKENDALL, P.F. VARADI (1971).  
An automated microprobe under PDP-8 control, using an  
IBM 360/65 for program and data storage.  
EPASA Proceedings, 6, 19.
- (5) - J.W. COLBY (1972).  
Microprobe analysis integrated automation computer system.  
EPASA Proceedings, 7, 67.
- (6) - K.F.J. HEINRICH (1960).  
Count distribution and precision in X-ray fluorescence  
analysis.  
Adv. in X-ray analysis, 3, 95-107.
- (7) - T.O. ZIEBOLD (1967).  
Precision and sensitivity in electron microprobe analysis.  
Anal. Chem., 39, 858-861.
- (8) - A. KOHN, J. ULMO (1958).  
Quelques considérations statistiques sur la mesure de  
l'activité de substance radioactives.  
Revue de Statistique Appliquée, 6, 9-55
- (9) - W.J. DIXON (1953).  
Processing data for outliers.  
Biometrics, 9, 74-89.
- (10) - F.E. GRUBBS (1950).  
Sample criteria for testing outlying observations.  
Annals of Mathematical Statistics, 21, 27-58.

Acknowledgement.

We would like to thank Dr. BASTENAIRE for the benefit of frequent discussions during the course of this work. This research is part of a larger project financed by the CECA.

VALEUR CONTROLEE	n	1 - $\alpha$ = 0,95	1 - $\alpha$ = 0,99
1	3	0,941	0,988
	4	0,765	0,889
	5	0,642	0,780
	6	0,560	0,698
	7	0,507	0,637
	8	0,468	0,590
	9	0,437	0,555
	10	0,412	0,527
	11	0,637	0,745
	12	0,600	0,704
2	13	0,570	0,670
	14	0,546	0,641
	15	0,525	0,616
	16	0,507	0,595
	17	0,490	0,577
	18	0,475	0,561
	19	0,462	0,547
	20	0,450	0,535
	21	0,440	0,524
	22	0,430	0,514
	23	0,421	0,505
	24	0,413	0,497
	25	0,406	0,489
	26	0,399	0,486
	27	0,393	0,475
	28	0,387	0,469
	29	0,381	0,463
	30	0,376	0,457

Table I - DIXON <sup>(9)</sup>

n \ $\alpha$	0,01	0,05
3	0,0001	0,0027
4	0,0100	0,0494
5	0,0442	0,1270
6	0,0928	0,2032
7	0,1447	0,2696
8	0,1948	0,3261
9	0,2411	0,3742
10	0,2831	0,4154
11	0,3211	0,4511
12	0,3554	0,4822
13	0,3864	0,5097
14	0,4145	0,5340
15	0,4401	0,5559
16	0,4634	0,5755
17	0,4848	0,5933
18	0,5044	0,6095
19	0,5225	0,6243
20	0,5393	0,6379
21	0,5548	0,6504
22	0,5692	0,6621
23	0,5827	0,6728
24	0,5953	0,6829
25	0,6071	0,6923

Table II - GRUBBS <sup>(10)</sup>

Performance Evaluation of FRAME — an On-line Theoretical  
Program for Electron Probe Microanalysis

R. L. Myklebust, H. Yakowitz, and K. F. J. Heinrich

Abstract

The program FRAME (Fitted Relations for Analytical Microprobe Equations) is based on the classical theoretical models for calculation of mass fractions from relative intensity data. It requires about 3.5K words of computer space and is primarily intended for on-line use in real time. FRAME requires as input only the operating voltage, the atomic numbers of the elements in the specimen, the x-ray lines used, the counting time, the x-ray intensities for specimen and standards, and their respective backgrounds. Alternately, FRAME accepts k-values and performs the appropriate calculations from that starting point. The program has provision for calculation of one constituent by difference.

The absorption correction function used in FRAME is that proposed by Heinrich and Yakowitz [1]. The atomic number correction is that of Duncumb and Reed [2]. The characteristic fluorescence correction uses the Reed [3] formulation. No correction for fluorescence excited by the continuum is performed. The program decides whether a characteristic fluorescence correction is needed. The mass absorption coefficients are calculated to agree closely with those of Heinrich [4]. A number of simplifications, such as a new fit for the backscatter factor,  $R$ , and the use of Moseley's law to obtain line and edge energies were made in order to render FRAME suitable for on-line operation with a small computer, and with the least possible amount of input.

In evaluating the performance of FRAME, we considered two criteria: (1) comparison of results for a wide variety of materials of known (analyzed) compositions, and (2) comparison of results from FRAME with those from two other NBS

computer programs for quantitative analysis (MULTI8 and COR2). The program MULTI8 [5] is comparable to the theoretical calculation procedures commonly used in microprobe analysis. The input for MULTI8 is somewhat cumbersome: the operator must provide atomic numbers, atomic weights, critical excitation potentials, fluorescence yields, and mass absorption coefficients, and he must decide where characteristic fluorescence corrections are needed. MULTI8 also requires background and deadtime corrected k-values as a starting point. While it yields accurate results, and can be used in a time-share system, it is unsuitable for on-line operation.

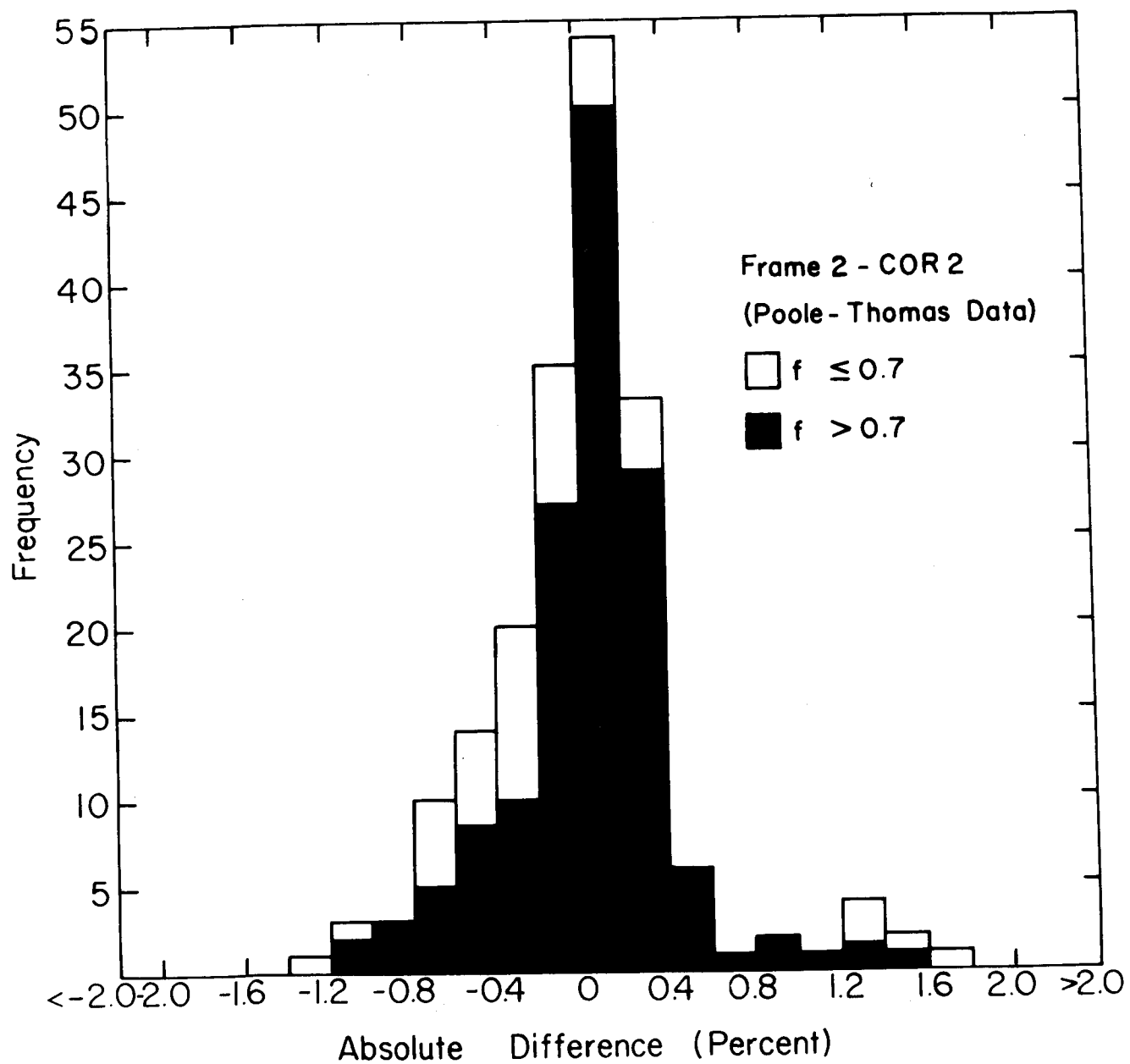
The program COR was written to be the most accurate program available for quantitative analysis [6]. COR2 includes the correction for continuum fluorescence and performs all the mathematical operations indicated by the correction models without short-cuts. The input of COR2 has become much simpler than that of MULTI8: COR2 requires only the atomic numbers, operating voltage and analytical lines as input. However, COR2 is a batch type program suitable only for relatively large computers. FRAME is meant to be as accurate as MULTI8, but usable on a minicomputer. In most cases, especially where continuum effects can be neglected, FRAME can be expected to give results as accurate as COR2.

We have compared the programs FRAME, MULTI8, and COR2 using the results 228 for binary specimens described by Poole [7]. Histograms of the differences are shown in Figure (1). The three give virtually the same results. Tests on a set of mineral specimens measured at NBS, and containing several elements, gave similar results. We conclude that the results obtained by FRAME are indistinguishable from those obtained with the most rigorous theoretical programs in use in the microprobe field.



References

- [1] Heinrich, K. F. J., Yakowitz, H., and Vieth, D. L.,  
"The Correction for Absorption of Primary X-rays,"  
in Proceedings Seventh National Conference on  
Electron Probe Analysis, San Francisco, CA (July 1972)
- [2] Duncumb, P. and Reed, S. J. B., Nat. Bur. Stand. (U.S.),  
Spec. Publ. 298, 133-154 (1968).
- [3] Reed, S. J. B., Brit. J. Appl. Phys. 16, 913-926 (1965).
- [4] Heinrich, K. F. J., The Electron Microprobe, McKinley,  
Heinrich, Wittry, Editors, John Wiley, New York, 296-  
377 (1966).
- [5] Heinrich, K. F. J., Myklebust, R. L., Yakowitz, H., and  
Rasberry, S. D., "A Simple Correction Procedure for  
Quantitative Electron Probe Microanalysis," U.S. Nat.  
Bur. Stand. Tech. Note 719, U.S. Government Printing  
Office (May 1972).
- [6] Hénoc, J., Heinrich, K. F. J., and Myklebust, R. L.,  
"A Rigorous Correction Procedure for Quantitative  
Electron Probe Microanalysis (COR 2)," U.S. Nat. Bur.  
Stand. Tech. Note 769 (in preparation).
- [7] Poole, D. M., Nat. Bur. Stand. (U.S.), Spec. Publ. 298,  
93-131 (1968).



## ELECTRON PROBE MICROANALYSIS OF THIN SPECIMENS

J. PHILIBERT <sup>+</sup> and R. TIXIER <sup>++</sup><sup>+</sup> Université de PARIS-SUD, ORSAY et C.N.R.S. 92190. MEUDON BELLEVUE.<sup>++</sup> I R S I D - 78104. SAINT GERMAIN-en-LAYE.

The increasing demand for microprobe analysis on electron microscopy specimens, the interest of thin foil properties and the development of specialized apparatus (1) for this kind of study led us to determine the optimal theoretical and experimental conditions for electron probe microanalysis of thin targets.

I - CORRECTIONS -

As in the case of massive targets any corrections have to be developed from physical principles. In fact the two kinds of analysis have to be consistent.

One knows how to correct X-ray intensities for massive specimens. Thin specimen corrections will have to be made by reference to thin standards or more frequently to massive standards.

I-1. Atomic number effect correction. For thin specimens, this correction was formerly discussed (2). Generally the back scattering factor of the specimen is practically equal to one. The second term in this correction arises from the following effect: the mean number of ionisations in a foil depends on the X-ray cross section for the element and the line considered.

The Bethe formula gives:

$$dn_j = c_A \frac{N}{A} \frac{\pi e^4}{E E_j^A} Z_j b_j \ln U_0^A d\rho_j$$

using the usual symbols in EPASA proceedings. In this formula, the energy losses of the electron are neglected. It is necessary to determine the limiting specimen thickness for which this assumption remains valid.

The most probable energy loss  $\Delta E$  for transmitted electrons has been calculated by LANDAU (3) as a function of mass thickness  $\rho_j$  :

$$\frac{\Delta E}{\rho_j} = - \frac{2\pi e^4 N Z}{m_0 v^2 A} \left[ \ln \frac{4\pi e^4 N Z \rho_j}{y_A^2 A (1-\beta^2)} - (\beta^2 + 0.37) \right]$$

$$\beta = v/c$$

Figure 1 shows the results calculated for gold and iron.

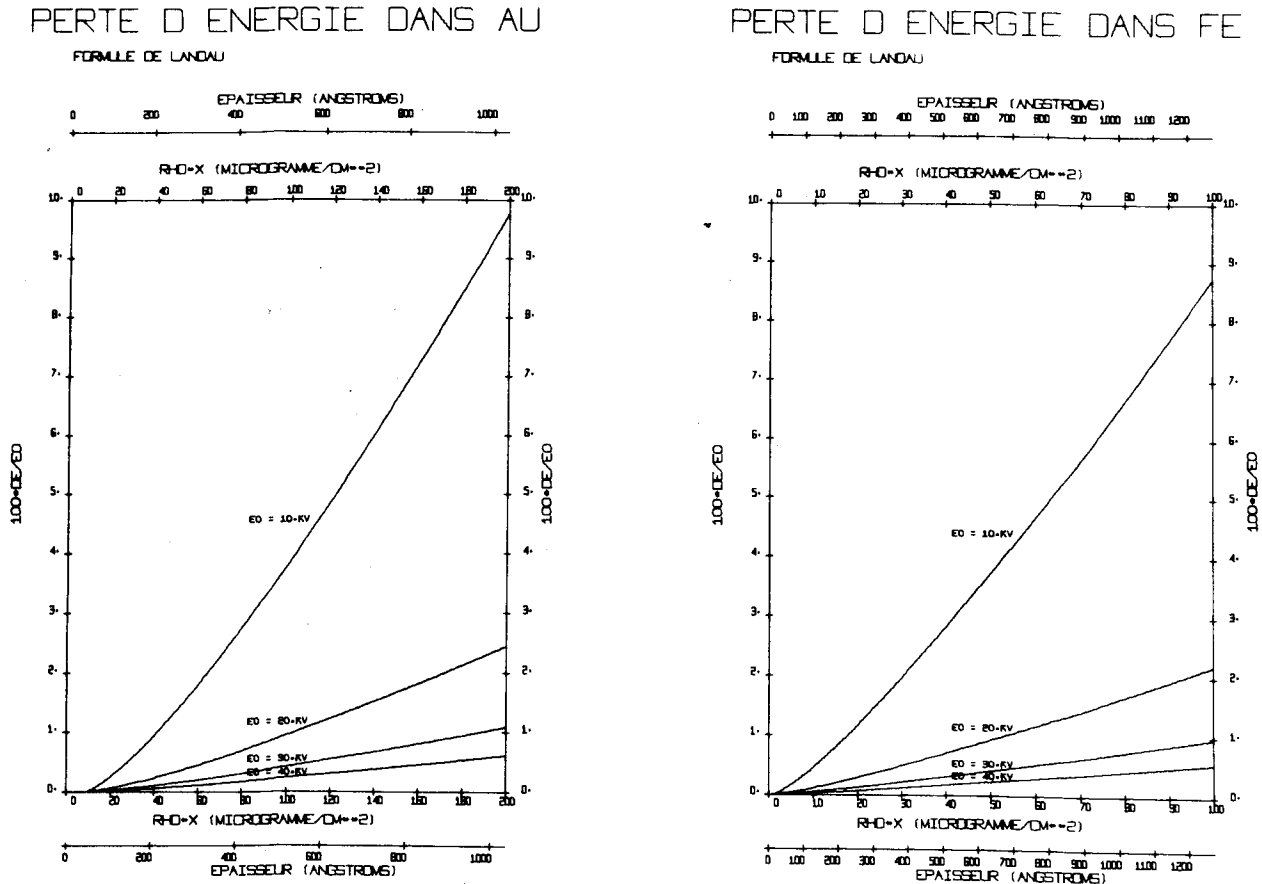


FIG.1. Energy losses calculated after LANDAU.

For thicknesses far larger than the limits for transmission electron microscopy, the energy losses are very small. For high over voltage ratio,  $dn_j$  will not be appreciably changed by such small energy losses. We therefore neglect calculated energy losses if they are smaller than 5 %.

I-2. Absorption correction - It has been shown (4) that the absorption correction is given by:

$$f(\chi) \approx 1 - (\sigma + \chi) \frac{\Delta \rho \beta}{2!} + \dots$$

and practically

$$f(\chi) = 1 \quad \text{if} \quad \chi \Delta \rho \beta / 2 < 0.1$$

It is even possible to bypass this correction when the absorption is not negligible. The technique consists in determining two intensity measurements, for at least two different mass thicknesses. One can extrapolate to thickness zero, the extrapolated value then only needs to be corrected for atomic number effect.

# I - 3. Fluorescence correction - 27c

## I - 3.1. by characteristic line -

The specimen is thin, but its lateral dimensions are not negligible; thus the correction has to be evaluated whether or not the secondary emission is important. It follows that:

$$\frac{I_A^f}{I_A} = 2 \omega_B C_B \frac{r_{A-1}}{r_A} \frac{A}{B} \mu_B^A \mu_B^{AB} \frac{\nu_A}{\nu_B} (\rho \delta)^2$$

Practically this will be negligible is  $\mu_B^{AB} \cdot \rho \delta \ll 1$ .

## I - 3.2. by continuous spectrum -

One obtains:

$$\frac{I_A^{fc}}{I_A} = 1.44 \cdot 10^{-33} \frac{r_{A-1}}{r_A} \rho^2 \delta^2 \frac{E_i^A}{\ln U_0^A} (\mu_{\nu_0}^A)^2 \nu_0^6 \left( \frac{1}{\nu_0^5} - \frac{1}{\nu_K^5} \right)$$

where  $\nu_0$  is the DUANE-HUNT frequency and  $\delta$  the A line weight in the K series. For this value of the constant factor, units are cm, seconds, eV.

Generally this correction may be neglected.

## II - CONSISTENCY -

The consistency of the corrections has been discussed in (5). We have shown that the corrected ratio of intensities, measured on standards, is invariant when the electron energy is changed (Fig. 2).

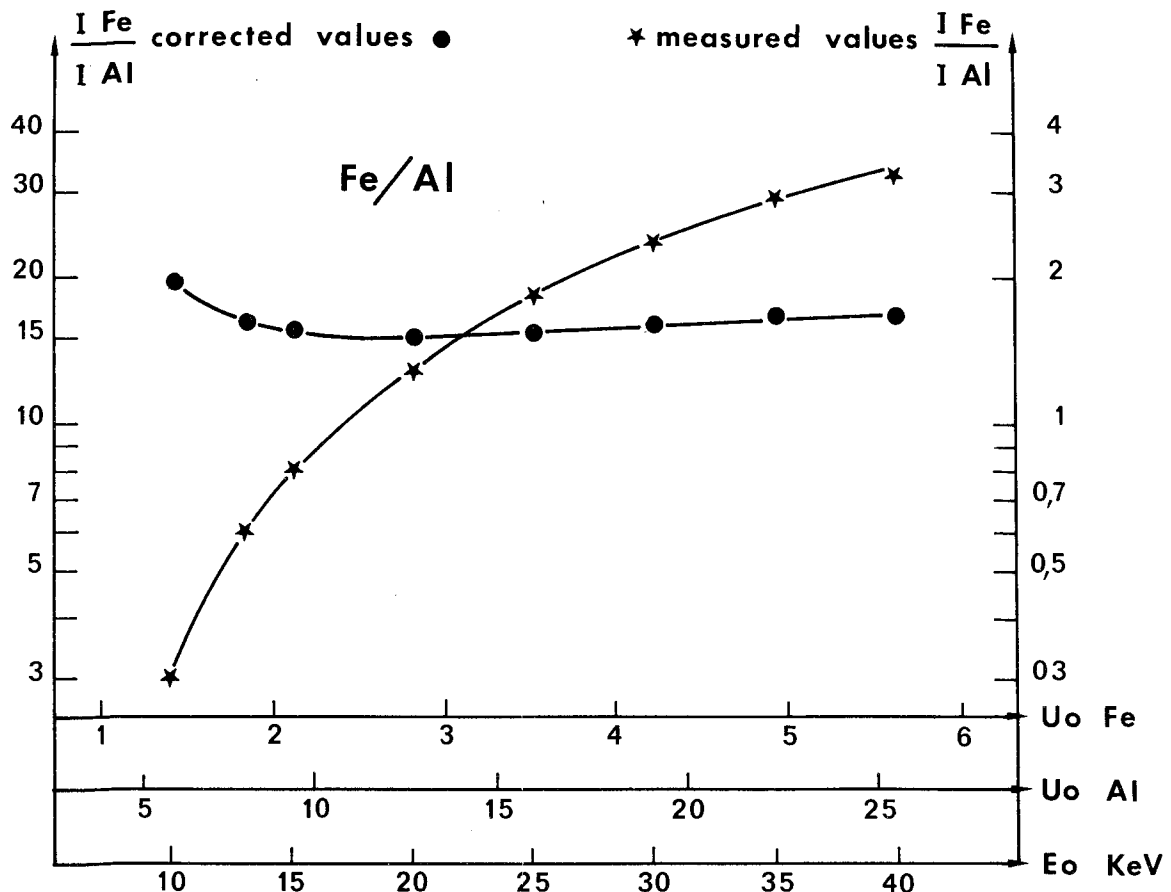


FIG. 2. Iron - Aluminium ratio.

One can make use of this property in order to analyse thin specimens at high voltages, 100 kV for instance, and measure the massive standards at a reasonable value for EPMA, 20 kV for instance.

### III - CRYSTALLINE SPECIMENS -

The anomalous emission of crystalline foils should not be a real problem as one measures only concentration ratios for two elements and as the electron beam should be focussed with a large divergence (larger than  $5.10^{-3}$  radian).

### IV - BIOLOGICAL SPECIMENS -

Our method can be compared with the calculations by T. HALL for biological specimens analysis (6). If the continuous spectrum cross-section is used - and not the KRAMERS formula, which is only valid for massive specimens, as utilised by HALL - the two approaches are similar. Either the intensities of an unabsorbed line or a low wavelength part of the continuous spectrum are proportionnal to specimen mass thickness.

### V - APPLICATIONS -

#### V-1. Thin standards -

Au-Ag and Au-Cu alloy foils were prepared. Thicknesses were measured using an X-ray interferometer technique, with an accuracy of  $\pm 2.5 \text{ \AA}$ . The corrected results were compared to independant measurements by X-ray fluorescence and diffractometry (Table I). Massive standards were also used, and both sets of values were consistent.

TABLE I.- Au-Cu atomic concentrations.  
Comparison of probe measurements and lattice  
constant measurements.

% at. EPMA	% at. d
12,4	11,5
17,7	17,7
28,5	26
22,3	23,5
86,3	83
81,2	83
81	83
54,6	54

V-2. Massive standards -

The formulae are easy to program:

$$\frac{k_A}{k_B} = \frac{C_A}{C_B} \cdot \frac{P_A}{P_B} \cdot \frac{f(X)_B}{f(X)_A}$$

with

$$P_A = \frac{\ln U_o^A}{E_j^A} \cdot \frac{1}{R[A]/S'[A]}$$

Various cases of measurements on extraction replicas have made possible the analysis of precipitates in steels.

The qualitative analysis, with X-ray scanning images, shows a very good resolution. Magnifications up to 4 000 times can be used.

VI - CONCLUSIONS -

A review of similar measurements on thin specimens reveals that most of the few published analysis were uncorrected or poorly corrected.

As dispersive or non dispersive spectrometers are now currently available as attachments for transmission electron microscopes, this kind of analysis will be more frequent and should be more rigorous.

Acknowledgments - We like to thank the cooperation of Dr RIVORY, Mr M. ANCEY, Mr A. QUENNEVAT and Miss BRYCKAERT. This work is part of a larger project sponsored by the C E C A .

- (1) COOKE C.J., DUNCUMB P. (1969).  
Performance analysis of a combined electron microscope and electron probe microanalysis "EMMA".  
Proc. V<sup>th</sup> Int. Cong. X ray optics and Microanalysis Springer (BERLIN), 245-247.
- (2) PHILIBERT J., TIXIER R. (1968).  
Some problems with quantitative electron probe microanalysis. N B S Spec. Pub., 298, 13-33.
- (3) LANDAU L. (1944).  
On the energy loss of fast particles by ionization -  
J. Phys. U.R.S.S., 8, 201-205.
- (4) TIXIER R., PHILIBERT J. (1969).  
Analyse quantitative d'échantillons minces.  
Proc. V<sup>th</sup> Int. Cong. X-ray optics and microanalysis Springer (BERLIN), 180-186.
- (5) PHILIBERT J., BRYCKAERT D. TIXIER R. (1971).  
Invariability of intensity ratios for standards.  
Proc. VI<sup>th</sup> Int. cong. X-ray optics and microanalysis OSAKA to be published.
- (6) MARSHALL D.J., HALL T.A. (1968).  
Electron probe X ray microanalysis of thin films -  
Brit. J. Appl. Phys. 1, 1651-1656.

# QUANTITATIVE ELECTRON MICROPROBE ANALYSIS OF THIN FILMS WITH MONTE CARLO CALCULATIONS

D. F. Kyser and K. Murata

IBM Research Laboratory  
San Jose, California

---

Quantitative analysis of thin films is a challenging problem for which there are at least two possible solutions. If the film thickness is sufficiently large to stop the electron beam before penetration into the substrate, then the conventional ZAF model can be utilized. This boundary condition often requires the use of soft x-rays with low excitation potentials, for example L and M lines, with subsequent uncertainties such as high mass absorption coefficients and absorption correction models. There can also be a low sensitivity for measurement of such soft x-rays. The second approach is to use high beam voltages and measure hard x-rays with their higher sensitivity and lower absorption correction. However, then a correction must be made for loss of intensity from the film due to penetration into the substrate, and also a correction for differential scattering and energy loss as the electrons cross the film-substrate interface. Previous work on the latter approach has been done by Hutchins,<sup>1</sup> Colby,<sup>2</sup> and Reuter<sup>3</sup> with some success using semi-empirical models. Bolon and Lifshin<sup>4,5</sup> have recently described the application of a simplified Monte Carlo calculation to the thin film problem.

The present work utilizes Monte Carlo calculations of electron scattering, energy loss, and ionization distribution with depth to calculate an intensity ratio  $k$  predicted between a thin film on a known substrate and a thick standard target. A single scattering model is used which has been described previously by Murata et al.<sup>6,7</sup> The model utilizes the Rutherford equation to describe the elastic scattering process, and the Bethe equation to describe the energy loss between elastic scattering events. The mean free path  $\Lambda$  of the electron is used as a step length between elastic scattering events. When the electron crosses the boundary between film and substrate, the ionization rate for elements in the film is set equal to zero unless the electron is subsequently backscattered into the film. Scattering and energy loss, characteristic of the substrate, continues as the electrons decelerate in the substrate. Typically the trajectories of 1200 electrons are calculated for statistical purposes on an IBM System 360, Model 195 computer.

The agreement between theory and experiment for Au and Ni films is indicated in Figures 1 and 2. The agreement is good over wide ranges in film thickness for elemental films at high voltage. It has been found necessary to introduce a factor  $\mu_s$  into the relation for  $\Lambda$  in order to obtain this agreement between theory and experiment. Thus  $\Lambda \propto \mu_s$  where  $\mu_s = (1 + \alpha)$ .



The value of  $\alpha$  which resulted in the best fit was determined by comparing experimental data and Monte Carlo calculations of  $k$  for thin films and back-scattered electron yield  $\eta$  for thick targets. For Au and Ni,  $\alpha = 0.25$  and  $0.10$ , respectively. Hence, it appears that the atomic number dependence of  $\mu_s$  is of the form  $(1 + Z/C)$  where  $C$  is approximately 300 at 20 kV. The primary energy dependence of  $C$  is not yet established, but may be similar to that proposed by Bolon and Lifshin.<sup>5</sup> A weak energy dependence in  $\mu_s$  may account for the difference observed for Au films at low beam voltage. The Monte Carlo calculation has also been applied to multi-element films and to the case of an inclined electron beam.

We would like to acknowledge and thank R. Bolon, E. Lifshin, and W. Reuter for sharing their experimental data with us.

- 
1. G. A. Hutchins, The Electron Microprobe, ed. by T. D. McKinley, K. F. J. Heinrich, and D. B. Wittry (Wiley and Sons, New York, 1966) p. 390.
  2. J. W. Colby, Advances in X-Ray Analysis, Vol. 11 (Plenum Press, New York, 1968) p. 287.
  3. W. Reuter, Proceedings Sixth International Conference on X-Ray Optics and Microanalysis, ed. by G. Shinoda, K. Kohra, and T. Ichinokawa (Univ. of Tokyo Press, 1972) p. 121.
  4. R. B. Bolon and E. Lifshin, Proceedings Seventh National Conference on Electron Probe Analysis (San Francisco, 1972) paper No. 35.
  5. R. B. Bolon and E. Lifshin, Proceedings Sixth Annual SEM Symposium, ed. by O. Johari and I. Corvin (IIT Research Institute, 1973) p. 285.
  6. K. Murata, T. Matsukawa, and R. Shimizu, Jap. J. Appl. Phys. **10**, 678 (1971).
  7. K. Murata, T. Matsukawa, and R. Shimizu, Proceedings Sixth International Conference on X-Ray Optics and Microanalysis, ed. by G. Shinoda, K. Kohra, and T. Ichinokawa (University of Tokyo Press, 1972) p. 105.

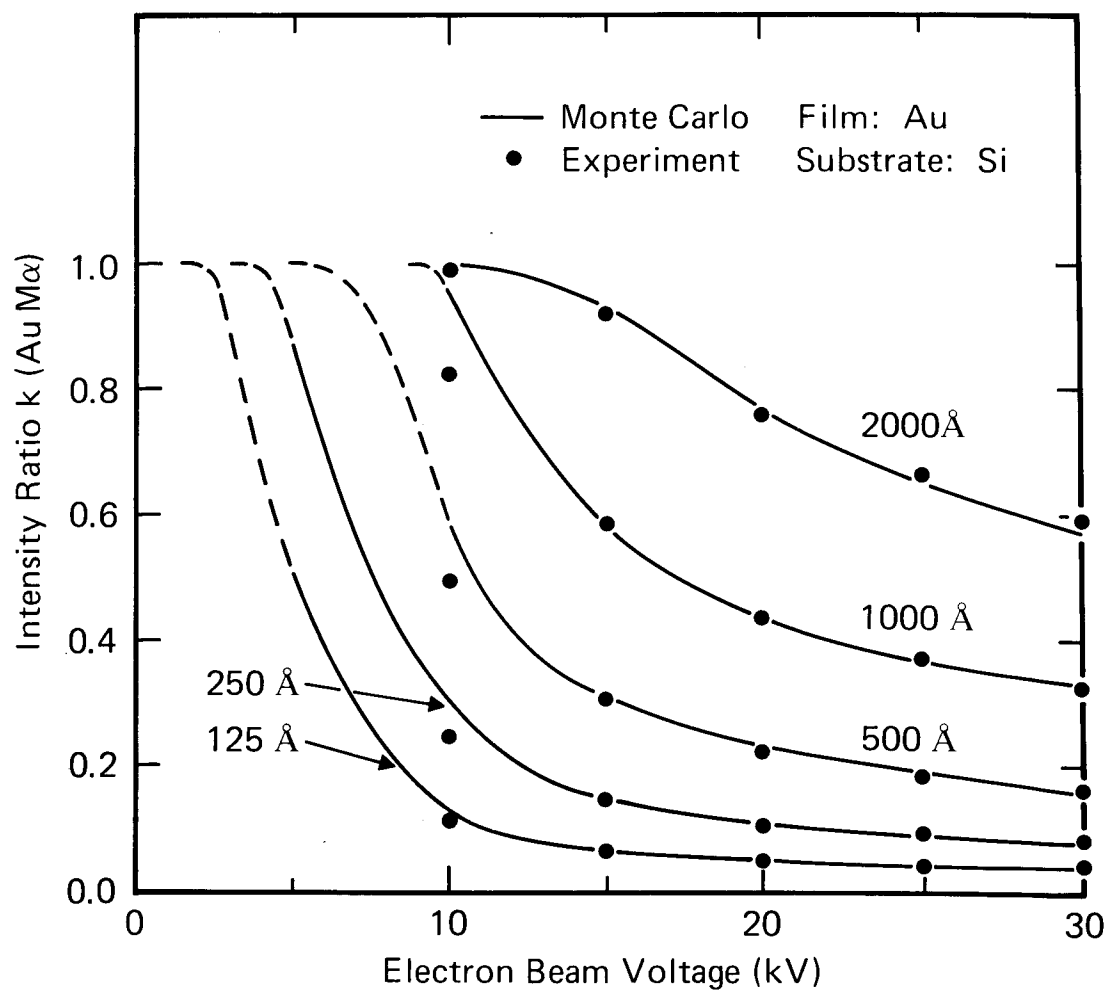


Fig. 1. Comparison of Monte Carlo calculations and experimental data of reference 4. The x-ray takeoff angle is  $18^\circ$ .

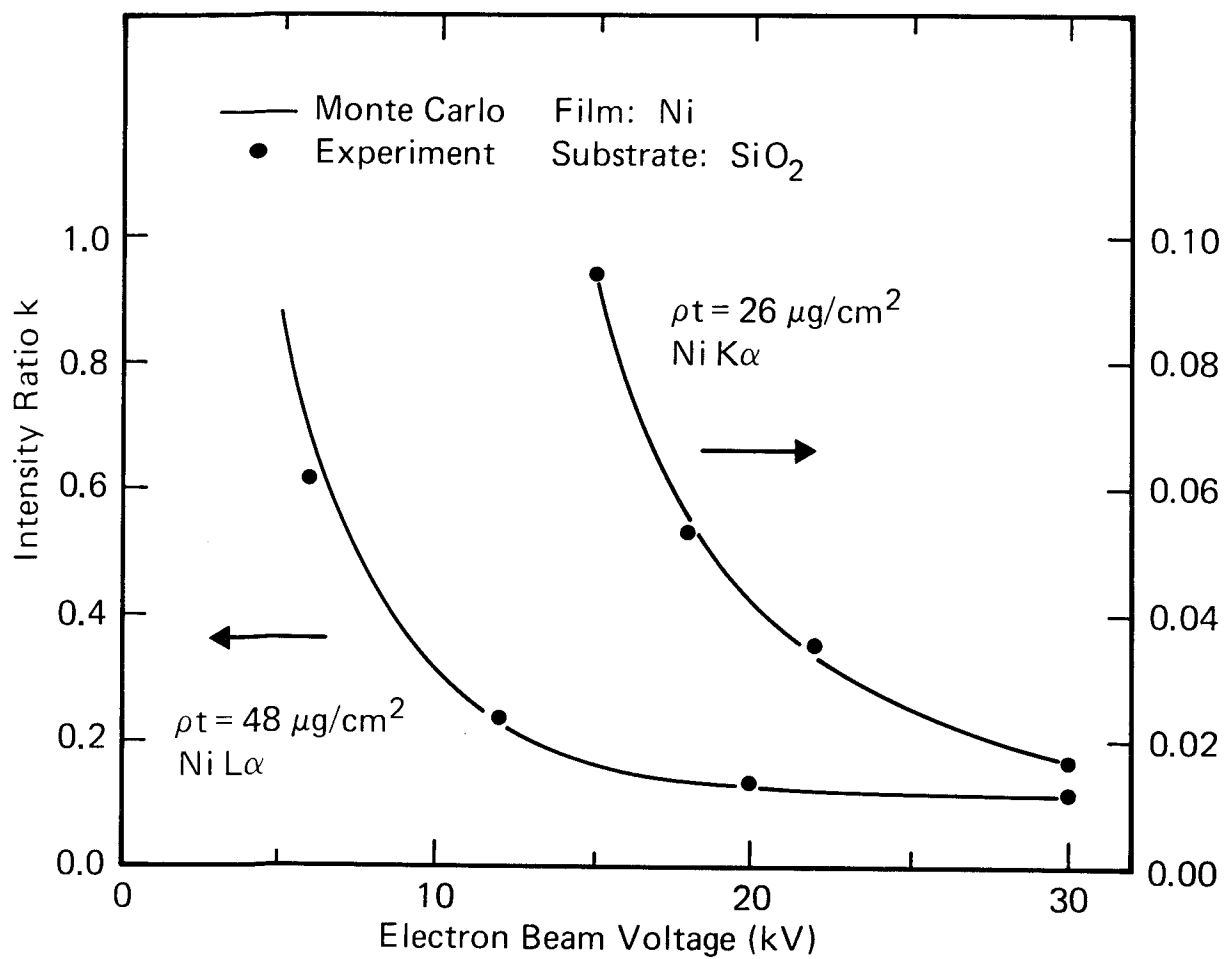


Fig. 2. Comparison of Monte Carlo calculations and experimental data of reference 3. The x-ray takeoff angle is  $52.5^\circ$ .

DETERMINATION OF THE ENERGY DISTRIBUTION OF THE CONTINUUM  
AND THE RATIO OF INDIRECT TO DIRECT X-RAY FLUORESCENCE

E. Lifshin, M.F. Ciccarelli, and R.B. Bolon  
General Electric Corporate Research and Development  
Schenectady, New York

There are two reasons why the x-ray continuum plays a significant role in electron probe microanalysis. First, it is the principal source of background and thereby, along with peak intensity and matrix composition, determines chemical sensitivity. Second, it can be a major cause of indirect x-ray fluorescence, influencing both quantitative accuracy and x-ray spatial resolution. In spite of its obvious importance, however, relatively few studies have been reported on the spectral distribution of the continuum as a function of beam voltage and target atomic number. In fact, both Springer<sup>1</sup> and Henoc<sup>2</sup> depend on the theoretical expression of Kramers':

$$I_{\nu} = kZ(\nu_0 - \nu) \quad (1)$$

(where  $I_{\nu}$  is the generated continuum intensity at a frequency  $\nu$ ,  $Z$  is atomic number,  $\nu_0$  is the minimum frequency which can be generated for a given electron beam energy, and  $k$  is a constant assumed to be independent of  $Z$  and electron beam energy)

to calculate the ratios of indirect to direct excitation used in their continuum fluorescence corrections. Recently the use of Kramers' equation in these corrections and the value of the associated proportionality constant,  $k$ , have been questioned by Rao-Sahib and Wittry<sup>4</sup>, Springer<sup>5</sup>, and Heinrich<sup>6</sup>.

Since the continuum fluorescence correction is often small and can be neglected<sup>7</sup>, it is unlikely that anything short of a major revision in Kramers' equation would significantly alter that

aspect of quantitative analysis. However, there clearly is a need for a better continuum model to facilitate background subtraction in the analysis of solid state x-ray spectra. Furthermore, Bolon and Lifshin<sup>8</sup> have recently shown that more accurate values of the ratio of indirect to direct x-ray fluorescence are necessary for the quantitative analysis of small second phase structures, since the contribution of indirect fluorescence to the measured intensity of such structures may be partially or totally absent relative to that of bulk reference standards.

The purpose of the present study was, therefore, to make a series of direct measurements of the x-ray continuum and compare the results with the empirical equation of Kuhlenskampff<sup>9</sup> which has been theoretically supported by Kramers. A solid state x-ray detector on a conventional microprobe was chosen because of the broad range of energy over which it has 100 percent collection efficiency, and also since the intensity data at all energies can be collected simultaneously with a multichannel analyzer in a convenient form for subsequent computer processing. Data communication between the multichannel analyzer and the computer was done using a 1200 baud asynchronous interface described previously by Lifshin<sup>10</sup>. The generated intensity distribution,  $I_g$ , was calculated from the observed,  $I_o$ , by the equation:

$$I_g = \frac{4\pi I_o}{\Omega f(\chi)} \quad (2)$$

where  $\Omega$  is the solid angle defined by the detector and  $f(\chi)$  is the absorption correction calculated by the equation proposed by Heinrich<sup>11</sup> et. al., last year:

$$1/f(\chi) = 1 + 3 \times 10^{-6} (E_o^{1.65} - E^{1.65}) \chi + 4.5 \times 10^{-14} (E_o^{1.65} - E^{1.65})^2 \chi^2 \quad (3)$$

where,  $E_0$  = the beam voltage,  $E$  = the energy of the emitted continuum energy (used instead of the critical excitation potential for a particular characteristic line), and  $\chi = \frac{\mu}{\rho} \csc \psi$ . The take-off angle is  $\psi$  and the mass absorption coefficient  $\frac{\mu}{\rho}$  can be calculated from Heinrich's equation <sup>12</sup>

$$\frac{\mu}{\rho} = C_i \lambda^{ni}$$

It was found that the spectra calculated from equation 2 did not appear to follow the linear dependence on the emitted frequency predicted by Kramers' equation. This can be interpreted as either a failure of that equation or the present inability to properly correct for continuum absorption by equation 3. This problem is not unique to the use of Heinrich's equation, since previous attempts to correct for absorption of the continuum by Reed and Ware <sup>13</sup> using the Heinrich modified Philibert equation <sup>14</sup> and Rao-Sahib and Wittry <sup>4</sup> using the Anderson-Wittry correction <sup>15</sup> all implicitly assume that the depth distribution of the continuum production is identical to that of the characteristic intensity. This assumption is known to be an approximation since the ionization cross-section used by Kramers follows a  $1/E$  dependence while that for characteristic x-ray production follows a  $\frac{1}{E} \ln E$  dependence <sup>16</sup>, even though Philibert <sup>17</sup> assumed a constant ionization cross-section. The effect of these differences are presently under study by the authors using Monte Carlo calculations.

As can be seen from Figures 1a and 1b the use of a pulse pileup rejector was essential for accurate spectral representation. The discontinuity in the background of the observed K spectra of iron shown in Figure 1b was typical of the effect due to the large change in absorption coefficient on either side of the absorption edge which is obscured by the  $K_\beta$  peak. It was interesting to observe, however, that this discontinuity which was eliminated

following the absorption correction, disappeared with increasing atomic number, thereby supporting the argument that a point source located near the surface of the sample could be used for the purpose of calculating the continuum fluorescence, particularly since continuum fluorescence increases with increasing atomic number. It was also possible to use the generated continuum distribution to calculate the ratio of indirect to direct excitation without the need for Kramers' equation or simplifications in the calculation of the mass absorption coefficients. Furthermore, since the characteristic line intensities are measured simultaneously with the background, experimental values can be used in preference to the theoretical values used by Springer and Henoc. Some results for the emitted radiation obtained at 40 kv and a  $40^\circ$  takeoff angle as follows:

<u>Z</u>	<u>Element</u>	<u><math>I_{\text{indirect}}/I_{\text{direct}}</math></u>
24	Cr	.010
29	Cu	.024
34	Se	.047
40	Zr	.069

#### REFERENCES

1. Springer, G. (1967) "Neues Jahrbuch fuer Mineralogie Abhandlungen, 106, p. 241-255.
2. Henoc, J. (1968) Quantitative Electron Probe Microanalysis, K.F.J. Heinrich, Ed., National Bureau of Standards Special Publication 298, p. 197-214.
3. Kramers, H.A. (1923) "Philosophical Magazine", 46, p. 836-871.
4. Rao-Sahib and Wittry, D.B. (1972) Proceedings of the Sixth International Conference on X-Ray Optics and Microanalysis, G. Shinoda, et. al. eds., University of Tokyo Press, Tokyo, p. 131-137.

5. Springer, G. (1972) Proceedings of the Seventh National Conference on Electron Probe Analysis, San Francisco, July 17-21, Paper No. 4.
6. Heinrich, K.F.J. (1972) "Analytical Chemistry", 44, No. 2, p. 350-354.
7. Myklebust, R.L., Yakowitz, H., and Heinrich, K.F.J. (1970) Proceedings of the Fifth National Conference on Electron Probe Analysis, New York, July, Paper No. 11.
8. Bolon, R.B. and Lifshin, E. (1973) Proceedings of 1973 Symposium on Scanning Electron Microscopy, O. Johari, ed., IIT Research Institute, Chicago, p. 285-292.
9. Kuhlenkampff, H. (1923), Ann der Phys. LXIX, p. 548.
10. Lifshin, E. (1970) Proceedings of the Fifth National Conference on Electron Probe Analysis, New York, July 22, Paper No. 8.
11. Heinrich, K.F.J., Yakowitz, H. and Vieth, D.L. (1972) Proceedings of the Seventh National Conference on Electron Probe Analysis, San Francisco, July 17-21, Paper No. 3.
12. Heinrich, K.F.J. (1966) The Electron Microprobe, T. D. McKinley et.al., eds., J. Wiley and Sons, New York, p. 296-377.
13. Reed, S.J.B. and Ware, N.G. (1973) "X-Ray Spectrometry" 2, p. 69-74.
14. Heinrich, K.F.J. (1967) Proceedings of the Second National Conference on Electron Microprobe Analysis, June 14-16, Paper No. 7.
15. Anderson, C.A., and Wittry, D.B. (1968) "British J. Appl. Phys.", Ser 2, 1, p. 529.
16. Worthington, D.R. and Tomlin, S.G. (1956) "Proc. Phy. Soc.", A69, p. 401.
17. Philibert, J. (1963) Proc. Third International Symposium on X-Ray Optics and Microanalysis, H.H. Pattee, et. al., eds. Academic Press, New York, p. 379-392.



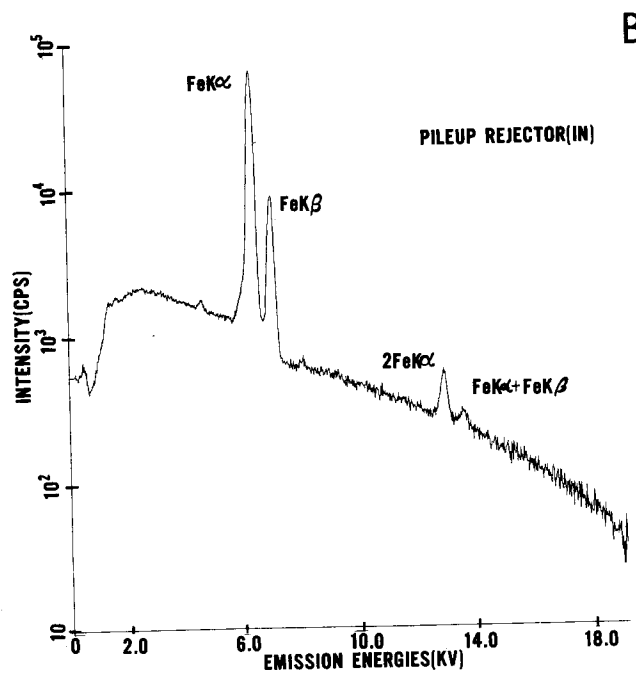
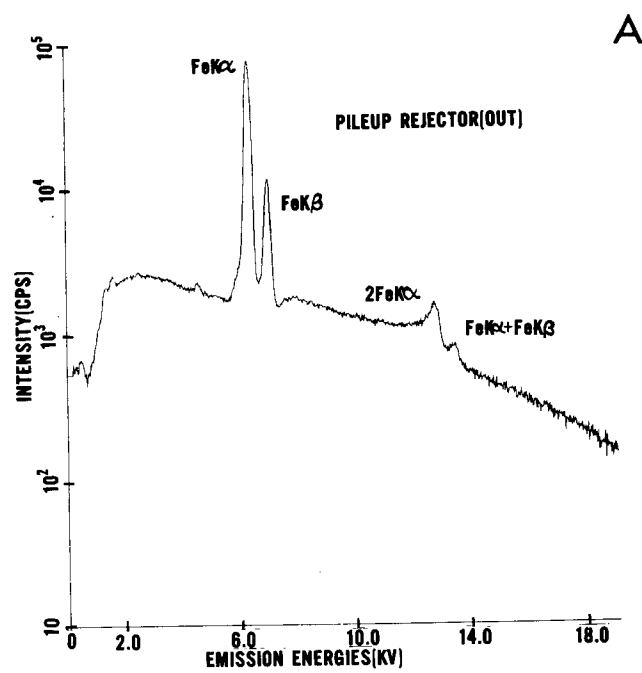


Figure 1. Solid State X-Ray Detector Spectra of Iron Without (a) and With (b) Pulse Pileup Rejection.

## QUANTITATIVE ELECTRON PROBE MICROANALYSIS OF PARTICLES

John C. Russ  
EDAX Laboratories  
Raleigh, North Carolina 27612

Attempts to obtain quantitative analysis of micron and sub-micron particles is generally difficult in the microprobe because of electron scattering into the surrounding matrix. A frequently used approach has therefore been the use of extraction replicas to remove the surface particles. If properly made, these replicas also contain useful information to relate particle position to structure, either the microstructure revealed by etching, or the topography of a fractive surface.

Analysis of the extracted particles is still difficult, beyond merely identifying the elements present, because the conventional ZAF-type of calculation cannot be applied. We have tested the use of an analytical model originally developed for thin-section analysis<sup>1</sup>, particularly of biological tissues, in the TEM and found that it gives fair accuracy for particles on replicas.

The model is derived from the elemental ratio model of Duncumb<sup>2</sup>, proposed for EMMA-4, in which

$$\frac{C_1}{C_2} = K_{12} \frac{I_1}{I_2}$$

relates the concentration  $C$  and intensity  $I$  of two elements in a section by an empirical constant  $K_{12}$ . The constant can be obtained by measurements on known areas, or indeed on the specimen as a whole since by definition x-ray absorption is negligible in the thin sections used.

The constant can also be calculated from fundamental constants. If we rewrite

$$C_1 : C_2 : C_3 : \dots = \frac{I_1}{P_1} : \frac{I_2}{P_2} : \frac{I_3}{P_3} : \dots$$

for  $C$  in atomic percent, then

$$P_i = Q_i W_i \cdot R_{\alpha/\beta_i} \cdot T_i$$

where

$Q$  = ionization cross section

$W$  = fluorescent yield

$R$  = relative intensity of the line measured (e.g.  $L_{\beta_2}$ )

$T$  = spectrometer efficiency

For the spectrometer efficiency, we use the term

$$T = \delta e^{-0.58/E^3} \cdot 1 - e^{-18700/E^3}$$

where  $\delta$  = detector solid angle

$E$  = x-ray energy

This applies to a silicon detector 3 mm. deep, behind a 7.5  $\mu$ m Be window. The difficulty of obtaining reproducible efficiency or expressing it analytically for a crystal spectrometer limits the use of this calculation to energy-dispersive x-ray analysis.

The key assumption in the model is that absorption of x-rays is negligible. If we accept as an upper limit 10% absorption, then

$$I/I_0 = .9 = e^{-\mu \rho t}$$

gives us a characteristic dimension

$$t = \frac{1.054 \cdot 10^3}{\mu \rho} [\mu\text{m}]$$

This suggests that for typical intermetallic compound with  $\rho$  of 4 to 6 and  $\mu$  in the 100 to 500 range, particles in the size range of a micron or less can be analyzed by this method, which has the major virtue of requiring no standards of any kind.

To test the accuracy of the proposed method, we have prepared specimens with stoichiometric compounds on carbon replicas<sup>3</sup>, and analyzed isolated particles of various sizes as summarized in the table below. The data were taken at 27.2 kV in an S600 Stereoscan, in times ranging from 40 to 400 seconds.

These results indicate that the model can provide accuracy of approximately 10% in most cases, which should be adequate to identify intermetallic compounds.

<u>Particle</u>	<u>Size (diameter)</u>	<u>Intensities</u>	<u>Calculated ratio</u>
Manganese	12.0 $\mu$ m	16917 : 16074	1 : 0.93
sulfate	2.5	1435 : 1393	1 : 0.95
Mn : S	1.1	1282 : 1349	1 : 1.03
1 : 1	0.8	497 : 467	1 : 0.92
	0.4	336 : 303	1 : 0.88
Calcium	5.5	4788 : 6839 : 7932	1 : 2.02 : 2.05
alumino-	1.2	5245 : 8085 : 8180	1 : 2.18 : 1.93
silicate	0.6	633 : 1008 : 997	1 : 2.15 : 1.86
Ca : Al : Si			
1 : 2 : 2			
Iron chloride	11.5	38440 : 115674	1 : 2.73
Fe : Cl	2.3	3078 : 10280	1 : 3.03
1 : 3	0.9	1246 : 4435	1 : 3.23
	0.7	960 : 3345	1 : 3.16

#### REFERENCES

1. Russ, J.C., "Obtaining Quantitative X-ray Analytical Results from Thin Sections in the Electron Microscope", ASCB Symposium, St. Louis, 1972.
2. Duncumb, P., Journal de Microscopie 7, 1968, p. 581.
3. Method suggested by Dr. J. Walinga, N.V. Philips Gloeliampenfabrieken, Eindhoven, Netherlands.

THE USE OF MONTE CARLO CALCULATIONS FOR  
QUANTITATIVE ANALYSIS AT NON-NORMAL  
ELECTRON BEAM INCIDENCE

by

R.B. Bolon and E. Lifshin  
Corporate Research & Development  
General Electric Company

Until recently most quantitative electron microprobe analysis has been performed at normal electron beam incidence. This configuration has the advantage that the distribution of generated x-rays is symmetric about the axis defined by the electron beam, which simplifies the derivations of the quantitative correction expressions. Furthermore, the same correction factors can be applied to multiple spectrometers providing they have the same takeoff angle. Normal electron beam incidence, however, is less frequently used in the scanning electron microscope where added flexibility is incorporated in the specimen stages to permit a wide range of specimen tilt and rotation control to improve secondary electron imaging. In addition, normal incidence cannot be used in any instrument which has the detector and specimen in a plane perpendicular to the axis of the electron beam as in the case where the crystal spectrometers have horizontal focusing circles or for some energy dispersive spectrometer systems. Since quantitative x-ray analysis is one of the major goals for instruments with combined SEM and microprobe capabilities, it is clearly important to develop analytical procedures for non-normal electron beam incidence.

Although the option remains open for a more general derivation of the ZAF correction expressions, the method chosen in this paper is a Monte Carlo procedure using a modified version of the Curgenven and Duncumb program which the authors have used with reasonable success on thin gold films on various substrates and TaC rods in a NiCr matrix<sup>1</sup>. In doing so it compliments work described last year by Shimizu, et. al.<sup>2</sup> on Fe-Al and Cu-Al using

Monte Carlo calculations based on the Lewis multiple scattering theory and Bethe energy loss expression. The present study used data collected with a solid state x-ray detector from the NBS Si-Fe, Cu-Au, and Cu-Ag standards at normal incidence and with sample inclinations of 20, 40, and 60 degrees about an axis perpendicular to the plane defined by the electron beam and a line from the sample to the detector. A comparison between Monte Carlo calculated and experimentally measured Si K $\alpha$  x-ray intensity ratios from Fe-3.22 Si is presented in Table 1 as well as the ZAF calculated intensity ratio for normal incidence. Figure 1 shows a comparison of Monte Carlo plots for normal incidence and a sample tilt of 40<sup>0</sup> for both pure Si and Fe-3.22 Si. The total number of x-rays shown in these figures is somewhat arbitrarily chosen so as to illustrate their in-depth distribution.

An added benefit of the M.C. method is that it provides a graphic presentation of the x-ray excited volume which can be useful for selecting tilt and voltage for thin film or small particle analysis.

### References

1. Bolon, R. B., Lifshin, E., Scanning Electron Microscopy /1973, (ed) O. Johari, IIT Research Institute, Chicago, Illinois, 1973, p. 286.
2. Shimizu, R., et. al., Proc. 7th Nat. Conf. on Electron Probe Analysis, (San Francisco, 1972), Paper No. 7.

TABLE I.

CALCULATED AND EXPERIMENTAL  
Si K $\alpha$  X-RAY INTENSITY RATIOS

Fe 3.2 Si  
E<sub>0</sub> = 10.0 kV

<u>ANGLE INCIDENT/TAKE OFF</u>	<u>M.C.</u>	<u>EXP.</u>	<u>ZAF</u>
90/40	0.0298	0.0280	0.0272
70/60	0.0321	0.0307	—
50/80	0.0325	0.0311	—
30/80	0.0339	0.0306	—

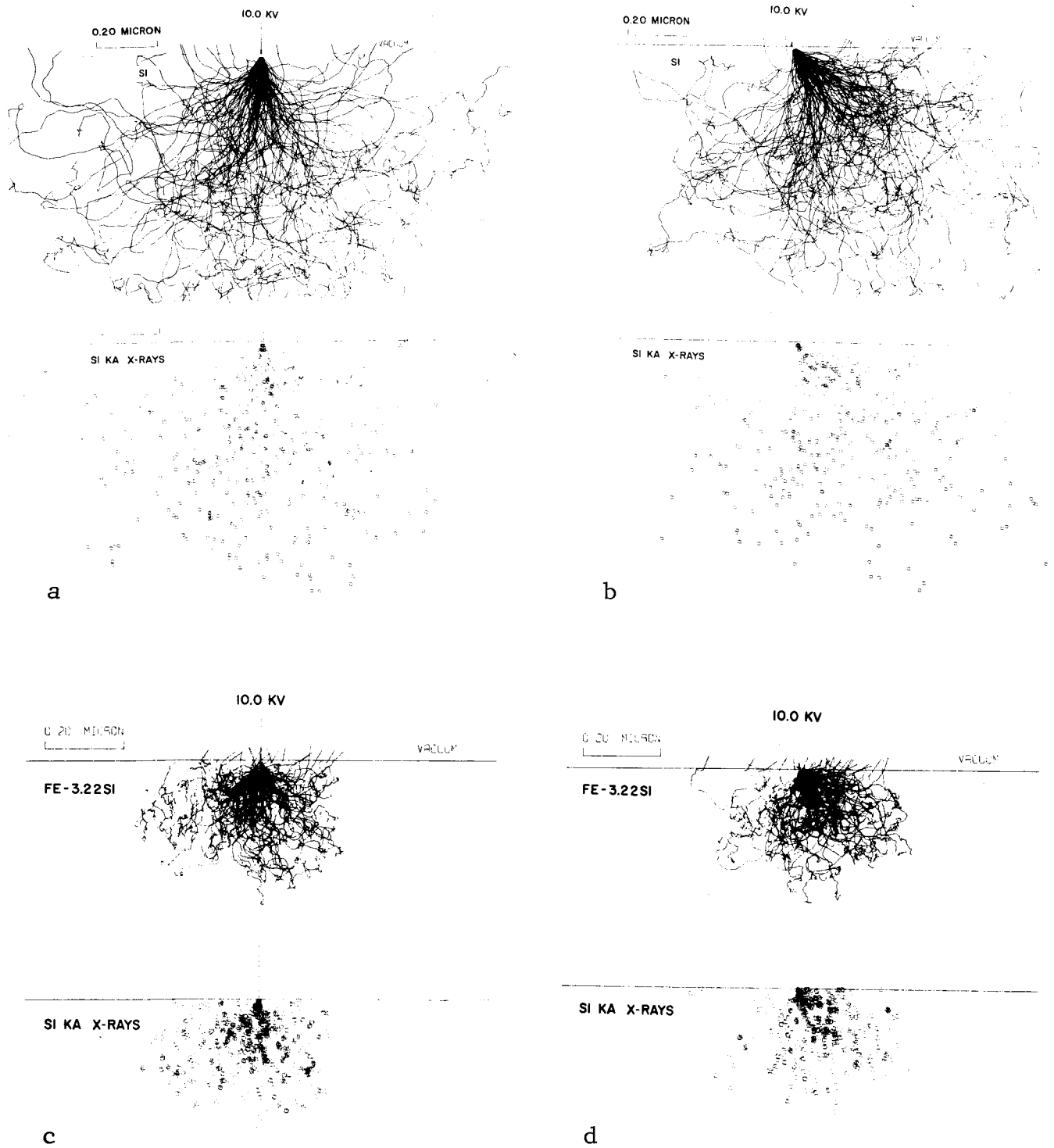


Figure 1. Monte Carlo electron and X-ray plots for:  
 a) Normal incidence on Si.  
 b) 40° to surface on Si.  
 c) Normal incidence on Fe-3.22Si.  
 d) 40° to surface on Fe-3.22Si.



## Analysis by Appearance Potential Techniques\*

J. E. Houston and Robert L. Park  
Sandia Laboratories, Albuquerque, New Mexico 87115

Elemental analysis of materials is usually accomplished by exciting atomic core levels with some probing particle and spectrally analyzing the characteristic decay products which result from the subsequent relaxation. An analysis can also be made by probing with monochromatic particles and noting the threshold energies at which additional decay products appear. The advantages of this appearance potential technique include (1) simplicity of the apparatus, since an energy analyzer is not necessary, and (2) simplicity of the resulting spectra, since only the core-level binding energies themselves are involved and not the term differences, as in a characteristic emission analysis. In the present paper we briefly discuss the various appearance potential techniques and contrast their advantages and disadvantages with the more standard methods of analysis. Emphasis will be placed on electron-excited soft x-ray and Auger appearance potential spectroscopies, which are very surface sensitive, and photon-excited Auger appearance potential spectroscopy, which is a bulk sensitive technique.

---

\*Supported by the U. S. Atomic Energy Commission.

SURFACE CAPABILITIES OF THE ELECTRON MICROPROBE  
USING THRESHOLD ISOCHROMAT INTEGRATED INTENSITIES  
AND OTHER TECHNIQUES

James S. Solomon

T. J. Wild

University of Dayton Research Institute, Dayton, Ohio 45469

and

William L. Baun

Air Force Materials Laboratory (LN), WPAFB, Ohio 45433

Conventional microprobe techniques, such as using excitation potentials two to three times the excitation potentials ( $E_K$ ,  $E_L$ ,  $E_M$ , etc.) of the various x-ray lines or bands, more or less disqualify the electron microprobe as a surface analytical instrument in light of the definition of a solid surface as the outermost atomic layer and the depth of penetration of the electron beam. At these  $E_o$  conditions the elemental information is generated in a microvolume ranging to several thousand angstroms in depth. Consequently, the characterization of surface atoms or thin films of 10 to 1000 Å thickness is obscured by the x-radiation emerging from this microvolume of surface plus bulk material.

One technique to reduce the size of the microvolume excited is to operate at threshold and near threshold excitation conditions; thus reducing the mean free path of the electron to less than 250 Å for elements with  $z > 12$ . This means that x-ray excitation takes place very near the surface since electrons penetrating more than say 120 Å in the case of Cu suffer an energy loss,  $\Delta E$ , such that

$$E_o - \Delta E < E_{Cu K_\alpha}.$$

One obvious difficulty with this technique is low x-ray yield at near threshold conditions. To overcome this the excitation method used in appearance potential spectroscopy (A.P.S.) was adapted to the electron microprobe in a modified fashion. This technique is employed as follows:

1. The beam voltage is set either above or below the excitation potential of the x-ray line to be measured.
2. The specimen is biased with a programmable high voltage supply (either analog or digital).
3. The x-ray spectrometers (dispersive and nondispersive) were setup to record the single x-ray line.

The programmable supply is swept positive when  $E_o$  is below the excitation potential and negative when  $E_o$  is above the excitation potential to satisfy the following equation:

$$E_o + \Delta E \geq E_{\min}.$$

The integrated x-ray intensity is recorded over an arbitrary range of  $\Delta E$ . Figure 1 shows the  $\text{Cu K}_\alpha$  line isochromats on a normalized scale. The difference between the "turn on" point of both lines corresponds to the difference in their  $E_K$  values. One principal advantage of this technique is the sensitivity of the integrated intensity to very thin coatings, regardless of atomic number. Therefore this technique affords a unique method to determine film thickness and the presence of a contaminate oxide layer in the range of 10 to 1000 Å or greater.

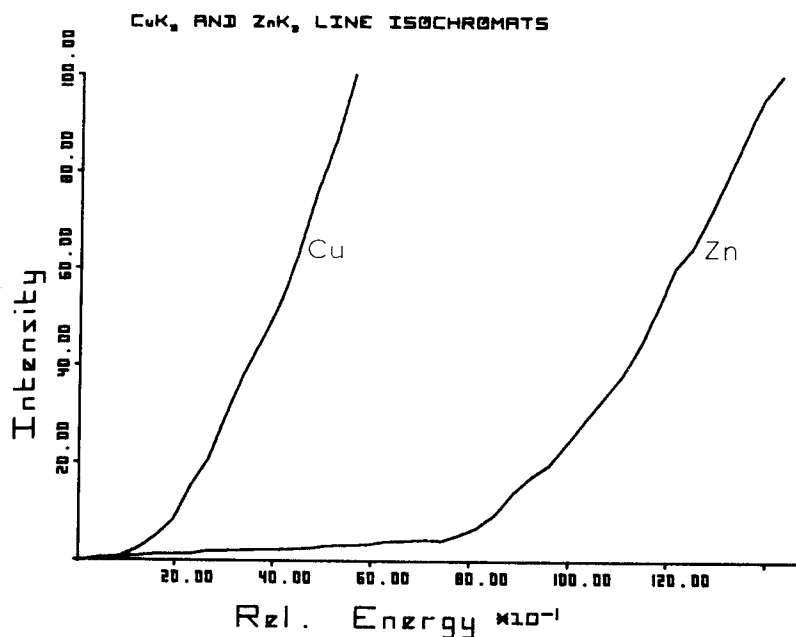


Figure 1.  $\text{CuK}_\alpha$  and  $\text{ZnK}_\alpha$  Line Isochromat Intensities (normalized) versus eV relative to  $E_{\text{CuK}_\alpha}$  and  $E_{\text{ZnK}_\alpha}$ .

Another surface sensitive technique employs the use of soft x-rays because of their extreme sensitivity to matrix absorption. The method used is expressed by the following simple relationship:

$$\frac{L_i}{L_m} \gtrless \frac{K_i}{K_m}$$

where  $K_i$  and  $K_m$  are the intensities of high energy lines such as the  $K_\alpha$  lines of the impurity (i) and matrix (m) elements respectively at a high beam potential such as 30 KV.  $L_i$  and  $L_m$  are then the intensities from low energy lines or bands such as  $L_\alpha$  of the impurity and matrix elements at a low beam potential, such as 5 KV.

If  $\frac{L_i}{L_m} > \frac{K_i}{K_m}$  the impurity is located on or very near the surface.

#### REFERENCES

1. R. L. Park, J. E. Houston, and C. G. Schreiner, R.S.I., 41, 1810 (1970).

# PROSPECTS AND DIFFICULTIES IN HIGH SPATIAL RESOLUTION SURFACE ELECTRON PROBES\*

T. W. Rusch and W. P. Ellis

Los Alamos Scientific Laboratory, University of California, Los Alamos,  
New Mexico 87544

Although electron microprobes with  $E > 5$  keV are highly developed and are used extensively for materials characterization, the range most sensitive to the outermost 2-4 atomic layers, i.e. 10-1000 eV, has received comparatively scant attention. The low-energy electron surface microprobe with high spatial resolution, i.e. with a beam diameter  $\sim 50$  nm and capable of operating in the scanning, diffraction, dark-field, and inelastic spectral modes, offers many fascinating possibilities worth exploring. Inhomogeneities and irregularities of the outermost 2-4 atomic layers, the identification of surface subphases in alloys and non-stoichiometric materials, the high resolution characterization of the surfaces of grains and grain boundaries of microcrystalline solids, and the growth of epitaxial nuclei are examples of an appealing array of subjects that could be examined and correlated with such a multi-functional instrument.

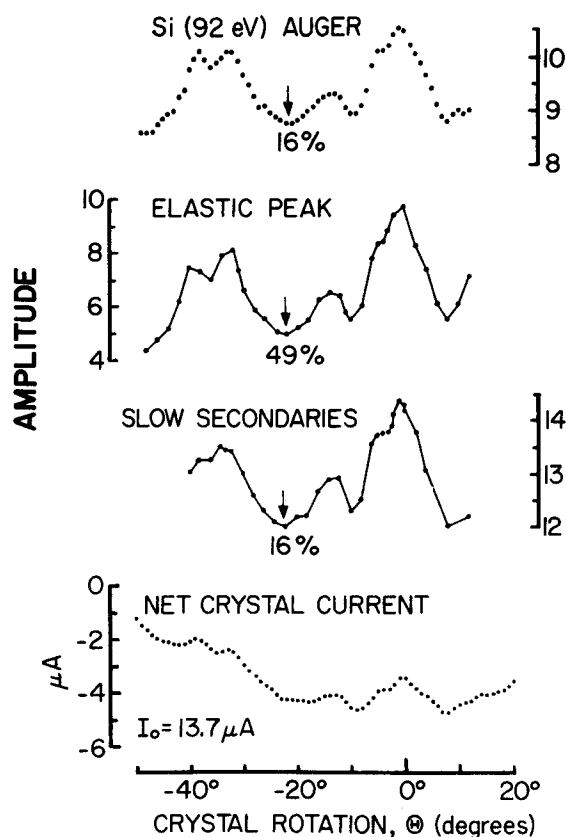
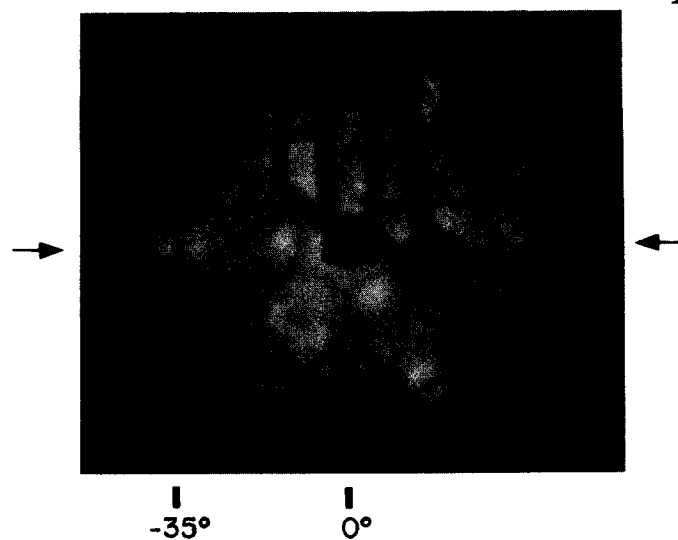
However, apart from the anticipated difficulties of instrumental design and the severe limitations imposed by beam damage, a surface sensitive probe is subject to complexities not associated with the bulk. In this talk some of the complexities specific to surfaces and surface microprobes will be discussed. In particular, examples will be taken from our work to illustrate (a) faceting and (b) the Kikuchi correlation in low-energy valence-band Auger emission (1), and their implications with respect to the study of microcrystalline solids.

As a separate concluding topic, the prospect of deriving atomic positions in epitaxial overlayers by means of a dark-field 100 eV electron microscope will be illustrated with optical analogs (2).

## REFERENCES

1. Ellis, W. P., Rusch, T. W., and Bertino, J. P.: "Kikuchi Correlations in Low-Energy Electron Spectroscopy." Oral presentation at the 33rd Annual Conference on Physical Electronics, Berkeley, CA, (28 March 1973). Submitted for publication.
2. Ellis, W. P.: In "Optical Transforms" (H. Lipson, ed.), Chp. 7, Academic Press, N. Y. (1972).

\*Work performed under the auspices of the U. S. Atomic Energy Commission.



The Kikuchi Correlation. Data shown for the  $(11\bar{0})$  plane of incidence (arrows) of Si(111),  $E_p = 1000$  eV. A strong correlation is observed among a) the Kikuchi display, b) the angle of incidence of primary electrons, and c) the amplitudes of features in secondary electron spectra from single crystals. As the angle of incidence is changed and the primary beam becomes parallel to the Kikuchi bright or dark zone, the flux of scattered electrons respectively increases or diminishes by as much as a factor of 2. With randomly oriented microcrystalline solids the correlation will be a prominent factor in the low E signal variation between different grains.

AN EXPERIMENTAL SYSTEM COMBINING MEDIUM ENERGY ELECTRON DIFFRACTION  
AND SCANNING ELECTRON MICROSCOPY

J. M. Cowley, F. A. Koch, and J. L. Albain  
Arizona State University, Tempe, Arizona

Abstract published in EMSA Proceedings

## SOFT X-RAY ABSORPTION SPECTROSCOPY USING THE ELECTRON MICROPROBE

D.G.W. Smith, Department of Geology, University of Alberta, Edmonton, Alberta, Canada  
K. Norrish, C.S.I.R.O. Division of Soils, Glen Osmond, S.A. 5064, Australia

In recent years it has become apparent that the electron microprobe can be used as a versatile tool in the study of soft X-ray emission spectra. To date the instrument has not, however, found a comparable rôle in investigations of the complementary absorption spectra. This paper describes techniques that have been developed which allow long wavelength absorption spectra to be obtained using the microprobe as the spectrometer and which are applicable to any substance that can be prepared as sufficiently thin films. The spectra reported here are in the region of O, Mg, and Si K absorption edges, but the basic technique should be suitable for any wavelength shorter than oxygen and can probably be extended to even longer wavelengths.

A late model Cambridge Instrument Company Geoscan microprobe was used in the experiments. The only modification was the addition of a small motor-driven unit which moved an aluminium frame supporting the film to be studied, in and out of the X-ray path in front of the detector slits and which could be switched from outside the spectrometer housing. This unit is illustrated in Fig. 1. In some experiments the frame carried a film 1  $\mu\text{m}$  or less thick of stretched polypropylene onto which was deposited the material being investigated. Polypropylene,  $(\text{CH}_2)_n$ , was used because it will not affect the shape of the absorption band in the region of the oxygen K edge and because it may be stretched to very thin and yet relatively strong films. Various high-purity metals in the sample position of the microprobe were used as targets and high probe currents (up to 10  $\mu\text{A}$ ), usually combined with an operating voltage of 15 or 20 KV, were employed to generate an intense continuum. Particular wavelengths were selected from the continuum by standard analysing crystals. The intensity of the diffracted radiation was measured by a flow proportional counter, with the absorber film alternately in and out of the beam to determine the attenuation produced. A range of wavelengths in the vicinity of absorption edges were studied in this way.

A major problem encountered was the elimination of unwanted radiation of different energy. Such radiation included fluorescent X-rays excited in the analysing crystal, higher orders of the target characteristic and continuum radiations, scattered and secondary electrons, cosmic rays and electronic 'noise'. Tight pulse height analysis was used to discriminate against all of these signals, but by itself, did not entirely eliminate them. It was found, however, that if methane was used instead of P-10 (90% Ar + 10% methane) as the counter gas, entirely satisfactory results could be achieved. Methane is not an efficient stopper of the harder, interfering radiations which consequently pass through the counter largely undetected, while the soft radiations of interest are efficiently absorbed. Use of methane also effectively eliminates a problem (which may become very severe, particularly with KAP analysing crystals) of low energy Ar escape peaks which pass easily through the discriminator window. To test whether unwanted radiation had been satisfactorily attenuated, the relatively thick mylar window, which can be inserted on this instrument to isolate the sample chamber from the spectrometer, was used: this window absorbs virtually all soft radiation and any intensity still recorded by the system is unwanted. Thus, to obtain more accurate data, small corrections can be made on the basis of the counts recorded with the mylar window in the X-ray path. Another important effect observed is one which occurs when a characteristic line rather than the continuum provides the X-ray intensity. There is a significant contribution of characteristic



radiation wavelength  $\lambda$  at spectrometer settings of  $\lambda \pm \Delta$ . This is due to the normal distribution in X-ray peaks diffracted by analysing crystals, and its contribution may swamp that of the adjacent continuum of true wavelength  $\lambda \pm \Delta$ . Consequently, targets with characteristic lines in the region being studied are only useful for providing accurate data points at the precise wavelength of that line. In general, for the rest of the region, a target material free of characteristic lines in the region of interest must be used.

To check further that unwanted intensity of all kinds had been satisfactorily eliminated, experiments were performed using two or more different target materials and two different analysing crystals. Essentially identical values obtained for  $\mu_{\ell}$  in each case, and close correspondence to values obtained at the exact positions of a few characteristic lines of other elements, indicated that the approach was successful.

Fig. 2 shows O, Mg and Si K absorption spectra and the associated  $K\alpha$  or  $K\beta$  emission spectra, obtained from thin films of vermiculite. The films were prepared by depositing the mineral from suspension onto a polypropylene supporting film. Different thicknesses of film were required, of course, to study the absorption of radiation in the three energy ranges. In general, detail on the absorption spectra is reproducible, clearly resolved and varies from element to element. The three spectra show interesting fine structure of the 'Kossel' and 'intermediate' types [1]. There may be some very fine structure in the immediate vicinity of the absorption edge which is not resolved. The position of the absorption edge for oxygen clearly indicates that there is no significant overlap of the absorption band onto the emission band and thus that changes in relative intensity within different parts of this emission band, which may be observed as the excitation potential is varied [2], must be related to phenomena other than absorption.

The oxygen K absorption spectra of two organic films studied (mylar and collodion) both show an interesting feature at about 531 eV, in the presence of an intense and sharp peak in the absorption spectra. This is a real effect and is not related to the analysing crystal used, appearing identically regardless of whether the X-rays were diffracted by KAP or clinocllore. Its energy corresponds exactly to that of the anomalous peaks in oxygen emission spectra, which have been shown to be produced as a result of reflectivity spikes of acid phthalate crystals [3].

The oxygen K absorption spectrum from  $\text{SiO}_2$  is interesting in that it differs from the vermiculite spectra in the lack of pronounced intermediate structure. It is, in fact, similar to Van Nordstrand's type IVa spectra [1], particularly in the presence of the small peak which occurs in this case at about 531 eV. This film was prepared by vacuum evaporation of  $\text{SiO}_2$  onto polypropylene and it is probably amorphous silica. The type IVa structure is characteristic of isolated tetrahedral ions [1]. A rather similar spectrum lacking intermediate fine structure but without the peak at about 531 eV was obtained from an SiO film produced in the same way.

Although spectra illustrated here show the variation of  $\mu_{\ell}$  (normalised to a value of 10 at peak) versus energy, there is, intrinsically, no reason why variations of  $\mu_m$  should not be studied successfully provided films of known thickness and density are used. It may thus prove possible to make useful and accurate measurements of mass absorption coefficients at long wavelengths where reliable data are at the moment very sparse. However, fine structure associated with these absorption edges emphasises the fact that, close to an edge, mass absorption coefficients at particular wavelengths for element absorbers are severely affected by factors such as the material in which the element is present, the bonding processes in which it is involved, the coordination state, crystallinity effects and possibly temperature.

Soft X-ray emission spectra are derived largely from the valence shells of atoms and it is becoming increasingly clear that they carry much useful information on the energies of the bonded levels. For some such spectra it has proved possible to make reasonable interpretations of the energy/intensity distributions by means of qualitative applications of molecular orbital theory [4]. Absorption spectra are the complement of emission spectra inasmuch as the structure at an absorption edge may be visualised as resulting from transitions to largely vacant antibonding levels. It can be anticipated, therefore, that a detailed study of the structure of such spectra may reveal interesting and useful information on the energies of these outer valence shells.

## References

- [1] Van Nordstrand, R.A. (1967): Fine structure in absorption-edge spectra. In: Handbook of X-rays (E.F. Kaelble, ed.), pp. 43-1 - 43-18, McGraw-Hill, New York.
- [2] Smith, D.G.W. & O'Nions, R.K. (1972): Investigations of bonding by oxygen  $K\alpha$  emission spectroscopy: further evidence concerning the true character of the oxygen  $K\alpha$  emission band. Chem. Geol. 19, 145-146.
- [3] Liefeld, R.J., Hanzely, S., Kirby, T.B. & Mott, D. (1970): X-ray spectrometric properties of potassium acid phthalate crystals. Advan. X-ray Anal. 13, 373-381.
- [4] Fischer, D.W. (1970): Molecular-orbital interpretation of the soft X-ray  $L_{II,III}$  X-ray emission and absorption spectra from some titanium and vanadium compounds. J. Appl. Phys. 41, 3561-3569.

Fig. 1. View of the special apparatus used, with spectrometer housing open. 1: motor unit. 2: Al frame with film mounted. 3: (methane) gas flow proportional counter. 4: sealed proportional counter.

Fig. 2. Composite of O, Mg and Si K absorption and emission spectra obtained for vermiculite. Intensity and  $\mu_{\lambda}$  normalised to 10 at peak. Solid and open circles represent data points obtained using different target materials and/or analysing crystals. Note that alignment of the three pairs of spectra is arbitrary and is based on the onset of the absorption edge.

Fig. 3. Oxygen K absorption band for mylar (polyethylene tetraphthalate) with superimposed oxygen emission spectrum from  $MgO$ . The latter was obtained using a KAP (potassium acid phthalate) analysing crystal. Note the precise correspondence at 531 eV\* between the anomalous peak in the emission spectrum and the first peak in the absorption band.

Fig. 4. Oxygen K absorption band for a collodion film. Again, note the presence of the sharp peak at about 531 eV\*.

Fig. 5. Oxygen K absorption band from vacuum evaporated  $SiO_2$  deposited on a polypropylene supporting film. Cf. type IVa structure in ref. [1].

\* All energies determined by reference to the position of the 7th order Cd  $L\gamma_1$  line ( $\lambda$  eff. = 23.349 Å).

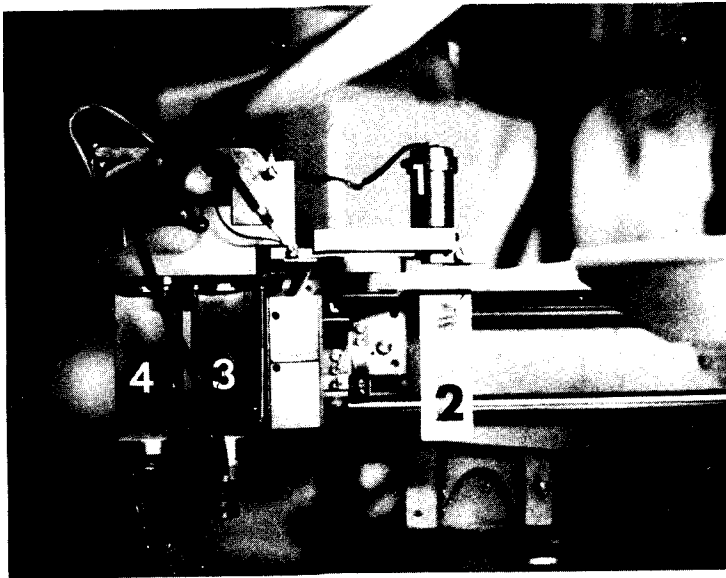


FIGURE 1.

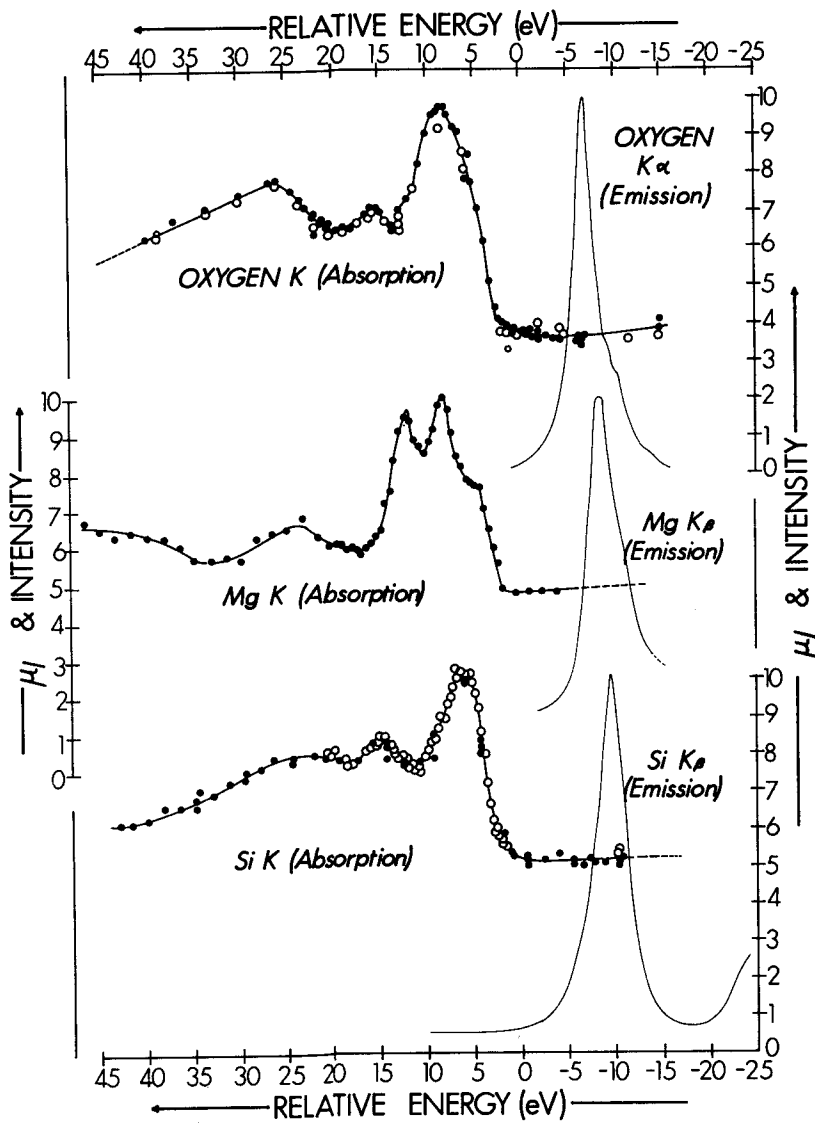


FIGURE 2.

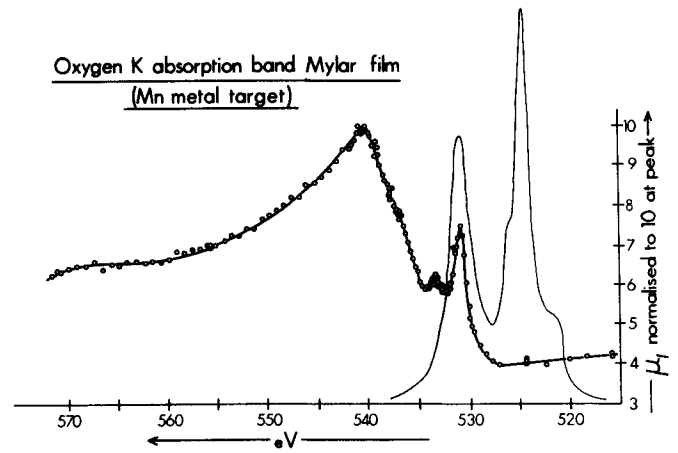


FIGURE 3.

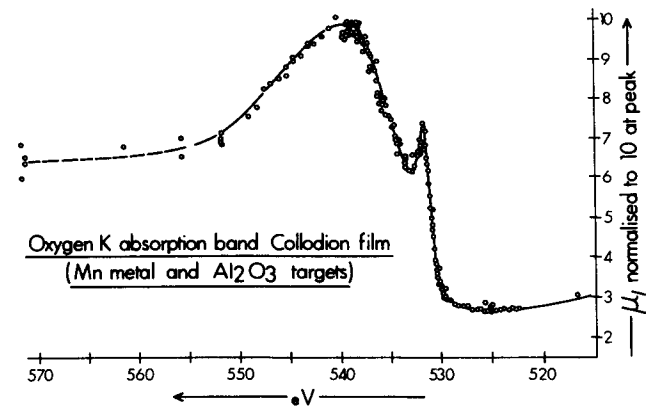


FIGURE 4.

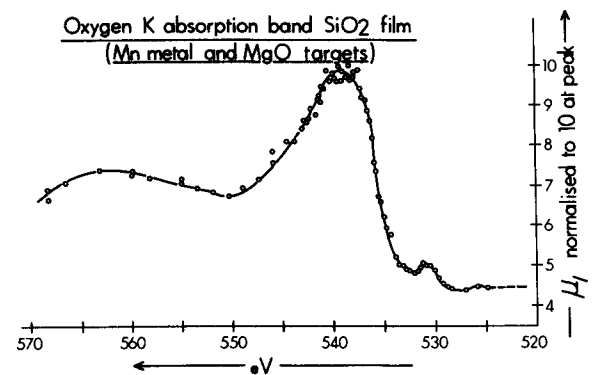


FIGURE 5.

A Universal Type Pressure Controller for  
Thin Window Flow Proportional Counters\*

Charles E. Hugenberger  
Wayne J. Steele

Lawrence Livermore Laboratory

ABSTRACT

Recent work at the Lawrence Livermore Laboratory has demonstrated that Thin Window Flow Proportional Counters when adjusted to critical sub-atmospheric pressures show a marked improvement in performance.

Factors that affect the performance of counters are the operating voltage, type of gas, spectrum wavelength, geometry of the counter and even the variations in leak rate of supposedly identical counters.

The critical pressure of any given counter can be determined experimentally by the operator using a newly developed pressure controller. The following described apparatus will not only pump down and vent the counter along with the electron microprobe but can be infinitely adjusted to produce or reproduce any desired operating pressure.

General Operation

Referring to Figure 1, the controller is connected as follows:

- C-5, to a small vacuum pump
- C-6 and C-7, to the proportional counter
- C-8, to the counting gas supply
- C-9, to the electron microprobe

Valves V-3 and V-4 are controlled by the vacuum switch, and are set to close at pressures below the set point, and open at pressures above the set point.

Valves V-1 and V-2, by balancing the action of the vacuum pump against the supply pressure of counting gas, can be set to maintain any desired pressure whenever valves V-3 and V-4 are closed.

Because valves V-3 and V-4 have greater conductance than valves V-1 and V-2, their action is to overpower any pressure settings derived from V-1 and V-2 adjustments.

The sequence of operations is as follows:

1. During installation of a thin window flow proportional counter into the electron microprobe, the vented condition of the microprobe is sensed by the vacuum switch which in turn opens V-3 and V-4.
2. During the rough pumping of the microprobe, both the counter and microprobe are common and are pumped down together.
3. At a discrete pressure (below lowest usable counter pressure and yet above the diffusion pump head pressure), valves V-3 and V-4 close, thus allowing the counter to shift slowly to the pressure derived from the settings of V-1 and V-2.

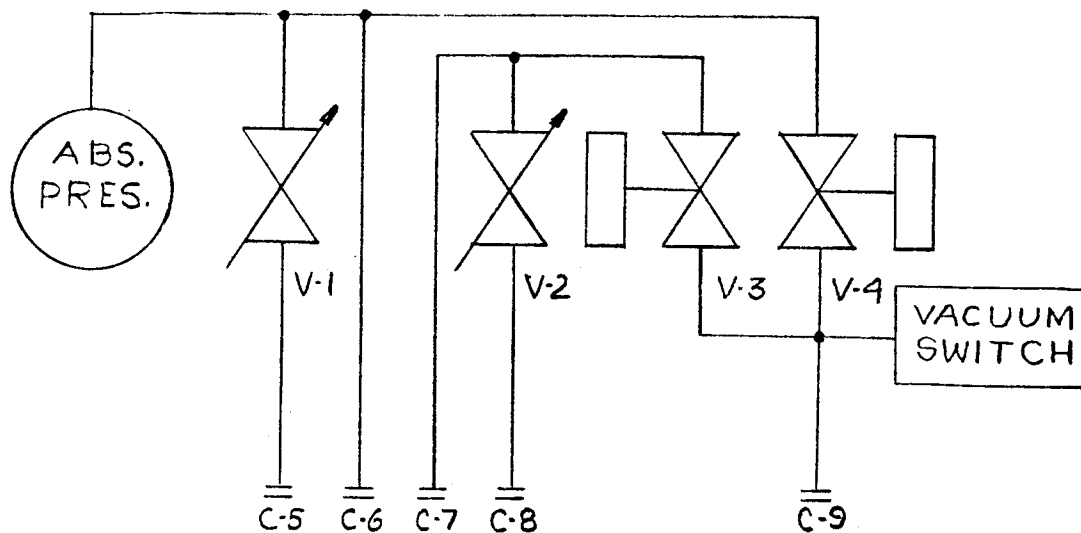
4. Whenever the microprobe is vented, the rising pressure is immediately sensed by the vacuum switch to open valves V-3 and V-4 so that the counter can be vented along with the microprobe.

The electromagnetic radiation emanating from solenoid valves V-3 and V-4 is present only during the roughing and venting cycles of the microprobe. During counting operations there is no trace of radiation and therefore no interference with sensitive counting circuits.

The use of the described pressure controller allows the operator to change the operating pressure and flow characteristics at will, in order to optimize the counting rate from various soft x-ray energy levels.

\*Work performed under the auspices of the U.S. Atomic Energy Commission.

FIGURE 1



SCHEMATIC, PIPING T.W.F.P.C. PRESSURE CONTROL

A PHOTOEMISSION ELECTRON MICROSCOPE USING AN ELECTRON MULTIPLIER  
ARRAY

W. J. Baxter and S. R. Rouze  
Research Laboratories, General Motors Corporation, Warren, Michigan

Abstract published in EMSA Proceedings

PHOTO STIMULATED EXOELECTRON EMISSION FROM SLIP LINES -- A NEW  
MICROSCOPY OF METALS DEFORMATION

W. J. Baxter and S. R. Rouze  
Research Laboratories, General Motors Corporation, Warren, Michigan

Abstract published in EMSA Proceedings

AUGER ELECTRON EMISSION MICROGRAPHY AND MICROANALYSIS OF A STAINED  
SURFACE OF PURE IRON PLATE

S. Hayakawa, H. Okano, S. Kawase, and S. Yamamoto  
Central Research Laboratory, Hitachi Ltd., Kokubunji 185, Japan

Abstract published in EMSA Proceedings



The Sandia Approach to Electron Probe Automation\*

W. F. Chambers

Sandia Laboratories  
Albuquerque, New Mexico 87115

Sandia Laboratories, Albuquerque, has been one of the pioneers in the electron probe automation field. Our first computerized system was developed by linking an 8k PDP8/I mini-computer to a 1962 vintage ARL-EMX microprobe. A major goal was to be able to utilize the same system for multi-channel data acquisition and analysis and for instrument control. To achieve this purpose, it was decided to include a mass-storage device and to operate under a keyboard monitor--that is, to have a master program which is capable of calling any program stored on the mass-storage device.

The original hardware configuration for the system included an 8k PDP-8/I, a 256k-word disk, a cartridge tape unit, a teletype, an analog-to-digital converter, a CRT display, a stepping motor interface, and a Canberra interface coupled to the scaler-timer and digital-to-analog converter systems. The disk was chosen over magnetic tape in order to provide random access to data files and because at the time (1968) there was little cost difference between it and a tape system that could operate with a monitor. The cartridge tape was used almost exclusively as a back-up to the disk (a complete reload of the disk would take 30 minutes from the tape but about 15 hours from a teletype paper-tape reader. This system has recently been expanded to include 12k words of core, a dual DECtape drive, and a 30 character/second DECwriter.

Initial programming efforts were via the machine-language route. Soon, however, it was realized that it would take years to create a flexible operating system via this route, so the high-level languages

---

\*This work was supported by the United States Atomic Energy Commission

were examined. At the time, the available language group included compiler-level Fortran and Basic and the interpretive language FOCAL. Of these, FOCAL best suited our needs because it provided ease of program development, interrupt capability, and efficient core usage. Our effort, therefore, has been put into developing operating programs written in FOCAL and in developing an improved version of FOCAL. The latter effort has resulted in the development of OS/8 PROBE FOCAL, a FOCAL system which operates under the OS/8<sup>(1)</sup> monitor and is itself capable of issuing commands to the monitor. PROBE FOCAL is thus capable of program chaining and input-output to any peripheral device. It is also capable of driving a Calcomp plotter and, of course, the various stepping motors, scalars, timers, multiplexers, and analog-to-digital converters associated with an automated microprobe.

Within the past two years a second computerized microprobe, an ARL EMX-SM, has been installed at Sandia Albuquerque. In order to maintain software compatibility, this system was also designed around a PDP-8 series computer. It includes a 12k PDP-8/E with dual DECTape, a DECwriter, an analog-to-digital converter, a CRT display, and ARL interfaces to the stepping-motor, scaler-timer, digital-to-analog converter, and multiplexer systems. The major differences between this system and the original one are the use of a computer with 12k words of core memory and the use of a magnetic tape as the primary mass-storage device. The advantages of the tape system are lower cost and the ability to store data in a format that is compact and easily retrievable both by the mini-computer and by a large computer. The disadvantages of the tape system are its inability to randomly access single words within data files and its relatively slow response time as compared to a disk-operating system.

Most control software for the two machines is identical except for minor command differences that are hardware related. Standard control programs include spectrometer focus, spectrometer alignment, and data collection and reduction. Special data collection programs are written as they are required.

---

(1) OS/8 is a trademark of DIGITAL EQUIPMENT CORPORATION

As a multi-channel analyzer, the computer can store data in either of two memory areas, add or subtract areas, perform background subtraction and peak area integration, and display a marker. The multi-channel analysis capability is used with an energy-dispersive analyzer for qualitative analysis and to determine true operating voltages. It is also used to determine appropriate single-channel baseline and window settings.

Major applications of computer control in our laboratory have been in the examination of diffusion couples and in the development of homogeneous materials. For this work we use a control program that includes on-line data reduction via an iterative scheme similar to that used in Colby's MAGIC. Prior to running this program, all element-dependent concentration-independent data are calculated via a Fortran program and stored on a file in the mass-storage device. The operating program then references that file for the element-dependent data. The operating program cross-checks its element and operating voltage information with that in the referenced file before accepting the data. If the element data are acceptable, the program collects, reduces, and outputs data from the sample. In this process, the data reduction and output from one point are performed while data from the next point are being collected.

Examples of both quantitative and qualitative results will be presented.

TIME-SHARED COMPUTER CONTROL OF ELECTRON MICROPROBE  
AND X-RAY DIFFRACTION EQUIPMENT\*

W. Holzwarth, Elizabeth Quigg, and C. T. Prewitt

Department of Earth and Space Sciences  
State University of New York  
Stony Brook, New York 11790

INTRODUCTION

A time-sharing system for the Digital Equipment Corporation PDP-15 has been developed to control an electron microprobe, a single-crystal X-ray diffractometer, and a powder X-ray diffractometer. Each of these instruments is connected to the PDP-15 through Canberra Industries electronics and the DEC LT19 multistation control which handles five teletypes or teletype-like units. The Canberra units look like fast teletypes to the PDP-15 and send data and receive a repertoire of commands from the PDP-15 as teletype-like messages to control the experimental equipment.

The computer configuration includes a 16K PDP-15 with automatic priority interrupt, real time clock, three teletypes (one 35, and two 33's), three DECTapes for data storage, and a 250K word disk (RF15). Other peripherals include a card reader, a Vpl5A display scope, paper tape reader, paper tape punch, and Calcomp plotter, none of which are presently used in the time-sharing system. However, these devices are available for program development and for running various application programs. A telephone-line link with a PDP-10 will eventually allow the transmission of data to the Stony Brook Computer Center for data reduction and analysis. Currently, DECTapes must be carried to the Center to be read by the PDP-10.

Important features of this system are as follows:

1. Application programming is all in FORTRAN IV, thereby permitting students and staff to write new programs and change old programs with a minimum of difficulty.
2. Time-sharing program uses less core (16K) than would be required with commercially available time-sharing packages.
3. The concept of making each experiment look like a teletype to the computer allows for effective and inexpensive communication over relatively long distances between computer and experiment. This also permits updating and expansion of the system to be done with a minimum of effort.
4. On-line communication with a larger time-sharing computer such as the PDP-10 opens up unlimited possibilities for interaction with the experiments and the data they are producing.

---

\* Supported by State University of New York and NASA Grant No. NGR 33-015-123.

5. Unlike some systems of this type which are described but never satisfactorily operated, the system at Stony Brook has been in operation for one year and during that time has produced approximately 4000 partial and complete microprobe analyses and 40 sets of three-dimensional X-ray diffraction data. The latter include a number of data sets obtained at high temperatures (up to 1050°C) using the diffractometer furnace described by Brown, Sueno, and Prewitt (1973).

#### TIME-SHARING SYSTEM

The time-sharing system was designed to meet the following requirements:

1. To accommodate programs larger than will fit into 16K of core.
2. Provide independent control of three experiments using the three teletypes.
3. To provide the protection against crashes.
4. To insure compatibility with the DOS system software and to use the DOS resident monitor and device handlers.
5. To allow for the execution of utility programs.

All these features are provided by the Time-Sharing Monitor (T-S Monitor), an assembly language program that supervises the starting and stopping of individual experiments and their utility routines, all I/O to the Canberra units and the control teletypes, core-disk swapping, and software timers for the three experiments. Special handlers were written for the LT19 and for disk swapping.

The basic assumption in designing the system was that all programs are usually I/O bound, i.e., they are waiting for the completion of I/O on the Canberra or control teletypes rather than executing long sequences of calculations. Whenever I/O is initiated for one experiment, control is transferred to another experiment that has completed I/O. The T-S Monitor supervises the transfer of control from experiment to experiment as I/O is initiated or completed. On the PDP-15, a FORTRAN read or write hangs up the computer until I/O is completed. To provide compatibility between FIV and time sharing, all reads and writes are accomplished using encode/decode and calling subroutines in the T-S Monitor that initiate I/O in assembly language and allow for transfer of control to other programs until I/O is completed.

Disk-core swapping and overlaying of subprograms permit the accommodation of a series of many subprograms. The subprograms of all three experiments are not co-resident, but only reside in core when the particular experiment needs servicing. Each experiment can use all core available (i.e., that core not occupied by the DOS resident monitor, device handlers, and T-S Monitor). Disk swapping of current core images to and from three areas on disk (1 per experiment) provides this feature. The Chain and Execute

programs provided by Digital permit the overlaying of subprograms. The software for the time-sharing system resides on disk as two execute files, which are loaded by the Execute system program. During the chaining, the operator defines resident core (T-S Monitor and handlers) and a series of links that overlay each other (the subprograms for each experiment). During execution a link table keeps track of all core and disk resident links. Whenever a new link enters core, the old link and its variables are destroyed. The disk-core swapping of subprograms and link table associated with an experiment prevents their destruction whenever a link associated with another experiment must be called, and makes invisible to that experiment the execution of the other two experiments. For example, the programs to control the microprobe consist currently of 25 links, where a combination of any three of the 25 is always co-resident, sharing named common. The X-ray diffractometer program is only one link. While the time-sharing system is running, it occupies 173 blocks on the disk. An additional 506 blocks are needed for DOS system software and the three core images. There remain 345 free blocks for future expansion of the time-sharing system. The binary subroutines that are used as input in the chaining process currently occupy 175 blocks on DECTape.

The T-S Monitor provides software timers for each experiment to allow resetting hardware and restarting when hardware failures in the Canberra unit halt data acquisition, a recurring problem. The T-S Monitor intercepts system and FORTRAN IV errors created by subprograms to avoid crashing of the entire system. Each experiment can have its own utility programs that can be run whenever data acquisition has stopped.

The rest of this paper will describe the software for controlling the microprobe and X-ray diffractometer which has been used successfully for one year to collect data.

#### ELECTRON MICROPROBE

An ARL-EMX-SM electron microprobe with automation and interfacing by Canberra is one of the devices controlled by the PDP-15 in a time-sharing environment. Of the four spectrometers, three are automated and the fourth is semi-fixed. The programs are written in FORTRAN IV and when considered in totality would occupy approximately 14K of the 16K of core memory. Since core is needed for the supervisor time-sharing programs and system programs, use of a disk-core swapping and overlaying scheme was employed. Thus, less than 4K of the probe program is in core at any one time. The considerable program size is the result of the need of a highly interactive program to give the operator a large degree of flexibility with his data collection and the automated hardware, and the need of a complete reduction of the raw data for each analysis to allow real-time decisions on the analytical results. With the projected addition of yet more programs (i.e., plotting of data, data reduction for non-oxide analysis), and hardware (i.e., non-dispersive analyzer) for the automated probe, the use of a time-sharing link to a PDP-10 and/or the updating of the PDP-15 is planned.

At present, the microprobe program is useful only for oxide analysis. The program allows input of a maximum of 16 elements of geologic interest along with the necessary elemental parameters to control the spectrometers and for data reduction. The program gives the operator the ability to perform peak searching, define subgroups of elements called: mineral packages, obtain standard peak and background counts, and perform analyses with data reduction (Bence and Albee, 1968) for all the elements input or those in the mineral packages. The operator is able at any time to add, delete, or correct elemental parameters or mineral packages, and perform peak searching or collect new standard peak and background counts on one or all of the elements. The background counts are normally collected only once for each mineral package, but the option exists to collect new background counts. The form of the analytical printout is shown by the example in Table 1. The data for each element is in the order: unknown counts, unknown background counts, K-value, atomic fraction of cations, formula, detection limits, and weight percent. The average counting time for each element and the weight percent sum follows. If the formula was based on 4, 6, or 8 oxygens, an end-member analysis is also given for olivine, pyroxene, or feldspar, respectively.

Table 1

```

>CD/MP,OX
..75083,2,18  PYROXENE 13
..
..PYRX 6
..!BKG/X
..ANALYSIS
.SI      35366.67   900.00   0.4511   0.4710   1.8704   0.155   50.45
.AL      3380.50   883.00   0.0277   0.0368   0.1460   0.187    3.34
.TI      1536.00    74.00   0.0243   0.0186   0.0738   0.000    2.65
.FE      8044.00   220.00   0.0996   0.0878   0.3486   0.000   11.24
.MG     14636.00   448.00   0.1485   0.2440   0.9689   0.489   17.54
.CA     11895.00    70.00   0.1301   0.1360   0.5399   0.168   13.59
.CR       711.00   149.00   0.0073   0.0059   0.0235   0.000    0.80
.TIME =      26.05                                SUM =  99.61

.EN =  52.16
.WO =  29.07
.FS =  18.77
..!HYDOX
..

```

#### SINGLE-CRYSTAL X-RAY DIFFRACTOMETER

The single-crystal diffraction experiment was first set up with the computer dedicated to control and data processing for this experiment alone. When operated in this way, the program generated the hkl indices, calculated the necessary diffractometer angles, recorded the diffracted intensity peak, and calculated the observed structure factor and its error for each diffracted beam. The results were written on non-file-oriented DECTape for input to a large computer. When time-sharing was begun, this approach

proved to be impractical and the X-ray program was divided into two steps. In the first, reflection indices and angles are calculated and stored on non-file-oriented DECTape with space left over for the experimental results. Then, during data collection, these data are read in blocks of seven reflections each, the intensities are measured, and the entire set of data read out into the designated areas on the same DECTape. The program can be stopped and restarted at any point in the data collection process and a new set of angles can be generated at any time. Additional programs for crystal orientation and data processing have been written, but are not included in the time-sharing. Eventually, we plan to add automatic orientation (or re-orientation) programs to the time-sharing system.

Equipment has just been installed to transmit diffraction data over a private telephone line to the PDP-10 at the Stony Brook Computing Center. We expect to be able to transmit at a rate of 120 characters per second which will allow a set of 1000 structure factors to be sent to the large computer in less than four minutes. A separate remote terminal will then allow immediate data reduction and least-squares refinement on the PDP-10 without the investigator having to leave the laboratory.

#### POWDER X-RAY DIFFRACTOMETER

Automatic powder diffractometry has not advanced as far as the other techniques, but programs are just being finished which control the scanning of the powder diffractor, the identification and measurement of peaks, and least-squares refinements to obtain accurate cell parameters and peak intensity data.

#### REFERENCES

1. A. E. Bence and A. L. Albee (1968) Empirical correction factors for the electron microanalysis of silicates and oxides, *J. Geology* 76, 382-403.
2. G. E. Brown, S. Sueno, and C. T. Prewitt (1973) A new single-crystal heater for the precession camera and four-circle diffractometer, *American Mineralogist* (in press).



## PRACTICAL ASPECTS OF MICROPROBE AUTOMATION

W. B. Estill and D. E. Benthussen  
Sandia Laboratories  
Livermore, California

## ABSTRACT

An automated system for performing microprobe analysis will be described which consists of an ARL EMX-SM electron microprobe, a PDP-11 computer, Canberra hardware, software, and a PDP-10 time share system. The automated system (1) controls three X-ray spectrometers and performs a peak search routine, (2) moves the sample stage in the X, Y and Z directions, (3) makes PHA adjustments for each spectrometer and (4) collects and analyzes the X-ray data. The system is completely automatic following initial setup of the operating parameters. The initial input requires only notation of the accelerating voltage, the elements to be analyzed, the X-ray lines to be used, the X, Y and Z position of the samples and standards, and the number of times each sample is to be analyzed. The standards and samples can be placed in the same mount and need not be polished together since the Z axis is controllable. The system also simplifies various time-consuming microprobe operations, such as X-ray scanner calibrations. The concentrations of elements in Cu-Au NBS standards determined from an automated analysis agree to within 1% of the values determined manually.

ON-LINE QUANTITATIVE MICROPROBE ANALYSIS  
WITH A HOSTED IBM SYSTEM/7 COMPUTER

D. F. Kyser, G. L. Ayers, D. E. Horne

IBM Research Laboratory  
San Jose, California

---

Computer control of electron microprobes for data acquisition and analysis is becoming increasingly popular as evidenced in recent sessions of these conferences. There are two basic approaches to computer automation for on-line quantitative analysis. These can be described as "dedicated" stand-alone mini-computer and "hosted" mini-computer. The former approach is represented in the systems described by Eichen and Kunz,<sup>1</sup> Chambers,<sup>2</sup> Chodos and Albee,<sup>3</sup> and Colby.<sup>4</sup> The latter approach is represented by that of Kirkendall and Varadi.<sup>5</sup> A more general description of hosted-satellite computers in laboratory automation has been given recently by Grant, Lusebrink, and Taupin.<sup>6</sup>

In this laboratory we are utilizing the hosted-satellite computer concept with an IBM System/7 satellite computer connected via teleprocessing to the laboratory's main computer facility, a System/360 Model 195. The general system is shown schematically in Fig. 1. The System/7 is a small sensor-based computer with capability for priority interrupt. The main storage is 16K words of 16-bit length, and auxiliary storage of 2.5 M words is provided on-line via disk. The special telecommunication link between the host S/360 computer and the S/7 allows transmission rates of 50,000 bits/sec such that the host computer can completely load the main storage of the satellite in about five seconds.

The main role of the hosted S/7 is for instrument control and data acquisition. The main role of the host S/360 is for S/7 program preparation and subsequent data analysis. Program preparation is accomplished via a standard IBM 2741 terminal placed in the local S/7 area and utilizing the Time Sharing Option (TSO) of Operating System/360. Data transfer from S/7 to S/360 and back is also initiated with this terminal. For the data generated by the microprobe and transferred to the S/360, data analysis can commence immediately via MAGIC IV<sup>7</sup> or be stored indefinitely. A special S/7 command language named MAXOL, for Microprobe And X-Ray Operating Language, was created for internal IBM use only as described in reference 6. This language allows time-sharing of the S/7 for multi-instrument control.

Our ARL EMX-SM electron microprobe has been modified with non-commercial electronics to enable S/7 computer control of the X-ray spectrometers and timer-scaler system. High-speed stepping motors were incorporated into the normal gear wheel drive of the spectrometers without eliminating the existing

manual or DC motor drive capability. Stepping motor controllers were fabricated which allow both computer and manual commanding. Digitally controlled scalers with individual timers were also fabricated to overcome limitations in the reading speed experienced with the commercial scalers provided originally. These electronics are interfaced to the digital I/O terminals of the S/7 via a multiplexer which can also be manually controlled for diagnostic purposes. A special hardware feature of the system is an on-line Tektronix 4010 control keyboard and storage oscilloscope display console. This console contains hardware character generation and has been modified to interface with the multiplexer. Hence, each instrument can be controlled locally by its dedicated console, and the teletype console provided with the S/7 is used only for loading MAXOL from disk and for hard copy output. The teletype can also be used to control the instrument if desired, but must be placed with the remote S/7. The storage oscilloscope is used to display the command sequence typed before initiating a run, as well as to display data sets and spectra stored in the S/7. The speed and convenience of the Tektronix 4010 console, compared to a standard teletype, has greatly enhanced the practical use of the S/7 for our particular applications. Hard copy of information displayed on the oscilloscope is available via a commercial accessory.

Future plans include the use of conventional digital-analog converters coupled with the instrumentation described by Kyser and Horne<sup>8</sup> to provide computer control of electron beam current, voltage, and focus simultaneously.

We are pleased to acknowledge the assistance of Dr. Paul Grant for system engineering, Dr. Daniel Taupin for application programming and creation of MAXOL, and the Central Scientific Services Department of this laboratory for suggestions on electronic hardware design.

- 
1. E. Eichen, F. Kunz, and G. Matthews, Proc. 5th Nat. Conf. on Electron Probe Analysis (New York, 1970), paper No. 5.
  2. W. F. Chambers, *ibid.*, paper No. 7.
  3. A. A. Chodos and A. L. Albee, Proc. 6th Nat. Conf. on Electron Probe Analysis (Pittsburgh, 1971), paper No. 15.
  4. J. W. Colby, Seminar on Scanning Electron Microscopy and X-Ray Analysis, (Pittsburgh, 1971), Tutorial Notes.
  5. T. D. Kirkendall and P. F. Varadi, Proc. 6th Nat. Conf. on Electron Probe Analysis (Pittsburgh, 1971), paper No. 19.
  6. P. M. Grant, T. R. Lusebrink, and D. G. Taupin, Industrial Research, November 1972, pg. 50.
  7. J. W. Colby, Proc. 7th Nat. Conf. on Electron Probe Analysis (San Francisco, 1972), Tutorial Paper B(a).
  8. D. F. Kyser and D. E. Horne, *Rev. Sci. Inst.* 43, 1334 (1972).

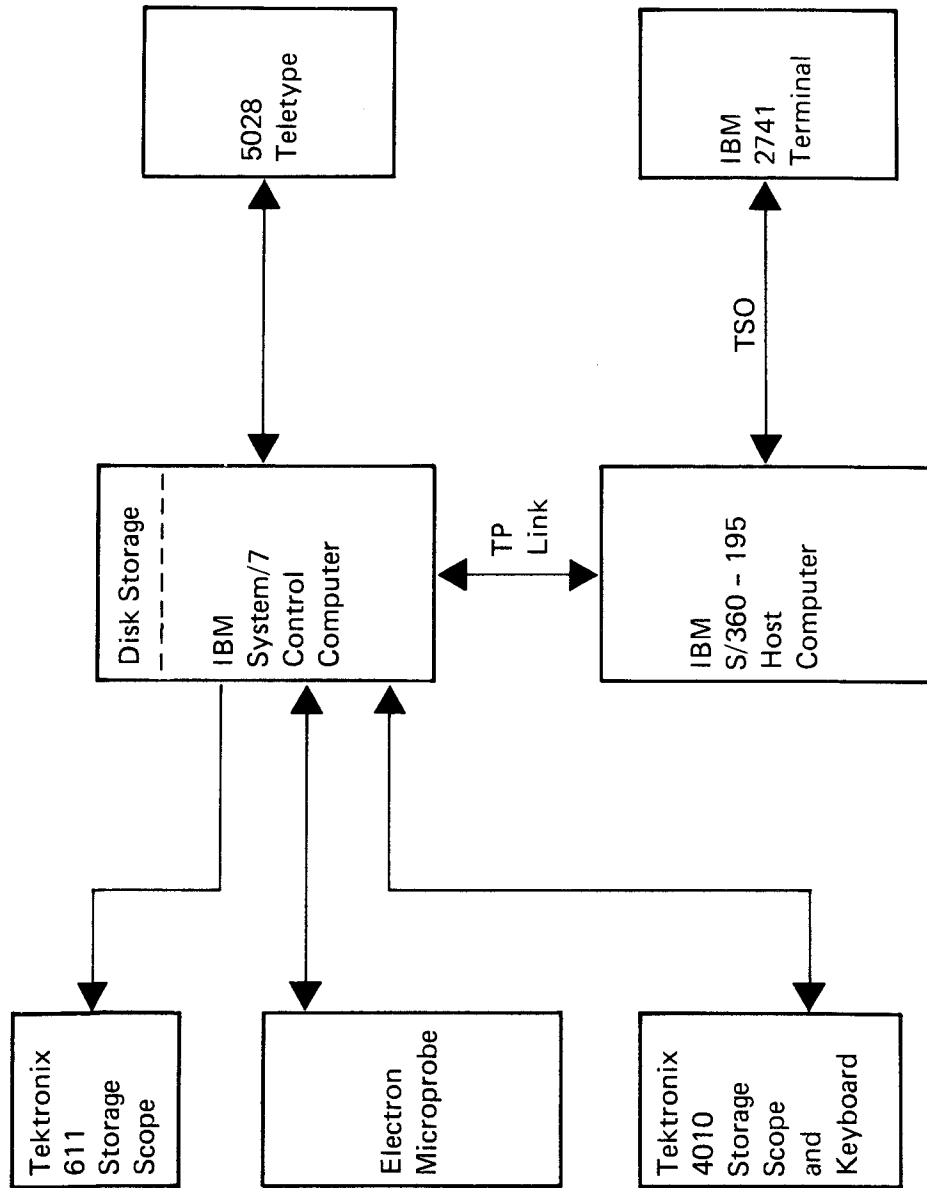


Fig. 1. Hardware schematic of hosted System/7 Computer and Electron Microprobe.



## OPTIMIZATION OF COMPUTER-CONTROLLED QUANTITATIVE ANALYSIS OF MINERALS

A. A. Chodos, A. L. Albee, A. J. Gancarz, and J. Laird

Division of Geological and Planetary Sciences  
California Institute of Technology \*  
Pasadena, California 91109

---

With the development of the computer-controlled electron microprobe, two basic approaches in programming the quantitative analysis of minerals have been used. In the first type of programming the instrument operator must input answers to a large number of questions before performing an analysis. The program is extremely flexible but requires the operator to have a thorough understanding of electron microprobe analytical techniques. In the second approach all choices, which include counting time, elements to be analyzed, and the order in which the elements are analyzed, are programmed for each mineral type. For this approach the operator does not require an extensive knowledge of analytical techniques to perform accurate quantitative analyses. This paper describes a computer program utilizing the second approach.

The program, ULTIMATE, is designed for quantitative analysis of most silicates, oxides, phosphates, carbonates, and sulfates. ULTIMATE is written in a high-level computer language, FOCAL (1969), and controls a Materials Analysis Corporation model 5-SA3 electron microprobe. The computer, a Digital Equipment Corporation 12K PDP-8/L, is interfaced to a Tennecomp Systems TP-1371 MiniDek magnetic cartridge tape deck. Control of the tape deck by FOCAL permits chaining in successive portions of the program during the actual analysis. FOCAL has been modified to include indexing of two-dimensional arrays and high speed calculation routines. These modifications increase the storage capacity for variables and constants by 67% and decrease calculation time from 50% to 80%. This increased efficiency results because the addresses of the doubly-indexed variables and constants are calculated by the computer rather than searched for by testing each entry in the list of variables and constants.

In writing ULTIMATE the main objective was to allow rapid quantitative analysis of the common minerals of geologic interest. Twenty-nine elements which are abundant in the common minerals and/or which have been shown to be significant to understanding the physical and chemical conditions of formation of the common minerals were selected to be analyzed. In addition, since all 29 elements never occur in any single phase, 22 mineral types were chosen, and the significant elements to be analyzed for each mineral type were selected from the list of elements. These combinations of elements and mineral types permit the analysis of all common rock-forming minerals and of nearly all different types of minerals in general.

The basic format of the program consists of: 1) an array of constant values, 2) a subprogram to run the standards, 3) the main portion of the program to control the acquisition of data and to compute the final chemical analysis, and 4) a subroutine for each of the 22 mineral types. The array of constant values consists of a 30 x 30 matrix of correction factors for the data reduction technique of Bence and Albee (1968) as modified by Albee and Ray (1970), stage coordinate locations of the standards for all elements, approximate peak position for all elements, and the constants for the calculations specific to each mineral type. Despite the size of the array, the modified version of FOCAL permits rapid location of the constants and consequently rapid calculation.

The standards subprogram moves each standard into position for analysis, searches for the precise peak, and collects counts on the standard. The peak search routine is a simple and rapid method for determining the peak position. Counts are accumulated for one second at each of 25 equally-spaced ( $10^{-4}$  Å apart) locations in an interval centered on the approximate peak. The location with maximum counts is determined, and those locations that have greater than 95% of the maximum counts are averaged to give the final peak position.

The main part of the program controls the actual data gathering and reduction. A peak search is done for those elements whose X-radiations are subject to wavelength shifts due to different crystallographic coordinations. Counts are accumulated for peak and respective background positions simultaneously for three elements. The counting time is 90 seconds unless counting statistics give a relative standard deviation of 1% in a shorter time interval. However, since there is only one scaler-timer for all three detectors, the actual counting time is the longest time calculated for any member of the triad of elements whose abundance is greater than about 1%. The final chemical analysis is calculated using the technique of Bence and Albee (1968).

The subroutine for each mineral type determines the sequence of elements to be analyzed. The triad grouping of elements was chosen for each mineral type to maximize the counting accuracy and minimize the counting time. The subroutines also contain specific calculations for each mineral type. For example, in the "opaque" subroutine the effect of the interference of  $Ti_{K\beta}$  on  $V_{K\alpha}$  radiation is calculated, permitting routine quantitative analysis of V. Additional calculations include determination of the amount of  $H_2O$  or  $CO_2$  present in the analyzed sample and correction of the other abundance values for the inter-element interferences due to  $H_2O$  or  $CO_2$ . To actually perform quantitative analyses, the appropriate subroutine is selected and the entire analysis is completed automatically.

The final chemical analysis is converted to cation percentages and formula proportions; the normalization factors for these values are set by the mineral subroutines. The formula proportions are used to calculate additional information for each mineral type. This information includes end-member mineral formulae, normative minerals, and significant element ratios.

Although the ULTIMATE program is very specific, it is written in a conversational language and can be readily modified to include analysis of additional elements and calculation of any other desired information.

#### Acknowledgements

FOCAL was modified by J. Crapuchettes of Frelan Associates. This work was supported by NASA grant NGL-05-002 and NSF grant GA-12867. The microprobe laboratory has been developed with the support of the National Science Foundation, the Jet Propulsion Laboratory, and the Union Pacific Foundation.

#### References

Albee, A. L. and Ray, L. (1970) Correction factors for electron probe microanalysis of silicates, oxides, carbonates, phosphates, and sulfates. Anal. Chem., 42, 1408-1414.

Bence, A. E. and Albee, A. L. (1968) Empirical correction factors for the electron microanalysis of silicates and oxides. J. Geol., 76, 382-403.

FOCAL (1969): Formulating On-line Calculations in Algebraic Language, Digital Equipment Corporation, Maynard, Mass.



MICROPROBE DIGITAL DATA ACQUISITION WITH  
THE MULTICHANNEL ANALYSER

by

W. T. Kane

Research and Development Laboratories  
Corning Glass Works  
Corning, New York 14830

Recently considerable development work has gone into the hardware for pulse height analysis for use with energy dispersive X-ray analysis on electron microprobes and scanning electron microprobes. Features such as character display, histogram generation, automatic energy calibration and X-ray line identification have done much to simplify an already fairly simple procedure, i.e., qualitative energy dispersive analysis (EDA). Self contained minicomputer data reduction programs have made possible quantitative analysis with EDA which is at least good as was possible with crystal spectrometers in 1965. Nothing which has been developed thus far has altered Beamans suggestion that electron probes (and SEM's used as probes) must be directed rather than administrated. On the other hand, the use of the multichannel analyser in multiscaler mode for data acquisition on electron probes or SEM's originally proposed by Solomon (1,2) has received rather little attention although it provides a significant extension of the analytical power of the instruments. Conventional X-ray imaging and profiling techniques involve the conversion of the digital count data generated by the instrument to an analogue form (film or strip chart recording) for purposes of display. Most options for quantification and/or data correction are usually irrevocably lost in the analogue conversion process. With a multichannel analyser properly equipped, the core memory is used as a scratch pad for the storage of X-ray intensity maps and profiles without compromising the digital nature of the data. When it is desirable to display the data in analogue format, it is done after the data collection phase is completed which gives the experimenter control over the process which is not possible in real time operation.

To accomplish multiscaler mapping and profiling, it is necessary that the analyser be equipped with an isometric display option, a time base generator, a display mode control and for control of the

probe electron beam, an x-y matrix generator. It is also desirable, but not necessary, that the analyser be equipped with a 4096-word memory, a four-channel multiplex buffer, an x-y recorder, and a computer compatible magnetic tape store. The block diagrams and the theory of operation for such a system have been discussed in detail elsewhere (3).

With the electron beam stepped across the sample surface under the control of the time base and matrix generator an array of sampled points is mapped into a corresponding array of analyser memory storage locations. With the aid of the isometric display option, the data may be displayed on the analyser scope as 1. a simple planar contour map, 2. an isometric projection (Figure 1) or 3. as a superposition profile. As there are only 4096 points in a 64 by 64 point array there is some degradation of the x-y spacial resolution which is compensated for by the vastly improved X-ray intensity resolution provided. The X-ray input for this type of mapping can be provided by either a crystal spectrometer or an energy dispersive spectrometer with a single channel analyser.

Selected areas of the matrix may be displayed to provide superposition profiles at any point in the array (Figure 2). In addition to the display flexibility, digital mapping is usually much faster than conventional X-ray imaging since multiple trials to get the proper exposure are not necessary. The data collection process may be stopped after each scan to determine if the statistics of the image are sufficiently good without loss of data. The data in the memory array can be dumped to magnetic tape and then corrected and plotted by a large computer to provide a highly detailed elemental concentration contour map (Figure 3). Direct background correction (not an electronic simulation) is carried out by detuning the spectrometer to the background and driving the beam an equal number of scans in the count subtract mode. The background correction shown in Figures 4 and 5 could not have been made using the delayed pulse comparitor technique.

A 4-input multiplex buffer allows inputs from 2 to 4 spectrometers to be mapped simultaneously into halves or quarters of the analyser memory. This mode of operation considerably shortens the time required to obtain multiple X-ray intensity images and in addition provides absolute register between the respective maps. Figure 6 represents 4 simultaneous maps of an ARL standard. Four single channel analysers (SCA) were paralleled on the amplifier output of an energy dispersive detector. The SCA outputs were connected to the multiplex buffer inputs.

In addition to the X-ray mapping modes discussed above we have used the ADC in multiscaling mode to digitize and map both sample current and cathodoluminescence data. It would be relatively simple to extend this technique to digitize the video output of an SEM secondary electron image to provide a rather good and inexpensive mode of quantitative image analysis.

In summary, the multichannel analyser has data handling capabilities useful in microanalysis which considerably exceed its use for pulse height analysis alone. The cost to implement these capabilities is a small fraction of the cost of the analyser equipped only for pulse height analysis.

#### REFERENCES

1. Solomon, J. L., Proceedings of the Fourth National Conference on Electron Probe Analysis, Paper No. 29 (1969).
2. Solomon, J. L., Use of the Multichannel Analyser to Make Concentration Maps in Conjunction with the Electron Microprobe, Septieme Congres International de Microscopie Electronique, Grenoble, France (1970).
3. Kane, W. T., and Williams, J.P., An Electron Microprobe Data Collection and Processing System Designed for the Microvolume Analysis of Glass, Proceedings of the IX Congres International de Verre, V. 1, P. 285-302 (1971).

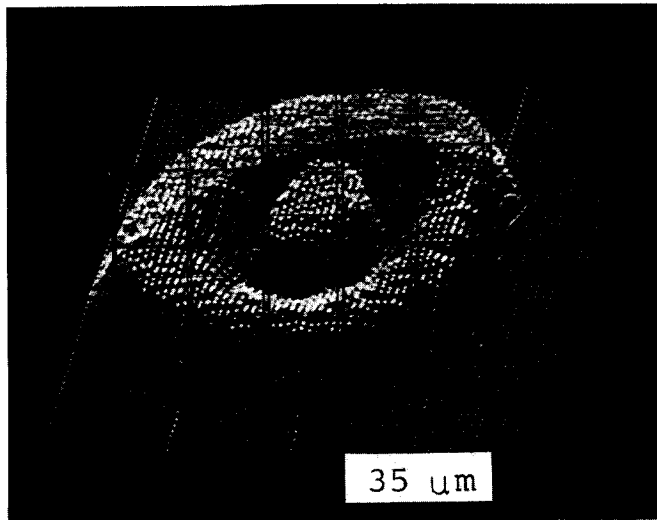


Fig. 1 An isometric X-ray intensity plot of the dopant level in a fiber optic filament.



Fig. 2 Superposition profile of 3 central x-lines from the data shown in Fig. 1.

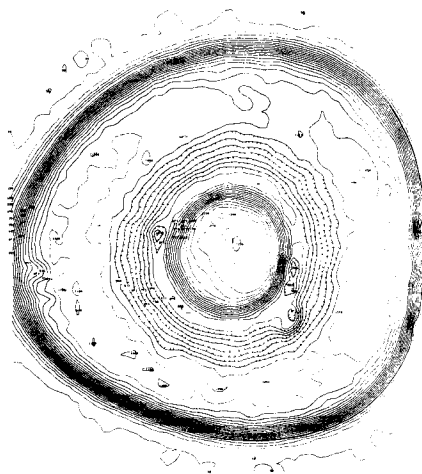


Fig. 3 A concentration contour map of the dopant element level on the same data as Fig. 1 which has been corrected and plotted off-line on a large computer.

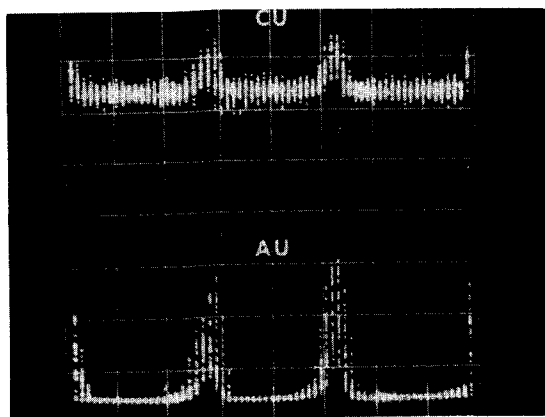


Fig. 4 Superposition profiles for Au  $M\alpha$  and Cu  $K\alpha$  taken on a ceramic capacitor. This data was taken in "add" store mode, and 40 scans of the matrix were made. Note that an apparent copper peak coincides exactly with the gold peaks. A careless interpretation at this point would assume that copper was present, alloyed with the gold.

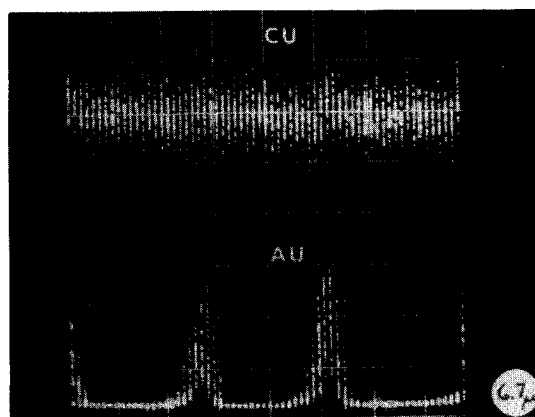


Fig. 5 After the data in Fig. 4 were accumulated, 40 more scans were made in the "subtract" store mode with the crystal spectrometers detuned just off the copper and gold peaks. This process removes white radiation background. Note that the "copper peaks" seen in Fig. 4 have disappeared, for they were actually the increased white radiation from the gold plates. The gold peaks remain, as they are real.

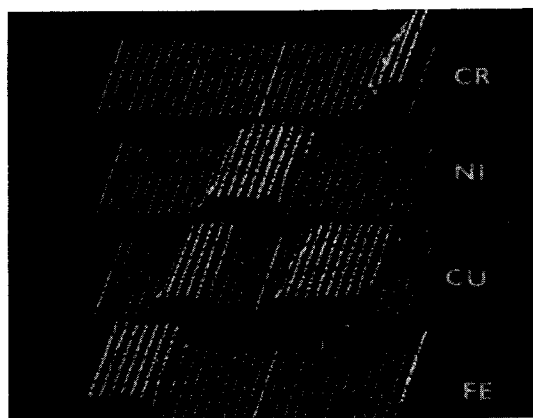


Fig. 6 Four 16 x 64 isometric concentration maps taken simultaneously using a single solid-state X-ray detector with four single-channel PHA's paralleled to the amplifier output. The sample consisted of an iron wire plated successively with copper, nickel, copper, and chromium.

ELECTRON MICROSCOPY AND X-RAY MICROANALYSIS IN FORENSIC SCIENCE

J. W. Johnson and J. L. Brown  
Georgia Tech, Atlanta, Georgia

Abstract published in EMSA Proceedings

DIRECT OBSERVATION OF FERROELECTRIC DOMAINS USING THE SEM

by

C. Michel, A. Sicignano

Philips Laboratories, Briarcliff Manor, N.Y.

The ability of the Scanning Electron Microscope (SEM) in the secondary electron mode of detection to detect changes in electrostatic potential by means of voltage contrast (VC) pictures has been widely used in the field of semiconductors and microelectronics.<sup>(1)</sup> This technique can also be used<sup>(2)</sup> to visualize directly ferroelectric domain structures associated with the surface charge perturbation induced by the electric polarization. Our study was devoted to ferroelectric materials, such as triglycine sulfate crystals (TGS), with domains of opposite polarization which cannot normally be directly observed with a polarizing microscope.<sup>(3)</sup>

Fig. 1 shows a typical SEM photomicrograph of the surface of a virgin, uncoated, multidomain TGS single crystal in the ferroelectric state; the VC mode of operation was used. To prevent the electron beam from poling the sample or damaging the surface, a low accelerating voltage (4 kV) with a low electron beam intensity ( $10^{-11}$  A) was used. The  $180^\circ$  domains, lenticular in shape and elongated along a preferential direction, are clearly delineated at the surface of the specimen.

In our study, a real time TV monitor coupled to a video tape recorder was used to display the VC signal, thus producing a direct recording of the motion of the domain walls. By using backscattered images on uncoated samples and VC images on gold coated samples, which are both insensitive to the electrostatic field caused by the electric polarization, the VC image of electrical origin could be unambiguously isolated from the surface topography of the sample. The observed domain patterns were quite unstable and very sensitive to the electron beam even with the real time display; polarization switching was observed as dark regions suddenly appearing on the TV monitor. Granular white spots (indicating a built-up surface charge distribution) were detected in the dark zones. A thin coating of carbon (200Å) was found to minimize this effect and also improve the stability of the VC image.

After several scans (or by increasing the electron beam intensity), the contrast between  $180^\circ$  domain patterns decreases rapidly. Fig. 1 is an example of such a flat contrast showing only the delineation of the ferroelectric domain walls. This effect is explained by a rapid neutralization of the positive surface charge by the electron beam. After few scans the electric field induced by the built-up surface charge is sufficient to reverse the polarization. The dark island created by this switching process is then compensated and the contrast disappears again leaving a larger delineated domain area. The initial and final states of this polarization switching process are clearly illustrated in the photomicrographs of Figs. 2, 3 and 4.

An electric field parallel to the axis of the spontaneous polarization was applied by means of a thin gold evaporated contact. The velocity of wall movements and the number of points at which domain growth starts were both found to increase with the strength of the applied field. The effect induced by a partial field scan, shown in Fig. 5, will be discussed. Local positive switching induced by the electron-beam scans appears as sets of parallel lines as shown in Fig. 6. Such lines are only visible in non-adjacent domains; thus providing a convenient means for characterizing the polarization state as well as the domain shape of a compensated specimen surface.

Preliminary SEM investigations in a dynamic mode extended to other single crystal and polycrystal ferroelectric materials will also be discussed.

### References

1. W. H. Hackett, R. H. Saul, R. W. Dixon and G. W. Hammlott, J. Appl. Phys., Vol. 43, No. 6, 2857 (1972).
2. Scanning Electron Microscopy; Applications to Materials and Device Science, P. R. Thornton, P. 300.
3. Ferroelectric Crystals, F. Jona and G. Shirane, Pergamon Press, 62, p. 47.



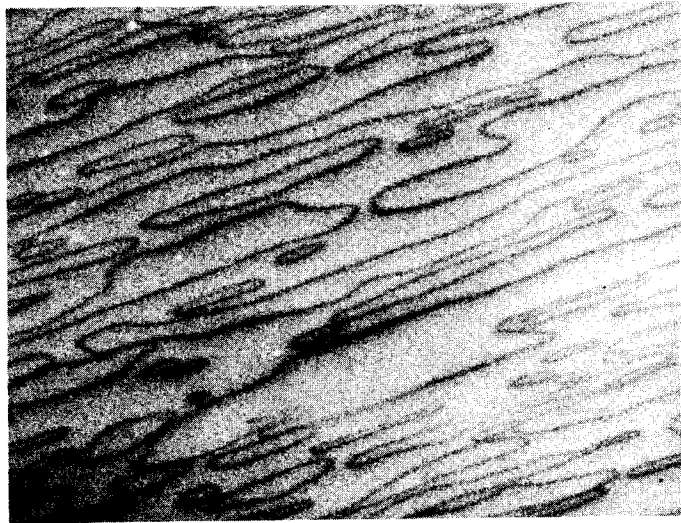


Fig. 1 - Typical domain structure of a TGS crystal, 200 X.

Fig. 5 - Effect of a partial field scan; the domain patterns are erased.



Fig. 6 - Traces of the electron beam scans are observed in the positive domains.



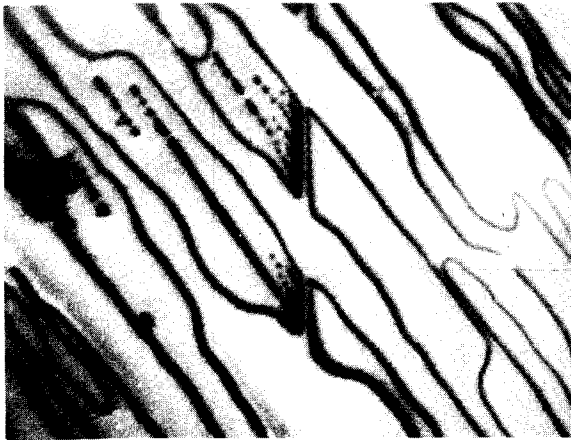


Fig. 2

Domain structure pattern before the polarization switching.



Fig. 3

The domain at the center has been switched by the electron beam and appears as a dark island characteristic of a positive domain.



Fig. 4

After the switching process the positive dark surface is compensated and the contrast disappears.

## MAGNETIC CONTRAST IN THE SECONDARY EMISSION MODE OF THE S. E. M.

R. P. Ferrier\* and D. F. Kyser

IBM Research Laboratory  
San Jose, California 95193

When the electron beam in an SEM is incident upon a magnetic specimen, the fringing fields above the surface, if present, will alter the angular distribution of the emitted secondary electrons in a manner dependent on the local field distribution. This mechanism is the basis for the techniques which have been developed for the direct observation of magnetic contrast in the secondary electron image. The first successful methods were described by Dorsey [1] who used the differential signal from a pair of detector plates located above the specimen and by Verstner [2] who used an energy analyser. The technique used by Joy and Jacobovics [3] was to place an aperture in the collector system and Banbury and Nixon [4] employed a directionally sensitive detector; this latter method has recently been the subject of further development [5] and detailed analysis [6]. Other methods have been described by Speth [7] who used a combination of screens and crude energy analysis, by Kammlott [8] who used a method designed to shield the collector from the directly emitted secondaries and by Wardly [9] who used a pair of energy analysers.

Although all the methods which are listed above allow the observation of magnetic contrast, it is not possible to directly compare their performance in terms of ultimate sensitivity. Since some of the methods involve non-trivial instrumentation, it would be useful to know if the added complication is justified in terms of improved performance. It is the purpose of this paper to attempt such an analysis.

For a specimen which exhibits only magnetic contrast, the minimum detectable change in the magnetic stray field configuration  $\Delta\phi_{\min}$  (measured in gauss-cm) will ultimately be determined by signal to noise considerations. It can be shown that if we measure the contrast  $C$  of the same magnetic feature of a given specimen by two different detection methods, the ratio of the ultimate sensitivities of the two methods is given by

$$\frac{(\Delta\phi_{\min})_1}{(\Delta\phi_{\min})_2} = \frac{C_2 (N_2)^{\frac{1}{2}}}{C_1 (N_1)^{\frac{1}{2}}} \quad (1)$$

\* Currently on sabbatical leave from Cavendish Laboratory, University of Cambridge, England

where  $N$  is the average number of electrons collected per picture point. The specimen chosen for comparison of the various methods was the polished prism face of a cobalt single crystal [see Fig. 1]. The contrast was measured by using  $y$ -modulation of the signal on line scan, the baseline being obtained by reducing the photomultiplier voltage to zero, as illustrated in Fig. 2. The ratio  $(N_2/N_1)^{1/2}$  required in equation (1) was obtained by first calibrating the photomultiplier gain control. A Faraday cage was used to determine the current incident upon its surface and then for varying incident currents the photomultiplier gain was read for an output signal at the mid-level of the wave form monitor; a graph of photomultiplier gain versus current was then drawn. In the comparison experiments using the cobalt crystal the beam current incident upon the specimen was always maintained at  $5 \times 10^{-9}$  A and the photomultiplier gain was adjusted to give the same mean signal level; the photomultiplier gain could then be converted to an equivalent current proportional to  $N$ .

The results obtained in this study are given in Table 1. The Nixon-Banbury detector used in this study was a commercially available model (Cambridge Scientific Instruments). It consists of a short cylinder with top and bottom plates with small holes in them to allow the beam to enter and impinge on the specimen, which is located immediately below the bottom plate. In part of the cylinder face is a gauze through which the electrons can pass to the scintillator (no collector cage is used in this method). Different voltages can be applied to each part of the detector and the highest contrast and sensitivity was found when  $V_{\text{gauze}} = V_{\text{cylinder}} = 350\text{V}$ ;  $V_{\text{bottom plate}} = V_{\text{specimen}} = -80\text{V}$ ;  $V_{\text{top plate}} = -120\text{V}$ . These are the voltages for Nixon-Banbury (1) in the Table. For Nixon-Banbury (2) the voltages on the top and bottom plates and on the specimen were reduced to zero. The other methods used were as closely similar to those of the original authors as possible, although in the original methods of Kammlott, Speth and Joy and Jacobovics the SEM used was a Stereoscan S2 which had the scintillator collector system at an angle to the horizontal whereas in this study a Stereoscan S4 was used which has the scintillator collector system horizontal. It is not believed that this will affect the results markedly. In the case of the Speth arrangement in which he used a collector voltage which was close to zero, we found in agreement with him that this leads to a significantly higher contrast than with the collector at 300V. However this contrast increase is only achieved at the expense of detected current and the overall sensitivity is much less; the sensitivity quoted in Table 1 is for the case of the collector at 300V. In addition to the other methods the results are also quoted for the case of a standard Stereoscan S4 arrangement with the specimen horizontal and at a level which is close to the bottom of the collector cage. It is perhaps the most surprising result that this method is only about 4 times less sensitive than Nixon-Banbury (1) and for many purposes would be entirely adequate. It is not possible to compare the present results with those of Dorsey, Verstner and Wardly. It may however be commented that in the case of the Wardly method the contrast which he obtained from the basal face of a cobalt crystal is no higher

than that obtained with the Nixon-Banbury detector in this work, and he also used a much higher beam current of  $5 \times 10^{-8}$  A. In addition he quotes that with  $\text{CrO}_2$  magnetic tape he could detect up to 8000 flux reversals per inch and this is comparable to the figure obtained in this study with the most sensitive method.

So far we have assumed that only magnetic contrast is present. However, in a real specimen we will also have topographic contrast and the conditions under which magnetic contrast is maximized will also maximize topographic contrast. The latter can swamp the magnetic contrast and we have been investigating methods to remove the effects of the topographic contrast or at least reduce them considerably. The results obtained using an optical bench to spatially filter the images of magnetic specimens will be discussed.

- 
1. J. R. Dorsey, Electron Probe Microanalysis, ed. by A. J. Tousimis and L. Marton (Academic Press, 1969), p. 291.
  2. V. N. Verstner et. al., Bull. Acad. Sci. (USSR Phys. Sci.) 30, 806 (1966)
  3. D. C. Joy and J. P. Jacobovics, Phil. Mag. 17, 61 (1968)
  4. J. R. Banbury and W. C. Nixon, J. Phys. E. 2, 1055 (1969)
  5. J. P. Ballantyne et. al. Proc. 25th Anniversary Meeting of E.M.A.G. 1971 (Institute of Physics, London), Conference Series No. 10, p. 194.
  6. E. Munro, Ph.D. Dissertation, University of Cambridge, England (1971)
  7. A. Speth, Rev. Sci. Inst., 40, 1636 (1969)
  8. G. W. Kammlott, J. Appl. Phys. 42, 5156 (1971)
  9. G. A. Wardly, J. Appl. Phys., 42, 376 (1971)

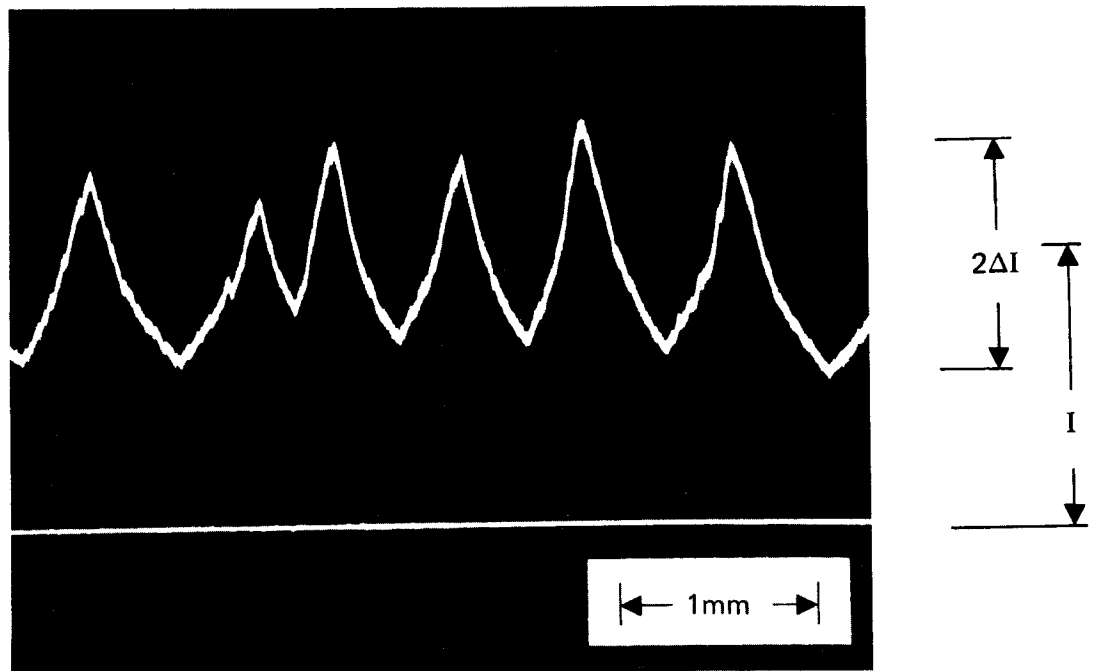
Table 1

The minimum detectable magnetic field for various detection methods (see text) measured relative to that for Nixon-Banbury (1)

<u>Method</u>	<u>Contrast</u>	<u>Detected current = constant x actual current (A)</u>	<u>Minimum detectable field</u>
Nixon-Banbury (1)	0.27	$1.1 \times 10^{-8}$	1.0
Nixon-Banbury (2)	0.23	$1.1 \times 10^{-8}$	1.2
Joy and Jacobovics	0.12	$1.2 \times 10^{-8}$	2.2
Speth	0.18	$1.95 \times 10^{-9}$	3.6
Kammlott	0.03	$3.8 \times 10^{-8}$	5.2
Standard Steroscan	0.02	$1.03 \times 10^{-7}$	4.2



**Figure 1.** SEM image of prism face of cobalt single crystal using Nixon–Banbury Method (1).



**Figure 2.** Oscilloscope trace showing magnetic contrast. The contrast is given by  $C = 2\Delta I / I$

## CRYSTAL HABIT OF IRON IN APOLLO 14, 15 AND 16 RECRYSTALLIZED BRECCIAS

Uel S. Clanton<sup>1</sup>, David S. McKay<sup>1</sup>, Robert B. Laughon<sup>1</sup> and Garth H. Ladle<sup>2</sup><sup>1</sup>NASA L. B. Johnson Space Center, <sup>2</sup>Lockheed Electronics Corp., Houston, Texas 77058

The highly metamorphosed and recrystallized breccias of Apollo 14, 15 and 16 contain euhedral crystals of iron growing on plagioclase and pyroxene crystals (Fig. 1). Terrestrial and meteoritic occurrences of iron crystals are rare; the common habits of iron are the octahedron, dodecahedron and cube. (1) Fragments of lunar recrystallized breccias with iron crystals are also rare, but when present, the crystals usually occur in abundance.

Based on crystal habit, three populations have been recognized in lunar samples. In the first group the trapezohedron (hll) predominates and the cube (100) faces are smaller (Figs. 2, 5, 11, 12). Rare crystals have been photographed that display two values for (hll) and a second set of trapezohedron faces are present. The second group of crystals has the cube (100) as the dominant form; the trapezohedron (hll) and tetrahexahedron (hk0) faces are smaller and about equally developed (Figs. 3, 4, 5, 6, 7). This group of crystals often shows four or five values of (hll) and has four or five sets of trapezohedron faces. The tetrahexahedron faces are covered with striations, or more correctly oscillatory combinations (Fig. 8). Each striation is formed by two narrow planes that correspond in position to faces of other crystal forms. This grooved surface is formed by the continual oscillation of the tetrahexahedron, trapezohedron and/or hexoctahedron forms. The dominant habit of the third group is the octahedron (111) with smaller but equally well developed cube (100) and dodecahedron (110) faces (Figs. 9, 10).

The development of crystal habit is related to rate of growth and environmental conditions. The first faces to appear on the nucleated crystal will be those of relatively high energy and will grow rapidly. The continued addition of material to these faces will build them at the expense of the less rapidly growing faces. As growth proceeds, the more rapidly growing faces become increasingly smaller, and perhaps disappear, to form a crystal of the slower growing more stable faces. (2)

Based on Energy Dispersive X-ray Analysis (EDX), the crystals are pure iron. Ni, P, Co and S if present, are less than 0.5%. The iron crystals shown in Figures 10 and 11 have an uneven coating of troilite. This hexagonal iron sulfide is selectively deposited on those faces with the most similar symmetry.

The euhedral crystals, the abundant growth steps, and the open network of substrate crystals clearly support the concept of vapor-phase crystallization (3) during thermal metamorphism of massive ejecta blankets. The composition of the vapor is somewhat speculative but the euhedral crystals and the overgrowths on crushed mineral grains suggests a vapor rich in components that would favor the growth of plagioclase, pyroxene, iron, troilite, ilmenite and apatite.

## References:

1. Palache, C., Berman, H., and Frondel, C. (1944) *The System of Mineralogy*, Vol. 1, John Wiley and Sons, Inc., New York, 834p.
2. Hurlbut, C. (1949) *Dana's System of Mineralogy*, John Wiley and Sons, Inc., New York, 609p.
3. McKay, D. S., Clanton, U. S., Morrison, D. A., and Ladle, G. H. (1972) Vapor-phase crystallization in Apollo 14 breccia. *Proc. Third Lunar Sci. Conf.*, *Geochim. Cosmochim. Acta. Suppl.* 3, Vol. 1, pp. 739-752, M.I.T. Press.

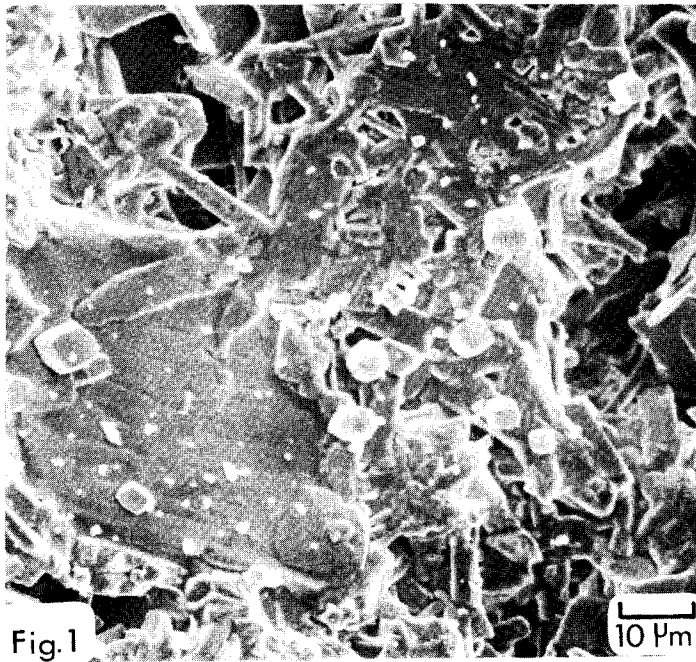


Fig. 1

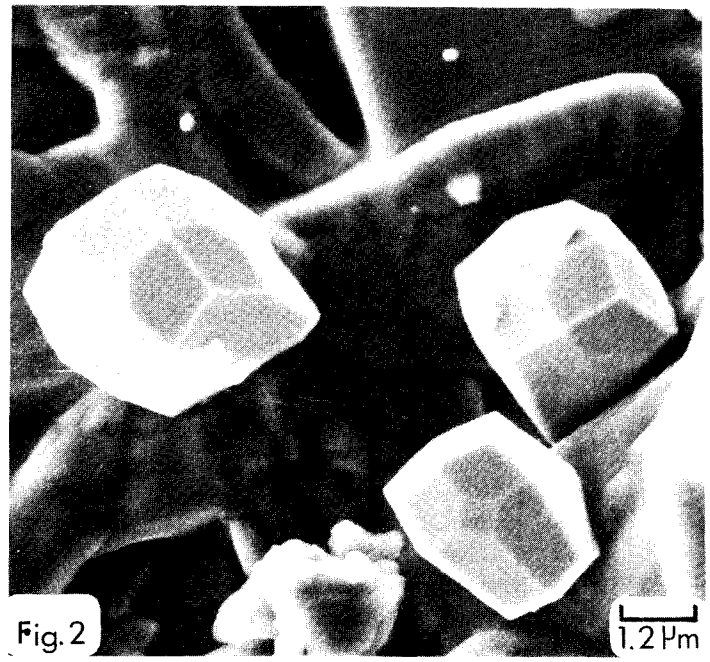


Fig. 2

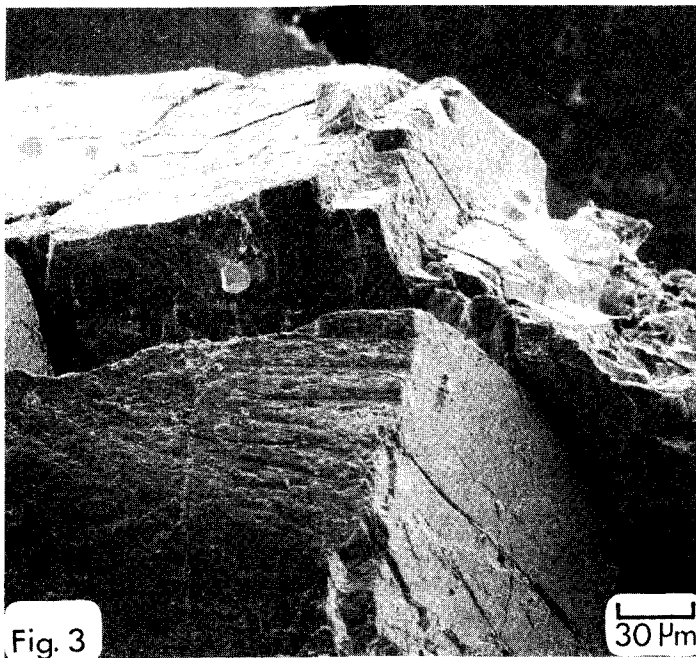


Fig. 3

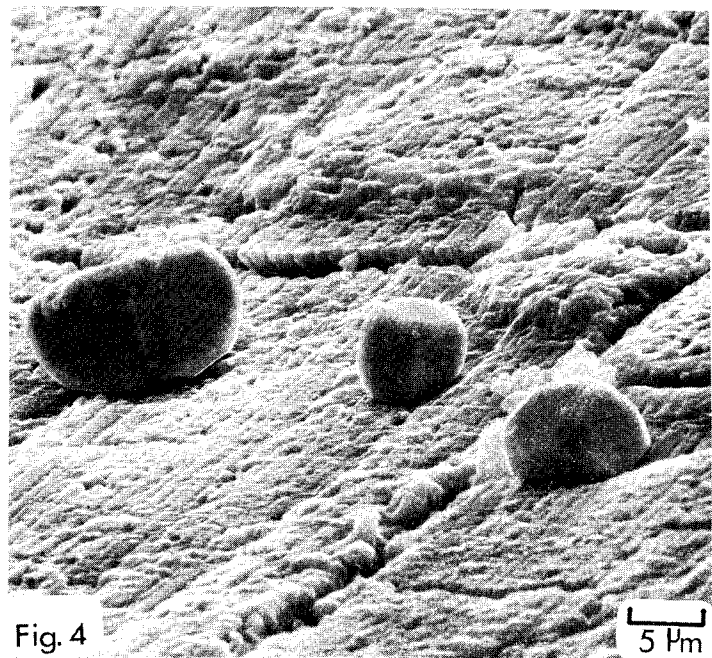


Fig. 4

## FIGURE CAPTIONS

- Fig. 1 - SEM photograph of a vuggy recrystallized breccia. Euhedral crystals of iron sit on a substrate of plagioclase and pyroxene crystals; the porosity extends well into the fragment (15402).
- Fig. 2 - SEM photograph of three euhedral iron crystals; the dominant crystal form is the trapezohedron, the cube faces are smaller (15402).
- Fig. 3 - SEM photograph of eight euhedral iron crystals on a grain of pyroxene. The iron crystals grow on surfaces and in fractures and are not related to the original crystallization of the pyroxene grain (15402).
- Fig. 4 - SEM photograph of three euhedral iron crystals on a grain of pyroxene. The iron crystals occur on the pyroxene overgrowth surface. The iron crystals are clearly late in forming, after the original grain was fractured and after the stepped pyroxene overgrowth (15402).



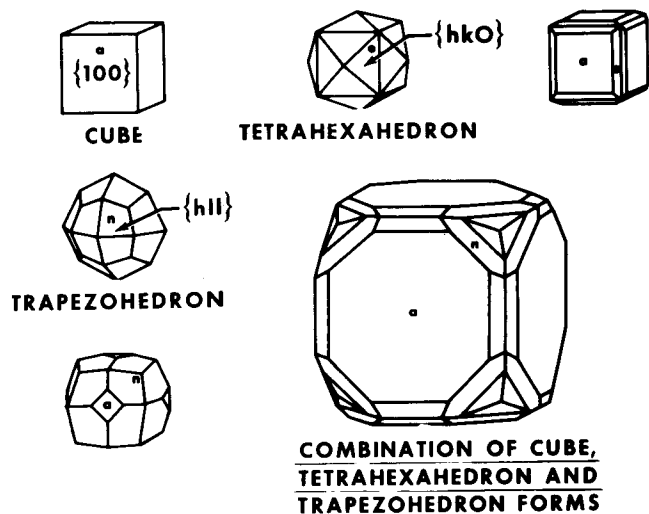


Fig. 5

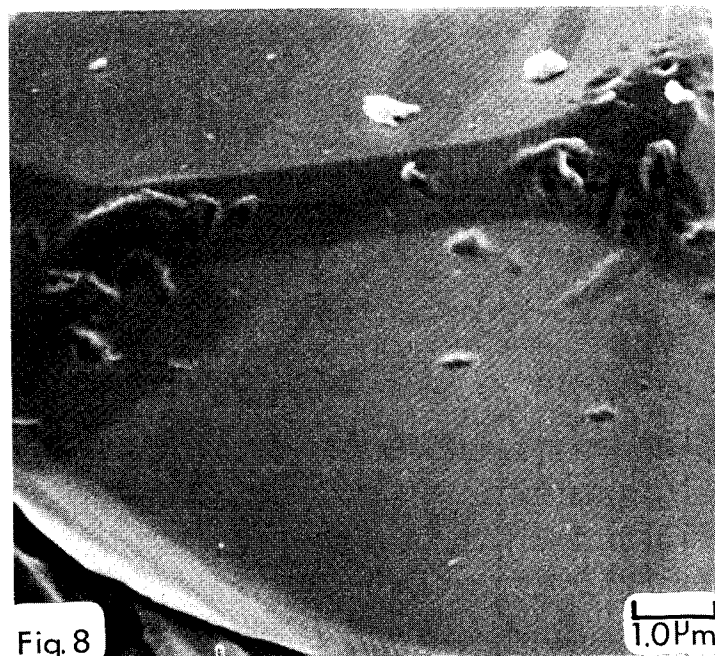
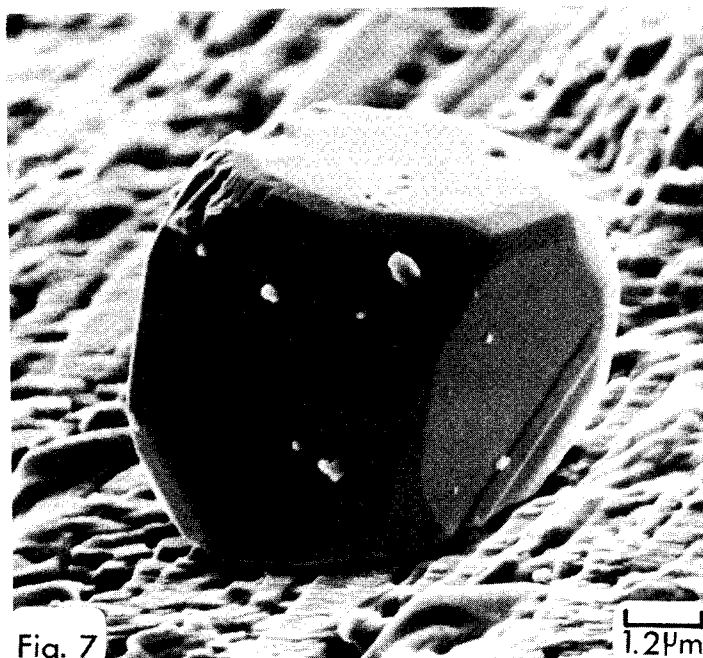
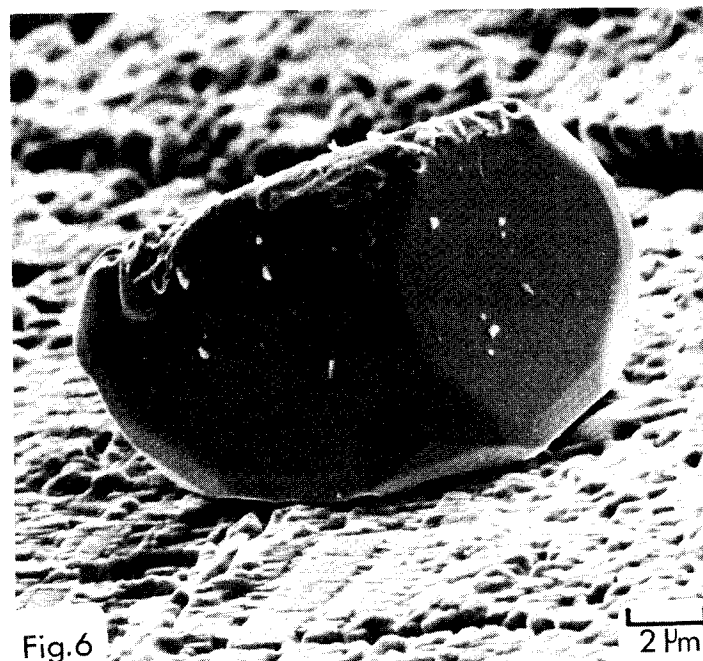


Fig. 5 - Drawing showing modifications and combinations of cube, tetrahexahedron and trapezohedron forms.

Fig. 6 - SEM photograph of an iron crystal; the dominant crystal form is the cube, the trapezohedron and tetrahexahedron faces are smaller. Five values for  $\{hll\}$  occur on this crystal; there are five sets of trapezohedron faces. The substrate is a pyroxene fragment; the bunched growth lines form  $150^\circ$  "growth steps" (15402).

Fig. 7 - SEM photograph of an iron crystal on a pyroxene substrate. The dominant crystal form is the cube; the trapezohedron and tetrahexahedron faces are smaller but equally well developed. Four values for  $\{hll\}$  occur on this crystal; there are four sets of trapezohedron faces. The iron crystal appears to have formed later than the growth steps on the pyroxene substrate (15402).

Fig. 8 - SEM photograph of an iron crystal. The striation are oscillatory combinations formed by two narrow planes that correspond in position to faces of other crystal forms. The striations are observed only on the tetrahexahedron faces (15402).

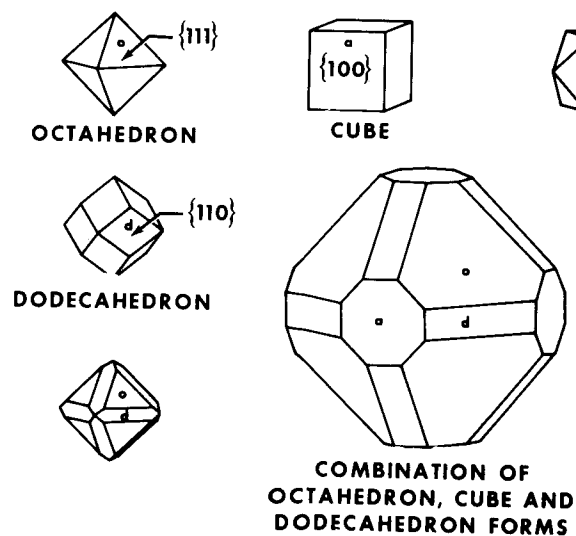


Fig. 9

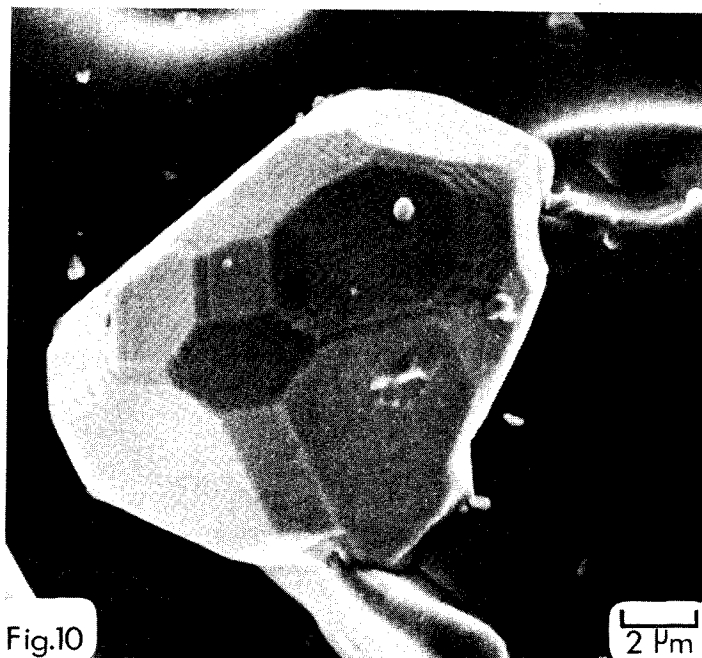


Fig. 10

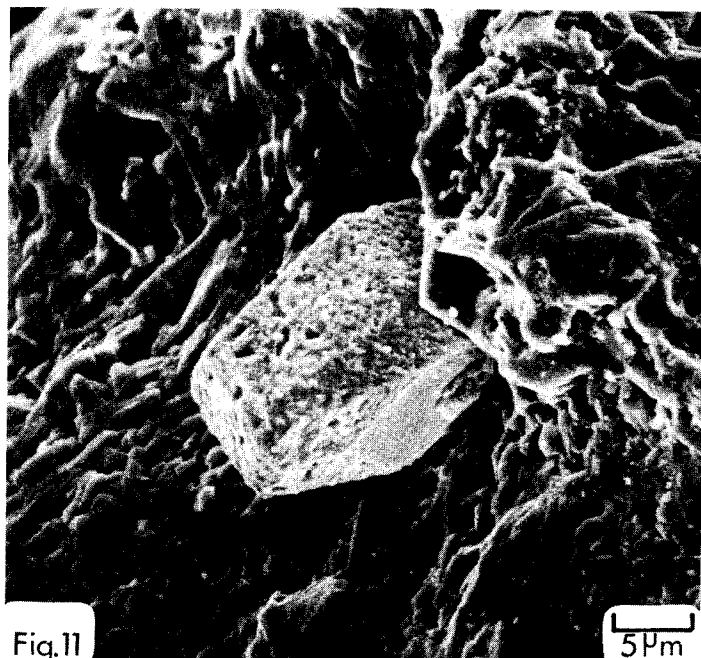


Fig. 11

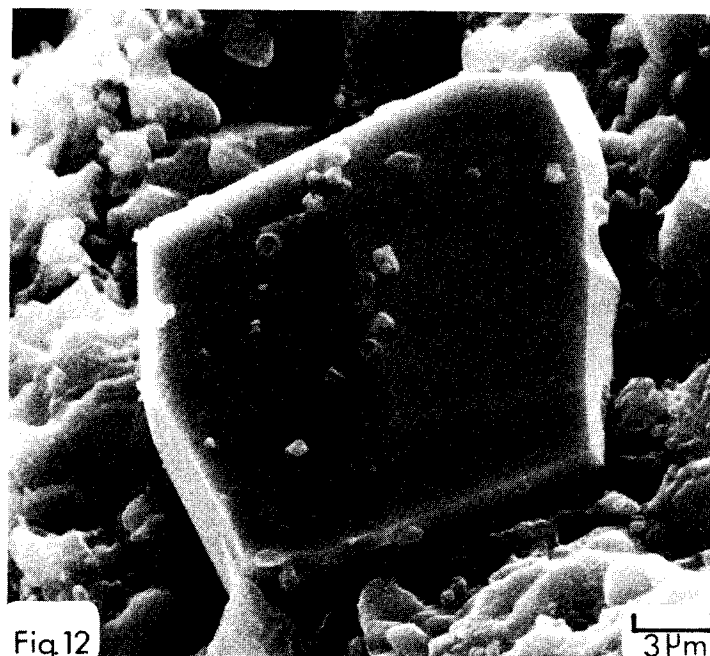


Fig. 12

Fig. 9 - Drawing showing modifications and combinations of octahedron, cube and dodecahedron forms.

Fig. 10 - SEM photograph of an iron(?) crystal coated with iron sulfide, presumably troilite. The dominant crystal form is the octahedron; the cube and dodecahedron faces are smaller and less well developed. This crystal sits on a "glazed" or "wetted" substrate. The glaze forms a coating that covers details of the previous surface (15402).

Fig. 11 - SEM photograph of an euhedral iron crystal partially coated with iron sulfide. The dominant form, the trapezohedron, has a rough troilite coating. The smaller cube faces are uncoated and smooth (14261).

Fig. 12 - SEM photograph of an euhedral iron crystal. Some iron crystals are distorted and not all faces are symmetrically developed. This view down the  $+a_3$  axis shows only trapezohedron faces; the  $-a_1$  and  $-a_2$  axes have not only trapezohedron faces but also small cube faces (67702).

CONSIDERATIONS IN MAKING STEREO MICROGRAPHS WITH THE SCANNING  
ELECTRON MICROSCOPE

E. R. Walter  
Union Carbide Corporation, South Charleston, West Virginia

Abstract published in EMSA Proceedings

S E M OBSERVATIONS OF MAGNETIC DOMAIN  
CONTRASTS IN SILICON-IRON CRYSTALS

----

A. GERVAIS<sup>\*</sup>, J. PHILIBERT<sup>\*</sup>, A. RIVIERE<sup>\*</sup>, R. TIXIER<sup>\*\*</sup>

Magnetic domains on iron samples were first observed by two of us (J. PHILIBERT, R. TIXIER (1969) ). This experiment shows that secondary electrons are unimportant for contrast observations and furthermore that domain contrast may arise for very small tilt angle.

The experiments presented here were carried out with (110) and (100) silicon iron crystals. In this case domain walls appear along 180° and 90° magnetization directions. For this study we limited ourselves to the domain structures which had their walls parallel to the easy direction of magnetization  $\langle 100 \rangle$  as determined from Kikuchi diagram.

Figure 1 shows typical 'tree' patterns of silicon-iron crystal with the surface being inclined at a small angle with respect to the 100 plane. Domains appear with 180° and 90° between magnetization vectors.

The experimental conditions are summarized below :

- accelerating voltage 20-45 keV
  - beam current 6-80 nA
  - beam divergence  $\delta\alpha$  up to 30 mrad
  - tilt angle  $\beta$  from 0° to 45°
- The contrast is not extinguished even at the 0° value of tilt angle where it becomes very faint. Figure 2 shows a (110) specimen tilted by 4°
- Azimuthal angle  $\theta$ . The reversal of contrast for  $\Delta\theta = 180^\circ$  is observed but is not crucial for the contrast formation since it is predicted in both the models B et C defined below.

---

\* Laboratoire Physique des Matériaux, C.N.R.S. 92190-MEUDON  
(France)

\*\* I.R.S.I.D., 78104, SAINT GERMAIN EN LAYE, France

52B



Fig. 1  $-(100)$  Si-Fe (3 % Si). Accelerating voltage 45 keV, beam current 10nA, specimen tilted by  $45^\circ$  image formed with specimen current.

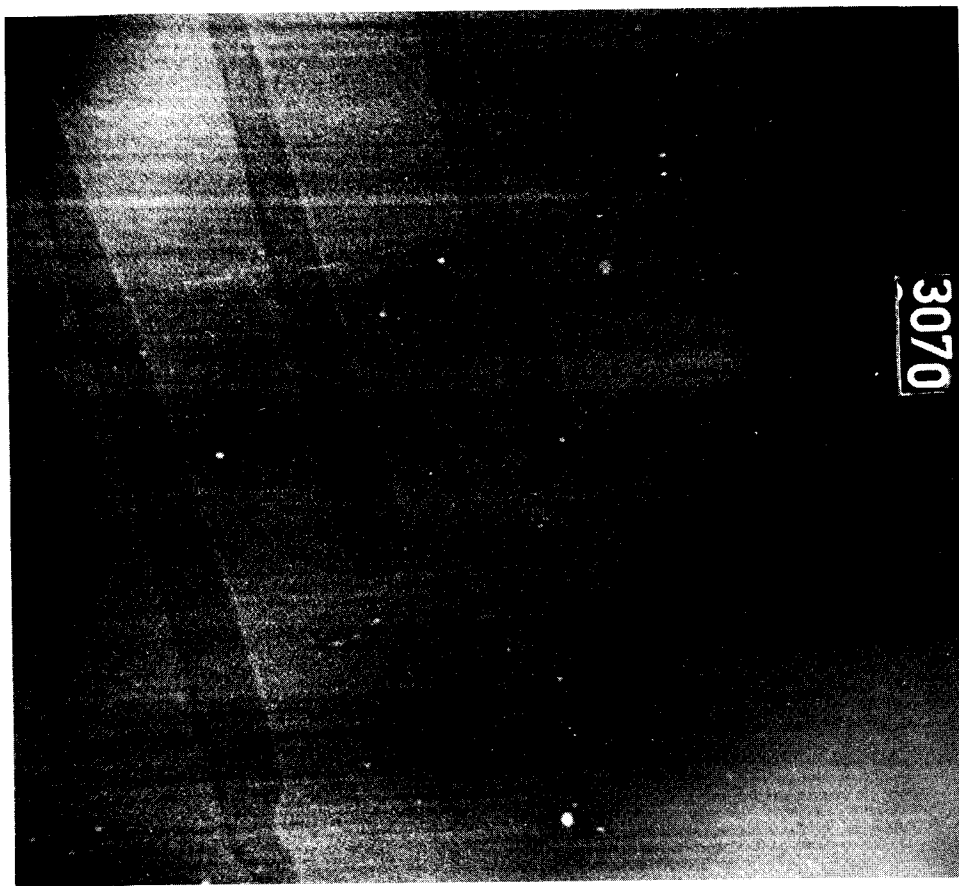


Fig. 2.  $(110)$  Si-Fe (3 % Si). Accelerating voltage 45 keV, beam current 30 nA, specimen tilted by  $4^\circ$ . The axis of the spikes is oriented along a  $(001)$  direction. The image is formed with specimen current.

However it is important to determine the orientation of the relevant magnetization vectors. Contrast extinctions and maxima in the S E M were compared with kerr magneto-optic effect observations.

- images are formed with backscattered electrons and specimen current modes.

We considered different models (denoted A, B, C) so as to understand the mechanism of contrast.


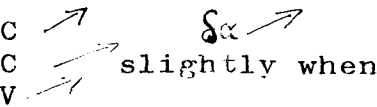
Model.A. the origin of contrast is due to magnetostriction. This interpretation was ruled out since we observed the domain structures on silicon-iron (6 % Si) for which magnetostriction vanishes.

Model. B. The contrast is due to the variation of the mean backscattering yield  $\eta$  or more exactly in the variation of the paths in backscattered electrons under the action of lorentz forces.

Model.C. The contrast arises from variation in the crystallographic part of the backscattering yield  $\Delta\eta$ .

For the cases B and C we examined the experimental conditions leading to extinction or appearance of magnetic domains. The two main difficulties encountered in the analysis are the determination of the magnetization vectors and of the diffraction conditions equivalent to a two beam case. This last requirement is necessary to examine the mechanism involved in the model C.

The extinction relations and the main features of the contrast change listed below for the models B and C will be successively examined.

	B	C
extinction relations	a) $\beta = 0$ b) $\vec{y} \cdot \vec{m}_S = 0$	c) divergence $\delta\alpha > 20\text{mrad}$ d) $g$ parallel $m_S$
contrast (C) change	 C reversal for $\Delta\theta = 180^\circ$	 C reversal for $\Delta\theta = 180^\circ$

$\beta$ ,  $\theta$  are respectively the tilt and azimuthal angle,  $V$  the accelerating voltage,  $\delta\alpha$  the beam divergence. The 20 mrad divergence value is estimated from  $g = 200$ ,  $\delta\alpha = 2/(g \cdot \xi_g)$  where  $\xi_g$  is the extinction distance at 30 keV  
 $y$  direction of the axis of  $\beta$  rotation.  
 $g$  reciprocal vector.

\* This variation was given by D.J. FATHERS, J.P. JAKUBOVICS and D.C. JOY.

From a naive model where the lorentz forces would act to deplace the sphere of complete diffusion it is not evident that the contrast variation with voltage must be that indicated by these authors.

When compared to experimental contrast changes it appears that none of the extinction relations predicted from B or C are completely realised. The mechanism leading to the magnetic domain contrast might not be found within one of these models alone.

J. PHILIBERT, R.TIXIER - Micron 1969 1 p. 174-186

D.J. FATHERS, J.P. JAKUBOVICS, D.C. JOY (1973)(to be published)

TEST SPECIMENS FOR HIGH RESOLUTION SCANNING ELECTRON MICROSCOPY

R. T. Greer

Department of Nuclear Engineering, Iowa State University, Ames, Iowa

Abstract published in EMSA Proceedings



SEM RESOLUTION AND TEST SPECIMEN

J. Temple Black  
University of Rhode Island, Kingston, Rhode Island

Abstract published in EMSA Proceedings

METAL CUTTING IN THE SCANNING ELECTRON MICROSCOPE

J. Temple Black  
University of Rhode Island, Kingston, Rhode Island  
and  
S. Ramalingam  
State University of New York, Buffalo, New York

Abstract published in EMSA Proceedings

AN EFFICIENT REDUCED RASTER AND MANUAL LINE SET CONTROL SYSTEM  
FOR JEOL JSM-U2 AND JSM-U3 SEMs

H. W. Estry, L. F. Allard, and W. C. Bigelow  
University of Michigan, Ann Arbor, Michigan

Abstract published in EMSA Proceedings

## A COMBINED SCANNING ELECTRON MICROSCOPE - ELECTRON PROBE MICROANALYZER

A. E. Zolla, R. S. Willing, A. Falco, and J. R. Seward

Applied Research Laboratories  
Sunland, California 91040INTRODUCTION

A wide variety of signals can be detected when an electron beam impinges on a solid surface. The observation of many of these various signals from electron probe instruments has become important in order to characterize a specimen with respect to composition, homogeneity, metallography, crystal structure and perfection as well as electronic or magnetic properties.

Instruments have been developed to concentrate on a particular phenomenon that occurs during electron impact and such instruments optimize the detection and processing of the signal that results. It is possible, however, to obtain similar performance in the many modes of operation using a single electron probe instrument thereby achieving maximum information for characterization of a given specimen. The desirable features of such a versatile combination instrument are the following:

- a. High spatial resolution and efficient signal detection.
- b. Capability of obtaining precise and rapid quantitative information on the elemental composition of a specimen.
- c. Capacity to accommodate a great variety of samples with a high degree of freedom for manipulation.
- d. Versatility in signal processing and data handling.

ELECTRON OPTICAL COLUMN

An electron optical system that provides a great versatility for signal detection and satisfies the above conditions is shown in Figure 1. The instrument utilizes a prealigned three electromagnetic lens system in order to provide sufficient demagnification of the electron probe for a spatial resolution better than  $100\text{\AA}$  in the secondary electron emission mode using a conventional tungsten source. A typical high resolution micrograph is shown as Figure 2. The two condenser lenses are of conventional design and the final objective lens is flat with a conical bore to provide optimum x-ray detection. This design permits detection of x-rays with a high take-off angle while the specimen is located at a short working distance from the lens as required for minimizing x-ray absorption by the sample and for maintaining a high current to electron probe diameter ratio.

The electron source is interchangeable. The gun includes external filament adjustments, anode, and total triode adjustments together with an internal adjustment for spacing of the cathode to Wehnelt grid cap. The gun includes an electrostatic beam blanking system.

Up to eight different apertures can be positioned above the objective lens by external selection in order to vary the convergence angle of the beam and to maximize the resolution in the SEM mode or to maximize the electron probe current in the x-ray microanalysis mode.

The electron beam scanning system employs a double deflection between the second and final lens. The same scan coils, scan drive circuitry and video amplifier circuitry are employed for all scanning rates from slow to television modes.

A sixteen coil - eight pole stigmator system incorporated into the final objective lens permits continuous control of astigmatism both in amplitude and direction through 360°.

### VIEWING OPTICS

A light optical viewing system, coaxial with the electron beam provides for simultaneous viewing of the specimen during electron bombardment and is used to set the sample surface to the focal circle of the x-ray spectrometers and for the collection of cathodoluminescence signals. The viewing system employs either a water cooled vertical illuminator or a transmitted light illuminator, both of which are located outside of the vacuum chamber.

### QUANTOMETER

The electron optical column is housed within an octagonal vacuum chamber providing eight readily accessible ports for detection of x-rays, backscattered and secondary electrons as well as for many other accessories. Such a housing can accommodate up to six scanning wavelength dispersive spectrometers, or twelve fixed wavelength dispersive spectrometers, or a combination of these with an energy dispersive system to provide simultaneous multielement analysis capability.<sup>(1)</sup> The relationship between secondary electron detector, electron and visual optical systems and scanning spectrometer is shown in Figure 3.

### SPECIMEN HANDLING

Three types of sample handling systems are available according to the applications bias of the user. A single sample stage intended for work directed towards secondary electron microscopy has X, Y, Z, tilt and rotation degrees of freedom. A separate high precision X-Y stage is an alternative for accurate microanalysis investigations when linearity and position repeatability are of the utmost importance. Both sample stages accept substages and accessories, including those for heating or cooling of the specimen, for studies of integrated circuit components, for transmitted light illumination or for detection of transmitted electrons. A third 'omnicentric' stage has the special features which maintain focus and field of view conditions during motion in the X or Y axes or during tilt or rotation.

### VACUUM SYSTEM

The materials used in construction have been selected with concern as to out-gassing and vapor pressure properties. Accepted vacuum standards have been met in both design and handling to achieve a vacuum of  $5 \times 10^{-7}$  torr with a low hydrocarbon partial pressure. Vacuum system operation is completely automatic

through the use of pneumatic valves controlled by a solid state electronic logic circuitry. The vacuum system includes three gate valves of high conductance for isolation of the electron gun, sample chamber and diffusion pump from the main chamber.

#### ELECTRON BEAM SCANNING AND VIDEO SYSTEM

A full complement of line and frame rates, T/V and power line synchronized scanning is available as single or continuous traces in area, line or line profile modes.

The magnification is selectable over a range of  $10^4$  and displayed on a log-scale meter. Raster size, position and rotation controls function in all modes. Dynamic control of focus and for eliminating foreshortening effects for tilted samples is included. Magnification and lens excitations are compensated for changes in beam energy.

Normal and inverted images are available over a 60 dB signal range with additional control of photomultiplier gain. The video amplifier provides a full complement of bias, roll-off, derivative and gamma functions for all detectors. Two CRT displays are provided with independently selectable signal inputs. Separate profile amplifiers and controls are available. Photographic setup is facilitated by integral waveform monitoring.

#### SUMMARY

The instrument described combines all the necessary features of both a scanning electron microscope and an electron probe microanalyzer. This type of versatile electron beam instrument should satisfy the need of the microanalyst to determine specimen structure and to perform accurate multielemental quantitative analysis.

#### REFERENCES

1. B. Kenessey, L. K. Griffith, and E. Davidson, "New X-Ray Spectrometers for a Multipurpose Scanning Electron Microprobe," Eighth National Conference on Electron Probe Analysis.

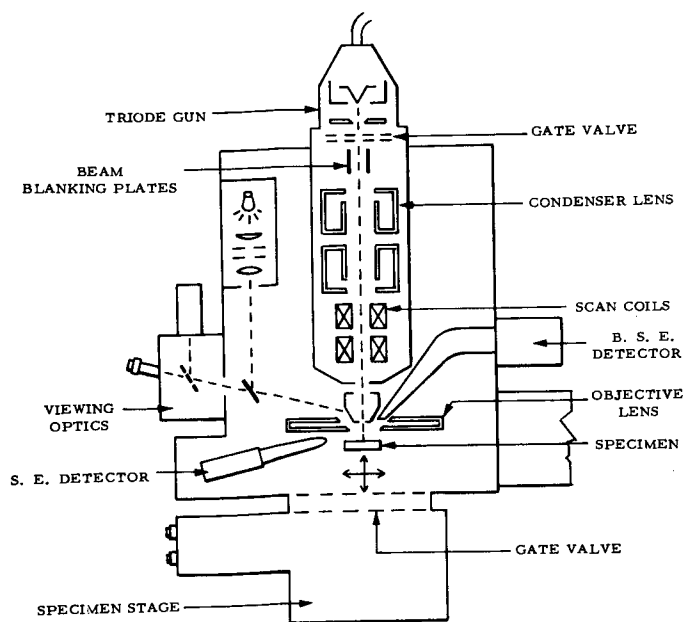


Figure 1

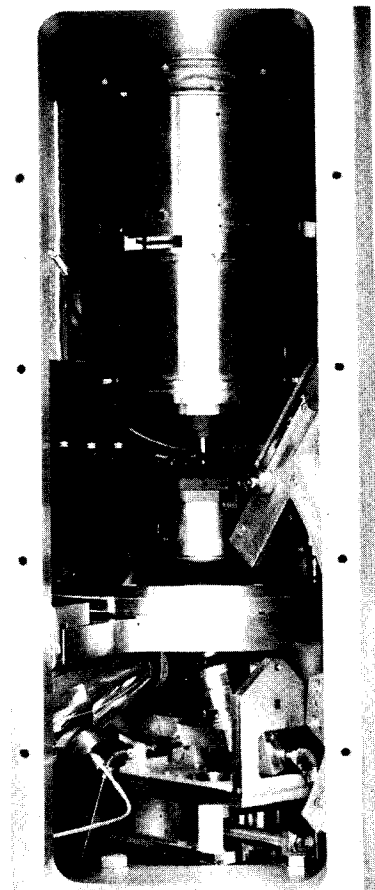
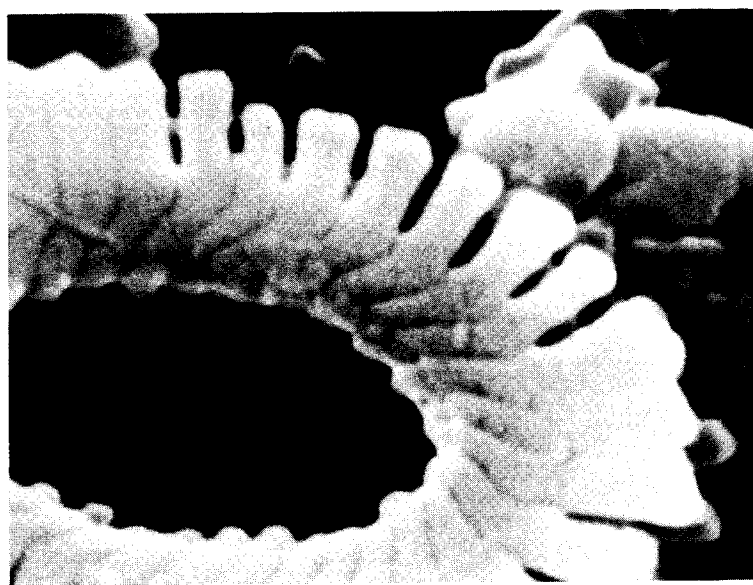


Figure 3



50,000X

0.2  $\mu\text{m}$ 

Figure 2

MODULAR MAGNETIC LENS ACCESSORY TO BASIC FIELD EMISSION SEM

A. C. Holmes, J. H. Cooper, J. J. God, and L. M. Welter  
Coates and Welter Instrument Corporation, Sunnyvale, California

Abstract published in EMSA Proceedings



## ELECTRON PROBE ANALYSIS OF SUBCELLULAR STRUCTURES IN BIOLOGICAL TISSUES

Lloyd V. Sutfin  
Department of Orthopedic Surgery  
Harvard Medical School  
Children's Hospital Medical Center  
Boston, Massachusetts 02115

## INTRODUCTION

With major emphasis being placed on structure and function at the molecular level of biological systems, an approach to electron probe analysis, different from those afforded by the typical commercial microprobes, is necessary if chemical information from structures of importance to current research is to be obtained. It is possible to perform qualitative electron probe analysis at the ultrastructural level with relatively simple, although not inexpensive, instrumentation. This capability is within the reach of any laboratory possessing a good scanning electron microscope and a nondispersive, semiconductor x-ray spectrometer. The standard microprobe is of value in biology when properly applied and, appropos of this discussion, as an adjunct for the preliminary localization of elements within tissues or within a cell because large regions can be analyzed for a limited number of elements relatively rapidly.

In order to analyze a structure with dimensions of the order of a few hundred angstroms, it is necessary to restrict the volume of material excited to a size approaching that of the structure of interest. Because scattering of an electron beam within a target material is unavoidable, the amount of material encountered by the beam must be restricted. This can only be accomplished by using a small diameter beam and a thin target suspended in space. In this case a thin target is one through which nearly all electrons pass and the diameter of the emergent beam is of the same order as the thickness of the specimen. [Obviously "thickness" or "thinness" depend on the accelerating voltage being used and the composition of the target (1).] Accuracy of analysis also places a restriction on the target thickness. If the thickness is much greater than the dimensions of the structure of interest, too much extraneous material will be excited and the analysis becomes meaningless at the ultrastructural level. Resorting to thicker sections and larger diameter beams, and probe currents, in order to keep x-ray counting rates high are not valid in analysis at the ultrastructural level.

## INSTRUMENTATION

In order to perform this type of analysis on a specimen with proper thickness relative to the size of the structure of interest, one must be able to visualize the ultrastructural morphology and accurately place a stationary probe on the structure of interest. Fortunately, a great deal of experience has been accumulated in preparing slices of tissue of appropriate thickness by electron microscopists and, although the techniques of stabilizing the tissues are too severe to preserve chemical integrity, they offer a starting point. The instrumentation should

have the following features to perform microprobe analysis using x-ray spectroscopy: 1. a finely focussed electron beam; 2. a stage which allows the thin specimen to be positioned; 3. a transmitted electron detector; 4. manually operated scanning coils for positioning the beam; 5. a very efficient x-ray spectrometer which implies a semiconductor detector; 6. some method of preventing electron beam induced contamination; 7. a method for monitoring the transmitted electron signal both during positioning of the beam and during the x-ray counting; and 8. electronic data processing equipment.

Currently, both conventional electron microscopes and scanning electron microscopes can be equipped to perform this type of analysis. However, when the development of this technique first began, the SEM was the only instrument available which provided a beam of appropriate diameter. Most of the other necessary features are commonly found in this type of instrument or can be readily adapted to it. The freedom from electron optical components below specimen makes the SEM the instrument of choice if experimentation and instrument development are to be carried out. However, if one has only the requirement of performing this type of analysis routinely, a conventional electron microscope, fitted with sufficient accessories to provide the features listed above, may be more useful in many biological laboratories.

Present improvements in the mechanical aspects of lithium drifted silicon semiconductor detector design are such that these detectors may be brought very close to the x-ray source. This type of spectrometer is several orders of magnitude more efficient than diffracting spectrometers, and it is still useful at x-ray signal levels which are not detected by diffracting spectrometers (2,3). Since the entire spectrum is accumulated simultaneously, analysis time is shorter, geometrical conditions are uniform, and radiation exposure is decreased. The relatively poor resolution of these spectrometers may prevent the detection of some elements in the presence of others; for instance, phosphorus in the presence of osmium, but continual improvement in semiconductor technology and in data processing techniques offers some hope of minimizing this drawback in the future. Because efficiency is most important, it is better to use a 10 mm diameter detector which increases the solid angle significantly over that of smaller detectors with 4 mm or 6 mm diameters. The increase in signal strength more than offsets the loss in peak to background ratio.

Specimen contamination can obliterate the structure being analyzed and mask its chemical composition. Two approaches for preventing it are available: 1. ultra-high vacuum techniques eliminate the contaminant at its source (4); and 2. small, inert gas jets may be directed onto the surfaces of the specimen so that the gas flow away from the specimen prevents the contaminant molecules from impinging on the surface (5,6). This latter technique is far less expensive than the former, can be more readily adapted to commercially available SEMs, but it is often less than totally effective. Gas jet decontamination has been, in our experience, good for obtaining qualitative analyses. (At present, specimen preparation techniques affect the chemistry so severely that attempts at quantitative analysis are useless anyway.).

A short description of how a spectrum was obtained from an ultrastructural feature in the size range of 500 to 1,000 Å on the modified Cambridge Stereoscan will illustrate the importance of the other features listed above. The special transmission stage incorporating the gas jets is shown in Figure 1. Thin sections, about 1,000 Å thick, mounted on collodion-backed EM grids were inserted into the stage and viewed in the scanning transmission mode. The image was very similar to that obtained with a conventional microscope. Gas flow was regulated as follows: the specimen chamber pressure gauge was disconnected, hence the vacuum logic system "sees" a perfect vacuum in the chamber. Argon gas was admitted through a flow meter and metering valves until the backing pressure reaches 0.1 torr. Dark field mode was used to prevent the direct beam from striking the scintillator of the transmitted electron detector. After locating the structure of interest, the static probe was positioned while observing the structure at magnifications of 20,000 or 50,000. There was an image shift when the microscope was switched from raster to line mode. Manually deflecting the line scan, which was still modulated by the transmitted electron signal, developed an image, and the stationary probe was positioned accurately using this image. The signal meter made it possible to maximize the scattered electron signal when a dense body was under analysis. This signal provides the most accurate positioning and afforded a method of monitoring contamination and guarding against beam drift. The x-ray spectrum was accumulated over whatever time period was desired.

Because x-ray production and detection are both statistical processes and because the signal level is low, random variations in signal level were present and made spectral interpretation very difficult. This and the large number of data points obtained in a single analysis make electronic data processing mandatory and the computer and its software, whether on-line or not, should be considered the last sub-system in the instrumentation. Data processing techniques can perform the following functions (7):

- A. Smooth data by removing much of the randomness introduced by the detection process,
- B. Operating on the smoothed data, x-ray peaks can be identified and tested for validity statistically and the number of photons belonging to one characteristic peak can be separated from those belonging to another and from those of bremsstrahlung radiation,
- C. Once the number of photons has been sorted, the conversion from x-ray intensities to chemical information can be carried out by the computer.

At present, we are using the empirical approach to quantitative analysis based on calibration curves obtained from suitable standards. However, since absorption and fluorescence are of minor importance in thin specimens, the theoretical approach to conversion from x-ray intensities to chemical data should be quite successful if an appropriate set of physical parameters is developed.

## APPLICATIONS

Our laboratories are currently using the system based on the Cambridge Stereoscan described earlier for the study of early mineralization of calcified tissues such as bones and teeth. We have been able to verify the suspected presence of calcium

and phosphorus in mitochondrial granules found within cells in bones, cartilage and teeth (8). Secretory granules formed by ameloblasts during the secretion of enamel have been shown to contain calcium when they are located intracellularly. Both these structures had dimensions which were of the order of a few hundred angstroms and thus, the analysis represents electron probe analysis on a truly ultrastructural scale. Figure 2 shows an example of the analysis as performed on secretory granules within Tomes process of an ameloblast. The tissue was fixed with Karnovsky's fixative without  $\text{CaCl}_2$  and further fixed with osmium tetroxide. The tissue was not stained. Twenty KV accelerating voltage was used. In this case, osmium made phosphorus undetectable, the chlorine, and probably sulfur, were attributable to the embedding material, the iron, copper and zinc were due to scattering from the stage, and nickel was from the grid. The calcium peak exceeded three times the square root of the background and was repeatably obtained.

Probably the most severe roadblock to meaningful applications of microprobe analysis of the sort described here is specimen preparation. The fact that elements are dissolved from the tissue due to exposure to aqueous solutions during electron microscopy preparation procedures is known and, in fact, demonstrated by microanalysis. It is not known to what degree fixatives such as glutaraldehyde or osmium may displace ions during these procedures, but as other techniques are developed to circumvent some of these problems, microprobe analysis can be used to reveal these effects. The most promising approach which we are taking to specimen preparation is cryosectioning, however, it is too early to report on the analysis of tissues so prepared.

### References

1. Cosslett, V.E. and Thomas, P.N. *Brit. J. Appl. Phys.* 15, 235-248 (1964).
2. Hall, J.A. IN *Physical Techniques in Biological Research*, V.I.A. C. Oster, ed. Academic Press, New York, 1971. pp. 172-183.
3. Sutfin, L.V. and Ogilvie, R.E. IN *Scanning Electron Microscopy/1970*. O. Johari, ed. ITT Research Institute, Chicago, 1970. pp. 17-24.
4. Bottoms, W.R. IN *Proc. 30th Electron Microscopy Soc. Amer. Mtg.* C.J. Arceneaux, ed. Claiters Publishing Division, Baton Rouge, La., 1972. pp. 422-423.
5. Castaing, R. and DesCamps, J. *Comptes Rendus* 238, 1506 (1954).
6. Brandis, E.K., Anderson, F.W. and Hoover, R. IN *Scanning Electron Microscopy/1971*. O. Johari, ed. ITT Research Institute, Chicago, 1971. pp. 505-510.
7. Vannier, M.W. and Sutfin, L.V. IN *Proc. 7th Natl. Conf. Electron Microscopy Analysis*, San Francisco, 1972. Paper #77.
8. Sutfin, L.V., Holtrop, M.E. and Ogilvie, R.E. *Science* 174, 947-949 (1971).

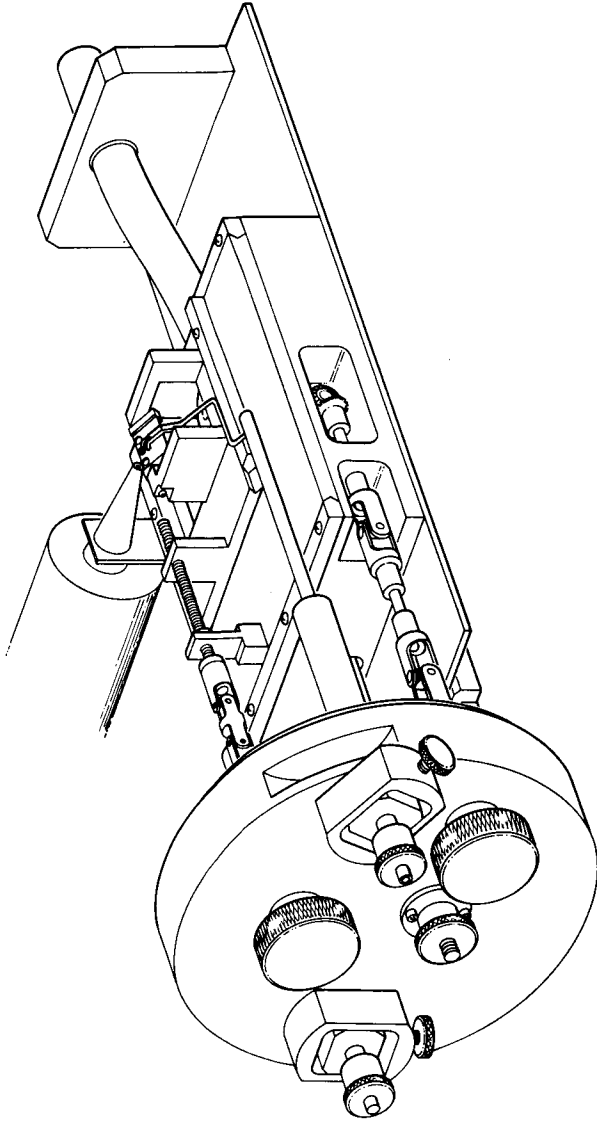


Figure 1 An isometric drawing of the special stage for the Cambridge Stereoscan.

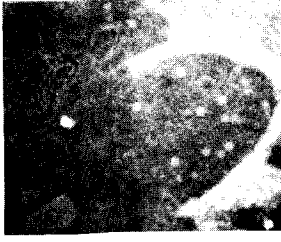
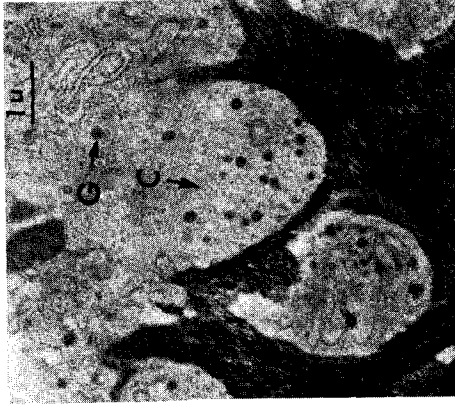
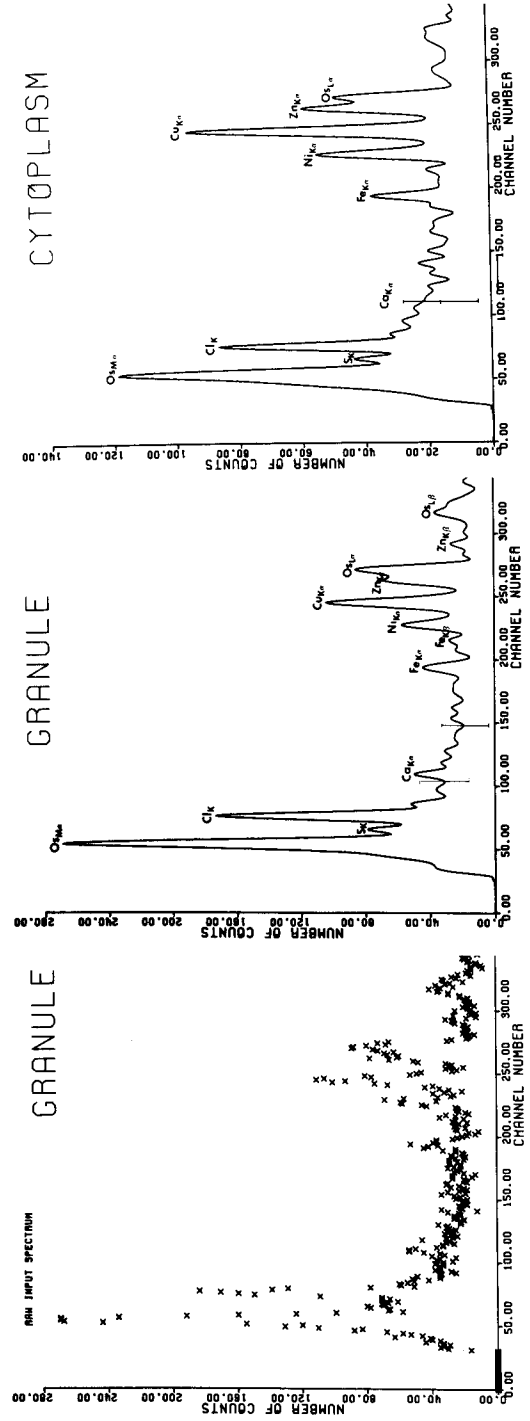


FIGURE 2 A conventional electron micrograph (above left) and a dark field scanning micrograph showing the secretory granules (G) and cytoplasm (C). STEM was taken just after (G) was analyzed. The diameter of the contamination spot is only slightly greater

than that of the granule. The randomness of the first spectrum (left) makes qualitative interpretation difficult. Smoothing (center) improves interpretation. Vertical bar is  $\pm 3 \sqrt{\text{Bkg.}}$



Sodium and Potassium Content of Single Cells:  
Effects of Metabolic and Structural Changes.

Eugene J. Barrett and James R. Coleman  
Department of Radiation Biology and Biophysics  
University of Rochester  
School of Medicine and Dentistry  
Rochester, New York 14642

Several laboratories (1,2) have developed procedures for enzymatic isolation of epithelial cells from complex tissues. The ability of these isolated cells to perform some metabolic activity and/or exclude a "vital" dye is commonly taken as evidence of the viability of the isolated cells. However, these criteria are of limited value for determining the functional homogeneity of the isolated cell preparation. The former measures only the activity of the cell population as a whole, giving no insight into the percentage of individual cells which are metabolically active. The latter criterion is not a direct measure of any metabolic property of the cell, but is frequently accepted as evidence that the cell membrane is intact. However, recent observations raise doubts about the reliability of this criterion. For, even when cells are fixed with  $\text{OsO}_4$ , a treatment known to make cell membranes permeable to large ions (3,4), the cells can continue to exclude the vital dye Trypan Blue for several hours (Barrett and Barrett, unpublished).

There is one property of cells that depends on both metabolic activity and an intact plasma membrane. This property is the ability to maintain a high intracellular potassium concentration and a low concentration of intracellular sodium. The electron probe can be used to measure this property in individual cells, and thus provide an indication of the viability of the individual cells that constitute a population of isolated cells. As part of a larger study we wished to know whether all the cells in a preparation of isolated intestinal cells were "viable" and had survived the isolation procedure intact.

Chicken erythrocytes were used to test the feasibility of using the electron probe to measure this property. These cells have the advantages of occurring as single cells, and thus are not liable to damage from isolation procedures, and their potassium and sodium contents can be manipulated by exposure to cold, a relatively gentle treatment, not known to permanently damage the cells. Erythrocytes suspended in 150 mM Tris were air dried on clean silicon discs. Analysis was at 22 KV with a 10  $\mu$  diameter beam, and 120 second counts for sodium  $K_{\alpha}$ , potassium  $K_{\alpha}$ , and phosphorus  $K_{\alpha}$ .

were recorded. Background counts were taken on the substrate at the peak for each element. Sodium and potassium counts were expressed as a ratio to phosphorus. This served to relate the sodium and potassium counts to the volume analyzed, since the intensity of the phosphorus signal can be taken as a measure of cell volume excited by the electron beam.

The phosphorus signal from the erythrocytes showed little variation from cell to cell with a mean of  $456 \pm 10$  counts/120 sec. ( $\pm$ S.E.). Since the dried cells have a rather uniform geometry, this confirms the value of the phosphorus signal as a measure of the volume analyzed. Figure 1 shows the distribution of the Na/P and K/P ratios in a population of freshly isolated erythrocytes. The means  $\pm$ S.E. for 120 sec. counts were Na =  $0.0 \pm 4$ ; K =  $825 \pm 16$ .

The concentration of Na and K within red cells was altered by incubating the cells for 120 hours at  $4^\circ$  in a 150 mM NaCl solution. Figure 2 indicates the resulting change seen in cell Na/P and K/P ratios. The mean  $\pm$ S.E. for 120 sec. counts in individual cold incubated cells were Na =  $284 \pm 15$ ; K =  $357 \pm 22$ ; P =  $513 \pm 11$ . The results indicate a significant increase in cell Na with a concomitant 2.5x decrease in cell potassium. This compares reasonably well with published reports showing a 2- to 5-fold decrease in cell  $K^+$ , following 5 days of cold incubation, determined by bulk analysis (5).

When isolated intestinal epithelial cells were analyzed the same way it was found that there were two morphologically identifiable groups of cells: single cells, and those that occurred in groups, or "clumps". The latter being cells that had not been completely dissociated from adjacent cells during the isolation procedure. The two morphological groups were characterized by quite different Na/P ratios. The "clumped" cells showed a rather narrow distribution of ratios with a mean near that found for normal red blood cells. The single cells showed a wide distribution of Na/P ratios with a mean similar to that found for cold incubated red blood cells. This suggested that the isolation procedure had damaged the cells in a way that permitted sodium to enter the cells.

This finding was consistent with electron microscopic observations in our laboratory and elsewhere which indicated that single isolated intestinal cells were likely to have suffered apparent structural damage to the plasma membrane. This damage typically occurred at sites where two adjacent cells had been joined by a cell junction. It now seems likely that this structural damage is sufficient to permit substantial quantities of sodium to enter isolated cells. Furthermore, it appears that cells in "clumps" are most likely to have normal metabolic and membrane functions, and probably represent the "viable" proportion of a population of isolated intestinal cells.

### Acknowledgements

This paper is based on work performed partially on USPHS Grants No. AM14272 and No. AM01004, and partially under contract with the U.S. Atomic Energy Commission at the University of Rochester Atomic Energy Project and has been assigned Report No. UR-3490-292.

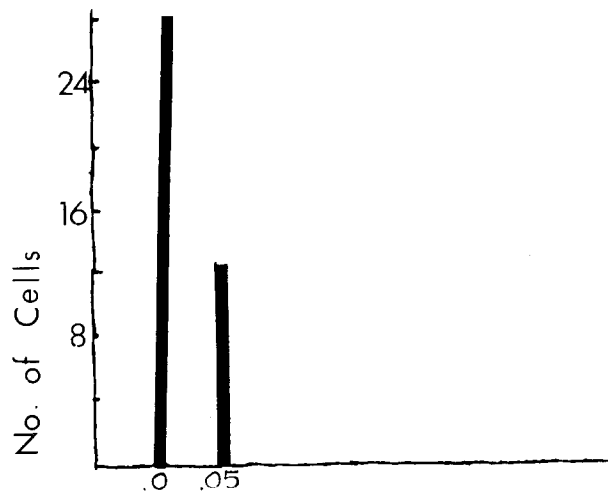
### References

1. Berry, M. N. and Friend, D. S., J. Cell Biol. 43: 506 (1969).
2. Kimmich, G. A., Biochemistry 9: 3659 (1970).
3. Page, S. G., J. Physiol. 205: 137 (1969).
4. Bulger, R. E., J. Cell Biol. 40: 79 (1969).
5. Harris, J. E., J. Biol. Chem. 141: 579 (1941).

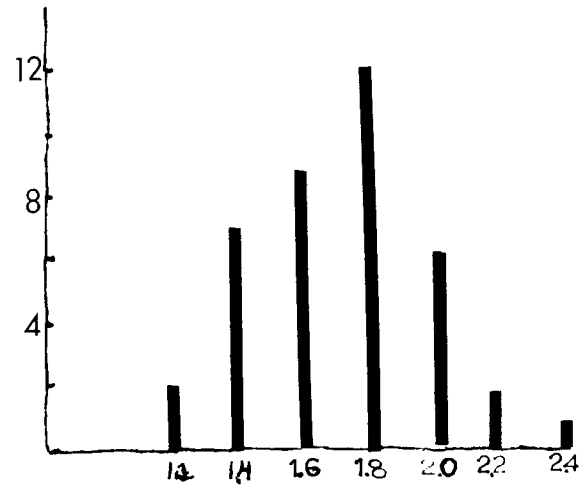
### Figure Legends

- Figure 1. Histograms showing ratios of sodium to phosphorus counts (left) and potassium to phosphorus counts (right) in population of normal chick erythrocytes. (Note difference in scales for abscissa.)
- Figure 2. Histograms showing ratios of sodium to phosphorus counts (left) and potassium to phosphorus counts (right) in population of cold treated chick erythrocytes.
- Figure 3. Histograms showing ratios of sodium to phosphorus counts in two morphologically distinct groups of isolated chick intestinal epithelial cells.



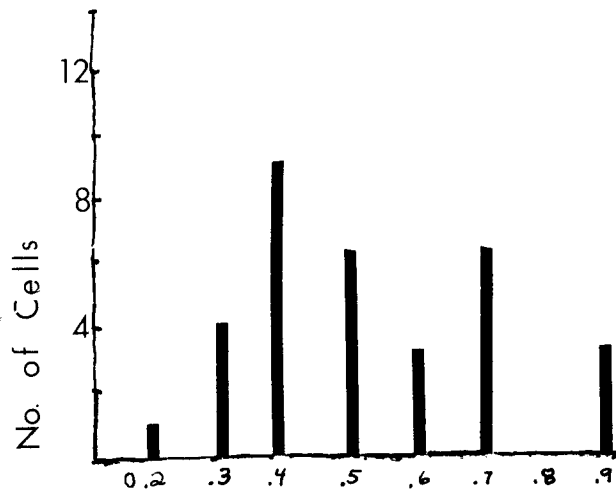


Na/P

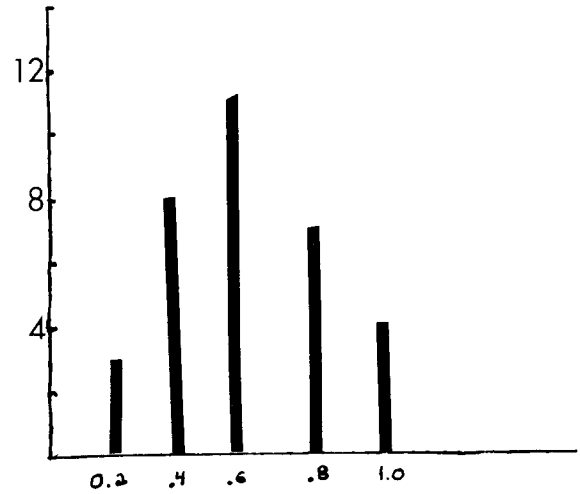


K/P

Fig. 1

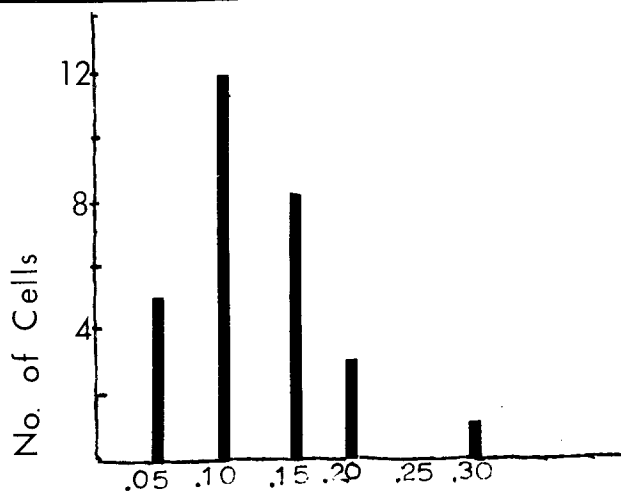


Na/P



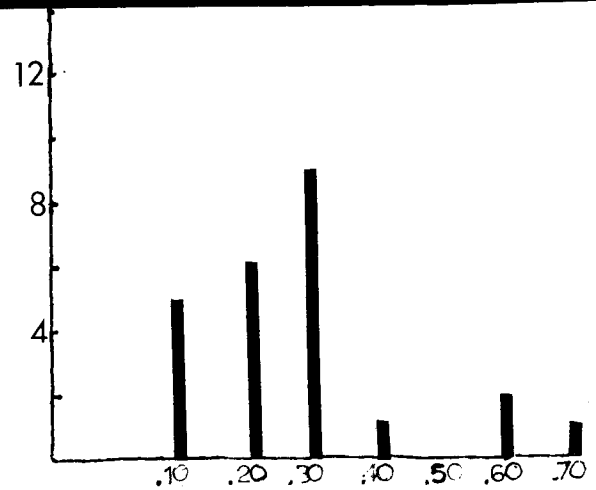
K/P

Fig. 2



Na/P

cells in clumps



Na/P

single cells

Fig. 3

## EVALUATION OF THE ELECTRON MICROPROBE FOR MEDICAL APPLICATION\*

P. S. Ong, W. O. Russell, M. Mandavia, and G. Sroka  
The University of Texas at Houston M. D. Anderson  
Hospital and Tumor Institute, Houston, Texas 77025

INTRODUCTION

The unique features of the electron probe microanalyzer make it an extremely valuable tool for medical applications. Spatial resolution, close to one micron, allows the study of elemental composition at the cellular level. Yet thus far, quantitative histological applications related to chemistry and morphology, remain at the developmental stage. No reliable method has been established which is suitable for routine diagnostic application.

The purpose of our program which was recently initiated at The University of Texas M. D. Anderson Hospital, was to evaluate the microprobe as a possible diagnostic tool for a selected field of application. We have concentrated our efforts on thyroid tissues, and intend to use the initial findings as a basis for future extension. There are several reasons for this choice. First, previous studies by Robison, et al. (1), and by Banfield, et al. (2) showed that elements such as iodine, calcium, and phosphorus could be measured with relative ease. These are essential elements related to many metabolic disorders. Secondly, sufficient quantities of research material are available from patients with various thyroid disorders at this institution. And thirdly, a wealth of experience and knowledge has accumulated from the study of thyroid tissue with various other techniques such as autoradiography, light and electron microscopy, and histochemistry. Initially, the program concentrated on the investigation of three major fields: Sample preparation techniques, beam induced damage, and quantitation of the results.

SAMPLE PREPARATION

Several investigators have devoted considerable effort to experimenting with a variety of sample preparation techniques with varying degrees of success. Coleman (3) reviewed the various aspects in last year's tutorial seminar of the 7th National Conference on Electron Probe Analyzer. Sample preparation reviews are also given by Hall (4) and Anderson (5).

An important part of our program was the comparison of the microanalytical results with the standard histochemical and optical observations. Therefore, a procedure had to be developed which allowed the same sample to be studied by the microprobe, light microscope, and possibly, the electron microscope. Generally, the optical microscope, incorporated into

\*This work was supported by a grant No. 166551 from the Kelsey-Leary Foundation.

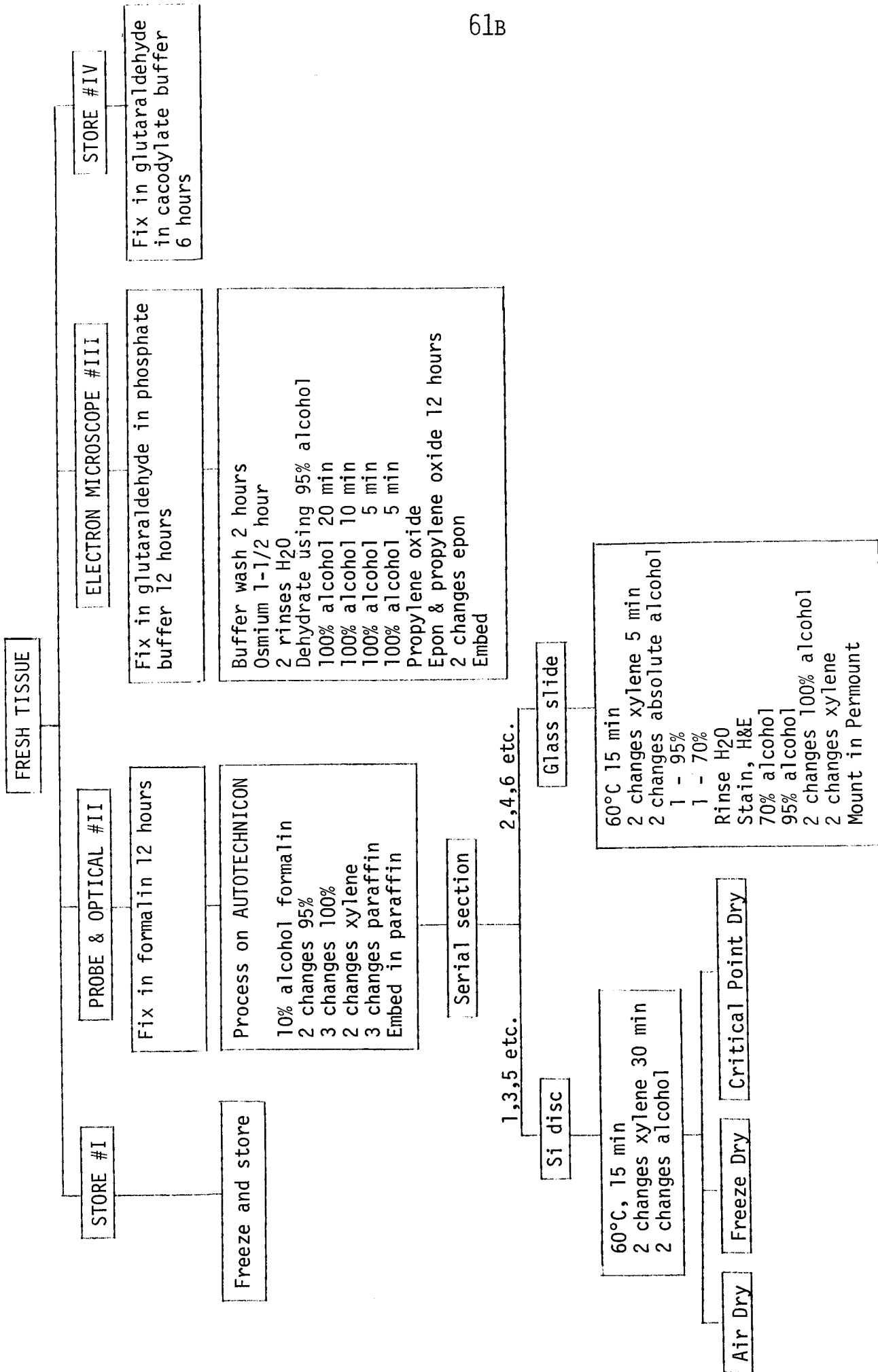
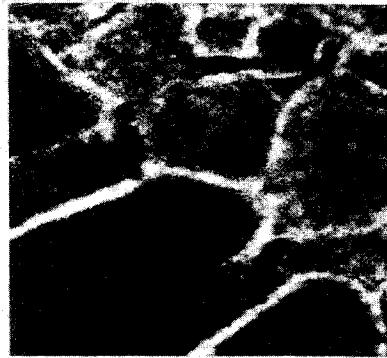


Fig. 1. Outline for tissue preparation procedure.

**15 $\mu$  Section of Thyroid Tissue****100 $\mu$** 

Electron Image



Phosphorous X-ray Image

Optical Photomicrograph  
of 5 $\mu$  Serial Section

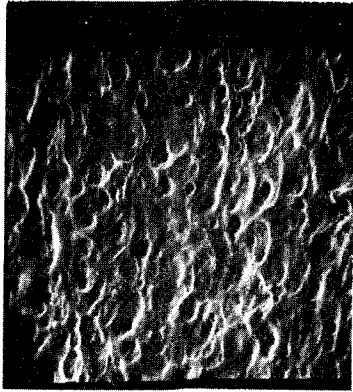
Calcium X-ray Image



Iodine X-ray Image

Fig. 2. Electron, optical, and x-ray images of air dried thyroid tissue.

## AIR DRIED



## C. P. DRIED

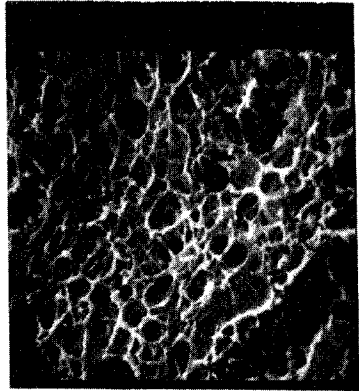
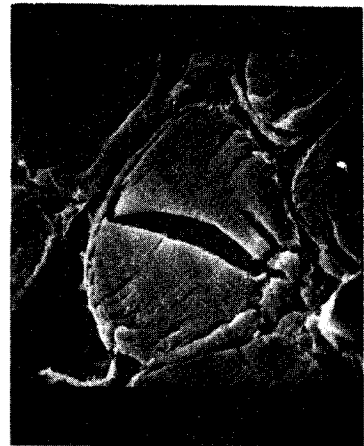


Fig. 3. Scanning electron microscope pictures of air dried and critical point dried thyroid tissue.

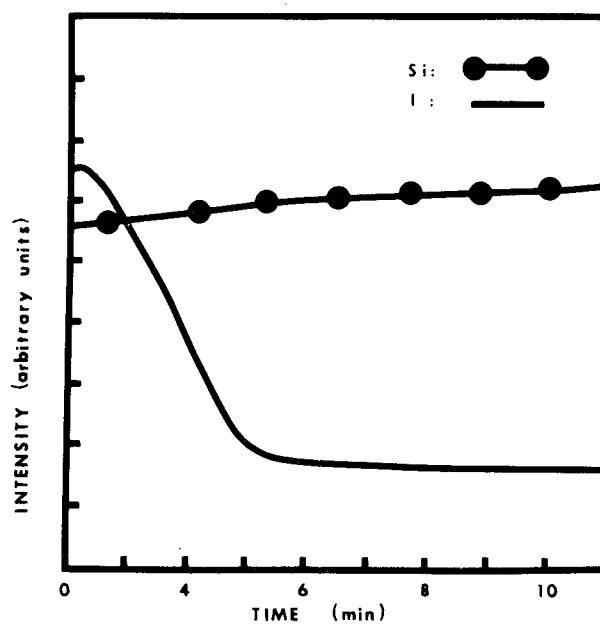


Fig. 4. Change of iodine and silicon intensities in a typical air dried sample.

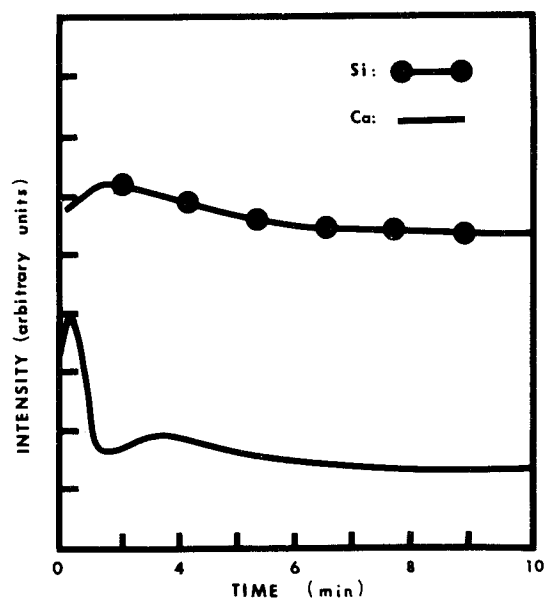


Fig. 5. Change of calcium and silicon intensities in a typical air dried sample.

the microprobe, is not of a high quality. In addition, good optical observation requires that the sample be properly stained and embedded. The method we followed was to use serial sections in which the consecutive sections were used for microprobe and light microscopic study. Because most of the fixing and sample handling techniques (3,4,5) proved to be equally effective, we followed the one which was basically the same as normally used for optical microscopy up to the point of staining and mounting (see diagram in Fig. 1). Although a slight gross distortion of the sample occurs during these processes, it is possible to identify the various parts of the tissue. Figure 2 shows an example of the images obtained with samples prepared as described and air dried.

One of the many questions which plagued us was the effect of structural changes that occurred when the sample was dried, particularly sample components such as follicles which consist of 90 per cent or more water. To answer this question, one air dried sample and one sample dried according to the critical point drying technique (6) were studied with the scanning electron microscope. The results are shown in Fig. 3. Contraction and distortion of the cells and a complete collapse of the follicles in the air dried samples can be observed. The critical point dried sample is better at preserving the overall structure. However, the follicles show a spongy structure with an inhomogeneous mass distribution which could lead to misinterpretation. For the sake of simplicity and uniformity in this investigation, the samples were air dried. A more extensive comparative study of the freeze drying, air drying, and critical point drying techniques is in progress.

#### BEAM INDUCED SAMPLE DAMAGE

Beam induced damage on biological samples can vary from loss of volatile components to complete charring and ashing. Recently, Hall (7) reviewed various aspects of beam damage. In general, the mechanism of beam damage is complex and several factors are involved. Lehrer and Berkley (8) reported that a stationary beam with a current as low as  $10^{-9}$  burned gelatin standards. On the other hand, other samples can withstand 10 to 100 times higher beam loads. This, and other observations, necessitated the study of the general behavior of biological samples under an electron beam.

The general qualitative changes in counting rate with time of iodine and silicon obtained from a typical air dried thyroid tissue on a silicon disc are shown in Fig. 4. In Fig. 5, the corresponding calcium and silicon intensities are shown. For both iodine and calcium, a small but rapid rise in intensity was first observed. This was followed by a drop in intensity, after which the intensity stabilized at a lower value. Associated with each element's intensity change was a small change in silicon intensity. The change in silicon intensity was opposite to that of iodine or calcium. The rate and extent of the intensity changes were dependent on the focusing condition and therefore on the current density. This is illustrated in Fig. 6 where the counting rates were observed for a focused and defocused

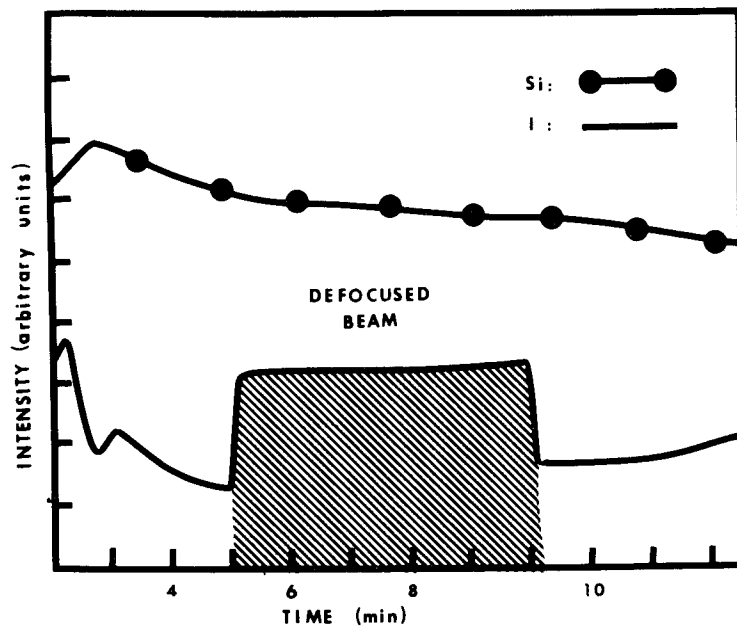


Fig. 6. The effect of a focused and defocused beam on the x-ray intensities.

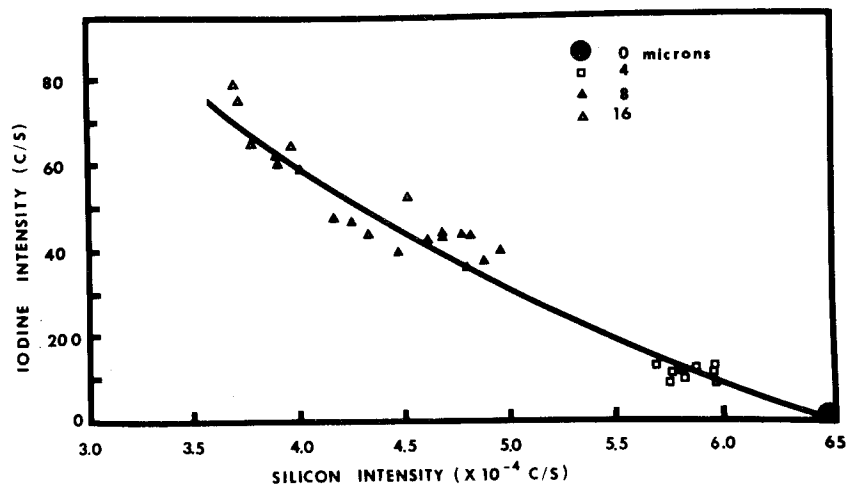


Fig. 7. A typical relationship of iodine and silicon as obtained from a follicle in normal tissue sections.



beam. Optically, a boiling phenomenon is observed which is followed by either a black deposit (contamination) or charring.

The effects described above were caused first by softening and displacement of the protein, followed by the boiling off of bound water which could not be removed by freeze, critical point, or air drying methods. This hypothesis was supported by experiments on air dried samples that were further dried for 3 hours in a vacuum at about 120°C. Samples prepared in this manner have a higher softening point; therefore, they remained stable under the beam and no change in x-ray intensity was observed even for a focused beam with a current as high as  $10^{-6}$ A.

### QUANTITATION

Accuracy of the data depends on a proper method of quantitation. Reliable and meaningful results must be expressed as a fraction of a reliable reference material. For medical application, this reference would be the dry mass of the sample. Various methods of quantitation based on dry mass have been developed and proposed in the past. The simplest and most efficient method is that proposed and used by Hall, et al. (9) and further developed by Hall and Werba (10). In this technique, the continuous radiation, which is proportional to the dry mass, is simultaneously measured. This method is correct only if the sample is mounted on an extremely thin substrate.

Where high specimen currents are necessary to obtain sufficient x-ray intensity, a thick substrate is necessary to act as a heat sink. A thick substrate is also required if the same sample is to be used for light optical observations before or after probe analysis. The method proposed by Warner (11) in his computer program Basic, and later modified by Warner and Coleman (12) in their computer program Bicep, is based on a thin sample on a thick substrate. These methods rely on the x-rays emitted from the substrate for the measurement of mass and require standards of known composition for quantitation.

A more direct approach would be to establish calibration curves for the various elements using the substrate x-ray intensity as a method of determining the dry mass, similar to the method described by Hutchins (13). Such a technique, however, must be based on the dry mass rather than on the thickness of the specimen (8).

To evaluate this technique, a thyroid sample was prepared and sectioned at 4, 8 and 16 micron thicknesses. A particular follicle was selected in the sample and iodine and silicon measurements were made at various locations in that follicle. The iodine intensity was plotted against the silicon intensity and is shown in Fig. 7.

This curve represents a particular iodine concentration, which was assumed constant within a follicle, and relates the iodine intensity to that of silicon. The absolute value of the iodine weight fraction was not known.

To obtain a family of curves of iodine intensity versus silicon intensity for various known weight fractions, the following method was used. Several solutions of gelatin were prepared with different iodine concentrations. The solution of each concentration was subsequently spread at random thicknesses on silicon discs, air dried and vacuum dried at an elevated temperature as previously described. Each of the samples yielded a number of data points with a variety of iodine and silicon intensities due to nonuniformity in mass. For a particular weight fraction, the data points fall on a single curve similar to that shown in Fig. 7. In this way, a family of curves is obtained for a range of iodine concentrations.

#### ACKNOWLEDGEMENT

The authors wish to acknowledge the competent technical assistance of Bessie Guillory and the dedicated assistance of Mary McCracken, Catherine Johns and Dr. Emanuel Solon in the preparation of the manuscript. The authors are also indebted to Dr. J. Anderson, The University of Texas M. D. Anderson Hospital, Department of Diagnostic Radiology, and D. Landis, Baylor College of Medicine, Department of Ophthalmology, for the SEM studies.

#### REFERENCES

1. Robison, W.L., L. Van Middlesworth, and D. Davis: Calcium, iodine and phosphorus distribution in human thyroid glands by electron probe microanalysis. *J. Clin. Endocrin. Metab.*, 32:786-795, 1971.
2. Banfield, W.G., P.M. Grimley, W.G. Hammond, C.M. Taylor, B. de Flores, and A.J. Tousimis: Electron probe analysis for iodine in human thyroid and parathyroid glands, normal and neoplastic. *J. Nat. Cancer Inst.*, 46:269, 1971.
3. Coleman, J.R.: Techniques for electron probe analysis of biological material. Proceedings of Tutorial Session of 7th National Conference on Electron Probe Analysis, San Francisco, 1972.
4. Hall, T.A.: The microprobe assay of chemical elements. In *Physical Techniques in Biological Research*. Vol. 1A, Optical Techniques, p158. G. Oster, Ed., Academic Press, New York, London, 1971.
5. Anderson, C.A.: An introduction to the electron probe microanalyzer and its application to biochemistry. In *Methods of Biochemical Analysis*, Vol. XV, p147. D. Glick, Ed., Interscience Publishers, 1967.
6. Anderson, T.F.: Electron microscopy of microorganisms. In *Physical Technique in Biological Research*, 3rd Ed. E.D. Oster and A. Pollister, Eds., Academic Press, New York, 1956.

7. Hall, T.A.: Preparation and examination of biological samples. Proceedings of 7th National Conference on Electron Probe Analysis, Paper No. 40, San Francisco, 1972.
8. Lehrer, G.M. and C. Berkley: Standards for electron probe microanalysis of biological specimens. J. Histochem. Cytochem. 20:710-715, 1972.
9. Hall, T.A., A.J. Hale, and V.R. Switsur: In The Electron Microprobe. Proceedings of the Symposium on Electron Probe Microanalysis. T.D. McKinley, et al., Eds., John Wiley and Sons, Inc., New York, 1966.
10. Hall, T.A. and P. Werba: The measurement of total mass per unit area and elemental weight fraction along line scan in the specimen. Proceedings of the 5th International Congress on X-Ray Optics and Microanalysis. G. Mollenstedt and K. H. Gaukler, Eds., Springer, Verlag, Berlin, Heidelberg, New York, 1969.
11. Warner, R.: A computer program for the analysis of biological material. Proceedings of the 6th National Conference on Electron Probe Analysis, Paper No. 42, Pittsburgh, Pa., 1971.
12. Warner, R.R. and J.R. Coleman: A computer program for quantitative microanalysis of thin biological material. Proceedings of the 7th National Conference on Electron Probe Analysis, Paper No. 41, San Francisco, 1972.
13. Hutchins, G.A.: Thickness determination of thin films by electron probe microanalysis. In The Electron Microprobe. Proceedings of the Symposium on Electron Probe Microanalysis. T.D. McKinley, et al., Eds., John Wiley and Sons, Inc., New York, 1966.

PURE CRYSTALS AS SECONDARY STANDARDS  
FOR QUANTITATIVE ELECTROLYTE  
STUDIES OF SOFT BIOLOGICAL TISSUE

F. Duane Ingram, Mary Jo Ingram and C. Adrian M. Hogben  
Department of Physiology and Biophysics  
University of Iowa  
Iowa City, Iowa 52242

Methods for the quantitative study of soft biological tissue have not been generally agreed upon. The tissue preparation for some methods involves a freeze-drying process in which aqueous solutions are not used for any step of the preparation. Standards are described here for the measurement of K, Cl and Na in samples prepared in this fashion. Pure crystals of KCl and NaCl have been referenced to these standards so that the easily procured pure crystals may be used routinely as secondary standards.

Freeze-drying in a vacuum at temperatures between  $-40^{\circ}\text{C}$  and  $-80^{\circ}\text{C}$  with subsequent embedding in Epon 826 polymer however, is accompanied by substantial volume changes (1). This was demonstrated by the use of radioactive isotopes to label solutions of 20% bovine serum albumin. The specific activity of that solution was compared with dried, embedded and trimmed drops of that same solution. Amphiuma whole blood and mouse muscle were also checked in the same manner. A shrinkage of 20% to 30% was found for each of the above types of samples.

Even if these volume changes were accurately known and allowed for, standard correction procedures would be unreliable. Correction factors for the electrolytes in an epoxy matrix are large, particularly for Na. Also, since these elements are present in only trace amounts, even a small error is quite significant.

It is thus necessary to reference measurements to well characterized standards prepared of a material similar in nature to that of the tissue to be studied with the electron probe. Solutions of 20% bovine serum albumin containing known quantities of K, Cl and Na have been used for this purpose. Drops were quick-frozen, freeze-dried in a vacuum

at about  $-80^{\circ}\text{C}$ , stained with osmium tetroxide vapor, embedded in Epon 826 polymer, and treated in every way like biological tissue (2, 3).

Two features of these specimens, however, render them as poor choices for routine use as standards. 1) Counting rates are low for specimens prepared with concentrations of the same magnitude as those found in typical tissues and 2) micro-inhomogeneities cause inter- and intrasample variations which require the obtaining of an average from a number of locations on a number of different standards samples, see Table 1.

These deficiencies may be overcome by referencing the counting on the albumin standards to counting on easily procured pure crystals of KCl and NaCl. These crystals possess the required homogeneity and yield the necessary high counting rates to make them excellent references. Subsequent electron probe measurements are then referenced to freshly prepared KCl and NaCl crystals as secondary standards.

Table 2 presents calibration factors for K, Cl and Na with the corresponding counting on KCl and NaCl crystals. The standards samples were prepared as described earlier. The 20% albumin solution was measured with a flame photometer to contain  $103.5 \pm 1.9$  and  $120.6 \pm 2.1$  mEq/kg of K and Na respectively. The Cl concentration was  $102.9 \pm 0.1$  mEq/kg measured with a Buchler-Cotlove Chloridometer. The confidence limits are the standard deviations of the mean of replicate measurements. Table 2 presents the counting obtained on a set of 11 standards blocks prepared from the albumin solutions. The probe specimens were prepared by facing the block with a steel knife microtome and mounting in an electron probe specimen holder next to crystals of KCl and NaCl. A thin, approximately 200 Å, carbon layer was cast on the specimen holder in a vacuum evaporator. Measurements were made with a 10 kv electron beam that registered 50 na on quartz. The electron probe counting on these blocks is presented in Table 2.

As the correction factors change with electron beam voltage and sample composition, the calibration factors presented in Table 2 can only be expected to yield meaningful values when used with a 10 kv electron beam and a sample embedded in plastic having a composition similar to that of the Epon 826 polymer, Table 3.

TABLE 1

## PROBE COUNTING ON ALBUMEN STANDARDS BLOCKS

 $E_0 = 10 \text{ kv}$  $i = 52 \text{ na (50 na on quartz)}$ 

Block No.	K - $K_\alpha$	Cl - $K_\alpha$	Na - $K_\alpha$
72-1-6f	929* $\pm$ 45**	1405 $\pm$ 47	640 $\pm$ 40
72-1-6g	990 $\pm$ 57	1415 $\pm$ 50	686 $\pm$ 23
72-1-6a	992 $\pm$ 53	1263 $\pm$ 58	631 $\pm$ 30
72-1-6c	971 $\pm$ 48	1274 $\pm$ 41	626 $\pm$ 28
72-1-6q	964 $\pm$ 79	1311 $\pm$ 113	659 $\pm$ 39
72-1-6s	921 $\pm$ 69	1298 $\pm$ 70	623 $\pm$ 22
72-1-6h	964 $\pm$ 82	1326 $\pm$ 98	649 $\pm$ 55
72-1-6m	948 $\pm$ 102	1311 $\pm$ 95	637 $\pm$ 65
72-1-6k	977 $\pm$ 64	1295 $\pm$ 110	664 $\pm$ 54
72-1-6o	917 $\pm$ 54	1384 $\pm$ 45	666 $\pm$ 26
72-1-6j	916 $\pm$ 59	1362 $\pm$ 85	644 $\pm$ 48
Average	954 $\pm$ 29	1331 $\pm$ 52	648 $\pm$ 19

\* Average of nine to eleven, 40 sec. counts

\*\* S.D. of the mean

Table 2

Calibration Factors for Converting X-ray Intensities  
To Numbers Representing Weight Concentrations\*

$E_o = 10 \text{ kv}$

$i = 50 \text{ na on quartz}$

Albumin Standards

	K	Cl	Na
Concentration of element (mEq/kg)	103.5 $\pm$ 1.9	102.9 $\pm$ 0.1	120.6 $\pm$ 2.1
Counting on Standards Blocks (Cnts/40 sec)	954 $\pm$ 29	1331 $\pm$ 52	648 $\pm$ 19
Off-Peak Background (Cnts/40 sec)	124 $\pm$ 4	132 $\pm$ 4	96 $\pm$ 2
Corrected Counts on Pure Plastic (Cnts/40 sec)	--	78 $\pm$ 11	--
Net Counting on Standards Blocks (Cnts/40 sec)	830 $\pm$ 29	1121 $\pm$ 53	552 $\pm$ 19
Calibration Factor (mEq/kg/Cnts/sec)	4.99 $\pm$ .19	3.67 $\pm$ .17	8.74 $\pm$ .34

Secondary Standards

Reference Crystal	KCl	NaCl	NaCl
Counting on Reference Crystal (Cnts/sec)	4079 $\pm$ 29	3143 $\pm$ 46	2199 $\pm$ 31

\*All values are listed plus or minus the standard deviation of the mean. The confidence limits on the calibration factors are estimates of the standard deviation obtained from the square root of the sum of the squares of the standard deviations for each of the components. The counting on the reference crystals has been corrected for off-peak background and for a 2  $\mu$ sec dead time.

TABLE 3

## COMPOSITION OF EPON 826 EPOXY POLYMER\*

Element	Concentration
C	71.33 wt. %
O	21.38
H	7.50
Cl	0.05
Density of Epon 826 Polymer	1.152 kg/liter

\*Determined by oxygen bomb combustion at Schwartkopf Micro-analytical Laboratory, 56-19 37th Avenue, Woodside, New York 11377.

References:

- 1) Ingram, F. D., A critical analysis of the freeze-dried, plastic embedded electron probe specimen preparation, Symposium on Microprobe Analysis as Applied to Cells and Tissues, Seattle, Washington, April 30 - May 2, 1973.
- 2) Ingram, F. Duane, Mary Jo Ingram and C. Adrian M. Hogben, Quantitative electron probe analysis of soft biological tissue for electrolytes. Journal of Histochemistry and Cytochemistry, 20:716-722, 1972.
- 3) Ingram, Mary Jo and C. Adrian M. Hogben. Procedures for the study of biological soft tissue with the electron microprobe, In: Developments in Applied Spectroscopy, W. K. Baer, A. J. Perkins, E. L. Grove, Eds., Plenum Press, New York, Vol. 6, 1968, p. 43-64.



Electron Probe Analysis of Calcium Containing  
Lipid Droplets in Tetrahymena pyriformis.

James R. Coleman

Department of Radiation Biology and Biophysics  
University of Rochester  
School of Medicine and Dentistry  
Rochester, New York 14642

Recent investigations indicate that cellular activity is directly involved in, and may exert a controlling influence over, bone mineralization. Several lines of evidence have led to the suggestion that the mineralization process includes the following steps (1): 1) accumulation of elevated concentrations of calcium and phosphorus as discrete spherules within bone cells; 2) excretion of these calcium and phosphorus concentrations as a vesicle or dense body; and 3) migration of the excreted body to sites of calcification on the extracellular matrix. Although of prime importance, it has proved difficult to study the cellular aspects of this hypothetical mechanism. The presence of large amounts of calcium in bone interferes with the in situ measurement of small changes in calcium concentrations that might be associated with cell activity. Isolation of cells from bone, so that cell calcium metabolism might be studied without the interference of high calcium concentrations in associated bone, has met with only limited success (2). Clearly, a model system to examine the cellular aspects of calcium and phosphorus accumulation should be useful.

Tetrahymena pyriformis is a ciliated protozoon which accumulates calcium and phosphorus within cytoplasmic lipid droplets, during the stationary phase of growth, and under certain environmental conditions. These lipid droplets, termed refractile granules, are difficult to isolate intact. Because they contain both lipid and inorganic components, and isolation procedures involve exposure to either aqueous or organic solvents, some losses have occurred with every isolation procedure so far employed. However, it has been possible to analyze the granules in situ, and individually, using the electron probe (3). Such analysis has shown that the amount of calcium, magnesium, potassium and phosphorus varies among granules, but the ratios of calcium to phosphorus, magnesium to phosphorus and potassium to phosphorus tend to be uniform among granules. These characteristics suggest that some aspects of the cellular accumulation of calcium and phosphorus which are important to bone mineralization might be studied conveniently in this organism.

One of the characteristics of the mineralization process is the discrimination of strontium from calcium (e.g., 4,5,6). Although strontium is incorporated into bone, it is not incorporated into bone in amounts proportional to its availability in the diet. This discrimination has been attributed to lack of absorption and to preferential excretion by the kidneys as well as to discrimination by forming hydroxyapatite. If, however, mineralization depends on a first step that involves intracellular accumulation of calcium and phosphorus, then discrimination between calcium and strontium may also occur at this level of operation. In order to test this possibility we cultured T. pyriformis under a variety of conditions to determine whether the refractile granules incorporated strontium in proportion to its concentration in the nutrient medium, or whether there was some discrimination against this element. Since adding strontium to the nutrient media would substantially alter the concentration of total divalent ions, we also cultured T. pyriformis in media to which calcium had been added in quantities sufficient to increase the total divalent ion concentrations to that found in the strontium-supplemented media.

T. pyriformis were cultured as described (3) in a) Proteose-peptone medium; b) Proteose-peptone medium to which 0.3 mM or 3 mM  $\text{CaCl}_2$  had been added; or c) Proteose-peptone medium to which 0.3 mM or 3 mM  $\text{SrCl}_2$  had been added; d) casein-yeast extract (Medium M) medium (7); e) casein yeast extract medium to which 0.3 mM or 3 mM  $\text{CaCl}_2$  had been added; f) casein-yeast extract medium to which 0.3 mM or 3 mM  $\text{SrCl}_2$  had been added; or g) defined medium (7). Cells were heat fixed as before and analyzed as previously described (3). Corrections were performed according to the BICEP procedure (8).

Results of the analysis are presented in Table I. The mean ratios for Ca/P and Mg/P were not significantly different in granules within cells cultured in any of the three normal, unsupplemented media. The mean K/P ratios were similar in granules within cells cultured in Proteose-peptone medium and Medium M, but was significantly lower within cells cultured in Defined medium. Supplementing the calcium content of the Proteose-peptone medium with 0.3 and 3 mM calcium depressed the mean Ca/P ratio and increased the mean Mg/P ratio of the granules, without altering the mean K/P ratio. Supplementing medium M with 0.3 mM Ca produced no significant change in the mean Ca/P, and Mg/P ratios but the mean K/P ratio decreased. When strontium was added, all granules incorporated this element. Adding 0.3 mM strontium to Proteose-peptone medium lowered the mean Ca/P of the granules, but did not affect the mean Mg/P or K/P ratios. Addition of 3 mM Sr to Proteose-peptone medium significantly reduced the mean Ca/P and Mg/P ratios but not the mean K/P ratio of the granules. However, the change in these ratios was not significantly different from that produced by the addition of 3 mM Ca. Addition of 0.3 mM Sr to medium M significantly reduced the mean Mg/P ratio, and increased the mean K/P ratio without affecting the mean Ca/P ratio. Addition of 3 mM Sr to the same medium significantly decreased the mean Ca/P ratio without

affecting the mean Mg/P or K/P ratios. The change in Ca/P ratio produced by 3 mM Sr in medium was significantly greater than that produced by an equimolar amount of Ca added to the medium. Addition of 0.3 mM Ca or 0.3 mM Sr to medium M produced similar changes in the K/P ratios.

These studies indicate that the metallic composition of refractile granules is not simply proportional to the concentration of these elements in the medium. Instead, there seems to be a rather complex relationship between medium concentration and granule composition. For example, increasing the calcium concentration in Proteose-peptone medium decreases the Ca/P ratio but tends to raise the Mg/P ratio. In contrast, raising the calcium concentration in Medium M has no significant effect on either the Ca/P, or Mg/P ratios. Furthermore, although all granules incorporate strontium if it is present in the medium, a tenfold increase in medium concentration doubles the Sr/P ratio in Proteose-peptone medium and raises the Sr/P ratio in medium M slightly more than threefold. In both Proteose-peptone medium and Medium M it appears that Sr is incorporated at the expense of both Ca and Mg, and does not compete specifically with just one element. Thus it appears likely that either the cell or the lipid components of the refractive granules exercise some control over granule composition, even though the mechanism for such control is not obvious.

#### Acknowledgement

This report is based in part on work performed under contract with the Atomic Energy Commission at the University of Rochester Atomic Energy Project and has been assigned report number UR-3490-299 and in part on work supported by U.S. PHS Research Grant AM14272.

#### References

1. Termine, J., 1972, Clin. Orthop. and Rel. Res. 85: 207.
2. Nichols, G., Jr., P. Hirschmann, and P. Rogers, 1971, in: Cellular Mechanisms for Calcium Transfer and Homeostasis (G. Nichols and R. Wasserman, eds). Academic Press, New York, p. 211.
3. Coleman, J.R., J.R. Nilsson, R.R. Warner, and P. Batt, 1972, Exptl. Cell Res. 74: 207.
4. Jethi, R.K., M.G. Mackey, P.D. Meredith, and C.L. Wadkins, 1972, Calc. Tiss. Res. 9: 310.
5. Bachra, B.N. and H.R.A. Fischer, 1969, Calc. Tiss. Res. 3: 348.
6. Neuman, W.F. and M.W. Neuman, 1958, The Chemical Dynamics of Bone Mineral. Univ. of Chicago Press, Chicago.
7. Holz, G.G., Jr., J.A. Erwin, and R.J. Davis, 1959, J. Protozool. 6: 149.
8. Warner, R.R. and J.R. Coleman, 1973, Micron (in press).

	Medium	Ca/P	Mg/P	Sr/P	K/P
1.	Proteose-Peptone ( $10^{-4}$ M Ca; $10^{-3}$ M Mg)				
2.	" " + 0.3 mM Ca	0.44 $\pm$ 0.06	0.38 $\pm$ 0.12		0.12 $\pm$ 0.02
3.	" " + 3.0 mM Ca	0.29 $\pm$ 0.06	0.49 $\pm$ 0.09		0.12 $\pm$ 0.04
4.	" " + 0.3 mM Sr	0.23 $\pm$ 0.08	0.48 $\pm$ 0.09		0.12 $\pm$ 0.03
5.	" " + 3.0 mM Sr	0.33 $\pm$ 0.06	0.29 $\pm$ 0.06	0.15 $\pm$ 0.02	0.10 $\pm$ 0.06
		0.23 $\pm$ 0.08	0.27 $\pm$ 0.06	0.28 $\pm$ 0.08	0.09 $\pm$ 0.05
6.	Medium M ( $10^{-4}$ M Ca; $10^{-3}$ M Mg)				
7.	" " + 0.3 mM Ca	0.41 $\pm$ 0.06	0.31 $\pm$ 0.10		0.14 $\pm$ 0.06
8.	" " + 3.0 mM Ca	0.39 $\pm$ 0.09	0.30 $\pm$ 0.05		0.19 $\pm$ 0.03
9.	" " + 0.3 mM Sr	0.50 $\pm$ 0.10	0.26 $\pm$ 0.08		0.08 $\pm$ 0.06
10.	" " + 3.0 mM Sr	0.39 $\pm$ 0.20	0.26 $\pm$ 0.02	0.08 $\pm$ 0.02	0.20 $\pm$ 0.02
		0.28 $\pm$ 0.13	0.27 $\pm$ 0.04	0.29 $\pm$ 0.06	0.19 $\pm$ 0.06
11.	Defined ( $7.5 \times 10^{-4}$ M Ca; $2 \times 10^{-3}$ M Mg)	0.43 $\pm$ 0.06	0.31 $\pm$ 0.02		0.10 $\pm$ 0.04

Table I. Ratios of metals to phosphorus in normal and supplemented media;  $\pm$  standard deviation of the mean. Values in parentheses are the concentrations of calcium and magnesium in the unsupplemented media.

## References

1. Borun, E. R., Figueroa, W. G., and Perry, S. M., The distribution of  $\text{Fe}^{59}$  tagged human erythrocytes in centrifuged specimens as a function of cell age, J. Clin. Invest., 36, 676 (1957).
2. Pranker, T. A. J., The ageing of red cells, J. Physiol., 143, 325 (1958).
3. Rigas, D. A., and Koler, R. D., Ultracentrifugal fractionation of human erythrocytes on the basis of cell age, J. Lab. & Clin. Med., 58, 242 (1961).
4. Garby, L., and Hjelm, M., Ultracentrifugal fractionation of human erythrocytes with respect to cell age, Blut, 9, 284 (1963).
5. Leif, R. C., and Vinograd, J., The distribution of buoyant density of human erythrocytes in bovine albumin solutions, Proc. Natl. Acad. Sci., 51, 520 (1964).
6. Danon, D., and Marikovsky, Y., Determination of density distribution of red cell population, J. Lab. & Clin. Med., 64, 668 (1964).
7. Bishop, C., and Prentice, T. C., Separation of rabbit red cells by density in a bovine serum albumin gradient and correlation of red cell density with cell age after in vivo labeling with  $^{59}\text{Fe}$ , J. Cell. Physiol., 67, 197 (1966).
8. Leif, R. C., Buoyant density separation of cells, in Automated Cell Identification and Cell Sorting, G. L. Weid and G. H. Bahr, Eds., Academic Press, 1970, pp.21-96.
9. Tousimis, A. J., Quantitative electron probe analysis of biological tissue sections, Sixth Nat. Conf. Electron Probe Analysis, 36 (1971).
10. Herz, F., and Kaplan, E., A microtechnic for the separation of erythrocytes in accordance with their density, Amer. J. Clin. Path., 43, 181 (1965).
11. Kimzey, S. L., and Burns, L. C., Electron probe microanalysis of cellular potassium distribution, Proc. N.Y. Acad. Sci., 1973 (In Press).
12. Lehrer, G. M., and Berkeley, C., Standards for electron probe microanalysis of biologic specimens, J. Histochem & Cytochem., 20, 710 (1972).



## ELECTRON PROBE MICROANALYSIS OF AGE DIFFERENCES IN HUMAN RED BLOOD CELLS

Linda C. Burns and Stephen L. Kimzey  
Cellular Analytical Laboratory  
Johnson Space Center, Houston, Texas 77058

Circulating erythrocytes in human blood represent a heterogeneous population of cells with a finite life span of approximately 120 days. As the red blood cell ages significant alterations occur in the physical and chemical characteristics of the cell which in turn affect its functional capacity. One of the changes occurring as a result of aging is an increase in cellular density which forms the basis for procedures to separate cells into fractions of similar age (1-8). The light cell fraction produced by centrifugation or density gradient separation techniques has been shown to consist of younger erythrocytes which contain more K, less Na, a higher content of total phospholipids, more ATP and 2, 3-DPG, a higher rate of glycolysis, and more resistance to osmotic lysis than the heavier fractions of older cells.

The use of the electron probe microanalyzer combined with a microtechnique for age density separation has allowed us to evaluate chemical differences between individual red blood cells from light and heavy cell fractions. This study describes differences found in intracellular x-ray intensities of K, S and P in age density separated fractions from normal human blood samples. Si substrate x-ray absorption by the cells was measured as an indication of dry cell mass.

All specimens were examined with an Applied Research Laboratories EMX-SM electron probe. Individual red blood cells were analyzed using a static electron beam with a measured diameter of 1.5  $\mu\text{m}$ , a 10 KV accelerating potential, and a sample current of 0.150  $\mu\text{A}$ . Wavelength dispersion detection systems were used for the analyses of K  $K\alpha$ , S  $K\alpha$ , and P  $K\alpha$  x-rays. An Ortec 7000 Series Si (Li) energy dispersive detection system was used for Si determinations. Data for K, S, and P are reported as counts/50 sec. corrected for background off the cell and changes in instrument efficiency. Si is expressed as  $\Delta\text{Si}$  and represents that portion of the substrate Si intensity which is absorbed by the cellular material. The technique is similar to that described previously for the determination of mass thickness in biological samples (9).

Age density separation of red blood cells was accomplished using a modification of the microtechnique described by Herz and Kaplan (10). A light cell fraction (top 10%) and a heavy cell fraction (bottom 10%) were isolated from 10 human blood samples. For microanalysis, a small sample of the red cell suspension was smeared in a thin film on a silicon wafer (2.5 cm in diameter by 0.02 cm thick) and air dried. Particular care was exercised throughout preparation and analysis to prevent external contamination of the specimen. The importance of adequate biological sample preparation cannot be overemphasized (11).

Standards were prepared from 16  $\mu\text{m}$  sections cut on a cryostat from solutions of 11.2% gelatin and specific  $\text{NaH}_2\text{PO}_4$ , KCl and L-cysteine-HCl concentrations, quick frozen in gelatin capsules in dry-ice cooled liquid Freon 12 and desiccated (12). A single standard approximating the intracellular counting rates of K, S, and P was selected for routine use in instrument calibration.

Table 1 compares microprobe data for K, S, P and substrate x-ray absorption ( $\Delta\text{Si}$ ) from pooled light cell fractions and heavy cell fractions (300 cells were analyzed in each fraction). Flame photometry data from identical samples are included. Although there are differences in the mean K, S and P x-ray intensities between light and heavy cell fractions which are consistent with reported differences in young and old red cells, the large standard deviations make these differences statistically insignificant. The higher K concentration in the light cell fraction measured by flame photometry and the decreased dry mass in this fraction measured by Si absorption indicate that this population consists of younger cells.

---

TABLE 1  
MICROPROBE AND FLAME PHOTOMETRIC ANALYSES  
OF LIGHT AND HEAVY RED CELL FRACTIONS

<u>MICROPROBE</u>	<u>LIGHT CELL FRACTION</u> (Net Counts/50 sec. $\pm$ 1 S.D.)	<u>HEAVY CELL FRACTION</u> (Net Counts/50 sec. $\pm$ 1 S.D.)
K	8995 $\pm$ 3997	8649 $\pm$ 2788
S	4062 $\pm$ 1040	4416 $\pm$ 1180
P	6644 $\pm$ 3658	5034 $\pm$ 3211
$\Delta\text{Si}$	3790 $\pm$ 874	4590 $\pm$ 1292
<u>FLAME PHOTOMETRY</u>	(Meq/Liter Red Blood Cells $\pm$ 1 S.D.)	
K	128.2 $\pm$ 11.7	87.1 $\pm$ 8.3

---

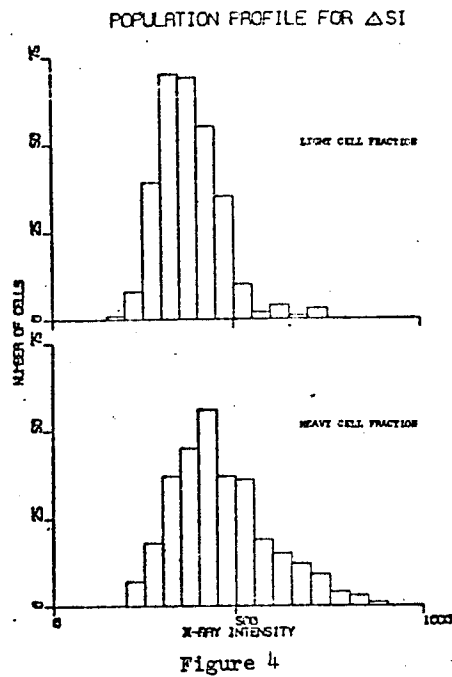
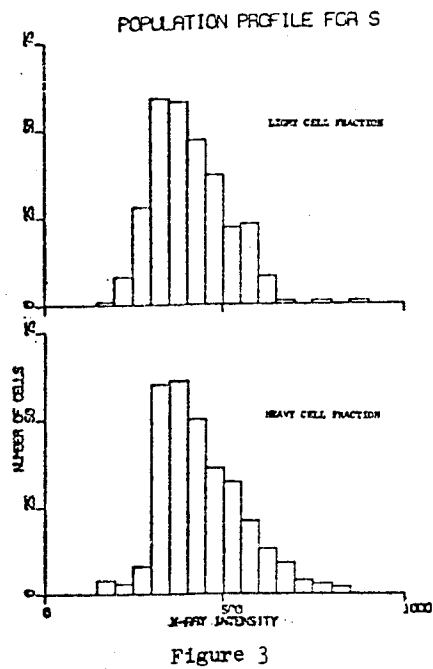
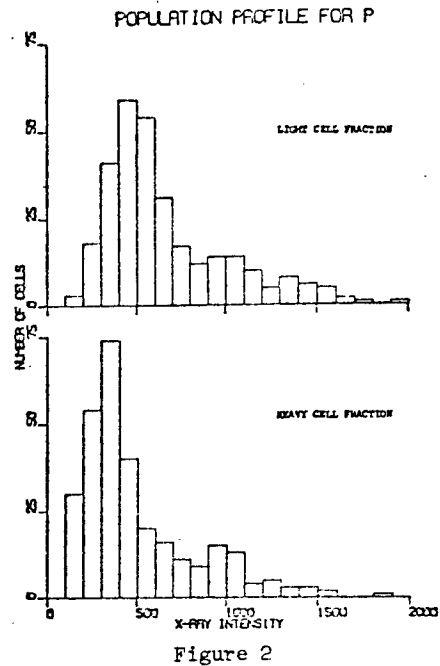
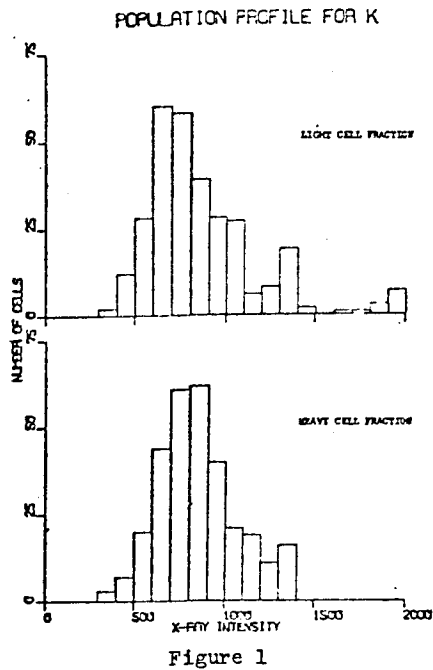


Although mean x-ray intensities for intracellular elements show no significant differences, the distribution profiles for these elements indicate distinct differences between the light and heavy cell fractions. Elemental population distributions for light and heavy cell fractions are shown in Figures 1 through 4. With respect to K distribution (Figure 1) the majority of the cells in the light fraction have a distribution similar to cells in the heavy fraction. However, a small subpopulation (5%) of red cells with high K intensities occurs in the young fraction. This subpopulation of high K cells varies with individual samples and has been observed to represent a significantly higher proportion of the light fraction under certain conditions. Routine flame photometric analysis for K shows increased K concentration in the light cell fraction, but it does not distinguish between contributions to the mean from the majority of the cell fraction and from small subgroups of cells. These observations suggest that the elevated K concentration reported in young cells is due to the existence of a small population of high K cells in this fraction.

The P distribution (Figure 2) in the light cell fraction is shifted to the right, indicating a higher content in the lighter cells. This finding is consistent with the higher levels of total cell phospholipid content reported to be present in light cell samples from age density centrifugation. However, the large variation in phosphate ester content in red blood cells makes interpretation of these data difficult.

The distribution of S x-ray intensities (Figure 3) is essentially the same in both fractions. The differences in substrate x-ray absorption, indicative of cell density (Figure 4), show the expected decrease in the total population of the light cell fraction. If the source of S x-ray intensity is primarily protein material, predominantly hemoglobin in the red blood cell, one would expect S and Si absorption to show similar distributions since both would be measurements of dry cell mass. These data suggest either a matrix effect with dry cell mass distributed differently in cells of each fraction or a contribution of other S containing compounds or anions to measured S intensity.

This study is an attempt to apply electron probe microanalysis techniques to the examination of age separated red blood cells to provide new data on differences in cellular composition related to the normal aging process. The electron microprobe provides the capability to establish distributions of element concentrations in separated cell fractions and to detect the occurrence of small subpopulations of cells which might not significantly alter the overall mean. Two types of population distribution profiles have been observed which relate to reported chemical measurements of cell content. The application of these microtechniques holds promise for the better resolution of age related differences in the chemical content of red blood cells.



FIGURES 1-4. ELEMENTAL POPULATION DISTRIBUTIONS FOR LIGHT AND HEAVY RED CELL FRACTIONS.

X-ray intensities corrected for background and instrument calibration are plotted against the number of red cells occurring at these intensities. Age density separated fractions were obtained from 10 blood samples taken from normal human subjects. 300 red cells were analyzed from each fraction.



## IMMATURE MUSCLE

## SODIUM AND POTASSIUM

## ELECTRON MICROPROBE INVESTIGATION

Buford L. Nichols  
D. Jane Sachen  
Carlton F. Hazlewood

Section of Nutrition and Gastroenterology  
Departments of Pediatrics and Physiology  
Baylor College of Medicine  
Houston, Texas 77025

Linda C. Burns  
Steven L. Kimzey

Cellular Analytical Laboratory  
Manned Spacecraft Center  
National Aeronautics Space Administration  
Houston, Texas 77058

Knowledge that the mineral content of animals changes with age has existed for more than one hundred years. In a recent publication<sup>1</sup> we reviewed the more recent literature on the changes in electrolyte content of muscle during postnatal maturation and presented original data confirming the fact that at birth the sodium content exceeds the potassium content of the rat gastrocnemius. Within a week of postnatal development, these values have been reversed, and by one month, have reached the adult concentrations.

In our previous publication<sup>1</sup> we attempted to estimate the theoretical intracellular concentration of muscle sodium and potassium by a variety of techniques. These included the assumptions that either muscle chloride is extracellular in location or that chloride is passively distributed as a function of muscle potential. These approaches led to the conclusion that intracellular sodium decreases insignificantly with development, a conclusion which is consistent with other investigators work. The decrease in intracellular Na between birth and 30 days was on the order of a factor of 10 regardless of how the cellular spaces were computed. Conclusions concerning intracellular K were not possible.

The application of the electron probe x-ray microanalyzer to analysis of cellular electrolyte composition has had increasing attention.<sup>2-6</sup> Using this procedure thin sections of freeze dried muscle can be directly visualized and the electron beam localized within individual muscle fibers. This provides the opportunity to determine directly the intracellular content of electrolytes unencumbered by theoretical assumptions concerning intracellular and extracellular volumes of water and electrolyte distribution. In this paper we report the results of such analyses of the electrolyte composition of muscle during maturation of the rat.

An applied Research Laboratories EMX-SM electron probe microanalyzer (EPM) located at the Lunar Receiving Laboratory was employed for all analyses. Three crystal wavelength dispersive spectrometers were used for the simultaneous assay of potassium, sodium and phosphorous. An Ortec 7000 Series Si(Li) energy Dispersive Detector system was used as a fourth spectrometer calibrated for silicon.

Preparation of the muscle tissue for microanalysis consisted of careful excision of the muscle fragments, excluding fat and connective tissue. The fragments were trimmed to 1 mm on a side and quick-frozen in Freon 12, pre-cooled in CO<sub>2</sub>-Acetone. Several fragments were mounted together and sectioned at 8 microns in a conventional cryostat. The sections were picked up on the warm polished surface of a silicon disc, 1" in diameter and .008" thick, and transferred immediately to a lyophilization unit. After 1 hour, the discs were transferred immediately to a vacuum desiccator prior to analysis.

In order to evaluate the precision and the sources of variation in our study we present a comparison of the coefficients of variation in Table I below. In the younger animals the major variation occurred between muscle fibers with the variation within a single fiber being much less. The variation between animals of like age was no greater than that between fibers in the same animal. There are several reasons why this might occur. Goldspink<sup>7-10</sup> has shown that muscle fiber diameters do not have a gaussian distribution but actually have several populations of morphologic sizes; the homogeneity of fiber diameters varying with age, muscle location and exercise. Figure 1 a and b presents scanning electron micrographs of representative muscle samples used in this study. Variations in muscle fiber diameter are evident. Younger animals demonstrate a larger degree of variation in fiber diameter.

Table I. Comparison of coefficients of variation counts in rat muscle fibers (Mean  $\div$  SD  $\times$  100).

<u>Age</u>	<u>Within Fibers</u>		<u>Between Fibers</u>		<u>Between Animals</u>	
	K	Na	K	Na	K	Na
10 days	11.4	12.5	21.6	22.4	23.6	14.6
33 days	7.1	7.9	11.9	14.4	11.4	18.6
Adult	13.0	17.3	15.9	18.9	14.3	17.4
Total	10.5	12.5	16.4	18.5	16.4	16.8

A second source of variation between muscle fibers may be the differentiation of fast and slow fibers in the gastrocnemius muscle. Goldspink<sup>10</sup> has shown that succinic dehydrogenase development is independent of fiber diameter but related to stage of maturation of the individual fiber. If muscle fiber hypertrophy were less than synchronous, as evidenced by Goldspink's work,<sup>7-10</sup> then it would be reasonable to find variation in the development of individual fibers during development of aerobic metabolic machinery. In the adult animal the major variability occurred within individual fibers and was not increased by comparison between fibers or animals. This must reflect decreasing homogeneity within the fiber with increasing fiber diameter, perhaps due to increased numbers of nuclei and other subcellular structures.

The intracellular localization of sodium is clearly indicated in Table II which presents the sodium Ka x-ray intensity from directly visualized muscle fibers (counts/minute  $\pm$  standard deviation). The sodium intensity from the 10 day old rats is twice that of the adult rats. The ratio of potassium/sodium intensities increases with age and is quite comparable to the molar ration of these ions in whole tissue<sup>1</sup>.

Table II. Localization of sodium, potassium and phosphorus of rat gastrocnemius muscle as a function of age (Counts/minute  $\pm$  standard deviation).

Age in Days	(N)*	Na	K	P	K/Na	Whole Tissue
						K/Na**
10	(6)	5,044	12,199	10,728	2.56	2.70
		$\pm$ 737	$\pm$ 2,877	$\pm$ 2,720	$\pm$ 0.80	
33	(5)	2,182	10,906	8,067	5.41	4.26
		$\pm$ 405	$\pm$ 1,253	$\pm$ 577	$\pm$ 1.56	
Adult	(4)	1,844	11,299	7,603	6.42	6.02
		$\pm$ 322	$\pm$ 1,619	$\pm$ 733	$\pm$ 0.80	

\* Number of Animals

\*\* Molar ratio based upon flame photometry<sup>1</sup>

In order to arrive at a more precise estimate of muscle fiber electrolyte content we have considered the possibility that although the frozen muscle sections were of uniform thickness the variable water content, known to be present as a function of age<sup>1</sup>, might result in a variable thickness of the freeze dried samples. To approach this problem we have monitored the absorption of the silicon Ka x-ray from the silicon substrate by the specimen. In unpublished work we have demonstrated that sample thickness and density are proportional ( $p < 0.995$ ) to the reduction in silicon substrate x-ray intensity. In Table III we present data corrected for the variable reduction in substrate intensity by the specimen. The % reduction in detected Si intensity increases as a function of age supports (63% at 10 and 33 days as compared with 70% at adult): These data verify the value of such a denominator. Between 10 days

Table III. Correction of sodium, potassium and phosphorus counts for section density by reduction in counts from silicon wafer ( $\text{CPM} \div \Delta \text{CPM Si}$ ).

Age in Days	(N)*	% Reduction				
		of Si Counts	Na	K	P	K/Na
10	6	62	0.64	1.53	1.32	2.55
		$\pm 7$	$\pm 0.17$	$\pm 0.30$	$\pm 0.24$	$\pm 0.78$
33	5	63	0.25	1.26	0.94	5.49
		$\pm 4$	$\pm .05$	$\pm 0.17$	$\pm 0.05$	$\pm 1.58$
Adult	4	70	0.19	1.23	0.83	6.53
		$\pm 6$	$\pm 0.01$	$\pm 0.17$	$\pm 0.05$	$\pm 0.87$
<u>Test of significance (t)</u>						
10 vs 33	11	-	4.925	1.719	3.392	4.010
10 vs Adult	10	-	5.088	1.823	3.921	7.494
33 vs Adult	9	-	1.950	0.329	3.057	1.165

\*Number of Animals

of age and 33 days of age intracellular muscle sodium falls significantly by a factor of two, a factor similar to that observed in whole tissue analysis. A slight reduction in intracellular K occurs; however, this is not a statistical significance. A fall in intracellular phosphorous occurs with each stage of maturation studied. These data confirm our previous conclusion<sup>1</sup> based upon indirect evidence that the high muscle sodium in the gastrocnemius of young rats is within the cellular compartment. It also indicates that the reduction in fresh immature muscle K is largely due to altered hydration, not a loss of intracellular potassium content; a point uncertain in our previous theoretical considerations<sup>1</sup>.

#### REFERENCES

1. C. F. Hazlewood and B. L. Nichols, J. Hopkins M.J., 125, 119 (1969).
2. F. D. Ingram, J. J. Ingram and C. A. M. Hogben, J. Histochem & Cytochem., 20, 716 (1972).
3. G. M. Lehrer and C. Berkley, J. Histochem. & Cytochem., 20, 710 (1972).
4. J. R. Coleman and A. R. Terepka, J. Histochem. & Cytochem., 20, 414 (1972).
5. S. Hodson and J. Marshall, J. Microscopy, 93, 49 (1971).
6. K. Gehring, A. Doerge, W. Nagel and K. Thureau, PRESENTATION, The International Symposium on Modern Technology in Physiological Sciences, Munich, West Germany, July 26-30, 1971.
7. G. Goldspink, Proc. R. Irish Acad., Sect. B., 62, 135 (1962).
8. R. W. D. Rowe and G. Goldspink, J. Anat., 104, 519 (1969).
9. G. Goldspink, Comp. Biochem. Physiol., 7, 157 (1962).
10. G. Goldspink, J. Cell. and Comp. Physiol., 63, 209 (1964).





Figure 1a: Scanning Electron Micrograph of Representative Tissue Preparation From Adult Rat Skeletal Muscle.

10  $\mu$



Figure 1b: Scanning Electron Micrograph of Representative Tissue Preparation From  
10 Day Old Rat Skeletal Muscle.

ULTRAHISTOCHEMICAL STUDIES OF MUCOSUBSTANCES: ELECTRON MICROSCOPE  
OBSERVATIONS OF MICROPROBE ANALYSIS OF THE CHICK EMBRYO CORNEA

T. Ohkura, H. Iwatsuki, and T. Watanabe  
Kawasaki Medical College, Kurashiki, Japan

Abstract published in EMSA Proceedings



Specific Metal Staining of Biological Tissues for the SEM  
Using Backscatter Electron or Specimen Current Imaging

by

Jerrold L. Abraham  
Phillip B. DeNee  
Albert H. Gelderman

Appalachian Laboratory for Occupational Respiratory Diseases  
National Institute for Occupational Safety and Health  
P. O. Box 4292  
Morgantown, West Virginia 26505

We have recently developed a technique to distinguish specific cell and tissue components with the Scanning Electron Microscope (SEM)<sup>1</sup>. This technique combines the old histochemical techniques of differential impregnation of tissue by heavy elements such as ammoniacal silver with the backscatter mode of SEM imaging. The backscatter imaging has long been used in metallurgy to reveal inhomogeneity of alloys due to topographical variation in atomic number<sup>2</sup>, but has not been utilized to date by biologists. Biologists using the SEM have great difficulty in correlating the surface images with the more familiar transmitted light or transmitted electron (TEM) micrographs. Our technique allows the biologist to utilize the vast experience of histochemical metal stains to localize specific cell and tissue components and to study the tissue with the SEM using secondary electron imaging and backscatter electron imaging. These techniques allow the microscopist to use the SEM as an extension of the light microscope and TEM with the added advantages of a large depth of field, surface morphology, histochemical identification of structures and high resolution. Further, the technique does not require the special tissue processing required by a TEM study. Large sections of routinely processed, paraffin embedded, stained tissues may be utilized.

The illustrations demonstrate the potential usefulness of the technique. The four figures show SEM images of the identical area of a 6  $\mu$ m paraffin section of a coal miner's lung<sup>3</sup> mounted on a glass slide, deparaffinized, stained with a modified periodic acid-ammoniacal silver stain<sup>4</sup>, critical point dried and coated with carbon. The secondary electron image (Fig.1) shows detail of the surface of the sectioned alveolar septum and portions of dust-filled alveolar macrophages in the alveolar space. The backscatter image of the same area (Fig. 2) reveals tissue elements which have been specifically stained with silver. This has been confirmed

by x-ray mapping (unpublished observations in our laboratory). In Fig. 2 one can see the silver stained nuclei and the basement membranes of the alveolar capillary. The backscatter image also shows silver stained nuclei beneath the surface of the sections, due to the greater penetration of the more energetic backscattered electrons ( $\sim 20$  keV) compared to the secondary electrons (50 eV or less). An unstained portion of an erythrocyte (RBC) is nearly transparent to the backscattered electrons (compare Figs. 1 & 2). As an adjunct to this technique, reversal of the polarity of the backscatter image (Fig. 3) results in an image closely resembling a light microscopic or TEM image. The spatial resolution of the SEM in the backscatter mode averages from about 500 to 1,000 Å which is about an order of magnitude better than the resolution for x-ray mapping and a factor of 2 to 4 better than that for the optical microscope. Thus, the backscatter mode is preferred over either x-ray mapping or optical microscopy. In addition, once the tissue elements have been identified in the backscatter image they can be more highly resolved using the secondary electron mode (100-150 Å resolution). For magnifications of up to 10,000 times the backscatter mode allows examination of much thicker and larger sections than in the TEM.

The use of higher accelerating voltages permits visualization of structures even deeper within the sample due to the increased depth of penetration of the electrons into the tissue (Fig. 4), although the higher voltage results in a slight loss of resolution. In our experience we have found glass to be the best supporting material, since (1) it does not react with the reagents used in metal staining, (2) it gives a low backscatter yield and (3) it allows light microscopic examination of the same section. We use carbon coating alone to provide conductivity, as heavy metal coatings tend to increase the backscatter yield.

We have successfully used stains containing Fe, Ag, La, W, Os, Au, Pb and U. In order to develop adequate contrast, the tissue must be somewhat overstained. An additional factor in the improvement of contrast is the backscatter detector itself. The present detector has a relatively small solid angle (approximately 0.1 steradian) but an improved, large solid angle detector is being designed which will fit just below the pole piece. The minimal concentration of various elements necessary for detection by this method are presently being investigated.

In our investigation of coal workers' pneumoconiosis<sup>3</sup> we are studying the connective tissue response to the inhaled dust particles. Adjacent sections of a single lesion may be used for x-ray microanalysis of dust particles, and for histo-

chemical staining of connective tissue. These techniques allow a complete study of lesions at high resolution and utilize the SEM as a bridge between the light microscope and TEM.

Metal stains are widely used for demonstration of tissue components and identification of immunological and enzymatic sites<sup>5</sup>. The means to apply these specific stains to the SEM, plus the ability to visualize more subsurface morphology than in the secondary mode, should make the backscatter mode or specimen current imaging enhance the usefulness of the SEM in biology.

#### References:

1. Abraham, J.L. and P.B. DeNee. SEM Histochemistry Using Backscatter Electrons and Metal Stains. Lancet, 1973 (in press).
2. Price, C.W. and D.W. Johnson. The Use of Backscattered Electron Images in Metallographic Analysis of Carbides. SEM/1971. Proceedings of the 4th Annual SEM Symposium. IIT Research Institute. Chicago, Illinois. April, 1971. p. 145-152.
3. DeNee, P.B., J.L. Abraham and A.H. Gelderman. Methods for a SEM Study of Coal Workers' Pneumoconiosis. in Scanning Electron Microscopy/1973, op.cit. pg. 411-418.
4. Jones, D.B. Nephrotic Glomerulonephritis. Am.J.Path. 33:313 (1957). Modified by Patsy Willard, ALFORD, NIOSH, Morgantown, W.Va. 26505
5. Shnitka, T.K. and A.M. Seligman. Ultrastructural Localization of Enzymes. Ann.Rev.Biochem. 40:375-396 (1971).

#### Figure Legends:

- Fig. 1 Secondary electron image. 20 keV, 0°. Portion of erythrocyte (RBC). Alveolar macrophage (AM).
- Fig. 2 Backscattered electron image. 20 keV, 0°.
- Fig. 3 Backscattered electron image with polarity reversed. 20keV, 0°. Nucleus (N). Basement membrane of alveolar capillary (BM).
- Fig. 4 Backscattered electron image with polarity reversed. 30keV, 0°.

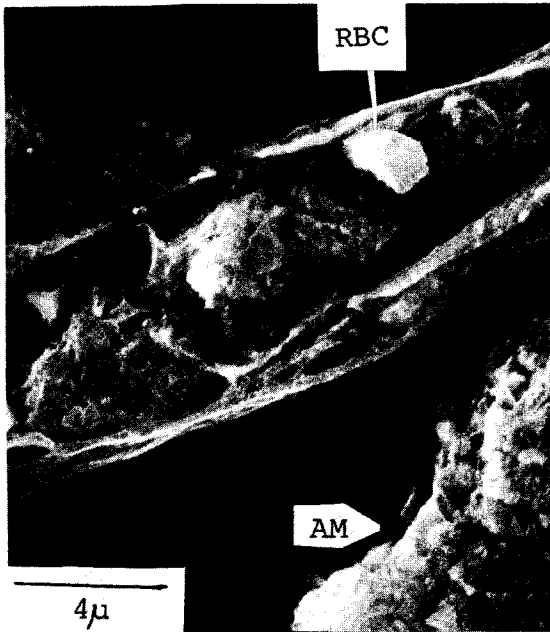


Fig. 1



Fig. 2

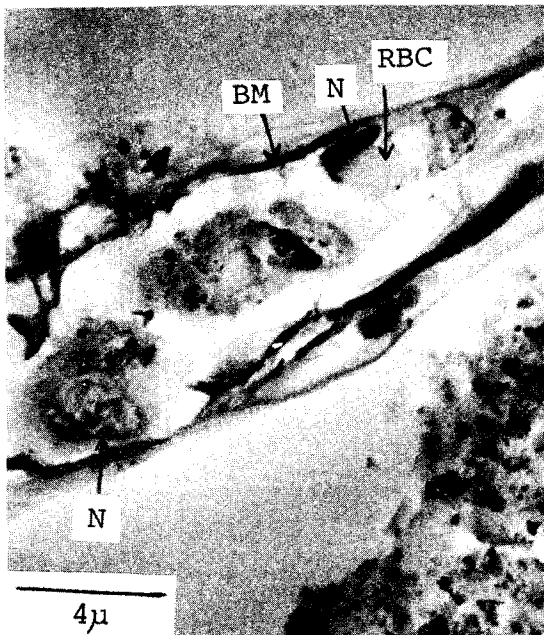


Fig. 3

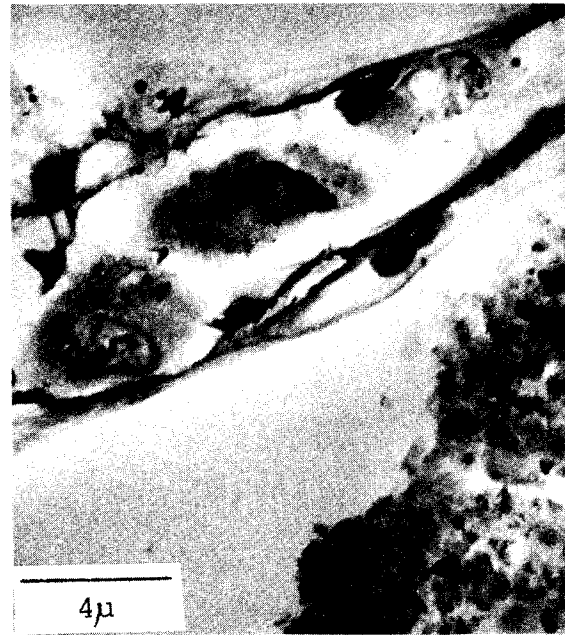


Fig. 4



APPLICATION OF ELECTRON AND ION MICROPROBES  
TECHNIQUES TO THE STUDY OF NUCLEAR FUELS

by

Carl E. Johnson

*Chemical Engineering Division*  
Argonne National Laboratory  
9700 South Cass Avenue  
Argonne, Illinois 60439

The nuclear fuel system presents an interesting system for scientific study not only for its practical interest but also because of the challenges it presents in chemical systems. There may be some who would suggest analogy with geologic systems however the significantly greater thermal gradients found in nuclear systems contribute to greater chemical complexity. When a virgin nuclear fuel is brought to power in a nuclear reactor the large ( $\sim 5000^{\circ}\text{C}/\text{cm}$ ) thermal gradient which is set up gives rise to transport processes which result in structural differentiation and transport. These gradients cause a redistribution of oxygen, uranium, and plutonium. Parallel with this is the continual change in fuel chemical content due to generation of fission products. These fission products encompass gases, metals, and non-metals and their distribution throughout the fuel is dependent upon temperature and thermodynamic activity in the region of interest.

The chemical state of the mixture of mixed oxide fuel and fission product elements which form during irradiation have a significant effect on the volume and hence the fuel swelling, the rate of reaction of fuel and cladding, and, should a defect in the cladding develop, the rate of reaction between the fuel and the liquid sodium coolant. By the post-irradiation examination of the mixed oxide fuel system one seeks to discover those aspects of the chemistry of the fuel system which significantly affect the life expectancy of the fuel pins and to use this chemical information to help establish specifications for fast breeder reactor mixed oxide fuels.

A variety of techniques have been used to elucidate chemical behavior in irradiated fuels. One technique that is ideally suited to this type of investigation is that of electron probe microanalysis which accomplishes microsampling and analysis directly. With this technique, fuel constituents and the distribution of fission products in the fuel can be determined and fuel-cladding interactions identified all on a micro-

scale. The technique has been used by various investigators to identify fission product inclusions in irradiated fuels. Studies have been carried out on single extracted particles, small sections, and complete radial cross sections in both shielded and unshielded probes.

The development of the ion microprobe mass analyzer has been invaluable in extending and complementing the established microprobe analytical technique in the analysis of the very complex irradiated fuel system. The capability for executing isotopic analysis at micron spatial resolution is invaluable in tracing the transport of species of interest throughout the fuel system.

Probably the single most important parameter contributing to the mass transport in the fuel is the local oxygen potential. The redistribution of oxygen which occurs when a fuel pin is irradiated depends on both thermodynamic and kinetic factors. For example, the increase in the oxygen potential with burnup will increase the thermodynamic driving force for oxidation of fission product molybdenum. The microprobe analysis for molybdenum in both the alloy and the oxide phases has provided a redox indicator system as a local in situ means of determining the oxygen potential as a function of radial position. Although this method is restricted to the hotter regions of the fuel it has been invaluable in providing the first measure of oxygen potential radial gradients in the fuel.

In conclusion it may be said that for the post-irradiation analysis of nuclear fuels no other instrumental technique has had as great an impact on the studies of nuclear fuels as microprobe analysis. Its ability to focus on microareas for complete elemental and isotopic analysis is unsurpassed.

#### References

1. B. T. Bradbury, J. T. Demant, P. M. Martin, and D. M. Poole, J. Nucl. Mater. 17, 227 (1965).
2. B. M. Jeffery, J. Nucl. Mater. 22, 33 (1967).
3. J. I. Bramman, R. M. Sharpe, D. Thom, and G. Yates, J. Nucl. Mater. 25, 201 (1968).
4. N. R. Stalica and C. A. Seils, Pro. Amer. Ceram. Soc., p. 211 (1969).
5. D. R. O'Boyle, F. L. Brown, and J. E. Sanecki, J. Nucl. Mater. 29, 27 (1969).
6. R. O. Meyer, E. M. Butler, and D. R. O'Boyle, USAEC-Report, ANL-7929 (1972).
7. C. E. Johnson, I. Johnson, P. E. Blackburn, and C. E. Crouthamel, Reactor Technology - Critical Reviews 15, 303 (1973).
8. I. Johnson, C. E. Johnson, C. E. Crouthamel, and C. A. Seils, Accepted for publication in J. Nucl. Mater. (1973).

MICROPROBE EXAMINATIONS OF IRRADIATED  
NUCLEAR FUELS\*

by

W. F. Zelezny, W. B. Hutchinson, R. E. Smith  
and E. A. Hakkila

University of California, Los Alamos Scientific Laboratory  
Los Alamos, New Mexico 87544

ABSTRACT

The shielded electron microprobe at the Los Alamos Scientific Laboratory (LASL) has been used extensively in the examination of irradiated liquid metal fast breeder reactor (LMFBR) fuel pins. The fuels are right cylindrical pellets having the approximate compositions  $(U_{.8}Pu_{.2})O_2$  or  $(U_{.8}Pu_{.2})C$  which are clad with stainless steel or Incoloy-800. The fuel and cladding are thermally bonded with helium for oxide fuels; or either helium or liquid sodium for carbide fuels. Fuel pins having undergone burnups ranging from  $< 0.1$  to 10% have been examined.

The high temperatures, together with the presence of fission products, over extended periods of time give rise to the possibilities of migration of the fuel constituents, migration (and segregation) of fission products within the fuel, and reaction of fuel constituents, fission products, or impurities with the cladding. Examples of each of these effects have been found by microprobe examinations at LASL.

One of the more interesting findings at LASL is the detection of segregated deposits of americium on the inner surface of the

cladding. Other interesting observations include the nitriding of stainless steel cladding by an impurity in the oxide fuel, uranium-rich deposits resulting from vapor-phase transport of oxide fuel, and carburization of stainless steel claddings by carbide fuels.

In the oxide fuels, there is a well-known tendency for the plutonium concentration to increase, relative to the uranium, in the fuel near the center where the fuel temperature has been the highest. This is thought to be due to preferential transport in the vapor phase of  $\text{UO}_2$  along the central void to a cooler portion of the fuel pin. Supporting evidence is the finding at LASL of deposits in the cooler region of the void which contained higher uranium and lower plutonium concentrations than the original fuel.

Deposits containing fuel constituents and fission products have been found along the inside diameter of the cladding, in many cases with no evidence of reaction with the cladding material. Uranium and plutonium usually are found together but sometimes there is a tendency toward preferential deposition of plutonium with little or no uranium. Deposits containing americium or one or more of the fission products cesium, iodine, barium, strontium, neodymium and cerium also have been found.

In other cases, reaction of the cladding with fuel or fission products has been observed. Carburization of stainless steel cladding by carbide fuels has been detected in a number of sodium-bonded fuel pins containing a sesquicarbide fuel. Similarly, nitriding of stainless steel cladding by an impurity in an oxide fuel was found. Both of these reactions could lead to reduced ductility of the cladding, with the possibility of crack initiation.

Studies of fuel pins that failed in service showed effects which could be associated with excessively high temperatures. These

include rupture of the cladding, pronounced chromium enrichment in the stainless steel grain boundaries in the vicinity of the rupture, grain boundary penetration in the stainless steel by plutonium and uranium, and irregular distributions of the stainless steel components in the fuel near the failure.

In summary, the shielded electron microprobe has proved to be a valuable instrument for studying the chemistry of irradiated nuclear fuel elements as evidenced by several described examples.

---

\* Work performed under the auspices of the Fuels and Materials Branch of the Division of Reactor Development and Technology of the U. S. Atomic Energy Commission.

INTERGRANULAR ATTACK IN LMFBR CLADDING

## A Comparison of Laboratory and In-Reactor Results\*

by

T.E. Lannin

E.A. Aitken

S.K. Evans

General Electric Company  
 Vallecitos Nuclear Center  
 Pleasanton, California 94566

Two types of cladding attack have been observed in irradiated mixed oxide fuel pins clad in 316 S.S.<sup>(1)</sup> A general type of attack which is almost erosive in character and an intergranular type of attack (Figure 1). The intergranular type of attack observed in irradiated fuel pins has been reproduced in this laboratory and a comparison of these results is the subject of this presentation.

Several attempts have been made to describe the role of certain fission products in LMFBR cladding attack<sup>(2)</sup>. A mechanism has been proposed<sup>(3)</sup> to describe the intergranular attack observed. To date, the mechanism remains as a complex problem, although recent laboratory results have simplified and isolated the major contributing elements and conditions necessary to cause or not cause intergranular attack of LMFBR cladding. Results obtained at G.E.'s Vallecitos Nuclear Center indicate Cs and Te in an environment with an oxygen potential above a certain threshold can cause intergranular attack of the S.S. cladding. Lowering this oxygen potential below the threshold results in no cladding attack. Previous results<sup>(4,5)</sup> indicate the cladding can act as an oxygen buffer at the fuel-cladding interface. The process of fissioning of (U,Pu)<sub>2</sub>O fuel leaves an excess of oxygen<sup>(6)</sup>. This excess oxygen leads to an increase in O/M of the fuel as the burnup process proceeds and an increase in oxygen activity of the fuel and at the fuel cladding interface.

---

\* Work sponsored by the AEC Contract AT(0-4-3)-189 P.A. #10 and P.S. #53.

Of the fission products created<sup>(7)</sup> some of these are relatively inert and precipitate out as metal ingots (Ru, Rh, Pd) in the oxide matrix. Others form oxides which are soluble in the oxide matrix such as Ba, Zr, Sr, Nd, Pr, etc. Of special interest are the volatile fission products such as Cs, Te, I, Xe, and those with low melting points such as Sn and Sb. Laboratory experiments focused attention on Cs and Te. Thermal gradient tests<sup>(8)</sup> indicated Cs and I combine and condense as CsI in the 200-400°C temperature range, while Cs and Te, presumably as  $\text{Cs}_2\text{Te}$ , remained in the 1000-1100°C temperature range. In all cases, the isotopically labeled elements or compounds were initially in the hot end of the capsule ( $\sim 1100^\circ\text{C}$ ). Radiolytic decomposition effects have not been assessed nor has the chemistry of the total radioactive decay scheme. For example, a typical decay process for Sn-133 is:  $\text{SN-133} \rightarrow \text{Sb-133} \rightarrow \text{Te-144} \rightarrow \text{I-133} \rightarrow \text{Xe-133} \rightarrow \text{Cs-133}$ .

The chemistry involved in analyzing a multiplicity of reactions with the Fe-Cr-Ni (S.S.) cladding becomes quite complex. In addition, considerable evidence exists for Cs-fuel compounds<sup>(8)</sup>. Sodium analogs of these compounds have been characterized<sup>(9)</sup>.

The laboratory results have indicated Cs and Te to be responsible for the intergranular attack of LMFBR cladding when the oxygen potential ( $\Delta\bar{G}_{\text{O}_2}$ , 800°C) is greater than about -120 kcal/mole (Figure 2). The oxidation threshold for Cr in S.S. is about -130 to -125 kcal/mole<sup>(8)</sup> (800°C). Stoichiometric  $(\text{U,Pu})\text{O}_{2.00}$  has an oxygen potential of about -95 kcal/mole. We have found where hypostoichiometric fuel ( $\text{O/M} = 1.97$ ,  $\Delta\bar{G}_{\text{O}_2} \simeq -150$  kcal/mole) is used no oxidation or intergranular attack of the cladding has occurred. A comparison of laboratory and irradiated fuel pin results of intergranular attack are shown in Figure 3.

## References

1. McCarthy, W. H., Perry, K. J., Bennet, W. J., and Hull, G. R., ANS Topical Meeting, Reactor Materials Performance, Hanford, Washington, April 23-26, 1972.
2. See for example: A. Crouthamel, C. E. and Johnson, C. E., "Reactor Development Program Progress Reports:
  - A. ANL-RDP-11, pgs. 6.14-6.17, November, 1972.
  - B. ANL-RDP-6, pgs. 5.21-5.29, June, 1972.
  - C. ANL 7825, pgs. 5.36, April-May, 1971.
3. Johnson, C. E. and Crouthamel, C. E., J. Nuc. Mat. 34 (1970) pgs. 101-104.
4. Lannin, T. E., Wolf, R. C., Rosenbaum, H. S., Melde, G. F., Proceedings Sixth National Conference on Electron Probe Analyses, pgs. 24A/24D.
5. Johnson, C. E., Johnson, I., Crouthamel, C. E., "Fuel Cladding Chemical Interactions in  $\text{UO}_2$ -20 wt.%  $\text{PuO}_2$  Fast Reactor Fuel Clad with Stainless Steel", Proc. Conf. Fast Reactor Fuel Element Technology, Ed. Ruth Faemakes, Am. Nuc. Soc., Hinsdale, Ill., 1971, pgs. 393-410.
6. Anselin, F., "The Role of Fission Products in the Swelling of Irradiated  $\text{UO}_2$  and  $(\text{U,Pu})\text{O}_2$  Fuel", Jan., 1969 (GEAP 5583).
7. Meek, M. E. and Rider, B. F., "Summary of Fission Product Yields for U-235, U-238, Pu-239, Pu-241 at Thermal, Fission Spectrum, and 14 MeV Neutron Energies", APED 5398A, October, 1968.
8. Aitken, E. A., Evans, S. K., Rubin, F. B., "Out-of-Pile Investigations of Fission Product-Cladding Reactions in Fast Reactor Fuel Pins", NEDO 12321, August, 1972.
9. Blackburn, P. E., Martin, A. E. Battles, J. E., O'Hare, P. A. G., and Hubbard, Proc. Conf. Fast Reactor Fuel Element Technology, Ed. Ruth Farmakes, Am. Nuc. Soc., Hinsdale, Ill., 1971, pgs. 479-493.



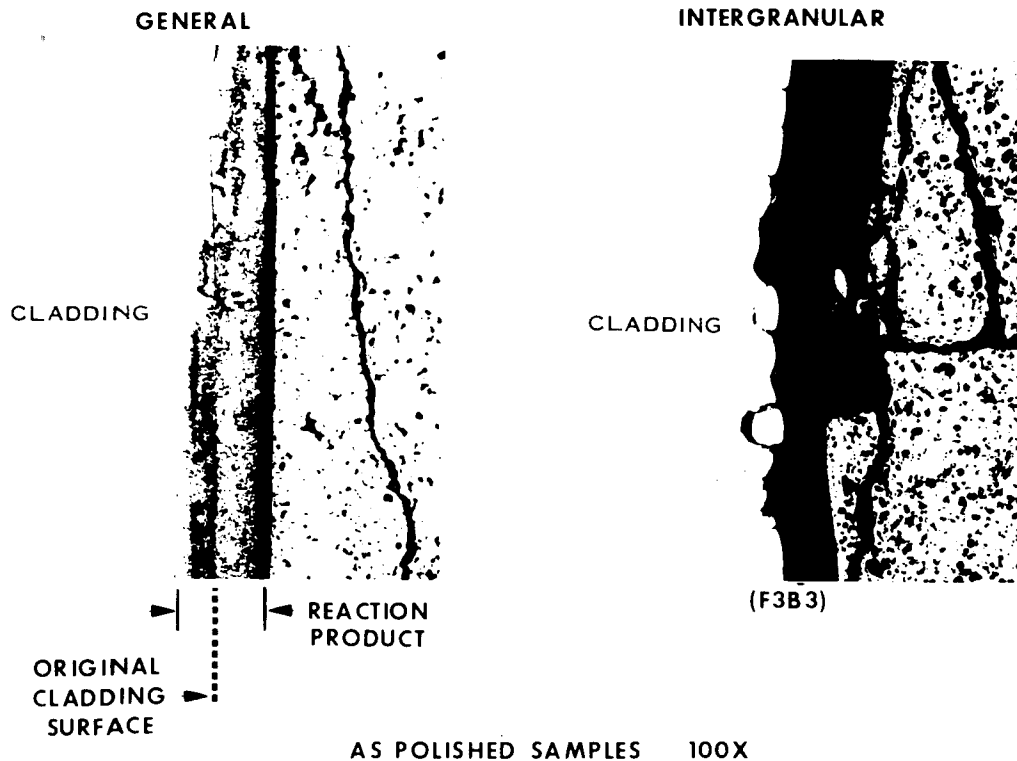


FIGURE 1. EXAMPLES OF GENERAL AND INTERGRANULAR ATTACK IN IRRADIATED MIXED OXIDE FUEL PINS

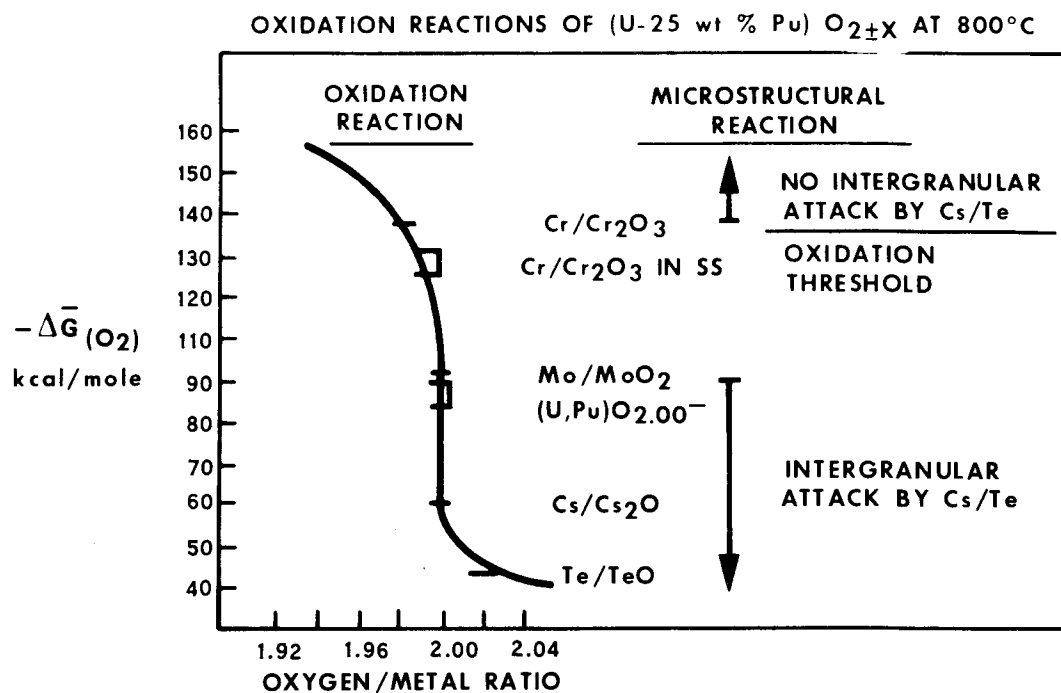


FIGURE 2. OXYGEN POTENTIAL VERSUS O:M OF MIXED OXIDE FUEL AT 800°C RELATIVE TO OXIDATION COUPLES FOR VARIOUS ELEMENTS

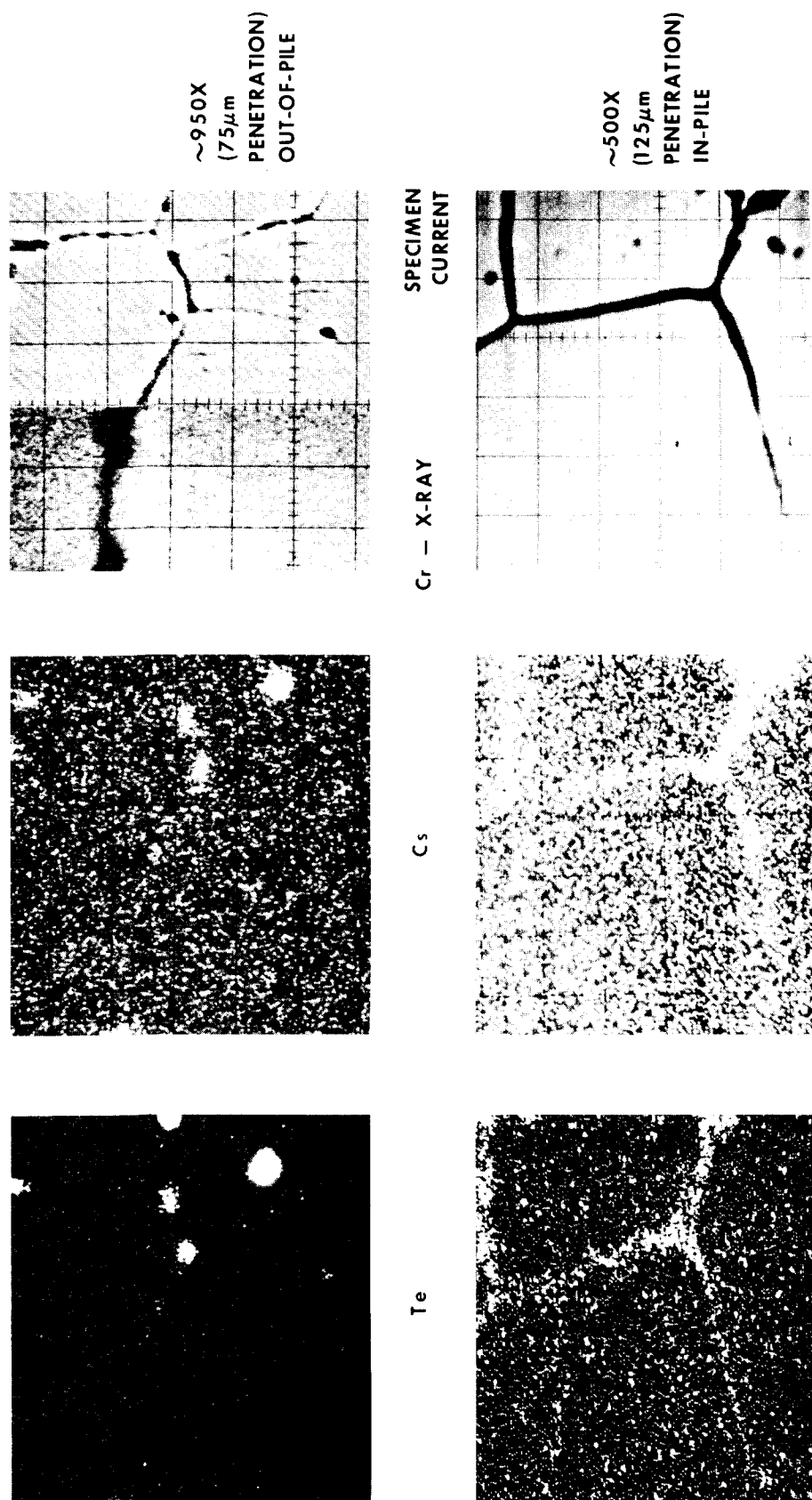


FIGURE 3. MICROPROBE SCANS OF INTERGRANULARY ATTACKED REGION OF OUT-OF-PILE THERMAL GRADIENT CAPSULE (100 HRS) CONTAINING CESIUM AND TELLURIUM AND OF CLADDING FROM AN IRRADIATED FUEL PIN

ELECTRON MICROPROBE DETERMINATION OF U, Zr,  
AND C IN MIXED CARBIDE FUEL ELEMENTS\*

E. A. Hakkila

University of California, Los Alamos Scientific Laboratory  
Los Alamos, New Mexico 87544

Uranium carbide and uranium zirconium carbide have been considered as possible fuels for various nuclear power applications. Studies of reactions between UC and ZrC, and the reactions of graphite or hydrogen with these materials, are of importance in perfecting a system stable at the proposed operating temperatures. To assist in these studies, the electron microprobe was applied to the quantitative determination of U, Zr, and C in these systems.

At the wavelength of the  $K\alpha$  x-ray for carbon (44 Å), it was anticipated that excitation voltage will have a serious effect on x-ray intensity due to the variation in depth of penetration for the incident electrons. For this reason, the intensity of the carbon  $K\alpha$  x-ray was measured from zirconium carbide and graphite at several excitation voltages, and the factor  $I/I_0$  was plotted as a function of voltage (Figure 1). The sensitivity for measurement of carbon in zirconium carbide increased as voltage decreased. Below voltages of approximately 10 kV, the effect of small changes in voltage on  $I/I_0$  becomes large, and small errors in voltage setting or fluctuations in power supply output seriously affect x-ray intensity. A voltage of 10 kV was selected as a compromise between optimizing sensitivity and precision.

Other factors to be considered are the shift in wavelength of the carbon  $K\alpha$  peak from graphite to a carbide, and the overlap of the N VI-O IV line of uranium with the  $K\alpha$  line for carbon (Figure 2).

These factors were considered in the successful development of an electron microprobe procedure for determining U, Zr, and C in mixed (U,Zr)C and ZrC. The precision of a single measurement expressed as weight fraction was estimated to be 0.007, 0.01, and 0.003, respectively, for measuring U, Zr, and C in  $(U_{0.1}Zr_{0.9})C$ .

---

\*Work performed under the auspices of the U. S. Atomic Energy Commission.

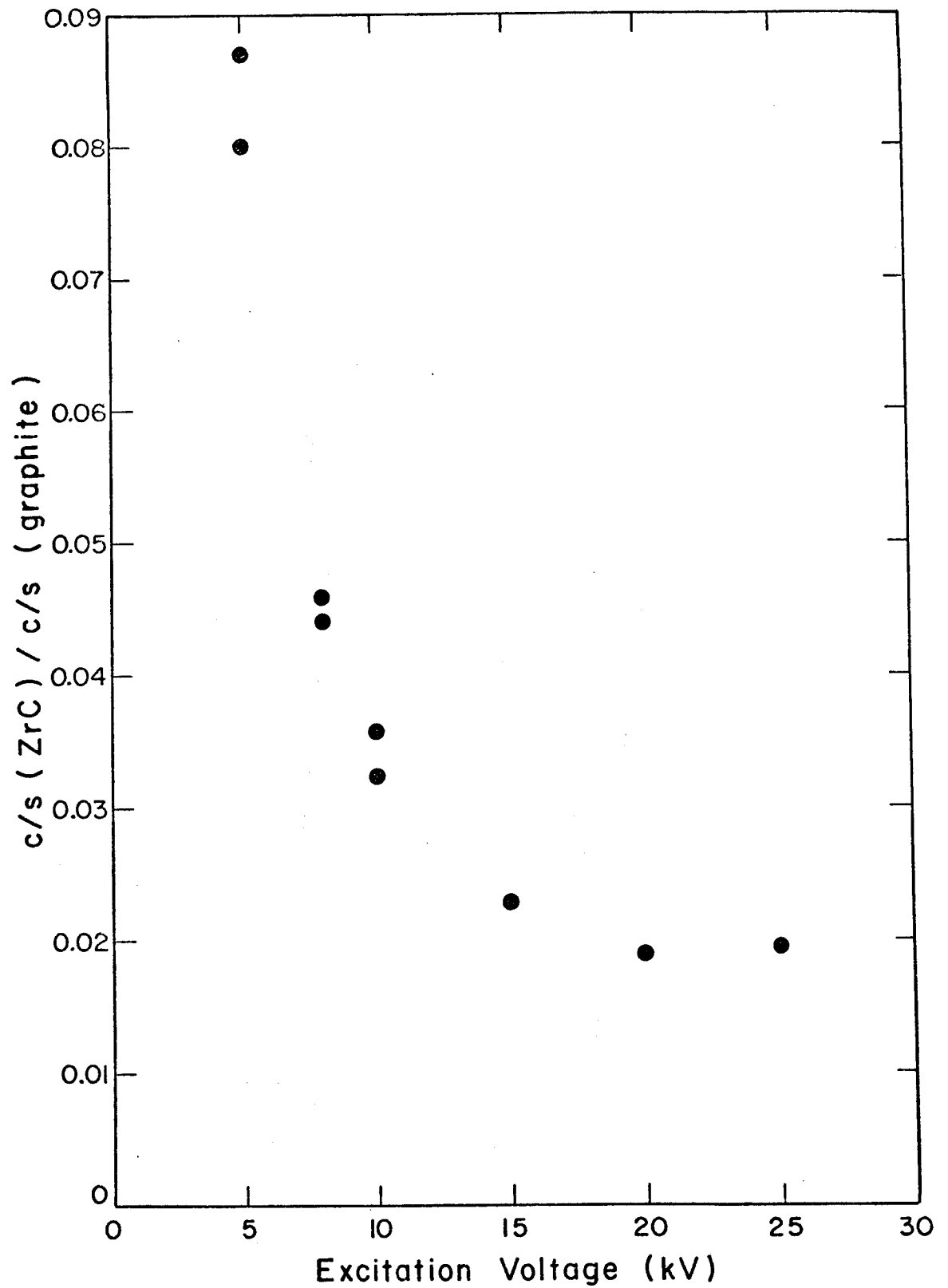


Fig. 1. Carbon x-ray intensity from ZrC, relative to intensity from graphite, as a function of excitation voltage.

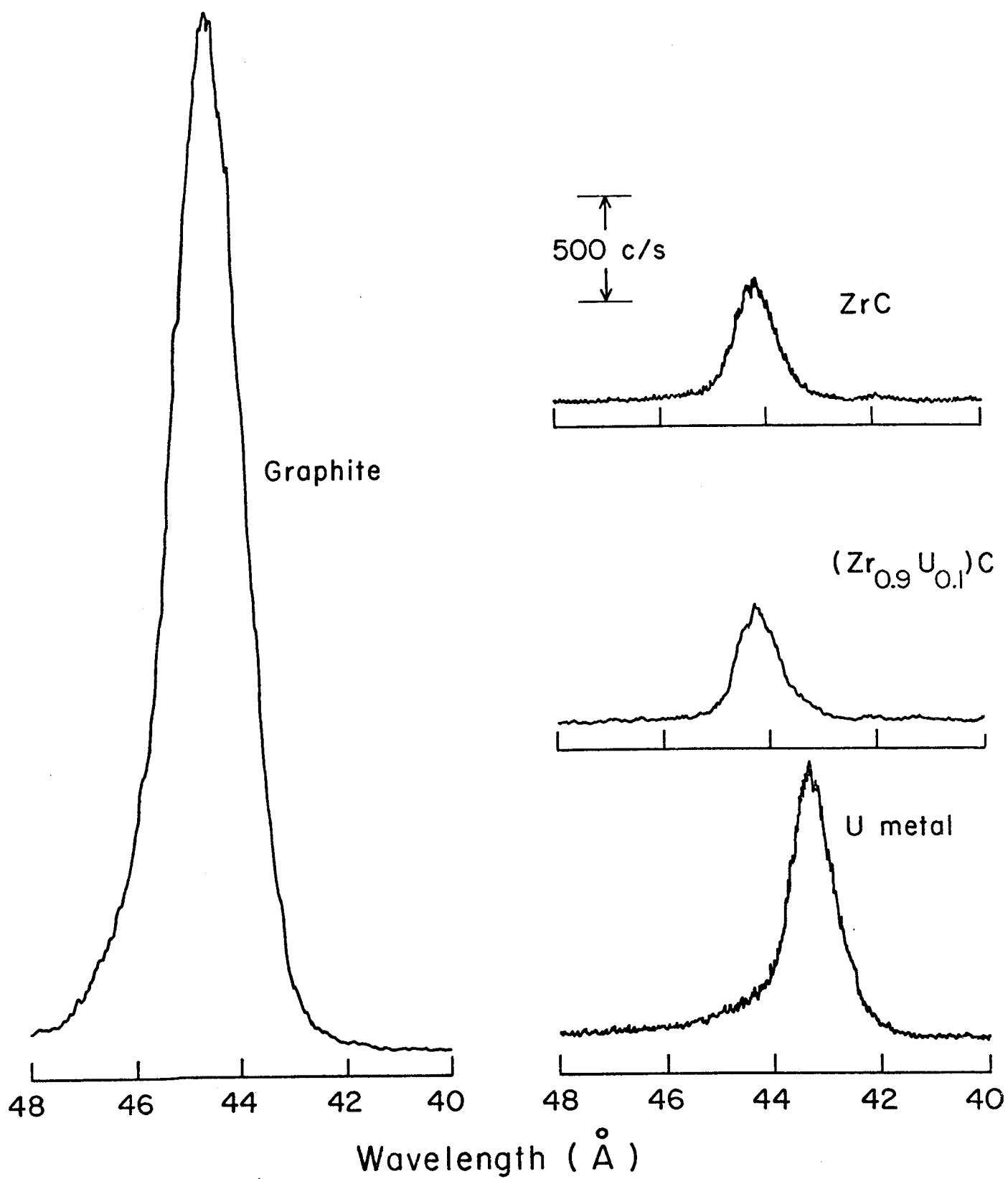


Fig. 2. X-Ray Intensities from graphite, ZrC,  $(\text{Zr}_{0.9}\text{U}_{0.1})\text{C}$  and U between 40 and 48  $\text{\AA}$ .

# DETERMINING THICKNESS OF $\text{SiO}_2$ AND $\text{Si}_3\text{N}_4$ ULTRA-THIN FILM COMPOSITES OF FET WAFERS AND DEVICES

Guilio Di Giacomo

IBM System Products Division, East Fishkill Product Assurance, Hopewell Junction, N.Y. 12533

A microprobe technique for determining the  $\text{SiO}_2$  and  $\text{Si}_3\text{N}_4$  thickness in P-SAG wafers and devices is described. The technique involves the measurement of oxygen and silicon X-ray intensities at 2.5kV for determining nitride ( $\text{Si}_3\text{N}_4$ ) thickness. However, the  $\text{SiO}_2$  thickness is obtained at the accelerating voltage of 10kV, because at this potential, its thickness is determined independently of the nitride overlay. Since the nitrogen intensity is excluded from the measurement (because of its low detectability), the nitride thickness is determined indirectly. Under these voltage conditions and for a 100-seconds X-ray count, an accuracy of  $10\text{\AA}$  was achieved. An empirical relationship expressing  $\text{Si}_3\text{N}_4$  thickness in terms of silicon and oxygen X-ray intensities (2.5kV) and  $\text{SiO}_2$  thickness (determined at 10kV) is derived.

Electron microprobe analysis of elements such as oxygen and lighter is restricted to a thin surface layer which may vary from a few hundred to a few thousand Angstroms. The depth limitation is due to the high mass absorption coefficients for these characteristic radiations.

For thin films smaller than these depth limits, the X-ray intensity varies linearly with the thickness of the film up to a point where the absorption and ionization intensity start to become a strong function of depth. For instance, the thickness of  $\text{SiO}_2$  ultra-thin films plots linearly with the  $\text{OK}\alpha$  X-ray intensity up to  $2500\text{\AA}$ . However, the measurement of nitrogen in silicon nitride films is restricted to a few hundred Angstroms due to its larger wavelength and higher absorption than oxygen. The nitrogen signal from such a layer is rather small superimposed on a relatively high background as  $\text{NK}\alpha$  is measured at the low extreme of the spectrometer using a lead stearate (LSD) crystal. Consequently, silicon nitride thickness of few hundred Angstroms cannot be determined with any degree of accuracy that is useful for this application.

Since the detectability and accuracy of nitrogen measurement proved to be grossly inadequate, a novel approach was tried, an approach which excludes nitrogen from the analysis. Briefly, the technique consists of measuring the oxygen intensity from the  $\text{SiO}_2$  layer beneath the nitride, and by total silicon intensity contributed by all layers at 2.5kV, see Fig. 1. The  $\text{SiO}_2$  layer is measured independently at 10kV because the nitride overlay does not affect this measurement at the stated voltage. The knowledge of the  $\text{SiO}_2$  thickness plus the oxygen and silicon intensities obtain at 2.5kV is sufficient to determine the thickness of the silicon nitride layer.

Composite strata of  $\text{SiO}_2$  and  $\text{Si}_3\text{N}_4$  are part of the structure of field effect transistors (FET). The requirement for monitoring the thickness of such composites prompted this work. The objective was to develop an effective microprobe technique for determining the thickness of oxide and nitride ultra-thin film composites with an accuracy of approximately  $10\text{\AA}$ . Using standards of various  $\text{SiO}_2$  and  $\text{Si}_3\text{N}_4$  thicknesses measured independently by ellipsometry, the oxygen and silicon X-ray data was obtained at accelerating voltages ranging from 2.5 to 10kV. On the basis of such data, an analytical expression was derived. This relationship expresses the  $\text{Si}_3\text{N}_4$  thickness in terms of the X-ray intensities of both elements and the oxide thickness of the sample and the standard. The empirical expression is:

$$t_N = \frac{1}{2} \left[ (\alpha - t) - \left\{ (t - \beta)^2 + \gamma \left( \frac{\text{Si}}{I_{sd}} \right) \left( \frac{\text{O}}{I_{sd}} \right) \left( \frac{t_{sd}}{t} \right) \right\}^{\frac{1}{2}} \right] \quad (1)$$

where  $t_N$  =  $\text{Si}_3\text{N}_4$  thickness,  $\text{\AA}$   
 $t$  =  $\text{SiO}_2$  thickness  
 $t_{sd}$  =  $\text{SiO}_2$  thickness of standard ( $300\text{\AA}$ )  
 $\left( \frac{\text{Si}}{I_{sd}} \right)$  = Si  $K\alpha$  intensity ratio of sample to standard ( $300\text{\AA}$   $\text{SiO}_2$  +  $200\text{\AA}$   $\text{Si}_3\text{N}_4$ )  
 $\left( \frac{\text{O}}{I_{sd}} \right)$  = O  $K\alpha$  intensity ratio of sample to standard  
 $\alpha = 2435\text{\AA}$ ,  $\beta = 1240\text{\AA}$ ,  $\gamma = 2.132 \times 10^6 \text{\AA}^2$

Figures 2 through 6 present the data on which the expression was based. The  $\text{SiO}_2$  thickness is determined at 10kV accelerating voltage using the calibration curve in Fig. 2. After this is determined, the  $\text{SiO}_2$  thickness value is substituted in the expression together with the intensity values of oxygen and silicon from the sample and the standard. Thus, the  $\text{Si}_3\text{N}_4$  thickness is calculated. Figure 3 shows the dependence of the silicon intensity on the sum of  $\text{SiO}_2$  and  $\text{Si}_3\text{N}_4$  thicknesses with the accelerating voltage as parameter. Figure 4 illustrates how the silicon ionization function varies through the layers and how the silicon substrate contributes predominantly to such dependence. However, Fig. 5 shows the oxygen X-ray intensity versus  $\text{Si}_3\text{N}_4$  thickness with  $\text{SiO}_2$  thickness as parameter. Again, the intensity dependence is illustrated in Fig. 6 where the  $\text{SiO}_2$  layer is seen intersected by the ionization function curve at its greatest slope so that a change in the nitride thickness causes a maximum change in the oxygen intensity. Optimum voltage for oxygen analysis is 2.5kV. Figure 7 illustrates how the oxygen intensity dependence on depth becomes stronger toward low voltages. However, at lower voltages, the X-ray signal to background degenerates because of the decrease in ionization cross-section. The Si intensity is also measured at 2.5kV, however, it is not restricted to this value and can be measured at any voltage between 2.5 to 3.5kV.

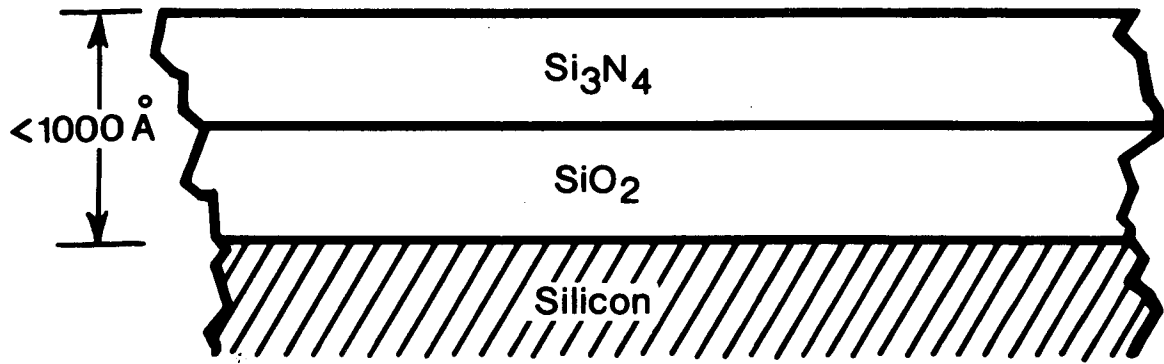


Fig. 1. Layer structure of gate.

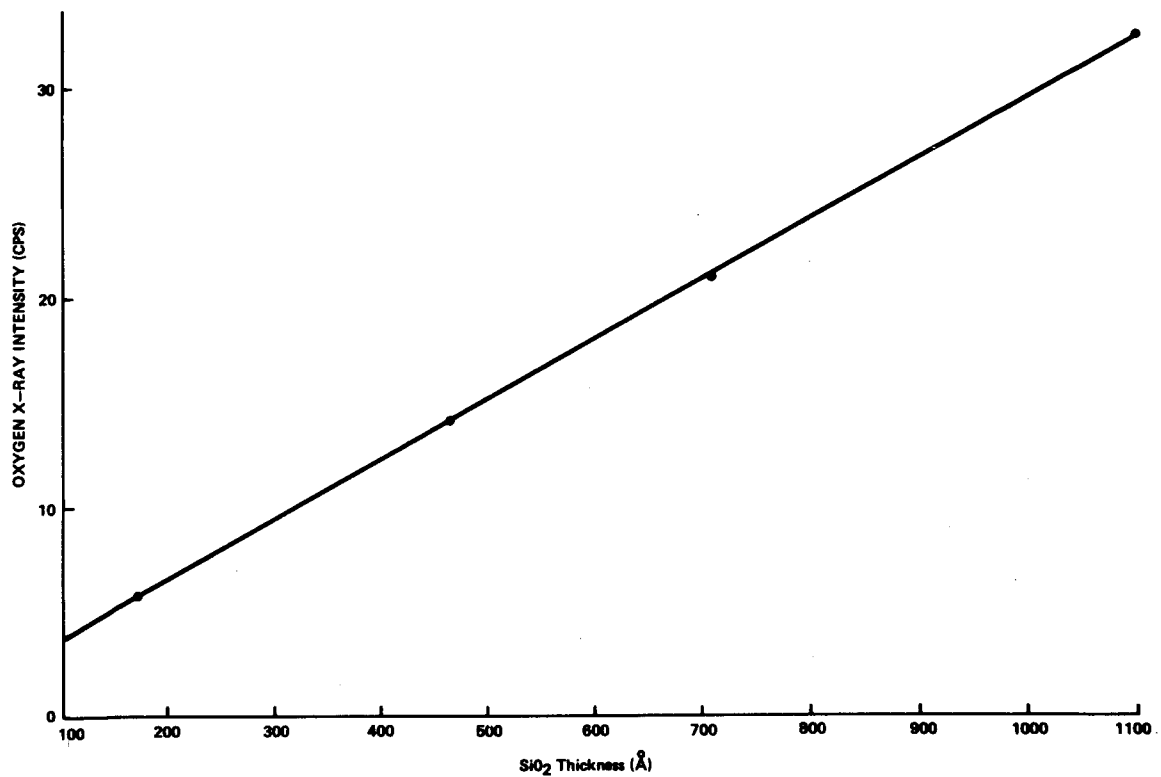


Fig. 2.  $\text{SiO}_2$  thickness calibration at various accelerating voltages with ellipsometric standards having no  $\text{Si}_3\text{N}_4$ .



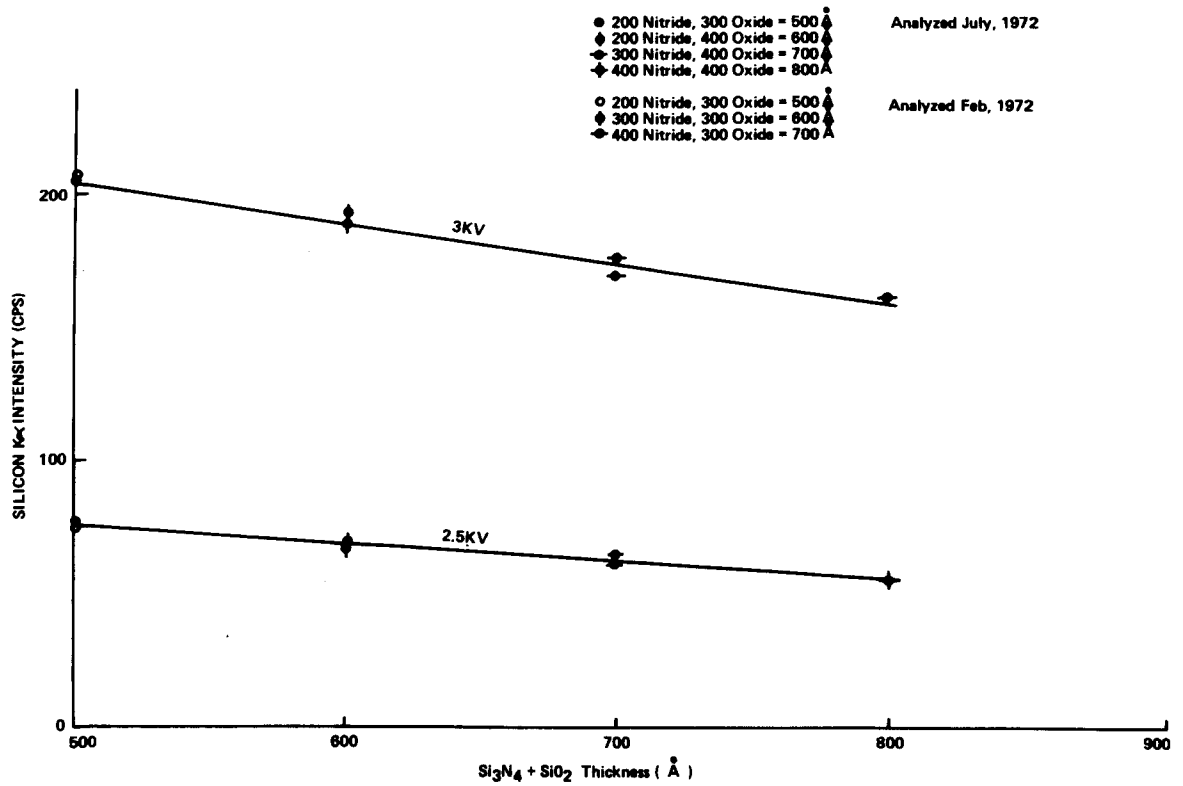
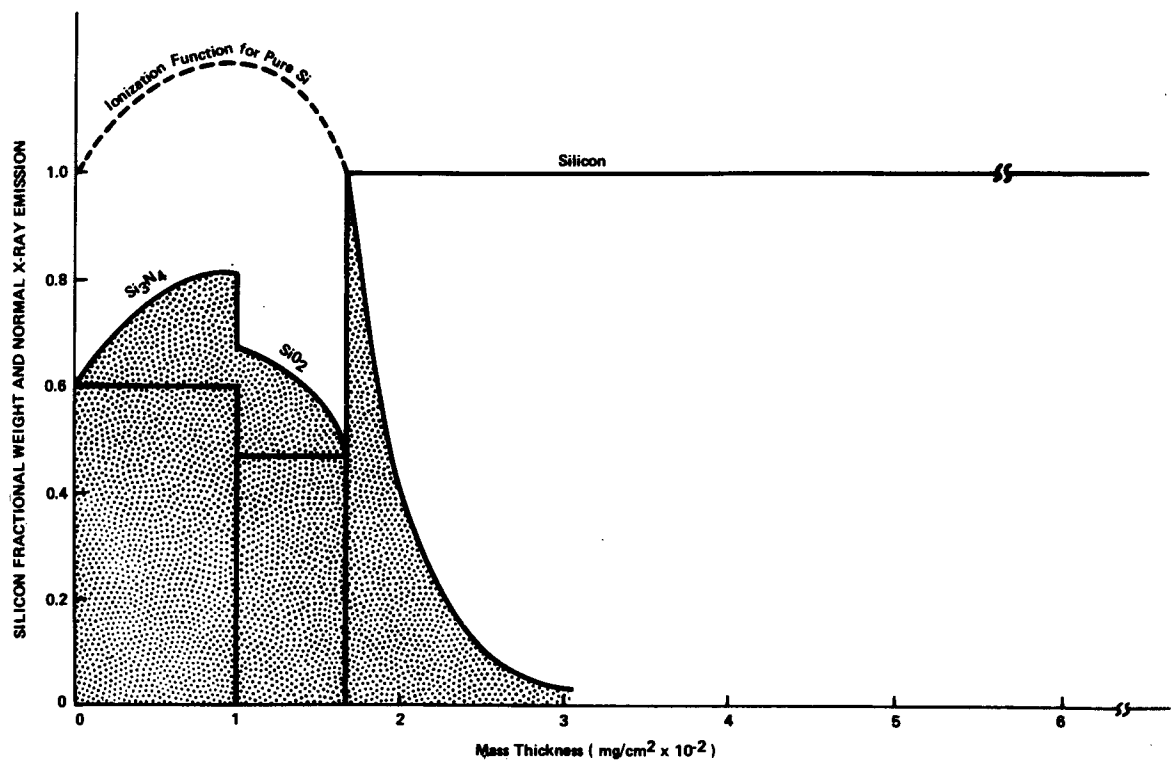


Fig. 3. Silicon X-ray intensity vs  $\text{Si}_3\text{N}_4 + \text{SiO}_2$  composite thickness at two voltages.



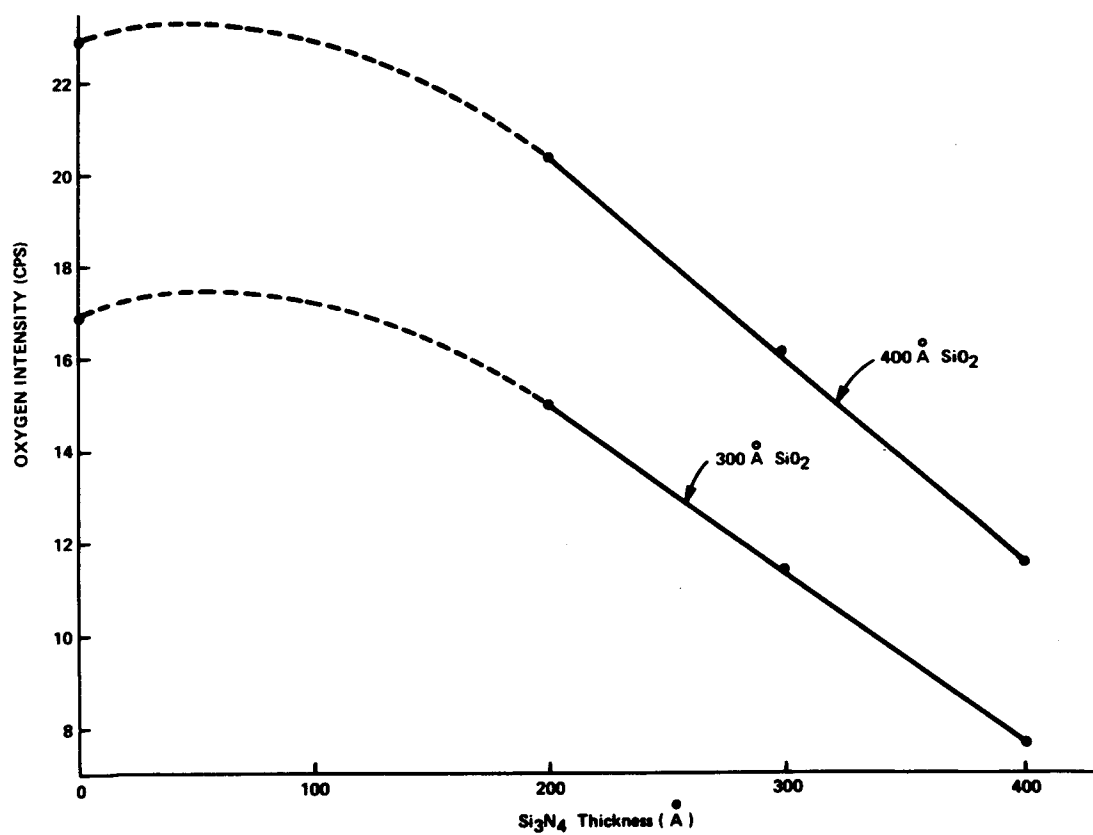


Fig. 5. Oxygen X-ray intensity vs  $\text{Si}_3\text{N}_4$  thickness for two  $\text{SiO}_2$  layers.

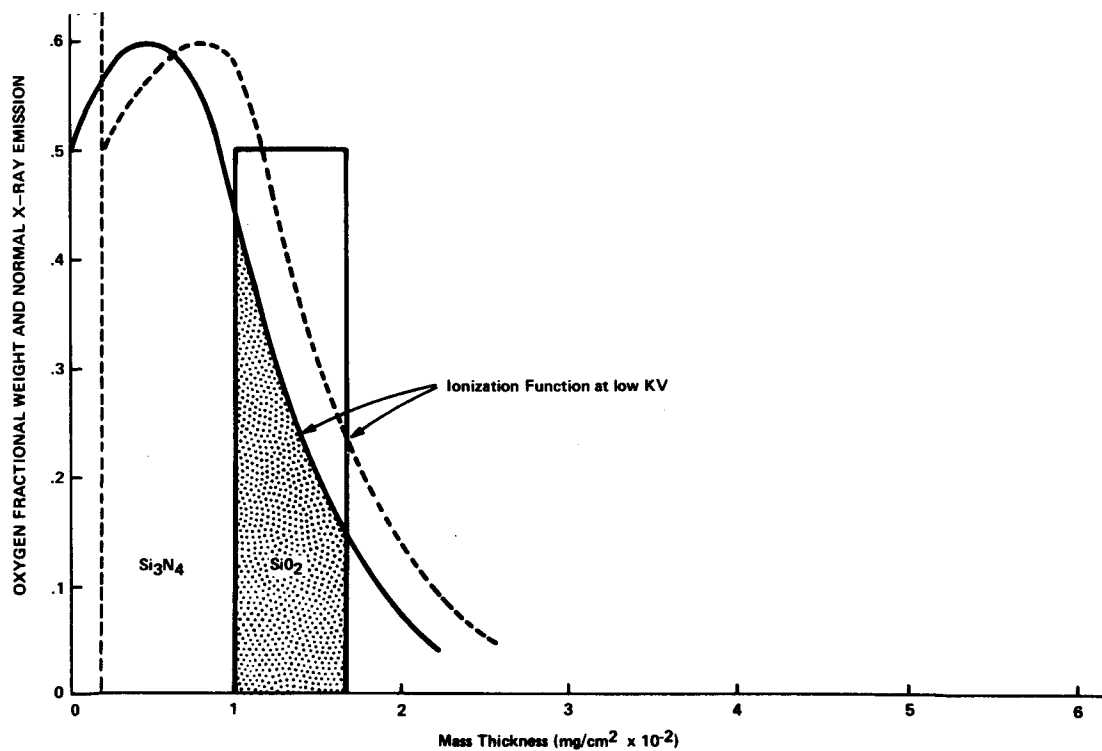


Fig. 6. Oxygen intensity distribution and shift in the ionization due to  $\text{Si}_3\text{N}_4$  layer removal.

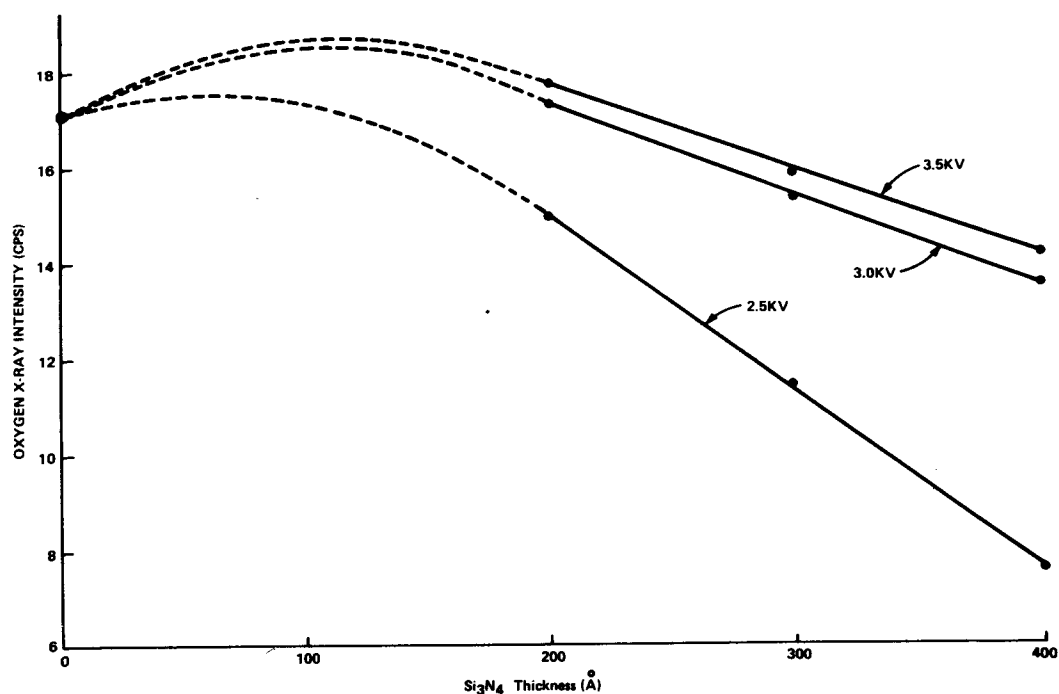


Fig. 7. Oxygen intensity from a 300Å SiO<sub>2</sub> layer vs Si<sub>3</sub>N<sub>4</sub> overlay thickness.

Table I lists the given SiO<sub>2</sub> and Si<sub>3</sub>N<sub>4</sub> values and those predicted by the relationship based on X-ray measurements.

TABLE 1. SiO<sub>2</sub> thickness values determined by electron probe at 10 kilovolts using calibration curves in Figure 7.

Sample	KV	Given Si <sub>3</sub> N <sub>4</sub> thickness (Å)	Given SiO <sub>2</sub> thickness (Å)	Oxygen X-ray intensity (cps)*	X-ray SiO <sub>2</sub> thickness (Å)
30	10	200	305	9.55	305
37	10	300	300	9.41	300
34	10	400	300	10.02	320
1	10	200	400	12.00	395
6	10	400	400	11.80	390
8	10	300	400	12.05	398

\*Every intensity value was obtained with a 100 sec. X-ray count.

## STUDY OF GaAs USING INFRARED MODULATED CATHODOLUMINESCENCE\*

W.N. Lin and D.B. Wittry

Department of Materials Science

University of Southern California, Los Angeles, California 90007

The study of deep impurity levels in semiconductors is important because of the influence that these levels have on the behavior of semiconductor devices. For example, in GaAs deep lying levels have been found to affect the behavior of diode lamps and transistors. The purpose of the present work is to study a possible new technique for the measurement of the energy of these deep levels.

The effect of light (with energies less than GaAs band gap) on the cathodoluminescence and sample current of semiinsulating GaAs was studied as a function of wavelength. Two Cr-doped and one undoped semiinsulating (resistivity  $\approx 10^8$  ohm.cm) single crystal GaAs samples were used in experiments performed at 300°K and 104°K. Steady light from a 150 watt quartzline lamp (color temperature 3200°K) passed through a Hilger and Watts D292 plane grating monochromator and was focused on the sample at the same position as the chopped electron beam. The light induced change in cathodoluminescence and sample current as a function of wavelength were recorded simultaneously. The typical curves obtained on the Cr-doped GaAs samples at 104°K are shown in Fig. 1(a). With wavelength  $\lambda$  longer than about  $1.6\mu$  (0.77eV), only small increase in cathodoluminescence  $I_c$  and sample current  $I_s$  were observed. As  $\lambda$  became shorter than  $1.6\mu$ , both  $I_c$  and  $I_s$  increased rapidly with decreasing  $\lambda$ . The energy threshold for the observed increase in  $I_c$  and  $I_s$  corresponds to the energy level introduced in GaAs by chromium<sup>1</sup>. The increase in  $I_c$  may be attributed to the excitation of electrons from Cr level to the conduction band by light since occupied Cr levels are very efficient hole traps. The increase in  $I_s$  is also due to the excitation of electrons from Cr level to conduction band which results in the change of sample conductivity and hence surface potential in such a way as to decrease the secondary electron yield. The energy threshold for the increase in  $I_c$  and  $I_s$  at 300°K was found to be about the same as that at 104°K (0.77eV). This is in agreement with the suggestion<sup>2</sup> that the Cr level is associated with conduction band and its distance from the conduction band edge is almost invariant with temperature. For the undoped GaAs sample, two threshold energies were observed at 104°K, namely, a sharp one at 0.77eV ( $1.6\mu$ ) and a much smaller one at 0.69eV ( $1.8\mu$ ) (Fig. 1(b)). At 300°K, only one threshold energy at 0.70 eV was observed. The observed threshold energies in this sample agree well with those reported<sup>3,4</sup> for the undoped high resistivity GaAs.

At constant beam voltage, within our experimental range, the percentage increase in  $I_c$  and  $I_s$  were found to be proportional to  $(I_s)^{-m}$ , where  $m$  is positive. A plot of this percentage change vs  $(I_s)^{-m}$  will give a straight line. The extrapolation of this straight line gives the value of  $I_s$  at which the light effect on  $I_c$  and  $I_s$  disappears. The concentration of excess electron hole pair density generated at this excitation should be proportional to the concentration of deep level

impurity responsible for the light effect. In Cr-doped samples, for which the Cr concentration is known, fairly good agreement was obtained between the estimated and true Cr concentration.

It was also found in this experiment, that in Cr-doped GaAs, especially with high Cr doping level ( $>10^{17} \text{ cm}^{-3}$ ), the distribution of Cr atoms tends to be nonuniform which results in the nonuniformity of sample conductivity. In addition to increasing the sample conductivity, the light was also found to make the conductivity more uniform.

From the foregoing, it may be concluded that by choosing a proper beam voltage and current, the light induced change in cathodoluminescence and sample current can be used to measure the energy of deep impurity levels in direct gap semiconductors. Furthermore, it can give information about the concentration of the impurity responsible for the deep level.

---

\* Work supported by the Advanced Research Projects Agency under grant No. DAHC 15-72-G7.

1. G.A. Allen, Brit. J. Appl. Phys., Ser 2, 1, 593 (1968).
2. A.T. Gorelenok, et al, Sov. Phys. - Semicond., 5, 95 (1971).
3. M.D. Sturge, Phys. Rev. 127, 768 (1962).
4. C.M. Gooch, et al, J. Appl. Phys. 32, 2069 (1961).

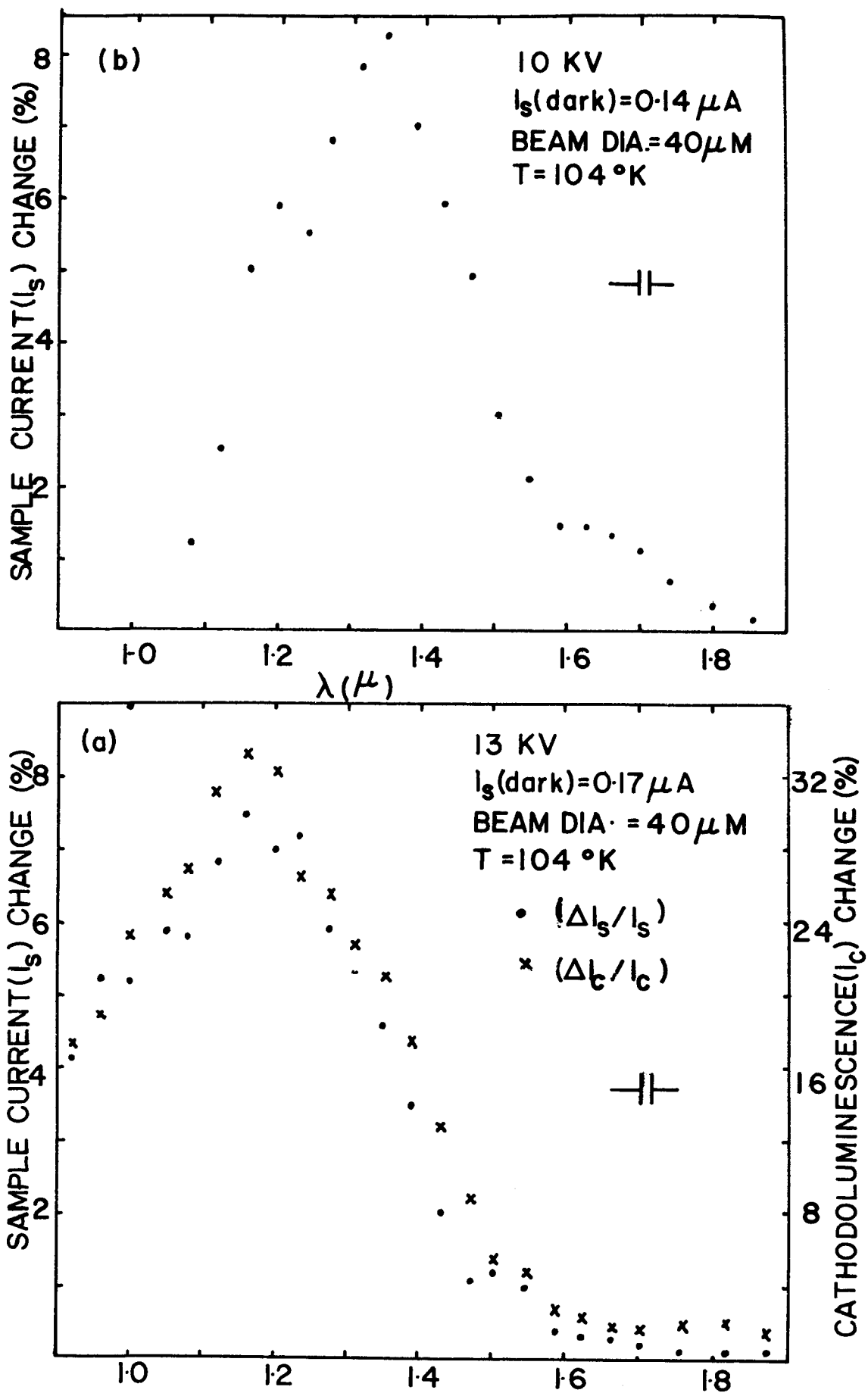


FIG.1. (a) Cr doped GaAs. (b) undoped GaAs.

INVESTIGATION OF THE ELECTRON BURN OF  $\text{MgF}_2$  DIELECTRIC MATERIAL

Paul J. Walitsky

Lamp Divisions  
Westinghouse Electric Corporation  
Bloomfield, New Jersey

The phenomena known as electron burn in cathode ray storage tubes has been examined by electron probe microanalysis and reflectance measurements. The analyses indicate that the burn is the result of the breakdown of the dielectric material on the backing electrode into free fluorine and colloidal magnesium. The evidence suggests that formation of a colloidal center is the cause of the observed discoloration.

The electron probe microanalysis was performed at the Lamp Divisions utilizing the Materials Analysis Company microprobe. The first analyses were performed in an attempt to find impurities in the burned areas. All elements in the periodic table from atomic number eleven (Na) to the number ninety two (U) were investigated. Only components of the backing electrode were detected. The possibility of oxygen or carbon impurity was also investigated, it proved negative.

A second group of analyses were performed in an effort to discover if color centers were responsible for the discoloration. Another aim of these analyses was to explore a possibility suggested by Dr. H. F. Ivey. Dr. Ivey suggested that a colloidal center caused by excess metal ion might be responsible for the discoloration.

In order to distinguish between color centers and colloidal centers, the exact location of the absorption band causing the discoloration was needed. Dr. Thornton of the Lamp Divisions provided a detailed examination of the reflectance spectra of the burned and unburned areas. Figure 1 shows a plot of wavelength vs the transmission ratio of the burned and unburned areas. If the sine waves (due thin film) effects are averaged it is apparent that maximum absorption occurs at approximately  $5800\text{\AA}$  ( $\sim$  yellow in the visible spectrum). The major color centers in  $\text{MgF}_2$  occur in the ultraviolet region (1,2,3,4). It appears that the discoloration is not due to color center formation.

The colloidal centers mentioned above are color changes which can occur if a dielectric with excess metal ions is irradiated with sufficient energy. A colloidal center could also occur if the radiation had sufficient energy to drive off the nonmetallic ion leaving excess metal. The distinction is important; the first type can be prevented by starting with stoichiometric material, the second type cannot be prevented even if the dielectric is stoichiometric. As far as can be determined, colloidal centers have not been previously investigated in  $\text{MgF}_2$ .

In order to determine if colloidal centers were forming on the  $\text{MgF}_2$  dielectric, an attempt was made to compare the Fluorine K x-ray<sup>2</sup> signals from the burned and unburned areas. During this effort it was quickly realized that the fluorine signal was dropping rapidly during exposure to the electron beam. Figures 2 & 3 show the result of plotting x-ray intensity vs time. The counts were accumulated in 10 second intervals with about a 2 second hold period between intervals. This experiment was done with 10-KV, and 4-KV electron beams. The beam current was 100 u amperes (.015 u amperes specimen current) and the beam size 3-5  $\mu$  in diameter.

The figure reveals drastic changes in the fluorine concentration in a relatively short time. Considerable darkening of the irradiated area was also observed in the microscope during irradiation. It seemed possible from this data that we were observing the formation of a colloidal center in situ. The results of monitoring the magnesium as had been done with the fluorine are plotted on figure 3 with the fluorine data. The magnesium rate rose quickly to almost double its starting value at all three kilovoltages. Thus, the decrease in fluorine count rate truly indicated the evolution of fluorine and the leaving behind on the electrode of excess magnesium.

If the colloidal center being formed was of the azide type, the starting composition would most likely be near stoichiometric. The actual Mg content was investigated using an  $\text{MgO}$  standard. The Mg count rate from the standard was compared with counts from the initial 10 seconds of counting from the  $\text{MgF}_2$ . The magnesium content came to within .5 weight percent of the stoichiometric value. The corrections for absorption and backscattering of the x-rays should not change this value very much. The evidence accumulated points strongly to the suggestion that the discoloration is a colloidal center of the azide type.

#### REFERENCES

1. H. F. Ivey, Photochromic Materials and Other Techniques for Real-Time Optical Processing and Display. W Research Report 68-1C1-COHAP-R2, 10/31/68, P.81.
2. A. Duncanson and R. W. H. Stevenson, "Some Properties of  $\text{MgF}_2$  Crystallized from the Melt", Proc. Phys. Soc. (London) 72 1001 (1958).
3. M. E. Hills and W. R. McBride, "Adsorption Bands of Irradiated  $\text{MgF}_2$ ", J. Chem Phys. 40, 2053 (A64).
4. R. F. Blunt and M. I. Cohen "Irradiation-Induced Color Centers in  $\text{MgF}_2$ ", Phys. Rev. 153, 1031 (1967).
5. S. D. McLaughlan and H. W. Evans, "Production of Colloidal Calcium by Electron Irradiation of  $\text{CaF}$  Crystals", Phys. Status Solid 27, 695 (1968).



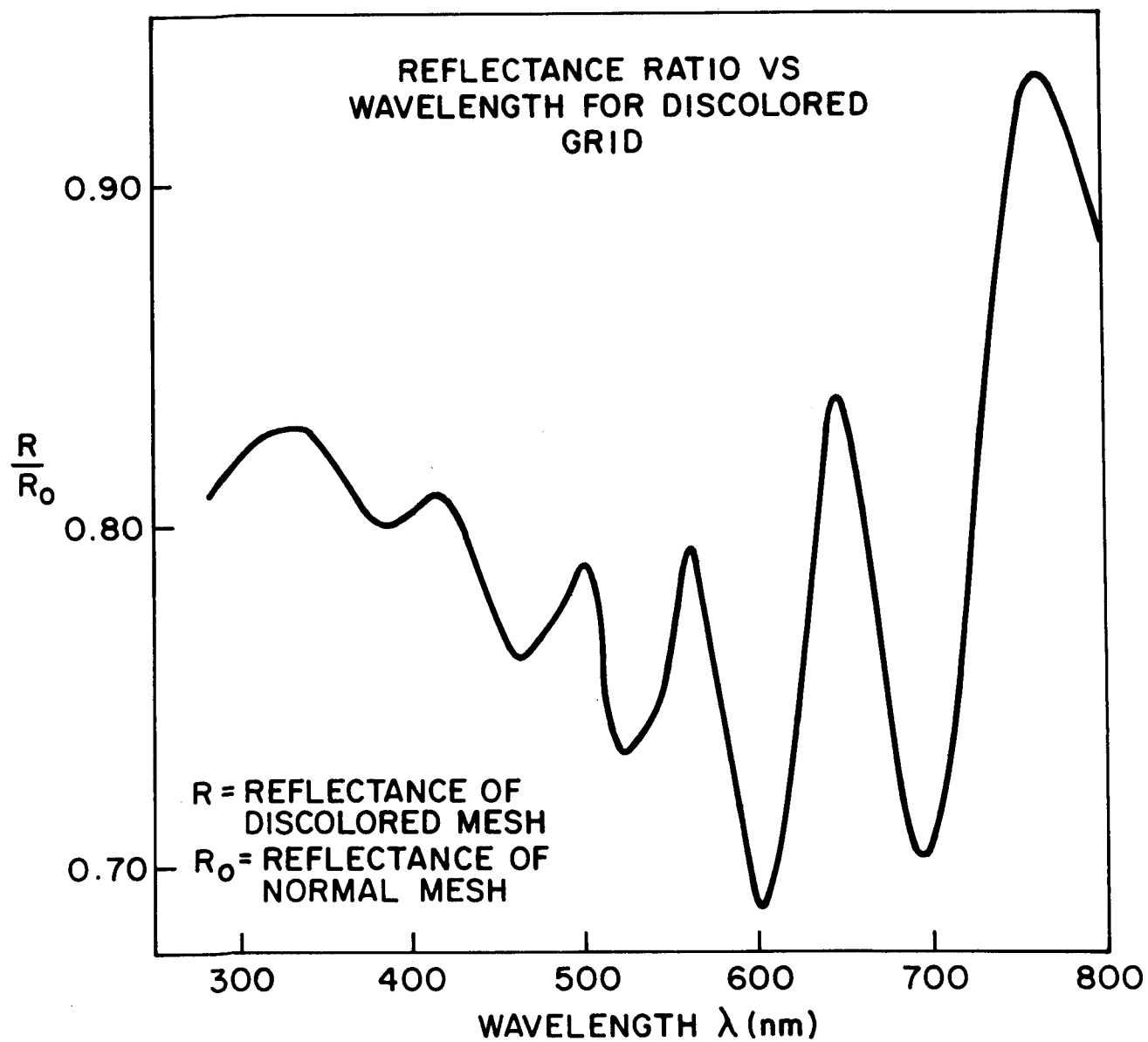


FIGURE 1

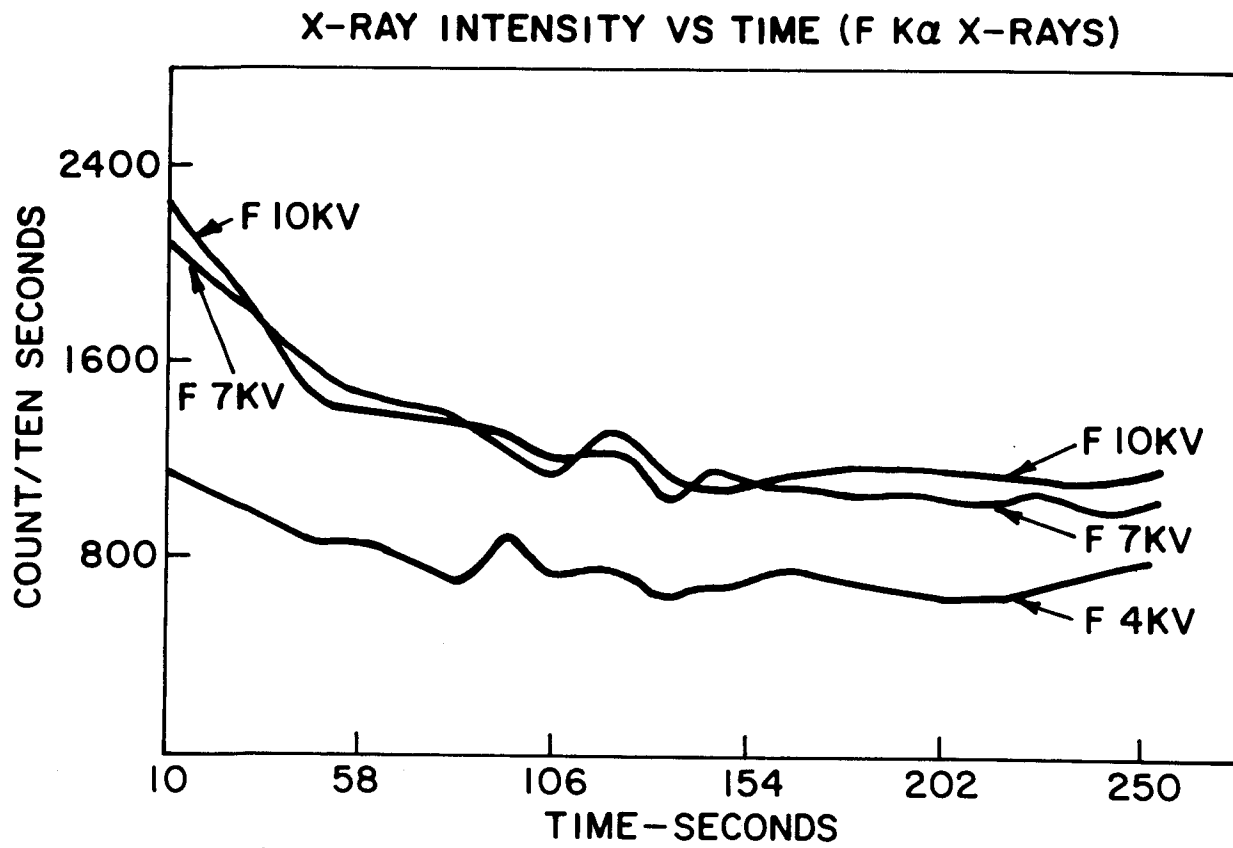


FIGURE 2

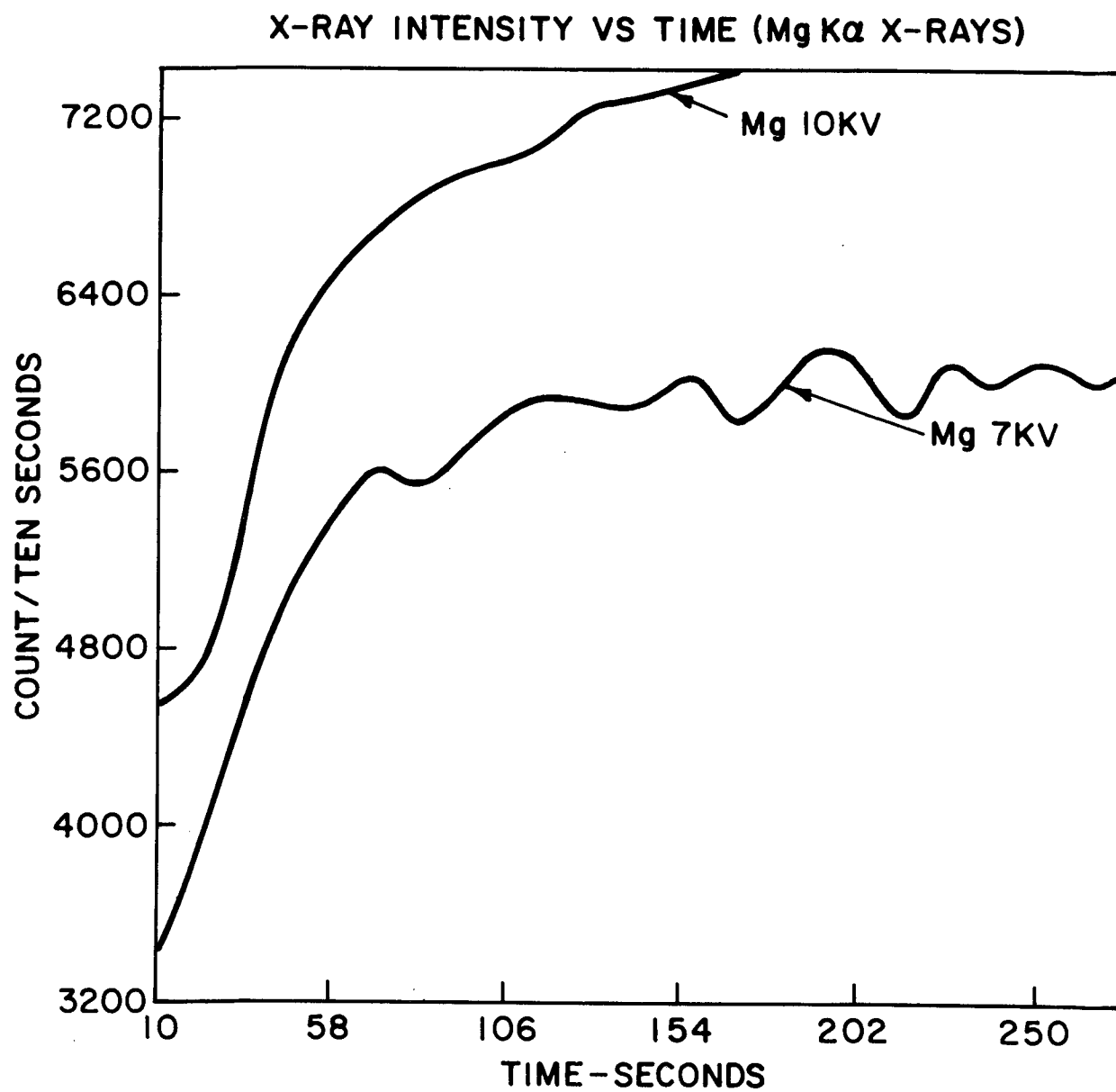


FIGURE 3

## THEORETICAL MODEL OF EBIC BIPOLAR CIRCUIT TESTING

P. C. Arnett  
IBM System Products Division  
Box A  
Essex Junction, Vermont

SUMMARY

In order to effectively use the EBIC technique for bipolar integrated circuit testing, a good understanding of the measurement is required. In general, the theoretical understanding of this measurement has been of a qualitative nature which allowed the prediction of the EBIC direction and, to some degree, the relative magnitude of the EBIC from two dissimilar irradiated junctions. In this paper, a quantitative description of EBIC phenomena is developed which allows prediction of the current magnitude to an accuracy approaching the accuracy (limited by junction defects, beam positioning, etc.) of the measurement.

Typically, in EBIC circuit testing, a p-n junction of the circuit is irradiated by the electron beam causing current to flow through the circuit by numerous paths to a limited number of external electrical contacts. The current detected at the external contacts is the EBIC. Consequently, in describing the EBIC signal, one must determine the following quantities: 1) the magnitude of the generated current, that is, the number of electron-hole pairs created by the electron beam; 2) the relationship of the generated current to the properties of the beam and the irradiated p-n junction; 3) the current-voltage property of the p-n junctions of the

circuit; 4) the maximum voltage across the p-n junction and its relationship to the generated current and p-n junction current-voltage characteristic mentioned above; and, finally, 5) the effective resistance offered by a p-n junction in order that it might be compared to other resistances present in the circuit.

With the above information, one can develop an equivalent circuit for the irradiated junction and the active elements of the circuit between the irradiated junction and the external contacts. The irradiated junction is modeled by a current source, whose strength is the generated current, in parallel with a forward-biased diode. The voltage developed across this junction drives current through the connecting circuit to the external contacts.

The application of Kirchhoff's laws to the equivalent circuit gives an expression for the EBIC. Calculations have been made beginning with the simplest cases (one p-n junction, two junctions in series, two junctions in parallel, etc.) and extending to complicated circuits. Comparison of the calculations with experimental results shows good agreement.

## METALLURGICAL APPLICATIONS OF THE ELECTRON MICROPROBE

Dennis O'Boyle

University of Wisconsin and Argonne National Laboratory  
Argonne, Illinois 60439

Since the first electron probe microanalyzer was described by Castaing in 1951, the importance of the instrument for analyzing the microstructure of alloys was well recognized. In his thesis, Castaing first applied the electron probe to metallurgical problems such as diffusion in solids, characterization of inclusions and impurity phases, the analysis of intermetallic phases, and crystallographic measurements by means of the Kossel line technique. During the past twenty-two years the electron probe has been utilized extensively in metallurgical research on many of these same problems as well as in many new areas. Recent improvements in electronic instrumentation and in correction procedures, have allowed the metallurgist to characterize the composition and structure of alloys more rapidly and accurately and to analyze a wide range of more complicated alloy systems. Often today the microanalyst has available in addition to the electron probe, instrumentation for energy dispersive analysis, scanning electron microscopy, low energy electron diffraction, and ion probe analysis, which not only permits the routine work to be done more rapidly but also which compliments and extends the capabilities of the electron probe.

Some developments that have extended the range of metallurgical problems that can be solved by electron probe analysis include 1) the general availability of computer programs for data reduction (largely based on the ZAF method), 2) the trend toward mini-computers for data acquisition and analysis, 3) the development of the shielded microprobe, which permits extremely gamma-active nuclear fuel specimens to be analyzed quantitatively. The shielded microprobe has led to major improvements in our understanding of fission product behavior and fission-product-induced grain boundary corrosion of cladding alloys.

In addition to these developments, the scope of metallurgical studies has been expanded by the greater use of stereometric analysis to characterize not only phase composition but also volume fraction, shape, and number density. The development of cathodoluminescence for metallurgical applications has extended the detectability limit for certain elements into the ppb range. Improvements that have been made recently in understanding chemical bonding effects on x-ray emission spectra, have been applied to both alloying studies and to oxidation studies of steel. In this paper we will review and discuss these developments as well as recent work on metallurgical phase studies, diffusion measurements, light element analysis, and the analysis of impurity phases.

## MICROPROBE ANALYSIS OF THE BULK COMPOSITION OF PHASE AGGREGATES

A. J. Gancarz and A. L. Albee

Division of Geological and Planetary Sciences  
 California Institute of Technology\*  
 Pasadena, California 91109

Introduction

Petrologic, metallurgic, and ceramic studies often require a knowledge of the total composition and/or average phase compositions of a heterogeneous aggregate of phases. Two approaches for obtaining the total composition, the "broad-beam" method and the "point-count" method, are readily possible with a computer-controlled electron microprobe. The advantages and disadvantages of each method will be discussed using the analysis of a lunar basalt as an example.

An aggregate of phases can be described by a series of mass balance equations:

$$C_{11}X_1 + C_{12}X_2 + \cdots + C_{1n}X_n = S_1$$

$$C_{21}X_1 + C_{22}X_2 + \cdots + C_{2n}X_n = S_2$$

$$\vdots$$

$$C_{m1}X_1 + C_{m2}X_2 + \cdots + C_{mn}X_n = S_m$$

where  $C_{ij}$  is the concentration of the  $i^{\text{th}}$  element in the  $j^{\text{th}}$  phase,  $X_j$  is the weight fraction of the  $j^{\text{th}}$  phase in the aggregate, and  $S_i$  is the concentration of the  $i^{\text{th}}$  element in the total aggregate. The "broad-beam" method attempts to directly determine the  $S_i$ 's, i.e. the bulk composition, by averaging the analyses of a large number of 30 to 50  $\mu\text{m}$  spots. The "point-count" method measures the  $C_{ij}$ 's and  $X_j$ 's, which are themselves exceedingly useful information and which also permit calculation of the  $S_i$ 's. It should be noted that the basic equation for each element is correct regardless of whether the phases are compositionally variable or homogeneous. However, obtaining the  $C_{ij}$ 's is much simpler for homogeneous phases, such as occur in petrologic or metallurgic systems in approximate thermodynamic equilibrium.

### Point-count method

Point counting is a standard microscopy technique (Chayes, 1956). Identification of the phase present at a statistically significant number of grid points on a surface provides an estimate of the volume percent of each phase. Volume percentages are transformed to weight percentages ( $X_j$ 's) by using the densities of the phases. If the phases are homogeneous a single analysis of each phase provides the  $C_{ij}$ 's, but if they are inhomogeneous a suitable average composition must be used.

The "point-count" method with the electron microprobe (Keil, 1965) applying the same principles as the standard microscopy technique, measures both  $C_{ij}$  and  $X_j$ .

The "point-count" technique was used to obtain the  $C_{ij}$ 's and  $X_j$ 's for lunar basalt sample 14276. With a MAC-5-SA3 electron microprobe completely under computer control, 5 second counts for Fe, Ca, and Si were made at 1949 one micron grid points on a polished thin section. The program advanced the stage position, identified epoxy-filled cracks or holes, moved to a new traverse line when the edge of the sample was reached, identified the phase analyzed at each point, determined the volume percentage of each phase, and calculated the average Fe, Ca, and Si counts for each phase. Total running time was less than 4 hours. A large number of complete analyses of the individual mineral phases had established the general compositional range of each phase (see Gancarz *et al.* 1972), and these ranges were used to establish the phase identification filter. A complete microprobe analysis with Fe, Ca, and Si counts closely corresponding to the average Fe, Ca, and Si counts was selected from all of the complete quantitative analyses to represent the average composition of each phase; these average analyses are included in Table 1. The bulk composition calculated by the "point-count" method is nearly identical to that obtained by chemical analysis (Rose *et al.* 1972), which is also presented in Table 1. Even minor elements can be determined with considerable accuracy by the "point-count" technique when they are concentrated in measurable quantities in low abundance phases.

In this rock the compositional variation in plagioclase could be expressed in terms of two components and formed a continuous series; hence plagioclase composition was expressed as a single average. The pyroxenes -- augite, pigeonite, and orthopyroxene -- show three distinct groupings within a nearly continuous compositional variation expressable by three components. Hence, the phase identification filter in the program was written to divide the pyroxenes into 3 groups and to provide three different pyroxene averages since a single average pyroxene composition would not correspond to any actual pyroxene in the rock.

Experience has shown that Fe, Ca, and Si analyses are sufficient to identify and average the phases in the lunar basalts. A different set of filters which identify the phase at each grid point on the basis of Fe, Ca, and Si X-radiation intensity, is written for each rock based upon numerous analyses of the minerals. Rewriting the filters is relatively simple because the program is written in FOCAL, a conversational computer language.



At the expense of increased analytical time, the program can be modified to analyze several elements on each spectrometer. Alternatively, a non-dispersive system with a number of preset windows could be used. Although such modifications make it possible to apply the "point-count" method to quite heterogeneous and less well known aggregates, it is necessary to have some prior compositional information on the phases in order to set up proper identification filters.

#### "Broad-beam" method

A bulk analysis of lunar basalt sample 14276 was also determined by the "broad-beam" technique and is given in Table 1. The program controlled the analysis and data reduction for 13 elements; 50 $\mu$ m spots spaced on a grid covering the polished thin section were used, and an average for the 50 individual analyses was calculated. This average analysis required about 15 hours of probe time. The resulting bulk composition is quite different from that determined by chemical analysis and by the "point-count" method (see Table 1). Especially notable are the higher  $Al_2O_3$  value and lower MgO and FeO values for the "broad-beam" method. These discrepancies are due to the combined results of at least 4 different biases, which could have been partially avoided by taking certain precautions.

One bias is due to the fact that the correction procedures for inter-element interactions assume a homogeneous sample. The "broad-beam" method assumes that the average grain size is so much smaller than the beam size that the area covered by the beam approximates a homogeneous sample. The grain size in this sample is too large. Hence, a large proportion of the X-rays are generated and pass through a single phase, but the corrections are based on the composition of the entire 50 $\mu$ m spot. As a result, Al, which is almost entirely in plagioclase ( $CaAl_2Si_2O_8$ ), is overcorrected because of the presence of pyroxene ( $(Ca, Fe, Mg)_2Si_2O_6$ ) within the analyzed spot. With some knowledge of the  $C_i$ 's and  $X_i$ 's, it would be possible to calculate correction factors weighted by the phase abundance in each spot, but this calculation becomes quite complicated. Moreover it can, at best, only be an approximation because of the difficulty of calculating an average path for the emergent X-radiation in grains of varied geometry.

Two different biases were introduced by the fact that pyroxene tends to pit more than plagioclase during polishing. The program allowed the operator to focus and inspect each 50 $\mu$ m spot and, if it was badly pitted, to move 1/4 of a grid distance normal to the grid traverse direction. In retrospect, this procedure introduced a definite bias toward plagioclase-rich areas. In addition, the higher degree of pitting on the pyroxene surface resulted in a change in the effective take-off angle, effective source volume, and effective depth of penetration. Both of these problems can be partially avoided by better polishing. An additional bias was due to the fact that some  $Al_2O_3$  used in polishing was lodged in cracks and pits despite ultrasonic cleaning. This amount of  $Al_2O_3$ , although small, is also overcorrected as explained above. This problem can be avoided by using other polishing materials.

## Discussion

Both the "broad-beam" and "point count" methods are useful for particular problems, providing proper precautions are taken. In most circumstances we have found the "point count" method provides more precise data in less time and provides valuable data on average phase composition and phase abundances as well as on bulk composition. In general, the use of a few "broad-beam" analyses as an estimate of the bulk composition is not a reliable procedure and can be highly misleading.

## Acknowledgments

We thank A. Chodos for his assistance and help with the computer programming. This work was supported by NASA grant NGL-05-002. The microprobe laboratory has been developed with the support of the National Science Foundation, the Jet Propulsion Laboratory, and the Union Pacific Foundation.

Table 1  
Phase abundances, "average" phase compositions and bulk chemical composition of 14276

	plagioclase	ortho- pyroxene	pigeonite	augite	mesostasis	ilmenite	Fe-metal	phosphate**	Bulk chemical composition		
									calculated	Rose et al.	"Broad Beam"
vol %	64.65±1.8 <sub>2</sub>	15.70±0.9 <sub>0</sub>	9.34±0.6 <sub>9</sub>	4.05±0.4 <sub>6</sub>	3.54±0.4 <sub>2</sub>	1.28±0.2 <sub>6</sub>	0.36±0.1 <sub>3</sub>	0.67±0.1 <sub>8</sub>			
wt %	59.9 <sub>2</sub>	17.9 <sub>8</sub>	10.7 <sub>0</sub>	4.6 <sub>0</sub>	3.1 <sub>5</sub>	2.0 <sub>3</sub>	0.9 <sub>1</sub>	0.7 <sub>2</sub>			
SiO <sub>2</sub>	46.25	53.52	50.67	51.73	73.58	0.24	n.a.	0.56	47.4 <sub>6</sub>	47.60	47.89
Al <sub>2</sub> O <sub>3</sub>	34.18	1.60	1.39	2.56	12.85	0.35	n.a.	0.06	21.4 <sub>5</sub>	21.34	26.13
Cr <sub>2</sub> O <sub>3</sub>	n.a.	0.56	0.48	0.81	<0.01	0.28	n.a.	n.a.	0.1 <sub>9</sub>	0.26	0.12
TiO <sub>2</sub>	n.a.	0.59	0.82	1.07	0.52	49.58	n.a.	n.a.	1.2 <sub>7</sub>	1.20	0.59
MgO	0.19	25.35	18.66	17.67	0.04	1.44	n.a.	1.15	7.5 <sub>2</sub>	7.10	4.98
FeO	0.21	16.41	20.81	12.49	1.21	47.62	91.71*	1.74	7.9 <sub>6</sub> ***	7.94	4.89
MnO	n.a.	0.27	0.29	0.22	<0.01	0.42	n.a.	n.a.	0.1 <sub>0</sub>	0.12	0.07
CaO	17.55	2.43	6.32	14.35	0.99	0.16	n.a.	47.96	12.6 <sub>7</sub>	13.18	14.57
Na <sub>2</sub> O	1.37	0.02	0.06	0.09	0.92	<0.01	n.a.	0.32	0.8 <sub>7</sub>	0.72	0.90
K <sub>2</sub> O	0.19	<0.01	<0.01	<0.01	7.41	0.01	n.a.	n.a.	0.3 <sub>1</sub>	0.48	0.55
BaO	0.05	n.a.	n.a.	n.a.	0.07	n.a.	n.a.	41.16	0.3 <sub>0</sub>	0.40	0.37
P <sub>2</sub> O <sub>5</sub>	n.a.	n.a.	n.a.	n.a.	n.a.	n.a.	7.45	n.a.	0.0 <sub>7</sub>	0.01	n.a.
Ni	n.a.	n.a.	n.a.	n.a.	n.a.	n.a.	n.a.	1.67	0.0 <sub>1</sub>	n.r.	n.a.
F	n.a.	n.a.	n.a.	n.a.	n.a.	n.a.	n.a.				
Total	99.99	100.75	99.50	100.99	97.97	100.10	99.16	94.62	100.24	100.34	101.08

\* Fe

\*\* average of apatite and whitlockite

\*\*\* total iron as FeO

n.a. not analyzed

n.r. not reported

References

- Chayes, F. (1956) Petrographic Modal Analysis, John Wiley & Sons, Inc.  
New York.
- Gancarz, A. J., Albee, A. L., and Chodos, A. A. (1972) Comparative Petrology of Apollo 16 Sample 68415 and Apollo 14 Samples 14276 and 14310, Earth Planet. Sci. Letters 16, 307-330.
- Keil, K. (1965) Mineralogic modal analysis with the electron microprobe X-ray analyses, Amer. Min., 50, 2089-2092,
- Rose, H. J., Jr., Cuttitta, F., Ansell, C. S., Carron, M. K., Christian, R. P., Dwornik, E. J., Greenland, L. D., and Ligon, D. T., Jr. (1972) Compositional data for twenty-one Fra Mauro lunar materials, Proc. Third Lunar Sci. Conf., Geochim. Cosmochim. Acta, Suppl. 3, 2, 1215-1229.

## USE OF EBM ANALYSIS IN THE PROCESS DEVELOPMENT OF A NEW GEAR MATERIAL

Norman M. Walter, Materials Engineering, The Boeing Vertol Company

At the present time the Electron Beam Microprobe provides the only "nondestructive" method for the analysis of the Carbon gradients associated with the carburized and hardened cases of steels used for bearings and gears. It is, of course, "nondestructive" only in the sense that a routine metallurgical cross section may be used.

In order to make effective use of the probe in the process development of an advanced gear material, the method should conform to a number of criteria such as:

1. Must be rapid
2. Must not impose undue hardships on the normal laboratory procedures.
3. Must provide data equivalent to standard combustion analysis of control slugs.
4. Must be applicable to the analysis of a broad spectrum of steels.
5. Must not be excessively costly.
6. Must be reproducible over periods of years.

During the past four years studies were undertaken in a variety of ways to determine the best way to achieve the above goals.

The first objective was to develop a working curve of Wt% Carbon vs. peak count rate which would have a reasonable standard error regardless of the matrix. It was purposely decided not to use a single set of Carbon standards, but instead, to use two types of standards. The first type consists of about twenty of the NBS chip standards used for combustion Carbon analysis. It was recognized that these standards may be made up from either a single heat or a composite of a number of heats. Therefore, a random sampling technique was decided upon. This simply consists of mounting a sample and analyzing a number of the chips at random (usually ten is adequate).

The second set of "standards" consists of samples of types of steels normally used in the manufacture of our aircraft; 4340, 9310, M50, 52100. These had been given routine analysis by the Quality Assurance Laboratory as well as by the vendors' qualification analysis.

The second stage was the selection of instrument operating conditions to be used. These were, for our ARL EMX-SM, beam potential-11KV specimen current, .1 uA, with 300 uA emission current.

The fixed Carbon wave length used, was the peak position of graphite, with Pulse Height Analyzer Base Line and Window Width settings to give about 95% of total radiation. A Lead Stearate Analysing crystal is used. The need for constant operating conditions is recognized when long term reproducibility is required. The data are collected for 10 uA-Sec. Deviations of as much as 10% of specimen current have been recorded which still gave repetitive analysis variations within the statistical limitations of total counts recorded.

The results of the calibration studies have given the present working curve shown in Figure I. The interesting feature here is the extrapolated 0% concentration background. The background corresponds to a value about 100% higher than would be expected by base-line extrapolation of higher and lower wavelength count rates. For the present this can only be explained on the basis of monochromator fluorescence. Higher order chromium radiation also does not appear to have an appreciable effect on the calibration curve.

In order to overcome the severe segregation of carbon that can occur during manufacture, under improper operating conditions, different methods of sampling were tried. Those used were (1) a single fixed point, (2) a fifty micron scanning line and (3) the finally accepted method of using a 125 micron x 125 micron raster scan, with a 10 millisecond Horizontal and 10 second Vertical sweep rate.

The 125 micron x 125 micron raster was sized to conform with the normal practice of 0.005 inch layer removal when using the combustion analysis method. This size also does not lead to severe spectrometer detuning, provided the spectrometers are properly aligned. In addition Chromium and Silicon are monitored during all Carbon analyses. This provides additional data as well as checks on the uniformity of steel heat lots. Table I shows a typical data typeout to show the variation that occurs.

These conditions are now being used in the development of process control conditions to determine optimum carburizing and heat treat conditions. The steel selected is a modified H-11 tool steel, vacuum remelted, with a nominal composition of:

Carbon	.15%	Mo	1.40%	P	.015 Max.
Mn	.30%	V	.45%	S	.015 Max.
Si	.90%	W	1.35%	Cr	5.0%

This steel was selected because of the excellent hot hardness and scuffing resistance properties which the material possesses. It is presently being used in the Heavy Lift Helicopter and other models under development.

The need for probe analysis in this type of program can be recognized when it is realized that it is impossible to use the combustion technique in determining the carbon case depth on the flanks and roots of individual gear teeth. In addition the particular material selected has peculiarities of chemistry which did not allow the same freedom of processing conditions used for 9310 steels, to be transferred to gear production with the new material. Therefore, it was necessary to analyze large numbers of specimens at each step to determine that the required conditions of hardness and case depth could be met. These studies have resulted in a proprietary carburizing and heat treat method. Representative examples of profiles will be shown and explained.

3-19-73  
EBM 1004  
TRACE A

T	uA-SEC	CR	SI	C	DEPTH
099.440	0100000	0105223	0018126	0013881	.0025"
099.081	0100000	0107772	0018591	0013356	.0075
099.049	0100000	0108719	0018833	0012508	.0125
098.999	0100000	0110174	0010174	0011714	.0175
099.261	0100000	0109859	0019175	0010300	.0225
100.228	0100000	0110020	0019588	0009546	.0275
100.437	0100000	0109470	0019891	0008979	.0325
100.495	0100000	0111134	0020111	0008275	.0425
100.404	0100000	0110983	0020103	0007672	.0525
100.463	0100000	0110467	0020276	0007003	.0625
100.395	0100000	0110564	0019996	0006841	.0725
100.382	0100000	0109996	0020220	0006370	.0825
100.236	0100000	0110220	0020119	0006210	.0925

TABLE I

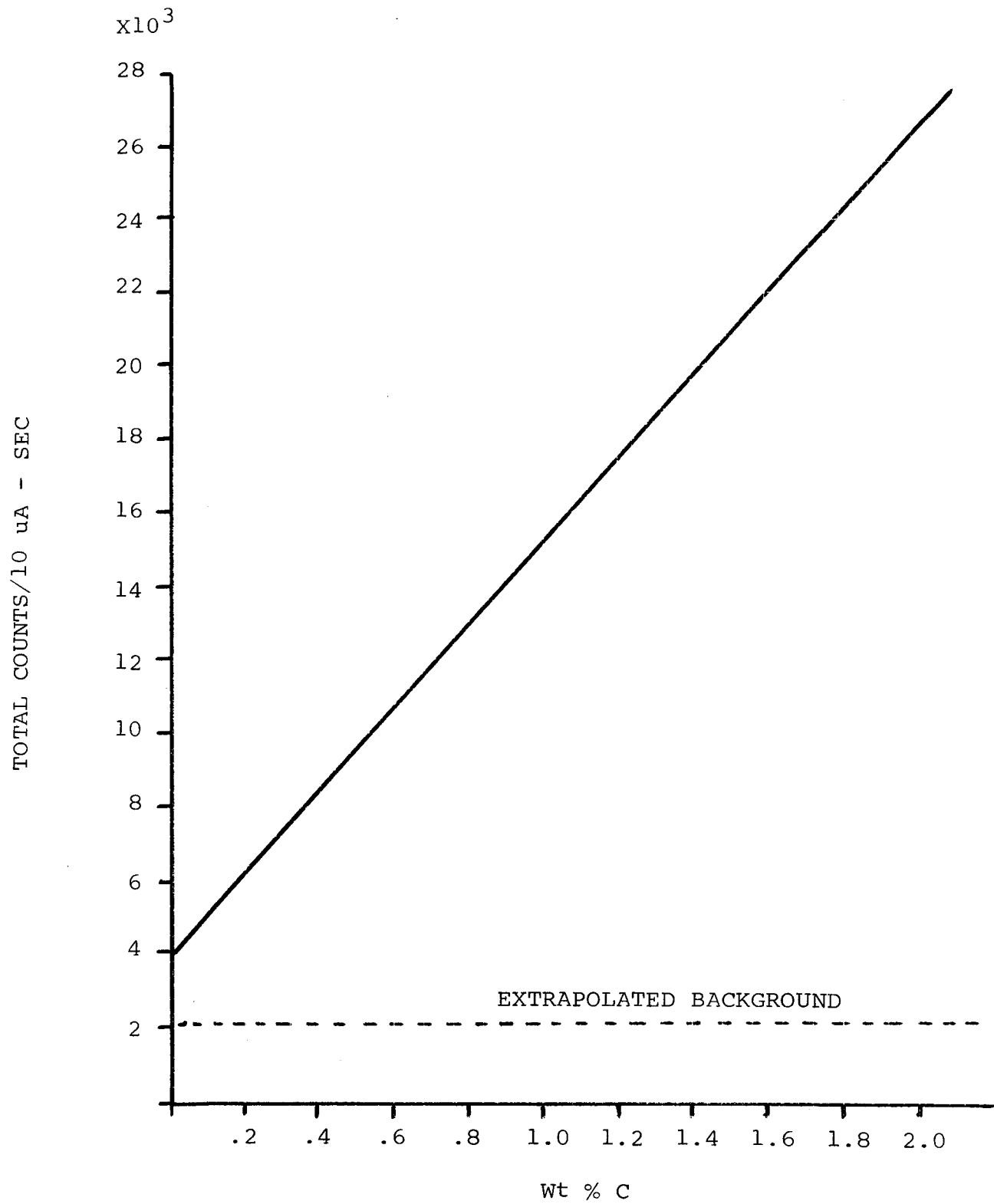


FIGURE I

## ION PLATED COPPER-STEEL GRADED INTERFACE

B. Swaroop and I. Adler

Kelsey-Hayes Research &amp; Development Center, Ann Arbor, Michigan 48105

The types of interfaces could be categorized as mechanical, monolayer, compound, and diffused. The diffused interface is characterized by a gradual change in composition across the interface. For such an interface to form, mutual solubility of at least two materials and some form of energy (generally heat) for diffusion are required. In this type of interface, interfacial stresses are distributed throughout the interfacial region. In addition, a graded diffused interfacial region can be prepared by impinging particles with high kinetic energy capable of penetrating into the substrate lattice without actually following a diffusion mechanism. This type of interface is generated by a "pseudodiffusion" mechanism and can be prepared by a process developed by Mattox<sup>(1)</sup> known as ion plating. The advantage of preparing a graded interface by this method over the graded interface produced by heat diffusion is that the stresses are evenly distributed over a small volume without the generation of a low strength or a brittle region.

## EXPERIMENTAL

Ion plating like sputtering involves the generation of a low pressure inert gas glow discharge. However, unlike sputtering the substrate is made the cathode and the depositing material originates from a thermal or electron beam evaporant source. In the actual process, positive ions from the glow discharge bombard the surface of the substrate in a fashion analogous to sputtering. This results in a continual cleaning of the surface before and during coating deposition. The coating material, a metal or alloy, is evaporated into the gas discharge where it is ionized. These ions are accelerated through the discharge, strike the surface of the substrate with a high kinetic energy ( $\approx 3000$  to  $5000$  eV) and become embedded in the surface. Further, the ions follow the electric field lines and because of this "throwing power" coat the part uniformly.



Using the above mentioned technique, copper was ion plated onto a steel substrate under an argon glow discharge of 50 to 60 microns. First, the substrate was sputter etched for 10 minutes and then the copper was thermally evaporated from a tungsten boat located at a distance of 7.5 cm from the substrate. The approximate time of ion plating was one minute. The resulting ion plated sample was cooled in the partial vacuum of the chamber. Metals like Cu, Ni, or Cr were chosen as potential candidates for ion plating onto steel in order to improve the fatigue life<sup>(2)</sup> of steel products.

The interface between steel and copper was analyzed by using a standard electron probe technique<sup>(3)</sup>. The electron beam was excited at 20 Kv giving a beam diameter of approximately 3 microns at the specimen. The intensity measurements of copper -  $K_{\alpha}$  or iron -  $K_{\alpha}$  were obtained using a mica crystal with P-10 gas flowing in the proportional counter. The measured intensities were as the peak intensity minus the off peak background. Point-analyses at steps of 0.0001" were conducted across the ion plated interface while x-ray photons were accumulated for a given period of time. Sample preparation for the probe analysis required reinforcing the copper film with a nickel layer so that the film was not damaged during polishing. The nickel layer was electroplated.

## RESULTS

Copper was ion plated onto a steel substrate at 3 kV dc under the conditions mentioned above. The front surface of the steel was found to be ion plated with a 12 to 15 micron thick layer of copper while the back of the specimen was plated with a 5 to 7 micron thick layer of copper. This disparity in the thickness of two surface coatings could be avoided if the substrate was rotated during deposition. Figure 1 shows a photomicrograph of a typical interface with a visible copper film having a thickness of 5 microns.

An electron probe point-analysis of the copper/steel interface is shown in Figure 2. In this Figure, the intensity of the Cu K $_{\alpha}$  radiation is plotted as a function of the distance, the electron beam travels in a direction perpendicular to the interface. This plot is divided in two sections. The first section (I) of the plot corresponds to increasing copper intensity for about 6 microns. The second section (II) corresponds to decreasing copper intensity and is about 7 microns. If one assumes that a sharp interfacial boundary between copper and steel exists along the dotted line indicated in Figure 2, then region II of the plot would correspond to a diffused region of copper in steel. However, this diffused region is not visible in the optical micrograph shown in Figure 1. The only visible copper layer in this micrograph corresponds to region I of the plot given in Figure 2. The dotted semicircles in Figure 2 indicate the respective positions of electron beam at each point-analysis.

The adhesion of the film to the substrate was examined by a ninety degree bend test. The sample was examined under the microscope before and after the test. For the purpose of comparison a copper film thermally evaporated onto steel also was prepared. The evaporation was carried out under the same conditions as the ion plating except that argon gas was missing; the substrate was not heated, and the pressure in the chamber was approximately  $10^{-5}$  torr. Both of these samples were given a  $90^{\circ}$  bend and were examined under an optical microscope for cracks and loss of coating adhesion. The thermally evaporated coating failed while ion plated film did not show a single crack along the bend. The standard "Scotch Tape Test" was also carried out on the ion plated and the thermally evaporated copper film. The test results show that the ion plated coatings indicated no sign of failure while thermally evaporated films failed during the first pull.

#### REFERENCES

1. D. M. Mattox, J. Electrochem. Tech. 2, p 295, 1964.
2. T. Spalvins, NASA, Lewis Research Center, Private Communication.
3. B. Swaroop, J. of Electrochem. Soc. 118, p 913, 1971.

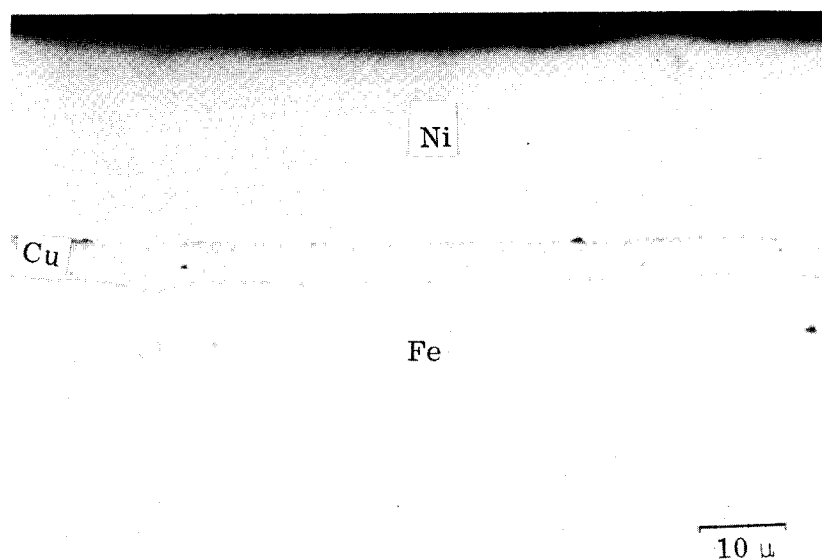


Figure 1: Photomicrograph of Ion Plated Copper onto Steel

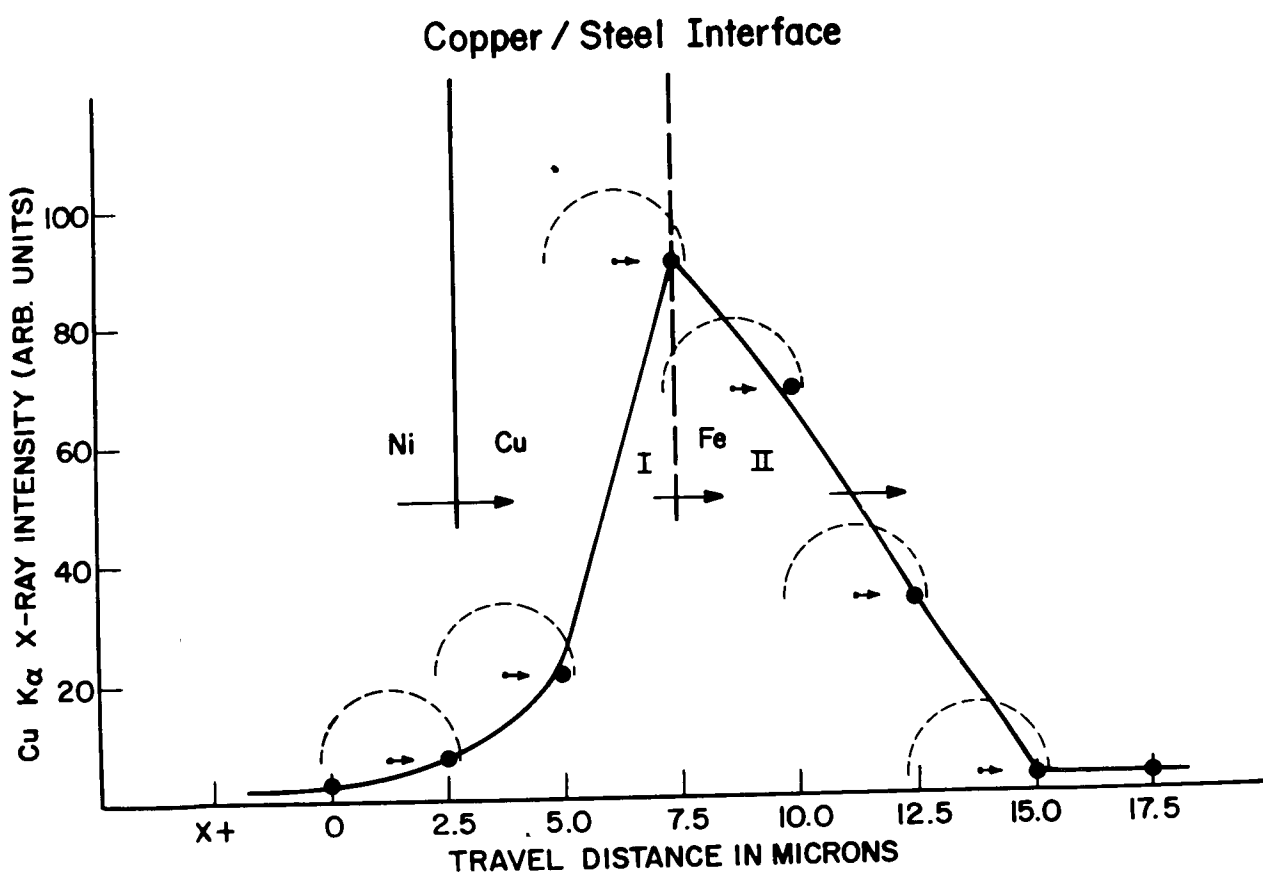


Figure 2: Point Analysis of Ion Plated Interface by Electron Probe

# REDUCING BACKGROUND AT THE SHORT WAVELENGTH END OF ARL CRYSTAL SPECTROMETERS

By

W. C. Bigelow, F. Bleicher, L. F. Allard & A. J. Mardinly

Dept. of Materials & Metallurgical Engr.

The University of Michigan

Ann Arbor, Michigan 48104

We have found that radiation scattered into the detectors of the spectrometers of our ARL EMX-SM Electron Microprobe from the cone of the optical microscope and nearby fixtures contributes significantly to the spectrometers' backgrounds at the low wavelength end of their ranges. This is background which is in addition to the necessary component which is due to the continuous spectrum radiation that is diffracted into the detectors by the analyzing crystals. It therefore causes an unnecessary decrease in the peak-to-background ratios of elements whose characteristic wavelengths fall at the lower ends of the spectrometers' ranges.

By installing shield boxes of the types shown in Fig. 1 we have been able to decrease this scattered background by a factor of one-half to one-third. However, observations made just prior to the deadline for submission of this abstract have revealed that the pattern of scattering is more complex than had been initially assumed, and that space limitations are such that the shields must be very carefully designed if they are to act effectively without damaging the crystals, grounding the detectors, or disturbing the alignment of the spectrometers.

It is anticipated that these requirements can be met and that an effective shield system will be described at the EPASA meeting.

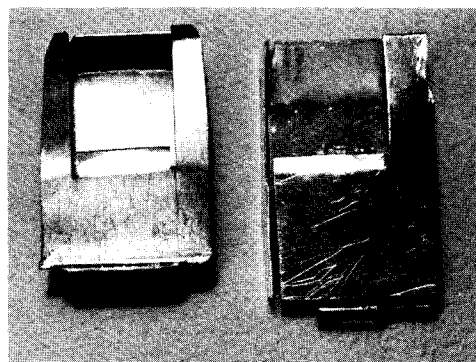


Fig. 1. Preliminary shield boxes for light (L) and heavy (R) element spectrometers.

NEW X-RAY SPECTROMETERS FOR A MULTIPURPOSE  
SCANNING ELECTRON MICROPROBE

B. Kenessey, L.K. Griffith and E. Davidson

Applied Research Laboratories  
Sunland, California 91040

### INTRODUCTION

The ideal x-ray detection system in an electron microprobe should provide high efficiencies in multiple element analysis, high precision in determination of major constituents and high sensitivity in determining trace elements.

All three of these requirements cannot be satisfied simultaneously for a given x-ray spectrometer since it is not possible to have maximum peak to background ratio while also having x-ray collection efficiencies.

The energy dispersive x-ray spectrometer provides for simultaneous analysis and provides a high signal collection efficiency. However, it has a number of disadvantages; namely, lower sensitivity for trace analysis, lower accuracy for concentrations of a few percent, more interferences due to peak overlaps and greater difficulty in detecting very soft x-rays. While the curved crystal spectrometer is superior in these respects, it generally provides a lower efficiency because only one characteristic x-ray line can be observed at a given time and the solid angle factor is usually about two orders of magnitude lower than the energy dispersive spectrometer.<sup>(1)</sup>

Because of these reasons, an optimum x-ray detection system must utilize more than one x-ray spectrometer. Such a system employing multiple spectrometers requires an integrated approach to the electron optics and the x-ray optics as discussed in another paper in these proceedings.<sup>(2)</sup> For such an instrument a possible x-ray spectrometer system is shown in Figure 1. The spectrometers utilized may be of three different types as described in the following.

### SCANNING X-RAY MONOCHROMATOR

The scanning x-ray monochromators (Figure 2) are based on a 5" radius focal circle and a linear crystal travel so that:

- a) The wavelength scale is linear
- b) The x-ray take-off angle remains constant

Compact size is achieved by using a vertical leadscrew and stainless steel band to transfer the motion to the crystal carriage. Also, a similar band is employed in a unique backlash free mechanical differential to develop the detector motion. The focal circle center is established by a carriage riding on precision ball bearing wheels in a circular track. A stepping motor located on the outside of the vacuum housing drives the leadscrew through bevel gears. The orientation of the leadscrew is such that the necessary spectrometer alignments can be provided without telescoping shafts and universal joints at the spectrometer drive. External alignments are provided to position the focal circle relative to the x-ray source and to rotate the crystal independently to achieve the correct Bragg angle relationship. The spectrometer may be controlled manually, remotely, or by computer. Easy accessibility is achieved by retracting the spectrometer from the main housing on a support rail.

### FIXED X-RAY MONOCHROMATOR

A fixed x-ray monochromator (Figure 3) has been constructed for use in multiple spectrometer instruments. The fixed spectrometer approach makes it possible to locate two spectrometers in the space normally occupied by a single scanning spectrometer.

In fact, it is possible to determine up to 12 elements simultaneously. One of the many possible combinations is illustrated in Figure 1. The two fully scanning spectrometers covering a range of  $1\text{\AA} - 150\text{\AA}$  and the eight additional fixed spectrometers may be preset to any eight spectral lines within the same range. It is also worth mentioning that the construction is such that they may be recalibrated for another spectral line after the initial installation.

Two external controls are provided for each channel, similar to the fully scanning spectrometers for crystal and focal circle adjustments.

### ENERGY DISPERSIVE DETECTOR

An energy dispersive detector for use in instruments that have capabilities for both high scanning electron microscope resolution and for high accuracy electron probe microanalysis must be matched to the direction and sensitivity of the secondary electron detector or the x-ray spectrometers. A single detector cannot provide this, since the specimen position may be different for SEM and for quantitative EPMA. For this reason a unique double detection system, cooled by a single cryostat has been developed (Figure 4). The lower detector is used for SEM on a tilted specimen; the upper detector is used for EPMA and receives x-rays at the same takeoff angle as the x-ray monochromators. This upper detector is provided with an externally switchable aperture so that detector sensitivity can be modified to permit operation either at the high sample currents used in EPMA or at lower sample currents as used in SEM.

### SUMMARY

It is apparent that a versatile and modular instrument concept employing various types of x-ray spectrometers can increase the effectiveness of many laboratories.

The energy dispersive detection system serves for rapid qualitative and semi-quantitative determinations at high signal collection efficiency. Computer controllable scanning spectrometers have the ability to perform sequentially qualitative as well as precise quantitative determinations of all elements down to and including beryllium, while fixed wavelength spectrometers provide rapid simultaneous analysis of a selected array of elements with equivalent precision.

### REFERENCES

- 1) E. Lifshin, "The Generation and Detection of X-rays in the Electron Microprobe and Scanning Electron Microscope." Seventh National Conference on Electron Probe Analysis. Tutorial Session (1972)
- 2) A. Zolla, R.S. Willing, A. Falco and J.R. Seward, "A Combined Electron Probe Microanalyzer-Scanning Electron Microscope." Eighth National Conference on Electron Probe Analysis. (1973)

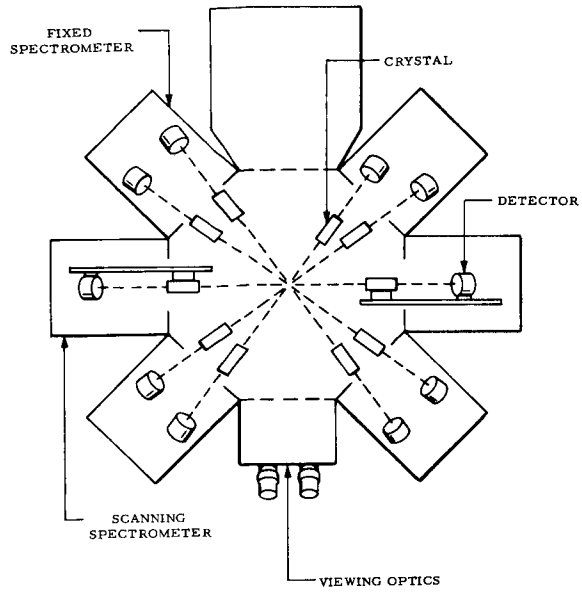


FIG. 1

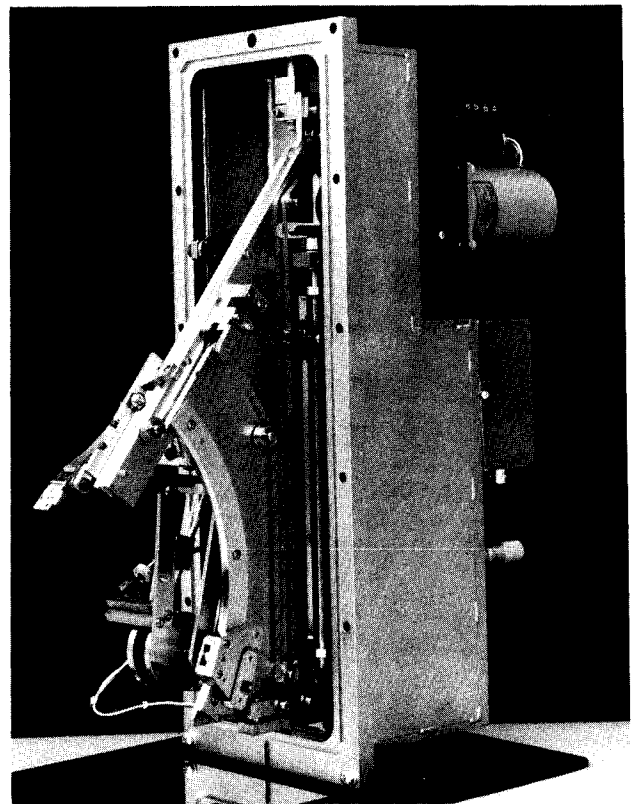


FIG. 2

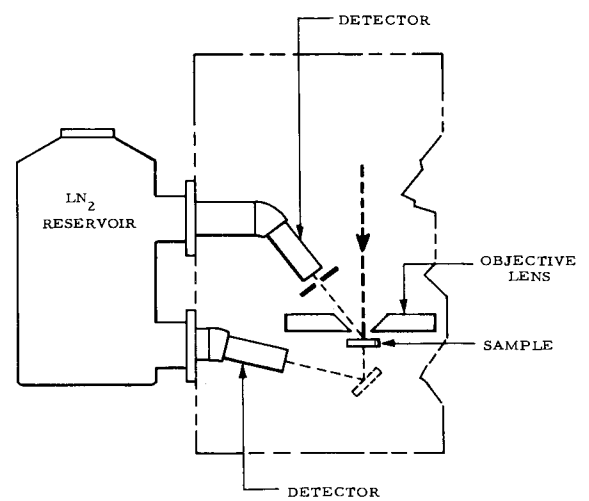
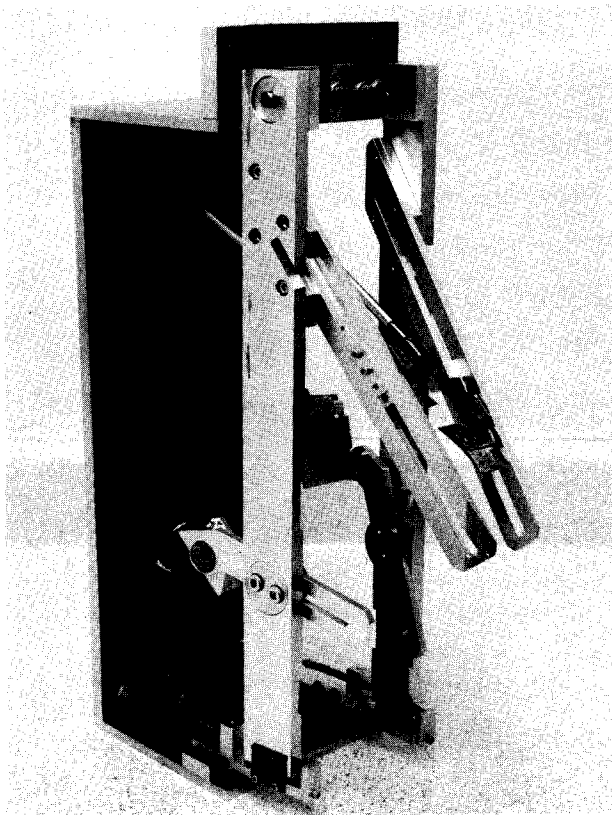


FIG. 4

# A SIMPLE DEVICE FOR VOLUME FRACTION ANALYSIS IN THE SCANNING ELECTRON MICROSCOPE

by

W.T. Hatfield, E. Lifshin, and M.R. Jackson  
General Electric Corporate Research and Development Center

Although the concept of direct volume fraction analysis in the scanning electron microscope and electron microprobe has been well established for some time, relatively few practical examples of applications of this method have appeared in the literature<sup>1-4</sup>. One possible explanation is the lack of a comparatively simple and inexpensive module which can be interfaced to most scanning instruments without the requirement of a computer for data processing or a separate scan generator to control the electron beam. Even without these limitations, other useful features such as multiple discriminators, associated logic circuits, and a variety of hardwired stereological functions are often unnecessarily expensive if the goal of a particular analysis is simply a volume fraction determination based on a single signal.

This paper describes a gating circuit to control a timer, which is turned on only when the beam crosses a preselected phase during the acquisition of a normal scanning electron micrograph. In samples where this phase is randomly distributed, the volume fraction is simply given by the fraction of the total scan time that the timer is on. The threshold level is selected by moving a DC level indicator across the profile monitor of the secondary electron image until the desired phase is isolated. Figure 1 illustrates this technique as applied to TaC rods and blades in a cobalt base superalloy. It shows the response of the system during one line of a thousand line picture. The basic counting interval and response time of the timer were chosen at



faster than one microsecond to reduce the possibility of systematic errors associated with gating the timer on and off a large number of times during a scan. This point was further checked by an experiment in which the beam was scanned over a homogeneous sample and blanked 50% of the time by a square wave to simulate a two phase structure with a constant volume fraction but with varying numbers of particles per unit volume. Table 1 indicates only minor variations in volume fraction over a wide range of blanking rates.

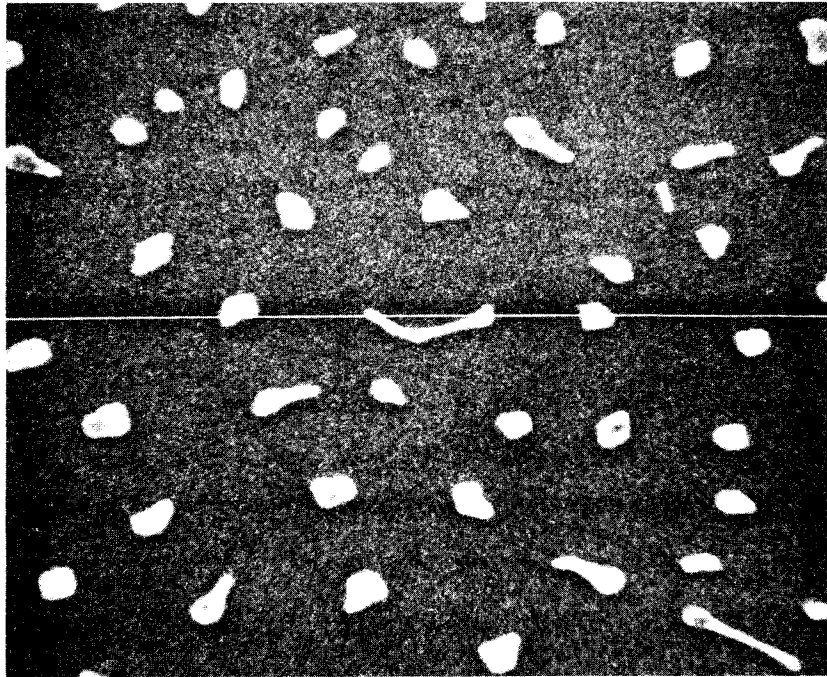
Results from several Co base TaC alloys are presented in Table 2, which shows both variations between alloys and between different fields for the same alloy. The gating technique has proved very useful for the analysis of this type of sample, and is shown to have many advantages including greater speed, accuracy, contrast, and resolution over competitive optical methods.

#### References

1. Heinrich, K.F.J., (1966) NBS Tech Note 401.
2. Dorfler, G., (1968) Quantitative Electron Probe Analysis, NBS Special Technical Publication 298, p. 215-267.
3. White, E.W., et. al., (1968), Proc. of the 1968 Symposium on the SEM, Om Johari, editor, IIT Research Institute, Chicago, p. 95-103.
4. Dorfler, G. and Russ, J.C. (1970) Proc. of the 1970 Symposium on the SEM, Om Johari, editor, IIT Research Institute, Chicago, p. 67-72.

82c

Line of scan



10  $\mu$

Threshold  
Secondary  
Electron  
Signal

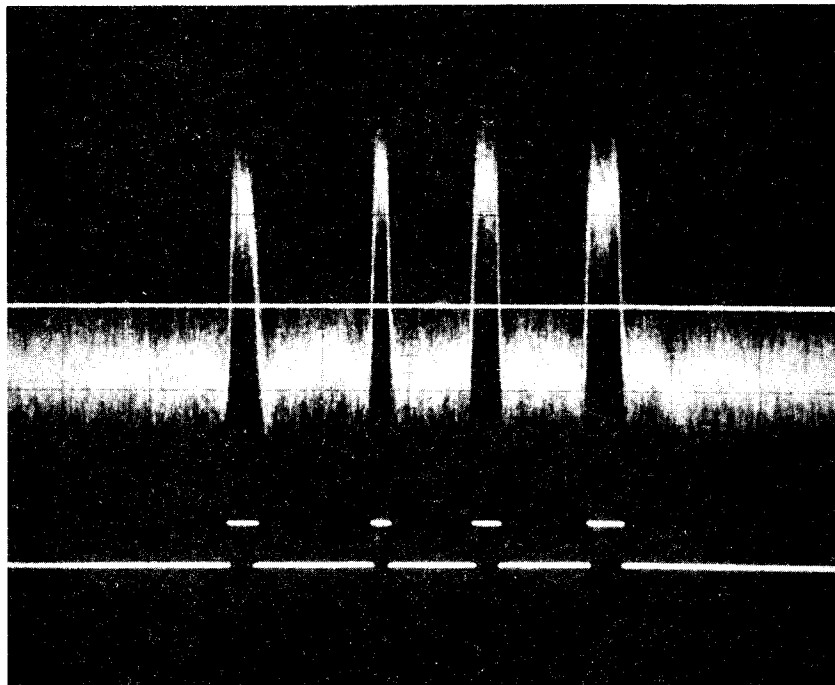


Figure 1 TaC in a Co Base Alloy

Table 1. Volume Fraction for 50 Percent Blanking

<u>Total Blanking/Frame</u>	<u>Volume Fraction</u>
$10^3$	$50.002 \pm 0.391$
$10^4$	$50.703 \pm 0.667$
$10^5$	$51.417 \pm 1.108$

Table 2. Volume Percent of TaC Obtained For Ten Different Areas on Three Cobalt Base Superalloy Samples.

<u>Sample A</u>	<u>Sample B</u>	<u>Sample C</u>
6.997	7.658	5.892
6.878	7.691	6.116
7.092	7.591	6.375
7.118	7.537	6.620
6.650	7.627	6.258
6.856	7.932	6.174
6.766	7.803	6.416
6.983	7.879	6.140
6.605	7.873	6.040
6.699	7.721	6.067

AN IMAGE COMPARISON SYSTEM FOR  
ELECTRON OPTICS INSTRUMENTATION

Gary Judd and Richard Wilson

Materials Division  
Rensselaer Polytechnic Institute  
Troy, New York 12181

Howard Weiss

Raytheon Company  
Equipment Development Laboratory  
Boston Post Road  
Wayland, Massachusetts 01778

---

In many applications of electron optics instrumentation techniques, especially in scanning electron microscopy, comparisons of sample topographies must be made. It is often required that a single sample be viewed both before and after a given treatment to determine the effect on the topography of the sample. Such studies have been limited by difficulties in the precise repositioning of the sample with respect to the electron beam and the electron detection system. This effect is particularly severe with irregular samples which may vary in thickness or tilt when mounted for SEM observation such that significant differences in apparent orientation may be created. It is desirable to remove these differences to facilitate qualitative and quantitative comparisons.

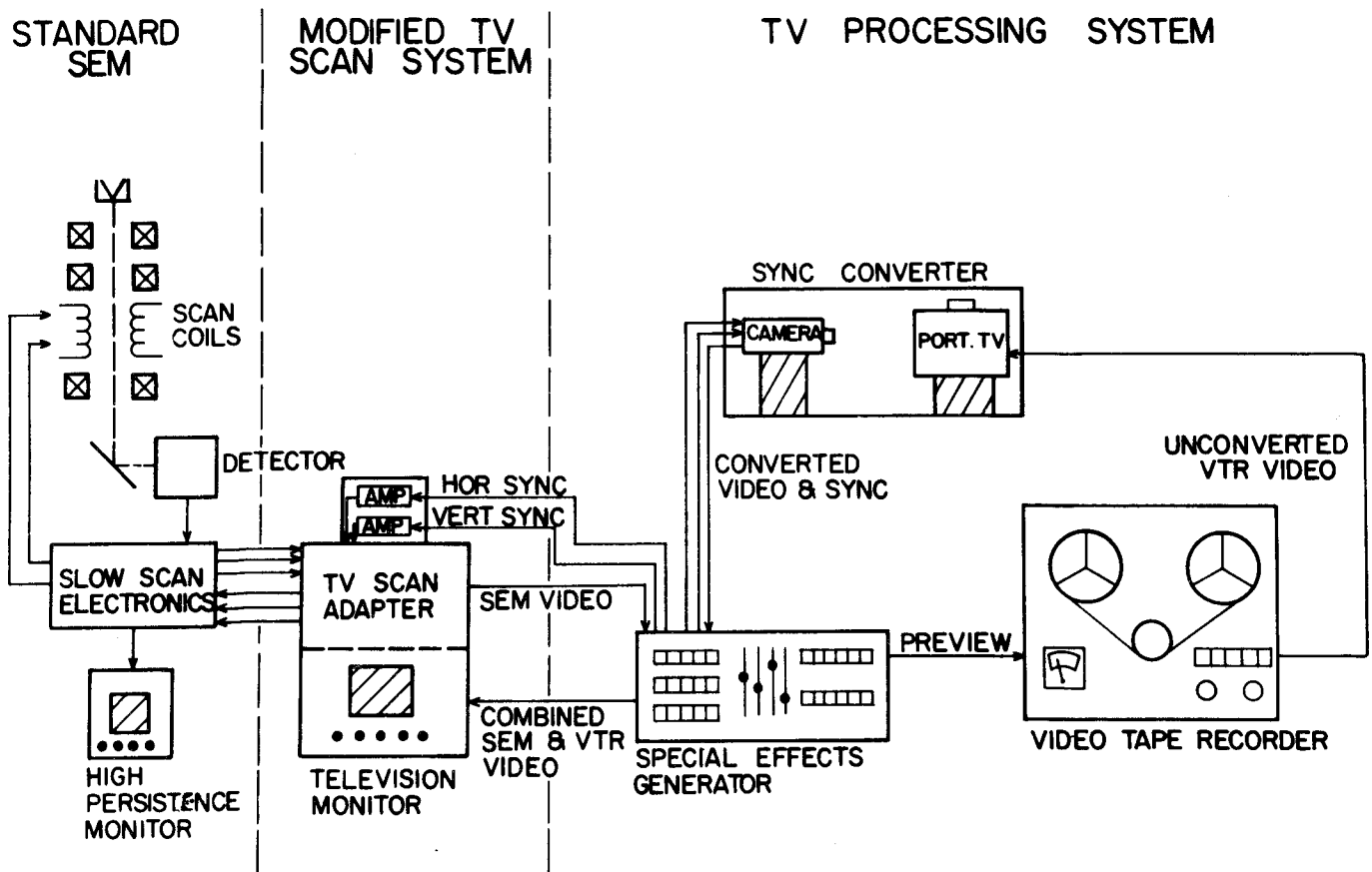
A system was developed<sup>1</sup> which allowed for the storage of images from the SEM for use in subsequent comparison displays. It assists the operator in rapidly and accurately positioning a sample so that orientation differences can be removed or minimized. The system employs a special effects generator as a control and image processing module for the SEM with TV scan imaging, a video tape recorder (VTR), and a TV display monitor. A "sync converter" was necessary to provide compatible synchronization for the developed system with the playback mode of the VTR, and an inexpensive design was employed for this purpose.

The comparison procedure consists of using split-screen and super-position images to determine the sample positioning changes that must be made in the SEM. The split screen technique employs a visual comparison of the recorded with

the live image on the same screen while the super-position method employs an electronic cancellation of topographical features when the live sample position duplicates the recorded sample position. Photography is not required except as a final record of the sample in the desired orientation. In addition, the ability to image a single frame on the VTR means that several different orientations or magnifications can be recorded in a few minutes and the tape can be stopped to give the recorded image indefinitely.

Although this system was developed and applied for forensic science applications, it could be successfully used in many investigations employing various types of electron optics instrumentation.

1. G. Judd, R. Wilson, and H. Weiss, "A Topographical Comparison Imaging System for SEM Applications", SEM-IITRI Symposium, 1973, pp. 167-172.



Schematic of the Comparison Imaging System

## MICROPROBE TECHNIQUES FOR THE ANALYSIS OF RADIOACTIVE MATERIALS

Dennis O'Boyle

University of Wisconsin and Argonne National Laboratory  
Argonne, Illinois 60439

Starting in the late 1950's, investigators recognized the importance of the electron probe in identifying microstructural features observed in irradiated nuclear fuels. As the trend toward higher fuel burnups continued, approaching ten atomic percent in fast breeder reactor fuels which results in twenty atomic percent of fission products, it became evident that to understand the behavior of nuclear fuels it would be necessary to analyze highly radioactive fuel specimens with the electron probe. In this paper we review the development of various experimental techniques for analyzing highly radioactive nuclear fuel materials.

The main problems of interest in nuclear fuel studies can be divided into four categories: 1) fission product behavior in the fuel, 2) cladding reactions with the fuel, fission products, and coolants, 3) radial redistribution of the fuel components, mainly uranium, plutonium, and oxygen, and 4) general problems such as precipitation of impurity phases, corrosion, and fuel homogenization. A review of the current understanding of many of these problems has been presented recently by Johnson<sup>1</sup>.

Following irradiation, nuclear fuel materials become intensely active gamma sources, emitting gamma rays having energies principally in the range from 0.4 to 1.0 Mev. The analysis of gamma-active fuel specimens presents the analyst with three separate problems: 1) instrument contamination, 2) reduced analytical sensitivity due to increased background, and 3) biological hazards to the probe operator. The first problem is eliminated by proper sample preparation and will not be discussed further. Both the increase in background, due to gamma-induced fluorescence of the detector materials, and the biological hazard depend strongly on the gamma activity of the specimen and the design of the instrument. In general if the activity of the specimen can be reduced by sample preparation to less than about 20 mR/hr at 30 cm, the specimen can be analyzed without any modification of the commercial microprobe. This technique has been used extensively by early investigators<sup>2,3,4</sup> of fission product behavior in irradiated oxide fuels and is commonly referred to as the "small sample approach." In all studies of irradiated fuel specimens, pulse height discrimination is utilized to reduce the background due to fluorescence. The lower the level of the gamma-induced background, the more effective is electronic discrimination in further reducing the background.

In order to analyze quantitatively fuel specimens of intermediate gamma activity, 100 mR/hr to 2 R/hr at 30 cm, it is necessary to reduce the gamma-induced background by means of heavy-metal shielding placed between the specimen and the x-ray detectors. Shielding materials used in the "limited shielding approach" are lead,<sup>5</sup> tungsten, and in one case<sup>1</sup> pure platinum.

Generally it is most convenient to examine irradiated fuel specimens that have been prepared for metallographic studies and are mounted in standard metallurgical mounts. Since the gamma activity of these specimens is extremely high, often several hundred R/hr at 30 cm, it becomes necessary to provide biological shielding for the probe operator in addition to improved shielding of the x-ray detectors. Commonly the biological shielding is designed to limit the exposure of the operator to ionizing radiation of 2.5 mrem per hour, corresponding to the occupational dose limit<sup>6</sup> of 5 rem per year. Electron microprobes with complete biological shielding have been described by Scotti *et al.*<sup>7</sup>, Giacchetti and Ransch,<sup>8</sup> and by Morlevat *et al.*<sup>9</sup> In addition to these user-modified probes, commercial shielded microprobes have been developed and are described by Macres *et al.*<sup>10</sup> (MAC-450) and by Bazin *et al.*<sup>11</sup> (Cameca MS-46 R). Computer programs for quantitative microprobe analysis of radioactive specimens have been developed by Natesh, Butler, and O'Boyle.<sup>12</sup>

Shielded microprobe laboratories often use one of two different methods for transferring specimens from the metallographic preparation hot cell to the microprobe: 1) transfer in a movable transfer cask or 2) transfer via a shielded tube to an interim transfer station located adjacent to the shielded microprobe. In this paper we will review these transfer methods as well as describe the shielded microprobe facilities at several national laboratories.<sup>13, 14, 15</sup>

### References

1. C. E. Johnson, Applications of Electron and Ion Microprobe Techniques to the Study of Nuclear Fuels, 8th National Conference EPASA, New Orleans (1973).
2. B. T. Bradbury, J. T. Demant, P. M. Martin, and D. M. Poole, J. Nucl. Mat. 17, 227 (1965).
3. D. R. O'Boyle, F. L. Brown, and J. E. Sanecki, Trans. Am. Nucl. Soc. 10, 462 (1967).
4. T. R. Padden, R. Burton, and C. E. Campbell, USAEC Report WAPD-TM-644, 1967.

5. W. F. Zelezny and R. A. Moen, p. 14, USAEC Report IDO-17191, 1965.
6. R. E. Bolz and G. L. Tuve, eds, Handbook of Tables for Applied Engineering Science, Chemical Rubber Co., Cleveland, p. 381 (1970).
7. V. G. Scotti, J. M. Johnson, and R. T. Cunningham, Advances in X-Ray Analysis, (G. R. Mallett, ed.) Plenum Press, New York, V. 9, p. 314 (1966).
8. G. Giacchetti and J. Ransch, V<sup>th</sup> International Congress on X-Ray Optics and Microanalysis (G. Mollenstedt and K. H. Gaukler, eds.), Springer-Verlag, Berlin, p. 250 (1969).
9. J. P. Morlevat, J. C. Janvier, and J. Roussignol, French AEC Report CEA-N-1507, (in French) (1971).
10. V. G. Macres, O. Preston, N. C. Yew, and R. Buchanan, V<sup>th</sup> International Congress on X-Ray Optics and Microanalysis (G. Mollenstedt and K. H. Gaukler, eds.), Springer-Verlag, Berlin, p. 248 (1969).
11. J. Bazin, N. Vignesoult, E. Roussel, C. Conty, and J. Guernet, VI<sup>th</sup> International Congress on X-Ray Optics and Microanalysis, Osaka, Japan (1971).
12. R. Natesh, E. M. Butler, and D. R. O'Boyle, USAEC Report ANL-7794 (1971).
13. R. Natesh, B. J. Koprowski, E. M. Butler, and D. A. Donahue, Proc. 16th Conference on Remote Systems Technology, Am. Nucl. Soc., Hinsdale, Illinois, 243 (1969).
14. E. L. Long, Jr. and J. L. Miller, Jr., Proc. 19th Conference on Remote Systems Technology, Am. Nucl. Soc., Hinsdale, Illinois, 132 (1971).
15. N. Vignesoult, J. Bazin, J. Monier, and G. de Contenson, Proc. 20th Conference on Remote Systems Technology, Am. Nucl. Soc., Hinsdale, Illinois, 123 (1972).



## A NEW TECHNIQUE FOR DECONVOLUTION OF COMPLEX X-RAY ENERGY SPECTRA

F. H. Schamber

Northern Scientific, Inc., Middleton, Wisconsin

The availability of high resolution Si(Li) detectors has stimulated serious interest in the use of X-ray Energy Spectroscopy (XES) for routine quantitative composition analysis. When compared to the well established Wave Dispersive Spectroscopy (WDS) technique, the XES approach is found to offer advantages in terms of sensitivity and simplicity but suffers from inferior spectral resolution. Although the X-ray energy resolution of modern solid-state detectors is quite adequate for most qualitative analyses, the resolution limitations have profound implications for quantitative analysis:

- 1) The Peak-to-Background ratio (P/B) of the characteristic radiation to the underlying continuum is decreased. The increased relative magnitude of the background correction not only increases the statistical uncertainty (degraded precision) but significant systematic biases can also be easily introduced.
- 2) Increased peak widths result in numerous overlaps in systems of practical interest ranging from relatively minor interference (e.g. Ni-Zn) to very severe (e.g. Pb-S). Failure to accurately account for such overlaps can result in grossly inaccurate determinations.

Since fundamental theoretical resolution limits are being approached by modern Si(Li) detectors, further drastic improvements in detector resolution are not to be anticipated and it thus follows that greater sophistication in data reduction techniques must play a major role in the full utilization of XES as a quantitative technique.<sup>(1)</sup>

It is the purpose of this paper to report on a new technique, "Multiple Least-Squares Fitting" (ML), which has recently been implemented for routine on-line deconvolution of complex spectra using a small dedicated digital computer. The most significant aspect of this technique is the ability to accommodate both of the above resolution induced effects and thus produce accurate measurements of peak intensities in the presence of both large background corrections and severe peak overlaps.

Previously available XES data reduction techniques have mainly concentrated on methods of "background subtraction". The "classical" background subtraction technique has been to assume a simple functional shape for the local continuum (e.g. a straight line), and measure the parameters (amplitude and slope) of the assumed continuum function at nearby peak free regions. The computed background shape is then subtracted from the spectrum and the remaining peak area is integrated. Under ideal conditions, this simple approach can give nearly optimal performance in terms of accuracy and precision. A serious practical problem is the frequent difficulty in locating nearby "background" regions from which the functional parameters can be inferred.

An alternative approach to background subtraction is the use of "frequency filters". The basic premise of this approach is that the spectral peak shapes

are characterized by intermediate frequency components whereas the continuum and channel-to-channel fluctuations can be characterized as dominantly low-frequency and high-frequency components respectively.\* Thus, a judiciously chosen digital filter is in principle capable of selecting out the frequency band (shape) of interest.<sup>(2, 3)</sup> A major difficulty in applying the technique to XES spectra is the variety of peak widths and shapes encountered. Since the filter must necessarily be "tuned" for peaks of a specific shape, it is not surprising that broad structures composed of weak unresolved lines are commonly interpreted as "continuum" components and erroneously suppressed.

Regardless of other merits and short-comings, "background subtraction" alone is incapable of offering relief for the major problem of overlapping peaks. To separate peak overlaps, it is necessary to resort to a regression analysis technique such as "least-squares fitting". Least-squares fitting using modified-Gaussian peak shapes is commonly employed in nuclear spectroscopy and is capable of excellent results.<sup>(4, 5)</sup> A practical difficulty in application of the technique is that the number of nonlinear peak shape parameters to be fitted (peak width, centroid energy, "tailing parameters", etc.) must be carefully limited if oscillating or divergent solutions are to be avoided. The most successful applications of this approach use calibrated peak shape parameters and fit for only centroid energy and peak area—even then, "difficult" overlap situations are usually treated via some form of direct operator intervention.

When applied to XES spectra, the fitting of Gaussian functional shapes becomes a very complex problem. Not only are peak overlaps very common, but nearly all characteristic X-ray peaks must themselves be treated as unresolved multiplets. Thus, although least-squares fitting is a very logical approach to XES spectral deconvolution, the logistical problems associated with accurate modeling of the peak shapes present a major difficulty. The ML solution to the above difficulties is to use measured pure-element spectra themselves as the fitting functions and thus simultaneously avoid the stability problems associated with heavily parameterized non-linear functions and still satisfy the requirement for an accurately detailed peak-shape model. Almost by definition, a measured pure-element spectrum with good statistics is the ultimate fitting function since all characteristic details of the spectral "fingerprint" for a given element are present—even detector "artefacts" such as escape peaks are accounted for.

In actual usage, the procedure is to acquire pure-element standard spectra for all elements likely to be present in the sample to be analyzed. These spectra are stored on magnetic tape for later usage. The unknown sample spectrum is acquired under identical excitation conditions (beam intensity, take-off angle, and excitation energy). A final set-up step is to roughly define the energy region-of-interest for the subsequent deconvolution and specify which standard

---

\* An argument which has been advanced in support of this technique for XES spectra would characterize absorption edges as "ultra-high" frequency components. This ignores the fact that the same statistical processes which degrade peak resolution also apply to every other component of the X-ray spectrum—absorption edges and peaks must appear in the same "frequency" band of the measured spectrum.

reference spectra are to be used. The ML program then proceeds to read-in the specified spectra and by an error-weighted linear least-squares computation the peaks characteristic of the respective standard spectra are simultaneously fitted to the peak content of the unknown spectrum. The output of this computation is the set of fractions ( $k = I/I_0$ ) which express the intensity composition of the unknown spectrum in terms of the assumed pure-element constituents. These ratios are the required input for any subsequent concentration analysis (e. g. ZAF correction program).

A significant virtue of least-squares fitting is that it allows the estimation of the statistical uncertainties in the computed parameters. Thus the ML output includes the precision ( $\pm \sigma_k$ ) predicted for each  $k$  value. Another important quantity appearing in the ML output is "CHI-SQUARED", a measure of the "goodness of fit". A large CHI-SQUARED value for an analysis provides a warning of inherent systematic errors in the fitting assumptions (e. g. unexpected peaks in the unknown spectrum).

It should be noted that the application of the technique imposes a minimum number of set-up details upon the operator. Specifically, the acquisition of pure-element standard spectra is always necessary for computation of  $k$  by any technique. When excitation conditions are adequately reproducible, a large library of standard reference spectra can be stored on magnetic tape and used for routine analyses. If measured pure-element standard spectra are not available, it is possible to synthesize the reference spectra from Gaussians.

The ML program has been used successfully to deconvolute complex SEM spectra containing from 2 to 6 overlapping components. A very large number of test cases have also been run using synthesized Gaussian peak shapes perturbed by random noise and curving backgrounds. The predicted statistical uncertainties are observed to approach the theoretical statistical limits for non-overlap test cases and increase gradually with increasing overlap interference as expected. Standard deviations actually measured for large numbers of runs are found to be adequately predicted by the computed estimates. No significant systematic biases have been observed in any of the tests conducted.

Complete analysis of a typical 6 element system requires about 75 seconds (including the retrieval of standards from magnetic tape and optional typing of the results). The program is written in assembly language for operation as part of the standard FLEXAN computerized analysis system and runs in an 8K PDP-11 computer.

# REFERENCES

- (1) D. R. Beaman and J. A. Isasi; "Electron Beam Microanalysis: The Fundamentals and Applications", Materials Research and Standards, Vol. 11, No. 11, Nov. 1971, p. 8.
- (2) A. L. Connelly and W. W. Black; "Automatic Location and Area Determination of Photopeaks", Nuc. Instr. and Meth., Vol. 82, 1970, p. 141.
- (3) T. Inouye; "Application of Fourier Transforms to the Analysis of Spectral Data", Nuc. Instr. and Meth., Vol. 67, 1969, p. 125.
- (4) R. G. Helmer and R. L. Heath; "Photopeak Analysis Program for Photon Energy and Intensity Determinations", Nuc. Instr. and Meth., Vol. 57, 1969, p. 46.
- (5) Jorma T. Routti; SAMPO, a Fortran IV Program for Computer Analysis of Gamma Spectra from Ge(Li) Spectra and for Other Spectra with Peaks, Lawrence Radiation Laboratory Report UCRL-19452, 1969.

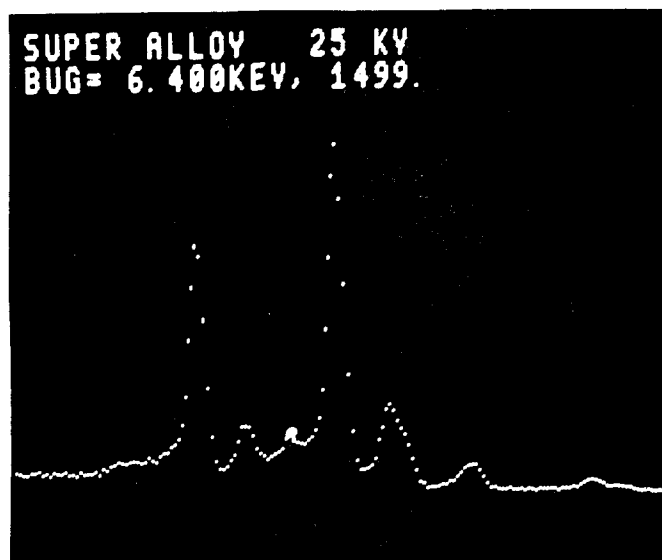


Figure 1. "Super Alloy" spectrum with Cr-Mn-Fe-Co-Ni-W overlaps.

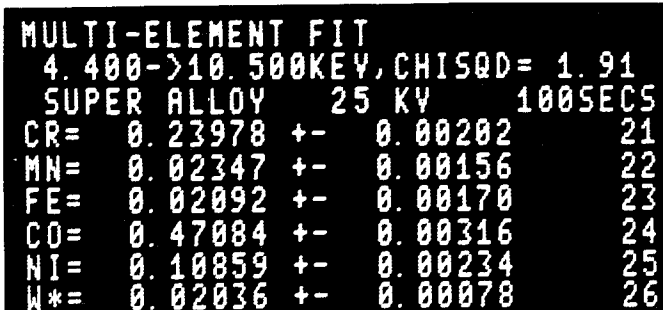


Figure 2. Output of ML deconvolution program.

OBSERVATIONS ON THE PRACTICAL APPLICATIONS  
OF SELECTED AREA ELECTRON CHANNELLING  
PATTERNS TO DEFORMATION STUDIES

J. A. Cornie, D. L. Harrod and C. W. Hughes  
Materials Science Section

METALLURGY AND METALS PROCESSING DEPARTMENT  
Westinghouse Research Laboratories  
Pittsburgh, Pennsylvania 15235

ABSTRACT

Experiments are presented demonstrating the practical applications and limits of the SAECP method as a microscopic tool for gauging plastic strain. Pattern resolution depends upon state of strain and residual stress as well as dislocation density and distribution. Inhomogeneous deformation on a microscopic scale leads to large but real variations in pattern resolution from grain to grain and from point to point within a given grain. The sub-structure resulting from high temperature deformation produces SAECP's with broader lines than those resulting from an equal amount of deformation at room temperature.

INTRODUCTION

The potential for using electron channelling patterns, particularly selected area patterns (SAECP), in plastic deformation studies has been impressively demonstrated by Stickler and Booker,<sup>(1)</sup> and their work has aroused widespread interest in practical applications of the technique. In addition to crystallographic information, SAECP's provide qualitative and quantitative measurements of plastic strain in selected areas as small as 5  $\mu\text{m}$  across and 100 angstroms deep. Further, the strain distribution over any desired area can be obtained by point-by-point observations. The technique is relatively new, however, and a number of problems arise in interpreting quantitative strain measurements. Some of these problems are discussed in this report.

The experiments described were run on 304 SS and were part of a more general and continuing study of plastic strain distributions at the microstructural level due to creep, fatigue and creep-fatigue interactions.

### EXPERIMENTAL CONDITIONS

The SAECP study was performed on a Cambridge Mk2 Stereoscan scanning electron microscope. Selected Area Channelling Patterns (SAECP) were produced by the deflection-focusing rocking beam method suggested by Schulson and vanEssen.<sup>(2)</sup> It is necessary to reduce beam divergence to some value less than the angular width of the channelling lines to be measured. Therefore, a 100  $\mu\text{m}$  aperture was substituted for the spray aperture above the second condenser lens.

Conjugate focusing<sup>(3)</sup> was used to insure simultaneously minimum SAECP spot size and SEM focusing. The current to the second condenser lens was reduced by a small but set amount during switching to the SAECP mode to decrease the beam divergence. Resolution is expressed in terms of line width measured in mm with an x-ray film reader and converted to milli-radians (R) by the appropriate factors.

The following instrument conditions were determined during a performance optimization study:

Lens Current (amps)	C <sub>1</sub>	C <sub>2</sub>	C <sub>3</sub>
	.35	.35*	.915
Work Distance:	2 mm		
Accelerating Voltage:	20 KV		
Beam Current:	$6 \times 10^{-9}$ amps		
Beam Divergence:	SEM - $5 \times 10^{-3}$ radian		
	SAECP - $< 1 \times 10^{-3}$ radian		
Recording Mode:	specimen current		
Spot Size:	5 $\mu\text{m}$ at WD = 2 mm		

Specimens machined from hot rolled bar stock of 304 SS were annealed for 30 minutes at 2000°F in argon and fast cooled. The as-annealed grain size was .04 mm.

### RESULTS

#### Baseline Calibration Curve

Specimens were strained 0, 5, 9 and 12% in tension at constant strain rate ( $0.005 \text{ min}^{-1}$ ) at room temperature. Transverse (T) samples

---

\* Pole piece of second condenser lens removed and inserted into first condenser lens.

were prepared from the middle of the gauge section and one SAECP per grain was recorded for fifteen to twenty grains. The resolution of the finest line is shown as a function of tensile strain in Fig. 1a where the vertical bars give the range of R values and the solid points give the averages. For the annealed condition ( $\epsilon_1 = 0$ ) the range of R values is about 1.2 mrad which reflects the combined effects of inherent variations in width of different finest lines and the ability of the operator to reproduce the measurements. The range of R values increases with increasing strain. Two factors contribute to this: (1) the finest lines disappear (get washed out in the background noise) at high strains; (2) plastic deformation is inhomogeneous at the microscopic level. Extremes in resolution are reproducible within about  $\pm 1$  mrad. Thus large variations in R reflect large but real variations in local defect structure.

It was thought that some of the variation in R might be due to the relative size of the electron beam spot ( $\sim 5 \mu\text{m}$ ) to grain size. As shown by the data in Fig. 1b, no such effect was found for the annealed condition. However, there might be an effect at high strains due to an influence of grain size on heterogeneity of strain.

A second set of measurements was made on the specimen strained 12%. The sample was repolished but not etched and the results are shown in Fig. 1c. There was no significant difference in the range of R values for the two sets of measurements but the mean values differed by  $\sim 3$  mrad. Whether this was due to surface effects or due to skewed sampling of the distribution of R values is not known. It is noted, however, that both sets of data were made on the same sample and the difference of 3 mrad in mean values of R corresponds, according to the slope of the dashed line in Fig. 1a, to an uncertainty in strain of  $\sim 5\%$ .

It is reasonable to suppose that pattern quality is influenced by the dislocation distribution as well as density. This factor is related to the heterogeneity of deformation mentioned in connection with Fig. 1a. A specimen was sectioned longitudinally, transversely and at an angle of  $45^\circ$  to the tensile axis after receiving 5% strain. The results shown in Fig. 1d indicate no influence due to the plane of sectioning in this fine grained material strained in tension.

The inhomogeneous deformation explanation for the increasing range of resolution values with increasing deformation was tested by comparing the average of one SAECP from central regions of many grains with the average finest line resolution of many SAECP's from various regions within a single grain. The results in Fig. 1e show that there is little difference in the averages of one SAECP from many grains vs many SAECP's from a given grain. However, the range of values is greater within a given grain. This experiment indicates that non-uniform deformation is responsible for the range of R values shown in Fig. 1a where fifteen to twenty grains were measured at each strain level.

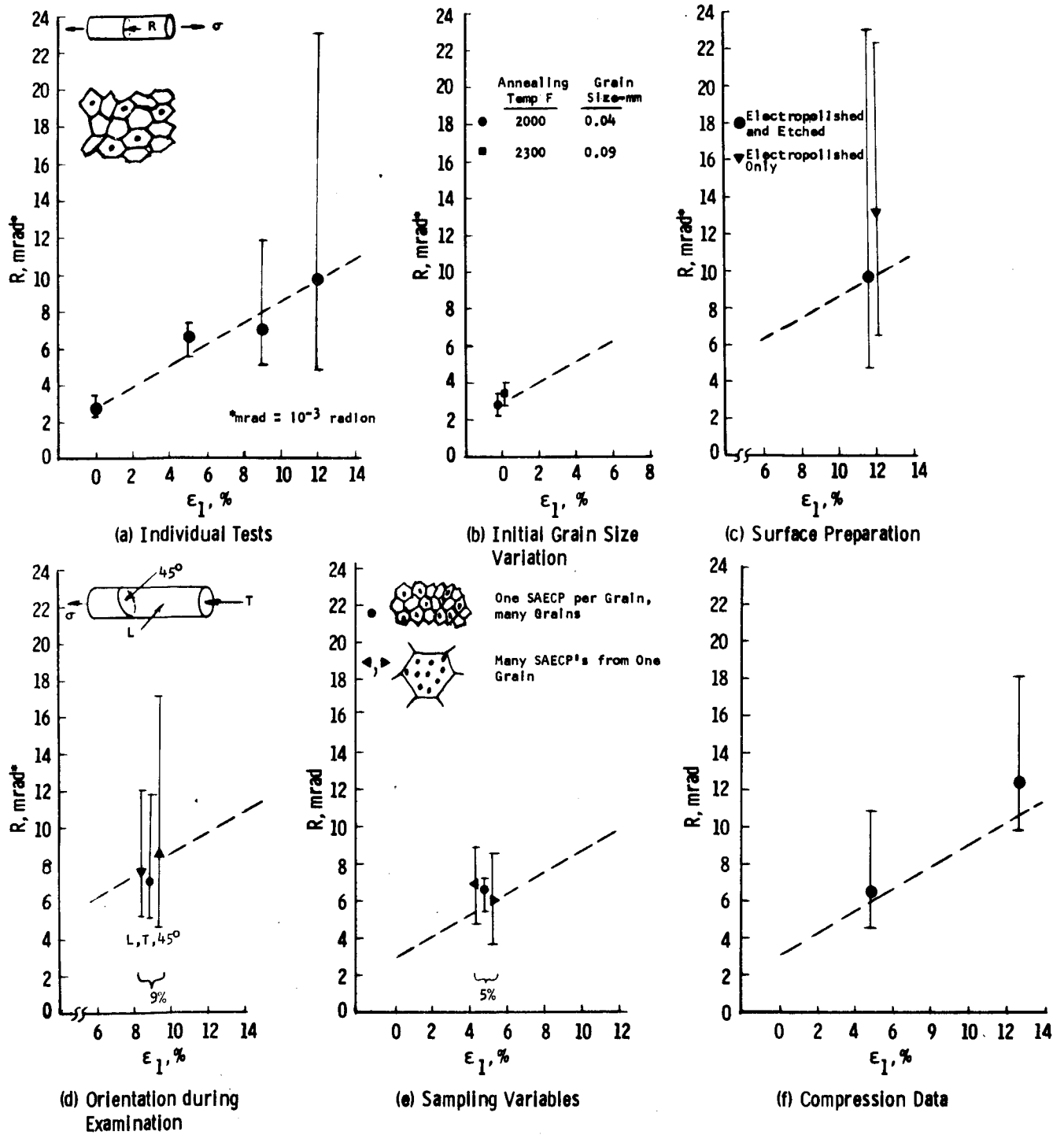


Fig. 1—Influence of experimental techniques on SAECP pattern resolution,  $R$



Compressive tests were also evaluated by SAACP resolution measurements. No significant difference between the tensile and compressive data could be detected from Fig. 1f.

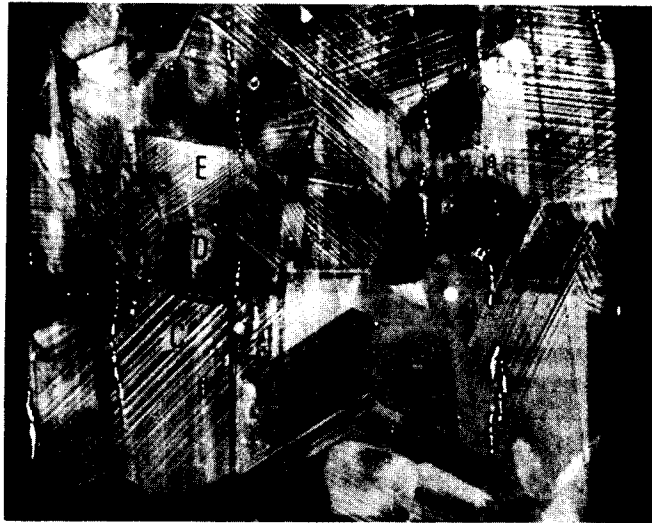
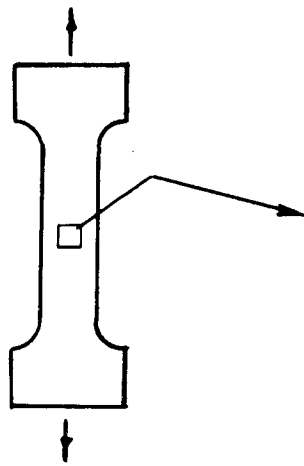
#### Individual (hkl) Line Variation with Strain

One would expect the pattern resolution of individual indexed (hkl) lines to increase uniformly with increasing strain with less variability in measured values than obtained in the finest line technique. An experiment was devised to follow the resolution of the finest lines of a few selected grains (Fig. 2a) after incrementally straining to 0, 2%, 4%, 7% and 10%. The orientations were located on the ECP map in Fig. 2b. The variation of the finest line in each grain is shown in Fig. 2c and averaged for the five grains in Fig. 2d. The increase in  $R$  with  $\epsilon_1$ , was not regular for all grains.

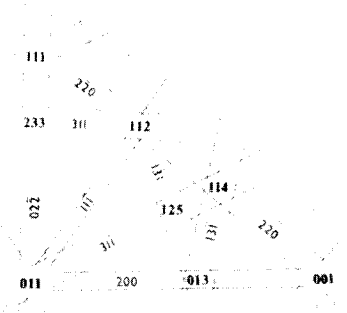
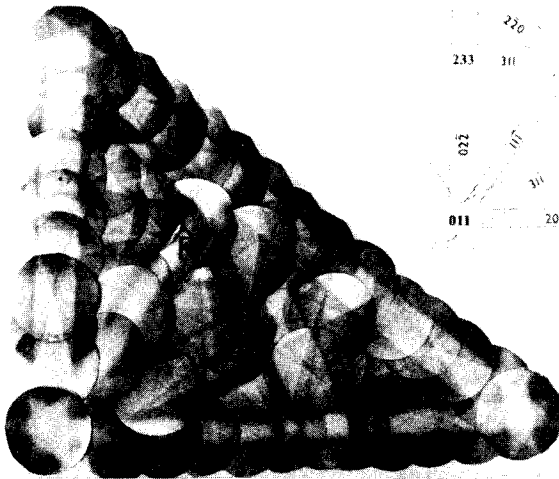
A number of lines were indexed for grain B and followed with incremental straining in Fig. 3. The SAACP's show the line identification and the usual deterioration of resolution with increasing deformation. The (220) line showed a uniform increase in  $R$  with increasing  $\epsilon_1$  -- as did the finest line. The  $(\bar{3}11)$  and  $(1\bar{3}1)$  lines which are of the same form differ radically in  $R$  and trend. Likewise pair lines of the  $\{420\}$  form have widely differing trends. The higher indexed  $\{133\}$  type lines were much better behaved and differed little from the finest line measurements.

These data are in disagreement with the findings of Stickler and Booker<sup>(1)</sup> who reported several selected (hkl) lines to increase uniformly at about the same rate as the finest lines. The variation of a given indexed line resolution from one strain increment to another may be related to the inhomogeneous deformation factors discussed in reference to Fig. 1e. However, at a given strain level the large difference in resolution between sets of (hkl) lines of the same form must result from other factors.

Room temperature deformation of 304 SS occurs by planar slip. Within a localized region deformation would be limited to one or possibly two slip systems. Thus the array of dislocations within this region could be described by one or possibly two  $\bar{b}$ . These data indicate that the resolution of a given line is influenced by its orientation with respect to  $\bar{b}$ . This statement has been recently confirmed by Joy<sup>(4)</sup> who reported that upon plastically deforming silicon crystals by bending, those lines perpendicular to  $\bar{b}$  are broadened while other lines of like (hkl) form but parallel to or at a small angle to  $\bar{b}$  are relatively unaffected by the deformation.



(a) Grains A, B, C, D, E after 2% Strain



(b) Orientation of Grains Examined

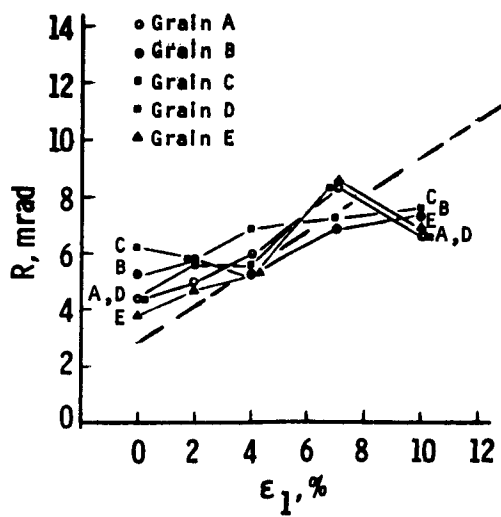
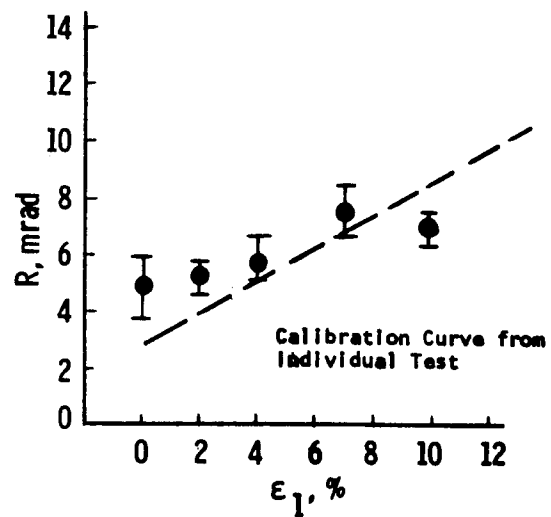
(c) R vs  $\epsilon$ , for finest lines on patterns (one per grain)(d) Average R vs  $\epsilon$ , for Grains A - E

Fig. 2 - Variation of resolution of finest lines in selected grains with incremental straining

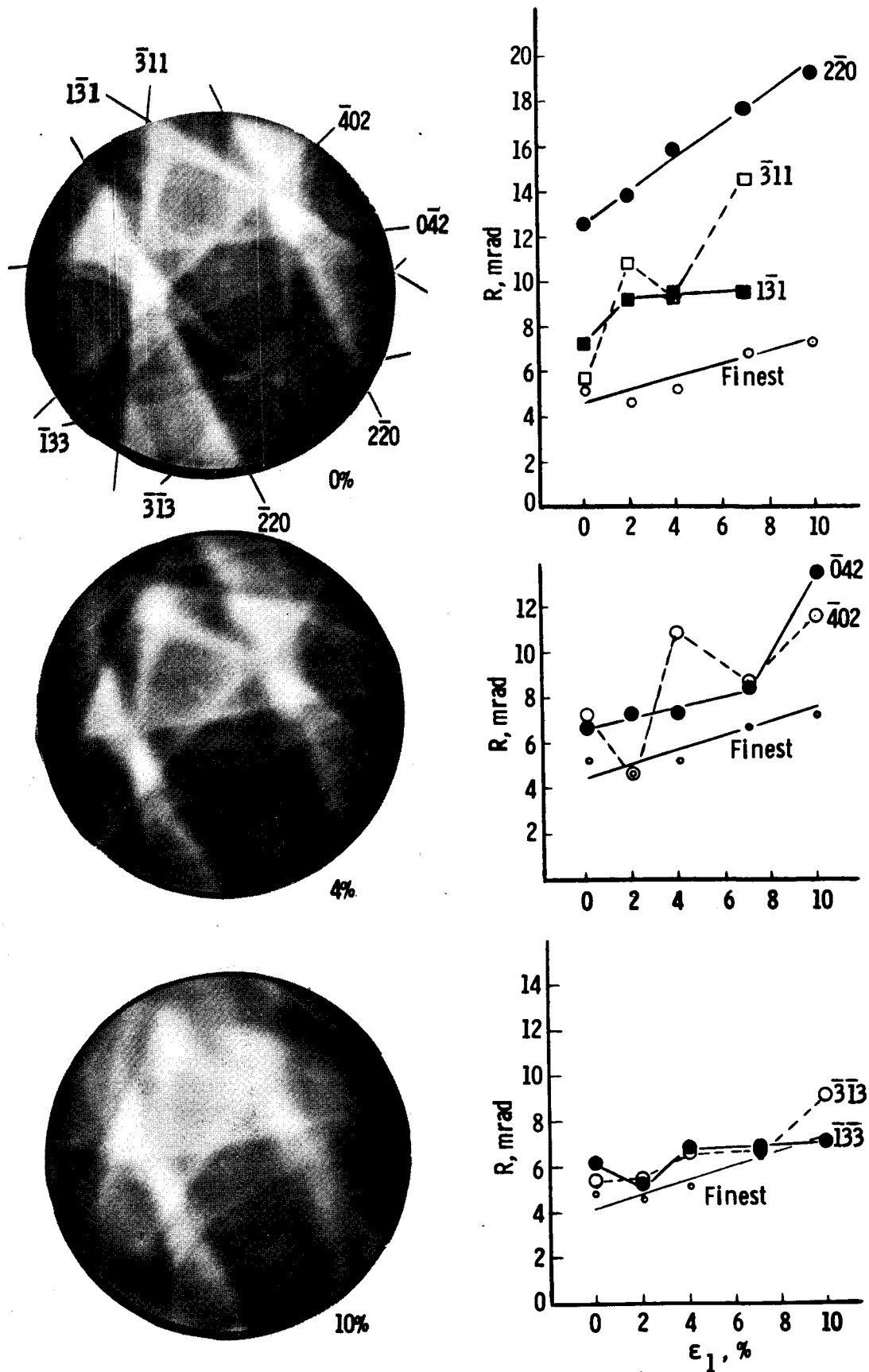


Fig. 3 — Effect of incremental strain on width of indexed lines from a selected grain (Grain B in Figure 2)

### Effect of Test Temperature and Creep Deformation on SAECP Resolution

Stickler and Booker<sup>(1)</sup> showed that recovery processes could be followed with SAECP measurements. Thus, we speculated that R should be lower for creep or hot tensile tests than for a like amount of deformation at room temperature. Surprisingly, this was not found to be so, as shown in Fig. 4. The 1200°F creep data lie somewhat higher and the 1200°F tensile data are significantly higher than the room temperature calibration curve.

The explanation of the higher R values for the 1200°F tensile and creep tests is not immediately obvious but may be related to a change of slip character from a planar slip mode at room temperature to a wavy slip mode at high temperature. Also the electron probe wanders about within the minimum SAECP spot during rastering due to spherical aberration of the final lens as described by Booker and Stickler<sup>(5)</sup> and demonstrated directly by Joy and Booker.<sup>(6)</sup> The effects of spherical aberration would be dependent upon details of the dislocation substructure.

### Effect of State of Strain on R

Pattern resolution is related to plastic strains. Since there are six components of strain, a question naturally arises as to which of these strain components is being measured. In particular, the relationship between R and the individual components of the strain tensor is important to failure analyses. To explore this, additional tests were run in torsion and flexure.

#### Torsion Tests

Torsion specimens were strained to maximum effective strains  $\bar{\epsilon}$  of 5% and 10% and sectioned as shown in Fig. 5. The strain should be a maximum at the O.D. and diminish to zero at some distance from the center of the section as shown schematically in Fig. 6. The SAECP traverse for the 10%  $\bar{\epsilon}$  specimen reveals such a gradient in Fig. 5. Each point along the gradient is an average of 5 SAECP measurements from adjoining grains. A similar gradient was noted for the 5%  $\bar{\epsilon}$  specimen. However, stains from the electropolishing solution were noted and the specimen was repolished and remeasured, and the resulting resolution gradient is shown in the lower curve of Fig. 5. Both curves for this specimen are shown to illustrate the importance of surface preparation in SAECP R measurements. The apparent peak at 2.3 mm may be spurious or it may be related to details of the residual stress distribution as shown schematically in Fig. 6. (Joy<sup>(4)</sup> recently reported that elastic strains caused considerable line broadening in silicon and that this is unexpected based on current theoretical considerations.) The general R level in the central region is 2-4 mrad greater than the initial pre-test resolution. This increase is most likely due to residual stress effects.

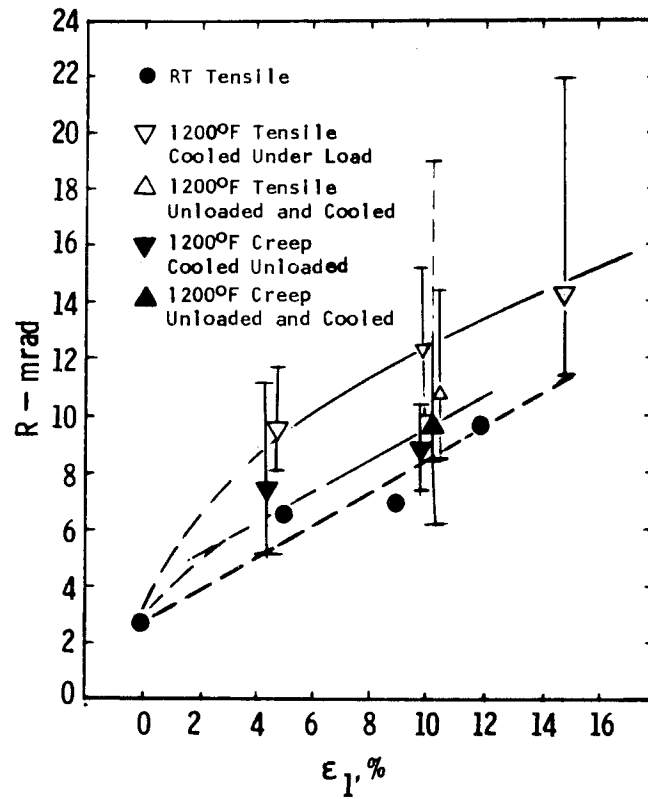


Fig. 4 – Effect of high temperature strain on  $R$

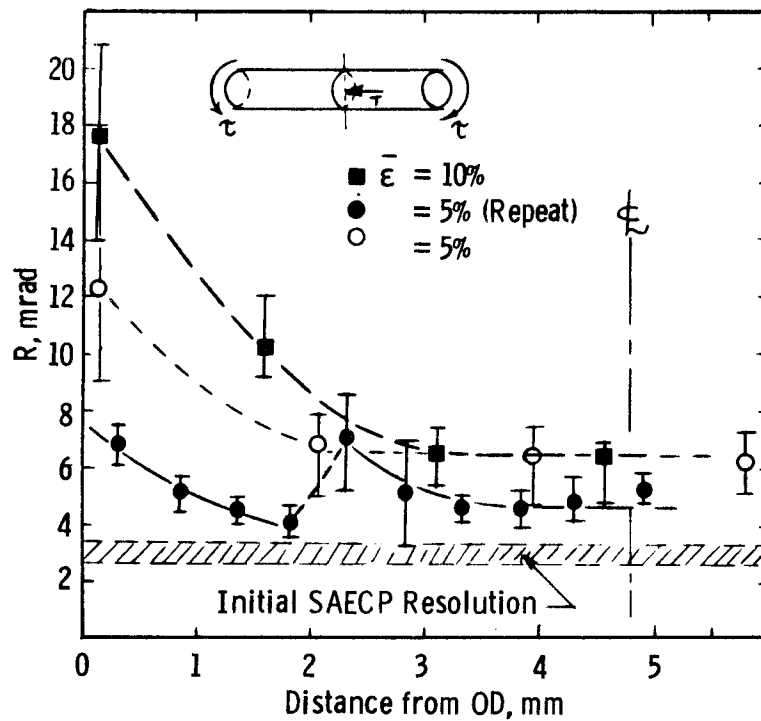


Fig. 5 – Resolution gradients in transverse sections of torsion strained specimens.  $\bar{\epsilon}$  at surfaces were 5% and 10%

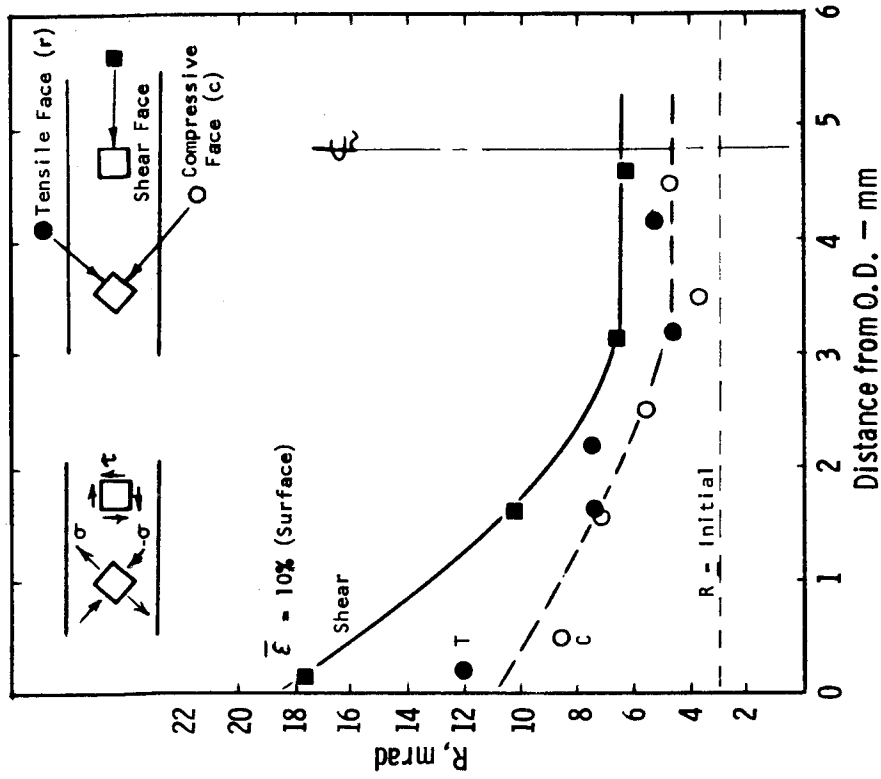


Fig. 7 — Effect of orientation on  $R$  in torsion test

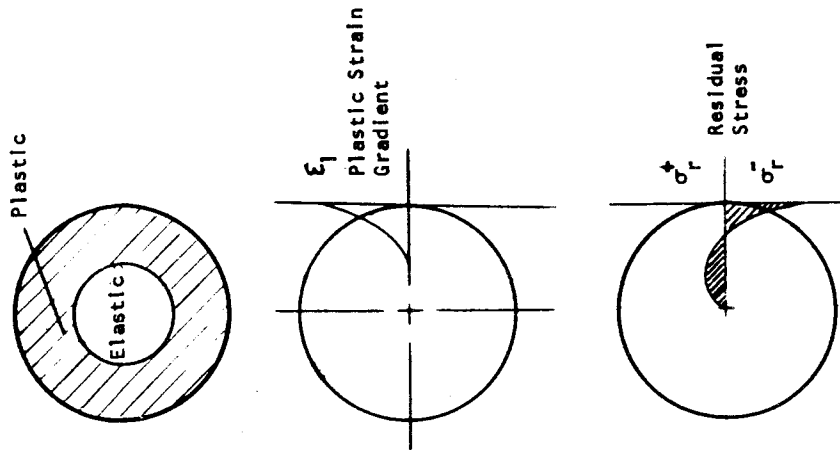


Fig. 6 — Schematic representation of plastic strain and residual stress distribution in torsion bar

The 10%  $\bar{\epsilon}$  specimen was sectioned perpendicular to the principal axes of tension and compression and gradients measured on these faces are compared with the shear face gradient in Fig. 7. Resolution gradients from the principal axial strain sections differed little from each other (i.e.,  $R_{\text{Tension}} = R_{\text{Compression}}$ ), as was noted earlier in Fig. 1e, but were significantly lower than the shear face (transverse section) gradient. Thus, for this torsion test the results did depend on the plane of sectioning.

### Flexure Test

The  $R$  gradient of a bend specimen deformed 5% in the outer fibers is shown in Fig. 8. The data was gathered from SAECP's taken on each grain encountered on a traverse across the section. All data fall within the limit of reproducibility, i.e.,  $\pm 0.5$  mrad. The central region was 2 mrad higher in resolution than in the pre-test condition and, as in the torsion test, this is probably an indication of an effect due to residual stresses.

### Comparison of States of Strain

The results of the tension, compression, torsion and flexure tests are summarized in Fig. 9 where  $R$  is plotted as a function of effective strain  $\bar{\epsilon}$ . The pattern resolution is seen to be dependent on the state of strain and the vonMises effective strain

$$\bar{\epsilon} = \frac{\sqrt{2}}{3} \sqrt{(\epsilon_1 - \epsilon_2)^2 + (\epsilon_2 - \epsilon_3)^2 + (\epsilon_3 - \epsilon_1)^2}$$

fails to provide a correlation of the results from different tests.

### Channelling Microscopy

Diffraction contrast is readily obtained in the SEM mode if the instrument is first conjugate focused in the SAECP mode to establish the optimum conditions. Thus contrast changes as the beam rasters from one well annealed grain to another, as shown in Fig. 10, is orientation and thus diffraction dependent. Those changes in contrast that do occur within a grain are due to the changing angle of incidence as the beam is rastered across the grain and thus across channelling bands. After deformation, the uniform bands are distorted into mottled regions in consequence to the changes in orientation from point to point. The degree of misorientation must be related in some way to the amount of plastic deformation. It is qualitatively apparent that the degree of mottling is proportional to the degree of plastic deformation. In one attempt to relate mottling to  $\bar{\epsilon}$ , the number of mottled regions within each grain in a 400 X field were counted. The average number of mottled regions per grain was then plotted vs  $\bar{\epsilon}$  for tensile and compressive specimens in Fig. 11.

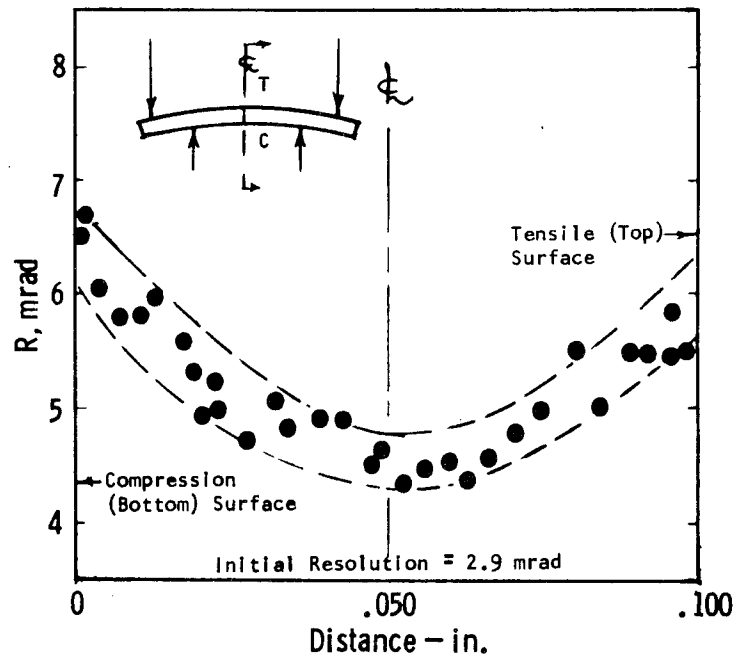


Fig. 8 – SAACP resolution gradient in in transverse section of flexure specimen.  $\epsilon_1 = 5\%$  at surface

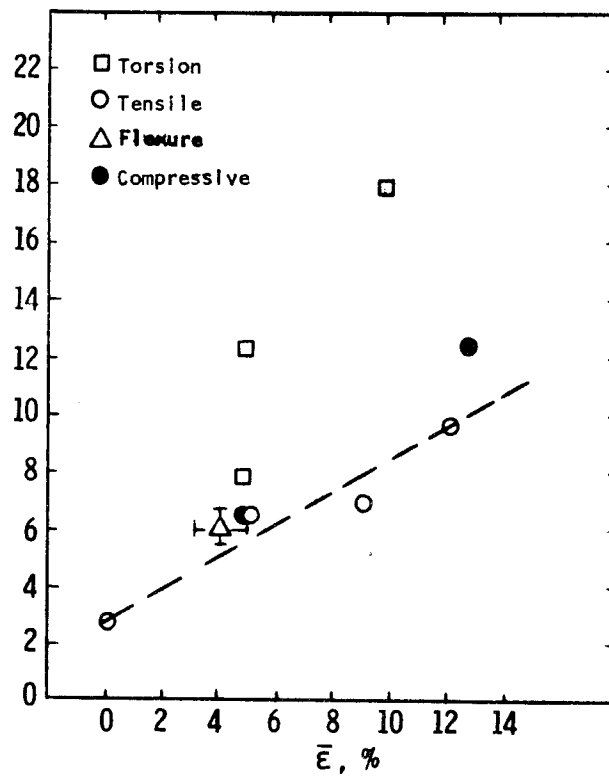
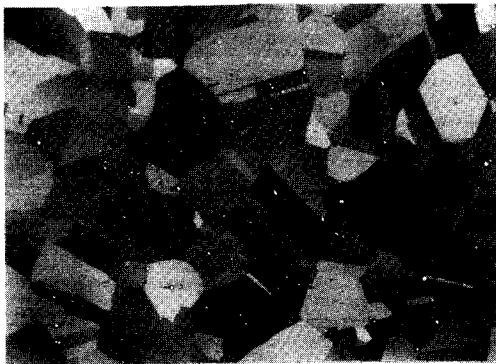
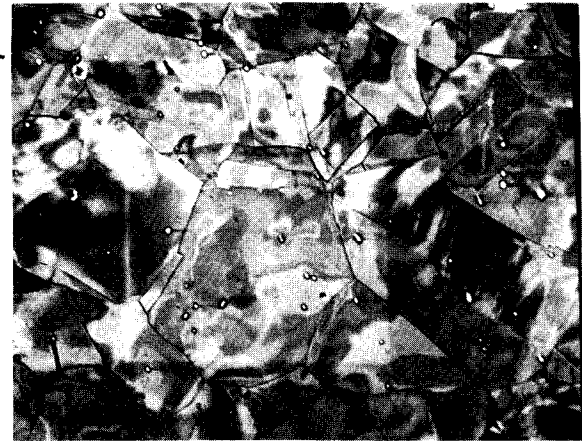
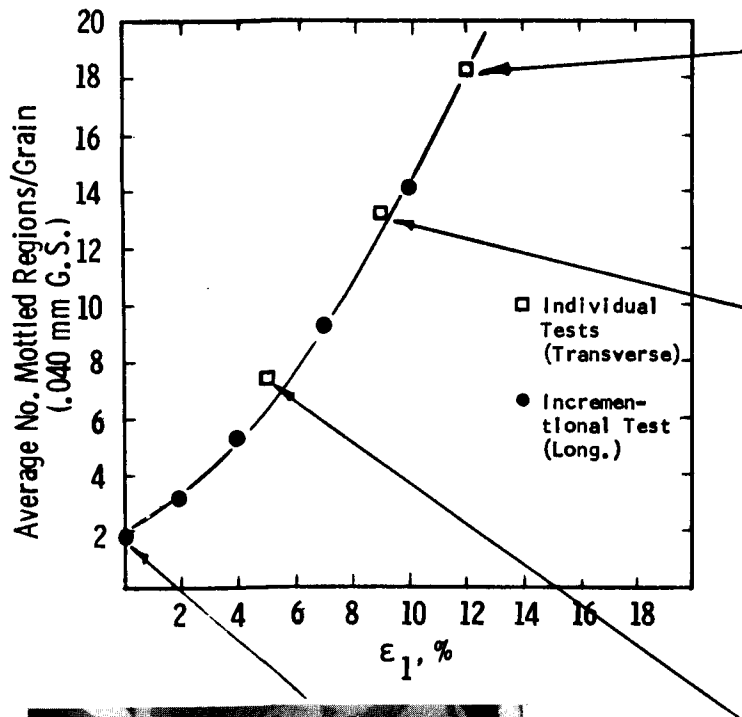
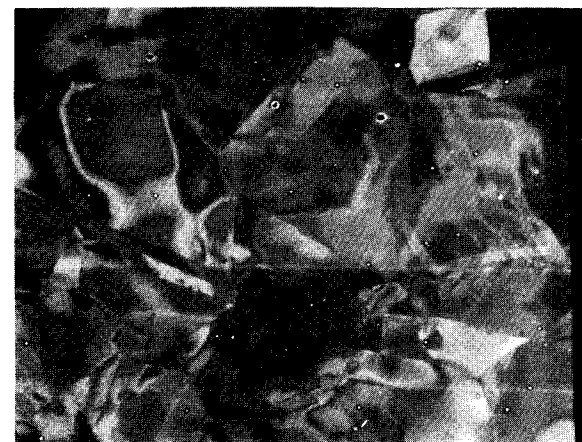


Fig. 9 – Effect of mode of deformation on  $R$





100 μm



100 μm

Fig. 10 — Variation of mottled structure with plastic strain

Although the counting method used here is rather subjective, the trend of the data was uniform, suggesting that there is a good possibility that quantitative metallographic techniques can be more universally applied. There is also a good possibility that this technique can be extended to high temperature deformation since details of dislocation arrangements would not be expected to affect the mottling to the degree as pattern resolution.

#### SUMMARY

The resolution of SAECP lines varies with state of strain and the results from tension, compression, torsion and flexure tests could not be correlated with the vonMises invariant strain function. Large variations in resolution are observed from point to point in a given grain due to the heterogeneity of deformation at the microscopic level and this variability increases with increasing macroscopic strain. Sufficient measurements are required to permit statistical analysis. The torsion and flexure test results suggest that elastic strains and residual stresses influence pattern resolution. Tensile creep and constant strain rate deformation at 1200°F produced greater line broadening than room temperature tensile deformation.

The SAECP technique remains an excellent tool for qualitatively analyzing plastic strain gradients. Such qualitative information is often sufficient for the solution of materials problems. The potential still exists for quantitative application of the SAECP tool. This work presented here should sharpen the focus for further investigation of the technique. Specifically, work should be concentrated upon determining the effects of elastic strains and dislocation substructures on R. Spherical aberration effects on R should be understood and/or eliminated. With the elimination of spherical aberration, methods of SAECP averaging through control of the minimum spot size could be developed.

The potential use of channelling microscopy as both a quantitative and qualitative tool was demonstrated. Quantitative metallographic methods must be developed to realize the potential of this new technique.

#### REFERENCES

1. R. Stickler and G. R. Booker, Proc. 5th International Materials Symposium (1971), 301, Electron Microscopy and Structure of Materials, G. Thomas, R. Fulrath and R. Fisher, Ed., Univ. of Calif. press, Berkeley (1972).
2. E. M. Schulson and C. G. vanEssen, J. Sci. Inst., 2, (1969), 243.
3. D. C. Joy and G. R. Booker, Proc. 5th Stereoscan Colloquium (1972), 77.
4. D. C. Joy, private communication.
5. G. R. Booker and R. Stickler, 5th Annual SEM Symposium (1972), 226.
6. D. C. Joy and G. R. Booker, 6th Annual SEM Symposium, (1973), 137.





# INDEX OF AUTHORS AND THEIR AFFILIATIONS

		<u>Paper Number</u>
Abraham, J. L.	U. S. Department of Health, Education, and Welfare, Appalachian Laboratory for Occupational Respiratory Diseases, National Institute for Occupational Safety and Health, P. O. Box 4292, Morgantown, West Virginia 26505	67
Adler, I.	Kelsey-Hayes Research and Development Center, Ann Arbor, Michigan 48105	79
Aitkin, E. A.	General Electric Company, Vallecitos Nuclear Center, Pleasanton, California 94566	70
Albain, J. L.	Arizona State University, Tempe, Arizona	35
Albee, A. L.	Division of Geological and Planetary Sciences, California Institute of Technology Pasadena, California 91109	45 77
Allard, L. F.	Department of Materials and Metallurgical Engineering, The University of Michigan, Ann Arbor, Michigan 48104	56 80
Ancey, M.	Groupe Metallurgie Physique, IRSID, 78104 Saint Germain- en-Laye, France	25
Andersen, C. A.	Applied Research Laboratories, Hasler Research Center, 95 La Patera Lane, Goleta, California 93017	4 9
Arnett, P. C.	IBM, Systems Products Division, Department G39, Building 966-2, P. O. Box A, Essex Junction, Vermont 05452	75
Autier, B.	Cameca Instruments, Inc., 101 Executive Blvd., Elmsford, New York 10523	5
Ayers, G. L.	IBM Research Laboratory, K33-281, Monterey and Cottle Roads, San Jose, California 95139	44
Bakale, D. K.	Materials Research Laboratory, University of Illinois, Urbana, Illinois 61801	7
Barnhart, M. W.	EDAX International, Inc., Raleigh, North Carolina	16
Barrett, E. J.	Department of Radiation Biology and Biophysics, University of Rochester, School of Medicine and Dentistry, Rochester, New York 14642	60
Baun, W. L.	Air Force Materials Laboratory (LN), Wright-Patterson Air Force Base, Dayton, Ohio 45433	33
Baxter, W. J.	Research Laboratories, General Motors Corporation, Warren, Michigan	38 39
Bayard, M. A.	W. C. McCrone Associates, Inc., 2820 South Michigan Avenue, Chicago, Illinois 60616	11

		<u>Paper Number</u>
Beaman, D. R.	The Dow Chemical Company, 574 Building, Midland, Michigan 48640	Tutorial
Benthusen, D. E.	Sandia Laboratories, Division 8312, Livermore, California	43
Bigelow, W. C.	Department of Materials and Metallurgical Engineering, The Univeristy of Michigan, Ann Arbor, Michigan 48104	56 80
Black, J. T.	University of Rhode Island, Kingston, Rhode Island	54, 55
Bleicher, J.	Department of Materials and Metallugical Engineering, The University of Michigan, Ann Arbor, Michigan 48104	80
Bolon, R. B.	General Electric Company, Corporate R&D Center, Schenectady, New York 12301	29 31
Brandis, E. K.	IBM, East Fishkill Facility, Hopewell Junction, New York 12533	20
Brown, J. L.	Georgia Tech., Atlanta, Georgia	47
Burns, L. C.	Northrop Services, Inc., P. O. Box 34416, Houston, Texas 77034	64 65
Castaing, R.	Laboratoire de Physique des Solides, Universite de Paris-Sud, 91405 Orsay, France	1
Chambers, W. F.	Sandia Corporation, Org. 1122, Box 5800, Albuquerque, New Mexico 87115	41
Chodos, A. A.	Division of Geological and Planetary Sciences, California Institute of Technology, Pasadena, California 91109	45
Christopher, J. L.	EDAX International, Inc., Raleigh, North Carolina	16
Ciccarelli, M. F.	General Electric Corporate R&D Center, Room 2C20, Bldg. K-1, P. O. Box 8, Schnectady, New York 12301	29
Clanton, U. S.	NASA, L. B. Johnson Space Center, TN6, Houston, Texas 77058	50
Colby, B. N.	Materials Research Laboratory, University of Illinois, Urbana, Illinois 61801	7
Colby, J. W.	Bell Telephone Labs., 555 Union Blvd., Allentown, Pennsylvania 18103	6
Coleman, J. R.	University of Rochester Medical Center, Dept. of Radiation Biology and Biophysics, Rochester, New York 14642	60 63
Conley, D. K.	Western Electric Company, 555 Union Blvd., Allentown, Pennsylvania 18103	21

		<u>Paper Number</u>
Cooper, J. H.	Western Electric Company, 555 Union Blvd., Allentown, Pennsylvania 18103	58
Cornie, J. A.	Westinghouse Research Laboratory, Pittsburgh, Pennsylvania 15235	86
Cowley, J. M.	Arizona State University, Tempe, Arizona	36
Davidson, E.	Applied Research Laboratories, 9545 Wentworth Street, Sunland, California 91040	81
DeNee, P. B.	U. S. Department of Health, Education, and Welfare, National Institute of Occupational Safety and Health, Appalachian Laboratory for Occupational Respiratory Diseases, P. O. Box 4292, Morgantown, West Virginia 26505	67
Di Giacomo, G	IBM System Products Division, East Fishkill Facility, Hopewell Junction, New York 12533	72
Dobrott, R. D.	Texas Instruments Inc., P. O. Box 5936, Dalas, Texas 75222	10
Ellis, W. P.	Los Alamos Scientific Laboratory, P. O. Box 1663, Los Alamos, New Mexico 87544	34
Estill, W. B.	Sandia Corporation, Livermore, California 94566	43
Estry, H. W.	University of Michigan, Ann Arbor, Michigan	56
Evans, C. A., Jr.	Materials Research Laboratory, University of Illinois, Urbana, Illinois 61801	7 Tutorial
Evans, S. K.	General Electric Company, Vallecitos Nuclear Center, Pleasanton, California 94566	70
Falco, A.	Applied Research Laboratories, Sunland, California 91040	57
Ferrell, R. E.	Department of Geology, Louisiana State University, Baton Rouge, Louisiana	15
Ferrier, R. P.	IBM Research Laboratory, San Jose, California 95139	49
Gancarz, A. J.	Division of Geological and Planetary Sciences, California Institute of Technology, Pasadena, California 91109	45 77
Gedcke, D. A.	ORTEC, Inc., Oak Ridge, Tennessee 37830	17
Gelderman, A. H.	U. S. Department of Health, Education, and Welfare, National Institute of Occupational Safety and Health, Appalachian Laboratory for Occupational Respiratory Diseases, P. O. Box 4292, Morgontown, West Virginia 26505	67
Gervais, A.	Laboratoire de Physique des Materiaux, C.N.R.S., 92190 Meudon, France	52

		<u>Paper Number</u>
God, J. J.	Coates and Welter Instrument Corporation, Sunnyvale, California	58
Goldstein, J. I.	Metallurgy and Materials Science Department, Lehigh University, Bethlehem, Pennsylvania 18015	Tutorial
Greer, R. T.	Department of Nuclear Engineering, 261 Sweeny Hall, Iowa State University, Ames, Iowa 50010	53
Griffith, L. K.	Applied Research Laboratories, 9545 Wentworth Street, Sunland, California 91040	81
Hatfield, W.	General Electric Corporate R&D Center, P. O. Box 8, Schenectady, New York 12305	82
Hakkila, E. A.	University of California, Los Alamos Scientific Laboratory, Los Alamos, New Mexico 87544	69 71
Harrod, D. L.	Westinghouse Research Laboratory, Pittsburgh, Pennsylvania 15235	86
Hayakawa, K.	Central Research Laboratory, Hitachi Ltd., Kokubunji 185, Japan	40
Hazlewood, C. F.	Department of Pediatrics, Baylor College of Medicine, Houston, Texas 77025	65
Heinrich, K. F. J.	National Bureau of Standards, Chemistry A121, Washington, D. C. 20234	3, 24, 26
Herfert, R. E.	Northrop Corporation, Aircraft Division, Hawthorne, California	18
Hinthorne, J. R.	Hasler Research Center, Applied Research Laboratories, 95 La Patera Lane, Goleta, California 93017	4 9
Hogben, C. A. M.	Department of Physiology and Biophysics, University of Iowa, Iowa City, Iowa 52241	62
Holmes, A. C.	Coates and Welter Instrument Corporation, Sunnyvale, California	58
Holzwarth, W.	Department of Earth and Space Sciences, State University of New York, Stony Brook, New York 11790	42
Horne, D. E.	IBM Research Laboratory, K33-281, Monterey and Cottle Roads, San Jose, California 95139	44
Houston, J. E.	Sandia Laboratories, Albuquerque, New Mexico 87115	32
Hugenberger, C. E.	University of California, Livermore Laboratory, 7000 East Avenue, Livermore, California 94550	37
Hughes, C. W.	Westinghouse Research Laboratories, Pittsburgh, Pennsylvania 15235	86



		<u>Paper Number</u>
Hutchinson, W. B.	University of California, Los Alamos Scientific Laboratory, Los Alamos, New Mexico 87544	69
Ingram, F. D.	Department of Physiology and Biophysics, University of Iowa, Iowa City, Iowa 52241	62
Ingram, M. J.	Department of Physiology and Biophysics, University of Iowa, Iowa City, Iowa 52241	62
Iwatsuki, H.	Kawasaki Medical College, Kurashiki, Japan	66
Jackson, M. R.	General Electric Corporate R&D Center, P. O. Box 8 Schenectady, New York 12305	82
Johnson, C. E.	Argonne National Laboratory, Chemical Engineering Division, 9700 South Cass Avenue, Argonne, Illinois 60439	68
Johnson, J. W.	Georgia Tech, Atlanta, Georgia	47
Judd, G.	Rensselaer Polytechnic Institute, Materials Division, Troy, New York 12181	83
Kandiah, K.	United Kingdom Atomic Energy Authority, Harwell, Didcot, Berks, England	12
Kane, W. T.	Research and Development Laboratories, Sullivan Park, Corning Glass Works, Corning, New York 14830	46
Karlovac, N.	ORTEC, Inc., Oak Ridge, Tennessee 37830	17
Kawase, S.	Central Research Laboratory, Hitachi Ltd., Kokubunji 185, Japan	40
Kenessey, B.	Applied Research Laboratories, 9545 Wentworth Street, Sunland, California 91040	81
Kimzey, S. L.	Biomedical Research Division, DB22, NASA, Johnson Space Center, Houston, Texas 77058	64 65
Koch, F. A.	Arizona State University, Tempe, Arizona	35
Kyser, D. F.	IBM Research Laboratory, K33-281, Monterey and Cottle Roads, San Jose, California 95139	28, 44, 49
Lachance, G. R.	Geological Survey of Canada, 601 Booth Street, Ottawa, Ontario K1A-OES, Canada	13
Ladle, G. H.	NASA, MSC-TN6, Houston, Texas 77058	50
Laird, J.	Division of Geological and Planetary Sciences, California Institute of Technology, Pasadena, California 91109	45
Lannin, T. E.	General Electric Company, Vallecitos Nuclear Center, Vallecitos Road, Pleasanton, California 94566	70

		<u>Paper Number</u>
Laughon, R. B.	NASA, L. B. Johnson Space Center, TN6, Houston, Texas 77058	50
Lewis, R. K.	Cameca Instruments, Inc., 101 Executive Blvd., Elmsford, New York 10523	5
Leys, J.	3M Company, Central Research Laboratories, P. O. Box 33221, St. Paul, Minnesota 55133	23
Lifshin, E.	General Electric Company, Corporate R&D Center, P. O. Box 8, Schenectady, New York 12301	29, 31, 82
Lin, W. N.	Department of Materials Science, University of Southern California, Los Angeles, California 90007	73
MacDonald, N. C.	Physical Electronics Industries, Inc., Edina, Michigan	19
Mandavia, M.	University of Texas, M. D. Anderson Hospital and Tumor Institute, Texas Medical Center, Houston, Texas 77025	61
Mardinly, A. J.	Department of Materials and Metallurgical Engineering, University of Michigan, Ann Arbor, Michigan 48104	80
McKay, D. S.	NASA, L. B. Johnson Space Center, TN6, Houston, Texas 77058	50
McKinney, J. T.	3M Company, New Business Ventures Division, St. Paul, Minnesota 55101	23
Michel, C.	Philips Laboratories, Briarcliff Manor, New York	48
Morabito, J. M.	Bell Telephone Laboratories, Inc. 555 Union Blvd., Allentown, Pennsylvania 18103	5 8
Murata, K.	Department of Applied Physics, Osaka University, Yamada-kami, Suita, Osaka, Japan	28
Myklebust, R. L.	National Bureau of Standards, Chemistry A121, Washington, D. C. 20234	3 26
Nichols, B. L.	Department of Pediatrics, Baylor College of Medicine, Houston, Texas 77025	65
Norrish, K.	C.S.I.R.O., Division of Soils, Private Bag No. 1, Glen Osmond, S.A. 5064, Australia	36
O'Boyle, D.	Materials Science Division, Argonne National Laboratory, Argonne, Illinois 60439, and University of Wisconsin, Madison, Wisconsin	76 84
Ohkura, T.	Kawasaki Medical College, Kurashiki, Japan	66
Okano, H.	Central Research Laboratory, Hitachi Ltd., Kokubunji 185, Japan	40
Ong, P. S.	University of Texas, M. D. Anderson Hospital, 6723 Bertner Avenue, Houston, Texas 77025	61

		<u>Paper Number</u>
Paulson, G. G.	Department of Geology, Louisiana State University, Baton Rouge, Louisiana	15
Parks, R. L.	Sandia Laboratories, Albuquerque, New Mexico 87115	32
Philibert, J.	Laboratoire de Physique des Materiaux, C.N.R.S., 92190 Meudon, France	52 27
Plant, A. G.	Geological Survey of Canada, 601 Booth Street, Ottawa, Ontario K1A-OE8, Canada	13
Potosky, J. C.	University of Southern California, Los Angeles, California 90007	2
Prewitt, C. T.	Department of Earth and Space Sciences, State University of New York, Stony Brook, New York 11790	42
Prince, J. L.	Texas Instruments, P. O. Box 5474, M/S 72, Dallas, Texas 75222	10
Quigg, E.	Department of Earth and Space Sciences, State University of New York, Stony Brook, New York 11790	42
Ramalingam, S.	State University of New York, Buffalo, New York	55
Rand, M. J.	Bell Telephone Laboratories, Inc., 555 Union Blvd., Allentown, Pennsylvania 18103	8
Rendina, J. F.	McPherson Instrument Corporation, 530 Main Street, Acton, Massachusetts 01720	22
Riviere, A.	Laboratoire de Physique des Materiaux, C.N.R.S., 92190 Meudon, France	52
Rouze, S. R.	Research Laboratories, General Motors Corporation, Warren, Michigan	38 39
Rusch, T. W.	University of California, Los Alamos Scientific Laboratory, Los Alamos, New Mexico 87544	34
Russ, J. C.	EDAX Laboratories, Division of Nuclear Diodes, Inc., 4509 Lindsey Drive, Raleigh, North Carolina 27609	16 30
Russell, W. O.	University of Texas, M. D. Anderson Hospital and Tumor Institute, Texas Medical Center, Houston, Texas 77025	61
Sachen, D. J.	Department of Pediatrics, Baylor College of Medicine, Houston, Texas 77025	65
Schamber, F. H.	Northern Scientific, Inc., Middleton, Wisconsin 53562	85
Schwettmann, R. N.	Texas Instruments, P. O. Box 5474, M/S 72, Dallas, Texas 75222	10
Seward, J. R.	Applied Research Laboratories, 9545 Wentworth Street, Sunland, California 91040	57

		<u>Paper Number</u>
Sicignano, A.	Philips Laboratories, Briarcliff Manor, New York	48
Smith, D. G. W.	Department of Geology, University of Alberta, Edmonton, Alberta, Canada T6G-2E	36
Smith, R. E.	University of California, Los Alamos Scientific Laboratory, Los Alamos, New Mexico 87544	69
Solomon, J. S.	University of Dayton Research Institute, Dayton, Ohio 45409	33
Sroka, G.	University of Texas, M. D. Anderson Hospital and Tumor Institute, Texas Medical Center, Houston, Texas 77025	61
Steele, W. J.	University of California, Lawrence Livermore Laboratory, 7000 East Avenue, Livermore, California 94550	37
Sutfin, L. V.	Orthopedic Research Labs., Children's Hospital Medical Center, 200 Longwood Avenue, Boston, Massachusetts 02115	59
Swaroop, R.	Kelsey-Hayes Research and Development Center, 2500 Green Road, Ann Arbor, Michigan 48105	79
Tixier, R.	Groupe Metallurgie Physique, IRSID, 78104 Saint Germain-en-Laye, France	25, 27, 52
Tsai, J. C. C.	Bell Telephone Laboratories, Inc., 555 Union Blvd., Allentown, Pennsylvania 18103	5
Vadimsky, R. G.	Bell Telephone Laboratories, Mountain Avenue, Murray Hill, New Jersey 07974	14
Walitsky, P. J.	Westinghouse Electric Corporation, Bloomfield, New Jersey	74
Walter, E. R.	Union Carbide Corporation, South Charleston, West Virginia	51
Walter, N. M.	Material Engineering, M. S. P38-21, The Boeing Vertol Company, P. O. Box 16858, Philadelphia, Pennsylvania 19142	78
Watanabe, T.	Kawasaki Medical College, Kurashiki, Japan	66
Weiss, H.	Raytheon Company, Equipment Development Laboratory, Boston Post Road, Wayland, Massachusetts 01778	83
Wells, O. C.	IBM Thomas J. Watson Research Center, Yorktown Heights, New York 10598	Tutorial
Welter, L. M.	Coates and Welter Instrument Corporation, Sunnyvale, California	58
Wild, T. J.	University of Dayton Research Institute, Dayton, Ohio 45469	33

		<u>Paper Number</u>
Willing, R. S.	Applied Research Laboratories, 9545 Wentworth Street, Sunland, California 91040	57
Wilson, R.	Materials Division, Rensselaer Polytechnic Institute, Troy, New York 12181	83
Wittry, D. B.	University of Southern California, Los Angeles, California 90007	2 73
Woodhouse, J. B.	Materials Research Laboratory, University of Illinois, Urbana, Illinois 61801	7
Yakowitz, H.	National Bureau of Standards, B118 Materials, Washington, D. C. 20234	26
Yamamoto, S.	Central Research Laboratory, Hitachi Ltd., Kokubunji 185, Japan	40
Zelezny, W. F.	University of California, Los Alamos Scientific Laboratory, Los Alamos, New Mexico 87544	69
Zolla, A. E.	Applied Research Laboratories, 9545 Wentworth Street, Sunland, California 91040	57



# ELECTRON PROBE ANALYSIS SOCIETY OF AMERICA

## BY-LAWS

July, 1971

### ARTICLE I. NAME

The name of the Society shall be the Electron Probe Analysis Society of America. The Society is duly incorporated under the laws of the State of New York.

### ARTICLE II. PURPOSE

The purpose of this Society shall be to provide continuity, advance planning, and a financing mechanism for annual meetings and to advance and diffuse knowledge concerning the principles, instrumentation, and applications of electron probes or related instrumentation, subject to the provisions of the Internal Revenue Code, Section 501(c)(3), (1954).

### ARTICLE III. MEMBERSHIP

The membership of the Society shall consist of Regular Members, Honorary Members, Student Associates, and Sustaining Members.

#### SECTION 1. Eligibility

- i. Regular Members: Any person interested in the use of electron microprobes or related instrumentation shall be eligible for Regular Membership in the Society. Every person desiring to become a Regular Member shall in person or by authorized representative make application in writing for such membership.
- ii. Student Associates: Any graduate or undergraduate college or university student interested in the use of electron microprobes or related instrumentation is eligible to become a Student Associate. Evidence of such interest must be certified by the faculty advisor for this student.
- iii. Sustaining Members: Any business or corporation interested in supporting the aims and objects of the Society may become a Sustaining Member upon acceptance by the Executive Council and payment of the annual dues set for Sustaining Members. The Sustaining Member may designate one individual in his organization who shall have voting rights in the name of the Sustaining Member.
- iv. Honorary Members: Any person whose contributions to the field of electron probe microanalysis are of the highest order is eligible for election to Honorary Membership in the Society. The number of Honorary Members shall not be increased so as to exceed one percent of the number of Regular Members.

#### SECTION 2. Nomination and Election

Application for all classes of membership except Honorary Members must be endorsed by at least two Regular Members and forwarded to the Secretary. Nominations to Honorary Membership must be endorsed by at least ten percent of the Regular Membership. A majority vote of approval of the members of the Executive Council present and voting at a regular or a special meeting shall constitute election to Honorary Membership.

### SECTION 3. Privileges

The right to vote at elections and to hold office shall be restricted to and vested in the Regular Members of the Society in good standing. Regular Members representing a Sustaining Member shall retain their privileges as individual Regular Members.

### SECTION 4. Termination of Membership

Membership in the Society may be terminated at any time for cause by a two-thirds majority vote of the Executive Council present and voting.

## ARTICLE IV. EXECUTIVE COUNCIL

The affairs of the Society shall be managed by an Executive Council consisting of the President, Secretary, and Treasurer of the Society, the President-Elect, the immediate Past President, and three Members-at-Large. A majority of the members of the Executive Council shall constitute a quorum.

A member of the Executive Council may designate an alternate to represent him at a specific council meeting with voting privileges. This alternate must be a member in good standing.

### SECTION 1. Election of Officers

Any regular member of the Society shall be eligible for election to any office in the Society. Each year a Nominating Committee, selected in the manner specified below, shall nominate two or more candidates for each of the offices of the Society which will become vacant at the end of the year.

The Secretary shall read the names of the nominees at the annual business meeting. At that time, additional nominations may be made from the floor provided that those whose names are placed in nomination do agree to serve if elected. All nominations from the floor shall require three seconding affirmations. Election shall be by secret, written ballot. The Secretary shall distribute written ballots prior to October first. The deadline for receipt of marked ballots shall be November first. Election shall be by a plurality of those voting for each office.

### SECTION 2. Terms of Office

The term of office for the President and President-Elect shall be for one year. The term of office of the Secretary and Treasurer shall be for two years with one of these officers to be elected each year. The Secretary's two-year term shall start in 1971 and the Treasurer's two-year term in 1972. One Member-at-Large shall be elected each year to serve a three year term; he shall replace the Member-at-Large whose term has expired. No officer except the Secretary and Treasurer may succeed himself in the same office.

The President-Elect shall become President of the Society upon the expiration of the President's term of office. If the office of the Presidency becomes vacant before expiration, the President-Elect shall assume the duties of the President. If a vacancy occurs in any other office, the Executive Council shall appoint a Regular Member of the Society to serve out the unexpired year of the term of the original officer. Thereafter the vacant office will be filled at the next regular election.



### SECTION 3. Duties of the Officers

i. President: The President shall be the executive officer of the Society, shall preside over all meetings of the Executive Council, and shall be responsible for the execution of all orders and resolutions of the Society.

The President shall appoint all committee members with the advice and assistance of the Executive Council.

ii. President-Elect: The president-Elect shall assume the duties of the President in his absence or incapacity and shall perform such other duties as may be delegated to him by the President or the Executive Council.

iii. Secretary: The Secretary shall keep precise and permanent records of the business of the Society including minutes of the annual meeting and the Executive Council meetings.

He shall be responsible for all matters relating to membership including updating of membership lists.

iv. Treasurer: The Treasurer is responsible for all financial records of the Society. He shall prepare a financial report for each meeting of the Executive Council and the annual business meeting.

## ARTICLE V. COMMITTEES

### SECTION 1. Standing Committees

Any committee established to provide continuing assistance to the Executive Council shall be considered as a Standing Committee. The President shall appoint the Chairman and members of a Standing Committee; their terms of office shall expire on December thirty-first following appointment. The Chairman of each Standing Committee shall be an advisory member of the Executive Council and shall be invited to Executive Council meetings.

i. Nominating Committee: The Nominating Committee for officers shall be appointed by the Executive Council not later than February first of each year. The Nominating Committee shall consist of four members and shall include at least two Regular Members who are not members of the Executive Council.

The Nominating Committee shall report in writing to the Secretary the names of those selected to be candidates for offices in the Society not later than two calendar months prior to the annual business meeting of the Society. The Committee shall ascertain, and so inform the Secretary, that each prospective nominee will serve if elected. The Secretary shall inform the membership of the names of the nominees at least one month prior to the annual meeting of the Society.

ii. Conference Committee: The Conference Committee shall consist of four members. The Chairman shall be the General Chairman of the National Conference for the present year. Other members shall be the General Chairman of the immediate past year and the two immediate future years. General arrangements and policy for the annual technical meeting shall be approved by the Conference Committee. The preliminary budget of an annual meeting shall be approved by the Executive Council in the fall of the year preceding that meeting.

iii. Legal Committee: The Chairman of the Legal Committee shall be appointed by the President. Other members of this Committee shall be the Secretary and one other Council member. This Committee shall advise the Executive Council on the legal matters of the Society.

## SECTION 2. Other Committees

The Executive Council shall have the power to establish such other committees as it may deem desirable to aid in the management of the Society. The President shall appoint the chairman and members of each committee and designate the term of appointment.

## ARTICLE VI. DUES

### SECTION 1.

The Executive Council shall fix the annual dues, these dues being payable on January first of each year.

- i. The dues for Regular Members shall not exceed ten dollars (\$10.00).
- ii. The dues for Student Associates shall be one-half that of Regular Members for the first five years of membership. After five years a Student Associate must apply for Regular Membership.
- iii. The dues for Sustaining Members shall not exceed one thousand dollars (\$1,000.00).
- iv. There shall be no dues for Honorary Members.

### SECTION 2.

A person elected to membership becomes a member in good standing upon payment of the designated dues. If the dues of any class of member remain unpaid on July first, the Executive Council shall be empowered to remove such a member from the membership list.

### SECTION 3.

For dues and other fiscal purposes, the fiscal year shall be January first to December thirty-first.

## ARTICLE VII. MEETINGS

### SECTION 1.

There shall be an annual technical meeting of the Society held in the period June through September whose location and exact dates shall be established by the Executive Council.

### SECTION 2.

There shall be an annual business meeting of the Society held concurrently with the annual technical meeting.

## ARTICLE VIII. LOCAL SECTIONS

### SECTION 1.

An organized group interested in becoming a local section of the Society may petition the Executive Council for local section status. The petition should include: a) a list of officers and the date of expiration of their offices; b) a copy of the Constitution and By-Laws of the local section; and c) a list of all current members of the local section. Approval of this petition by the Executive Council shall constitute establishment of the local section.

### SECTION 2.

The Constitution and By-Laws of such local sections shall be consistent and in harmony with the objectives and By-Laws of the Society. Authorization of a local section shall imply no financial obligations on the part of the Society, the Executive Council, or the local section.

### SECTION 3.

The local sections shall have the power to collect dues. All local sections shall submit an annual financial statement to the Treasurer of the Society at the end of each fiscal year (December thirty-first).

### SECTION 4.

Officers of the local sections must be Regular Members of the Society. The secretary of the local section shall inform the Secretary of the Society of the results of election of local officers. The secretary of the local section shall maintain a current roster of local members with the Secretary of the Society.

### SECTION 5.

The Executive Council has the power to suspend temporarily the affiliation of any local section not acting in the best interests of the Society. Permanent suspension shall be subject to confirmation by the membership of the Society.

## ARTICLE IX. AMENDMENTS TO THE BY-LAWS

Amendments to these By-Laws may be proposed by the Executive Council or by a petition to the President signed by at least two percent of the total number of Regular Members. The text of the proposed amendment shall be circulated to all Regular Members by the Secretary at least two weeks in advance of the annual business meeting of the Society at which discussion is planned on the amendment. Members shall vote by written ballot and the amendment shall be adopted if it is favored by three-fifths of the members voting.

## ARTICLE X. DISSOLUTION OF THE SOCIETY

In the event of either voluntary or involuntary dissolution of the Society, the funds or assets of the Society remaining after discharging all just debts of its officers in the name of the Society shall be distributed without encumbrance to a non-profit group, organization, or institution of learning within the contemplation of Section 180(c)(2) of the Internal Revenue Code (1954). The selection of the recipient or recipients shall be made by the majority vote of the Executive Council in office at the time of dissolution, but in no event shall the assets be distributed to any member or employee of the Society.



# PROGRAM CORRECTIONS AND ADDITIONS

EMSA--EPASA

## Page 38

9:40 (Change in paper to be presented)  
Resolution and Contrast in the Conventional and the Scanning High  
Resolution Transmission Electron Microscope--M.G.R. Thomson, The  
Research Laboratory of Electronics, MIT, Cambridge, Mass.

Page 61 (top) Friday PM, August 17 (Change from Friday AM)

Page 63 (Change ALL times as follow:)

9:00 to 1:30	10:10 to 2:40
9:40 to 2:10	10:25 to 2:55
9:55 to 2:25	10:40 to 3:10
	10:55 to 3:25

Page 68 (Change sequence to the following:)

2:50 Some Interelement Effects in Ion Microprobe--M.A. Bayard,  
W.C. McCrone Associates, Inc., Chicago, Illinois EPASA 10a

3:05 BREAK

3:20 Panel Discussion on Ion Microprobe Analysis--  
John Colby, Moderator, Bell Telephone Laboratories  
R. Castaing, University of Paris  
C.A. Andersen, Argonne Research Laboratories  
C.A. Evans, Jr., University of Illinois  
R. Baxter, Batelle Columbus

Page 69 (Additional paper)

3:30 Improvements in High Counting Rate Performance of Si (Li) Energy  
Spectrometers with a Novel Baseline Restoration Technique--N.  
Karlovac and D.A. Gedcke, ORTEC, Inc., Oak Ridge, Tenn. EPASA 15a

Page 79 (Time changes and additional papers as follow:)

2:00 Paper originally scheduled for 2:10

2:10 Paper originally scheduled for 2:20

2:20 Microprobe Techniques for the Analysis of Radioactive Materials--  
D. O'Boyle, Argonne National Laboratory, Argonne, Ill. EPASA 77

2:35 A New Technique for Deconvolution of Complex X-Ray Energy Spectra--  
F.H. Schamber, Northern Scientific, Inc., Middleton, Wis. EPASA 78

2:55 Observations on the Practical Application of Selected Area Electron  
Channeling Patterns to Deformation Studies--J.A. Cornie and D.L.  
Harrod, Westinghouse Research Laboratory, Pittsburgh, Pa. EPASA 79

3:10 Use of the Ion Microprobe for the Identification and Localization  
of Impurities in Cathodoluminescent Natural Materials--G. Remond,  
Bureau de Recherches Geologiques et Minieres, Orleans, France  
EPASA 80



DIRECTLY HEATED  $\text{LaB}_6$  CATHODES INTERCHANGEABLE WITH STANDARD SEM  
FILAMENTS

by

C. K. Crawford

Kimball Physics, Inc. Wilton, New Hampshire 03086, and MIT Particle Optics Laboratory,  
Cambridge, Massachusetts 02139

and

Henry L. Smith\*

Lincoln Laboratory, Massachusetts Institute of Technology  
Lexington, Massachusetts 02173

The advantages of boride cathodes are well known: substantially higher brightness, longer life, and smaller effective source size.<sup>1-5</sup> Unfortunately their promise has not been exploited significantly in the microscope field due to the difficulty of mounting borides at high temperature.

This paper presents a new method of constructing directly heated cathodes, which is low enough in power consumption to permit simple mounting on standard filament bases. The cathodes may then be run in existing instruments using existing filament supplies without modification.

The design is shown in Figure 1. A tiny boride block, (at present  $\text{LaB}_6$ ), weighing approximately one milligram, is mounted by means of two pure carbon heater strips which pass through a rectangular hole in the block. The heating strips in turn are mounted on refractory metal mounting posts which are spotwelded to an appropriate filament base. The junction between the heating strips and the posts must be cooled to prevent carbide formation. This is accomplished by inserting a pair of carbon cooling strips between the heater strips. The cooling strips perform the dual function of increasing the heat radiating area, and partially short circuiting the outer sections of the heaters (thus reducing the  $I^2R$  heat generation in the outer sections). The cathode structure has been intentionally designed with two mutually perpendicular planes of symmetry, to reduce thermal drift.

---

\*This work is sponsored by the Department of the Army.





Figure 2 is a low magnification scanning electron micrograph of a  $\text{LaB}_6$  cathode. The photograph was taken using an identical cathode as the electron source. The visible deflection of the carbon heaters where they pass through the  $\text{LaB}_6$  block provides just enough friction (due to the springiness of the heaters) to hold the block in place. The same deflection also insures good electrical contact between the heating strips and the cooling strips, along the latter's inner edges.

The cathode is sharpened to a point of several micrometers radius; the tip is about one-half millimeter above the heating strips. This distance has been deliberately kept small to minimize the thermal gradient between the heaters and the tip (a smaller cathode block also implies less heat radiating area and thus lower operating power). A disadvantage of this small distance is that the heater structure is close to the Wehnelt and care is required in turning the filament adjustment screw. Some work has been done using hairpin shaped heater strips which allow more maneuvering room, however curved strips are harder to make and assemble than straight ones.

Several cathodes have been run, and simple tests made, however the results must be regarded as preliminary. Typical heater operating parameters are 2.5 V and 3.5 A maximum, with good emission usually obtained at about 8 watts input power. Total emission currents in the milliamperage range are easily achieved. The ultimate destruction mechanism as the power is increased without limit is the evaporation of the  $\text{LaB}_6$  block (rather than any chemical reaction). No long term life tests have yet been run, nor have studies been made of the tradeoff between very high brightness and lifetime. The longest any cathode has been run as of this writing is about 200 hours, and this was in an auxiliary vacuum system using a planar anode, not in an SEM. Also, the only SEM tests run thus far were made in an ion pumped Ultrascan instrument. From the literature it would appear that there is little hope of successfully running high brightness boride cathodes in vacuums worse than  $1 \times 10^{-5}$  Torr, and that  $10^{-6}$  Torr or better should be provided for stable operation. Finally it should be noted that the electron optics for operation of pointed cathodes are different than for



tungsten loops. A much smaller Wehnelt aperture should be provided, and the cathode tip should be close to the plane of the exit surface for maximum brightness. Considerable work remains to determine optimum operating conditions for various instruments.

The authors acknowledge with pleasure the assistance of A. Soares in operating the scanning microscope.

#### REFERENCES:

- 1) J. M. Lafferty, J. Appl. Phys. 22, 299 (1951).
- 2) A. N. Broers, J. Phys. E 2, 273 (1969).
- 3) S. F. Vogel, Rev. Sci. Instr. 41, 585 (1970).
- 4) H. Ahmed and A. N. Broers, J. Appl. Phys. 43, 2185 (1972).
- 5) H. Ahmed, W. Blair, and R. Lane, Rev. Sci. Instr. 43, 1048 (1972).



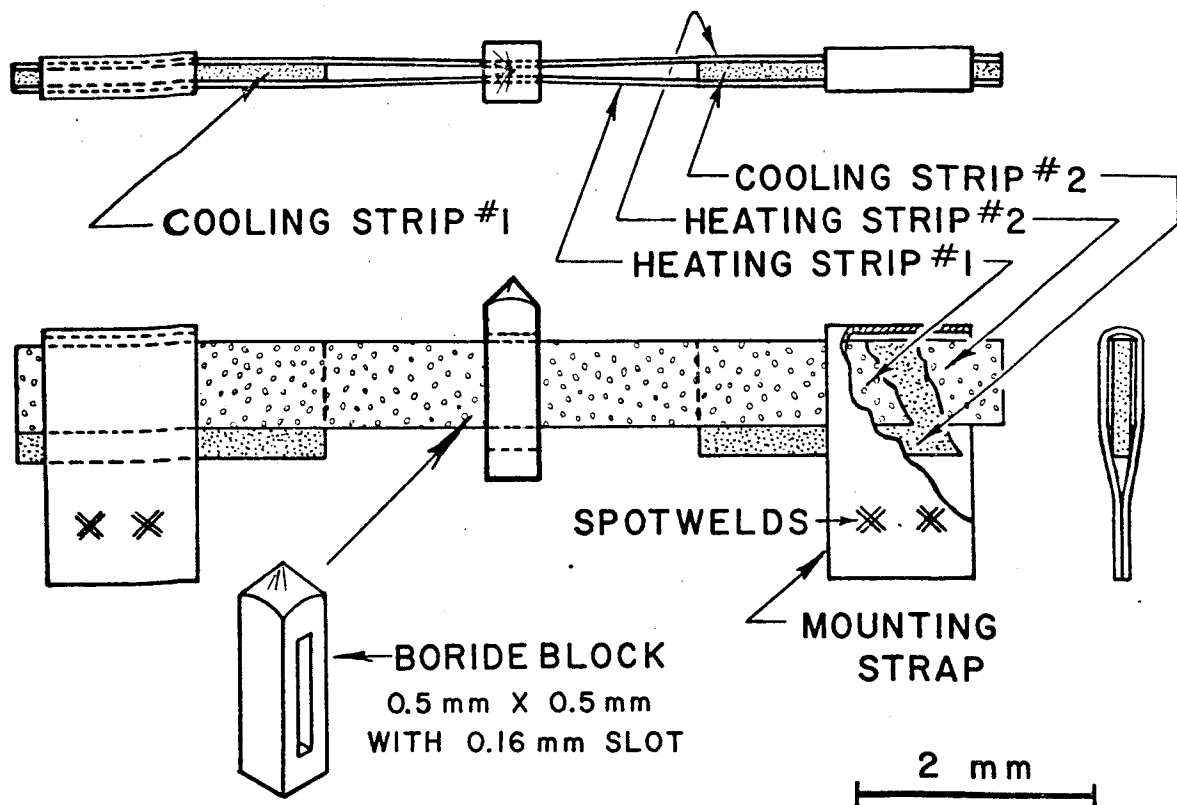


Figure 1. Construction method used to mount boride block on a double carbon heating-strip filament. Friction holds the block in place. Cooling strips electrically short the heating strips to keep the ends cool.

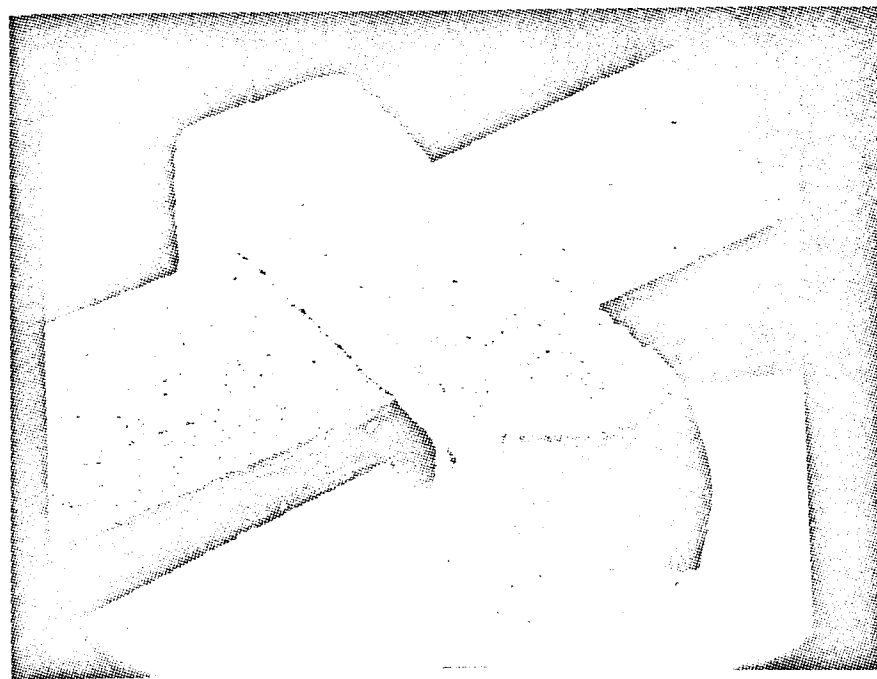


Figure 2. Low magnification scanning electron micrograph of a mounted boride cathode. The carbon heating strips retain their springiness even after long operation at high temperature.

